Aus dem Biomedizinischen Centrum
Lehrstuhl für Stoffwechselbiochemie
der Ludwig-Maximilians-Universität München
Vorstand: Prof. Dr. rer. nat. Dr. h.c. Christian Haass

Investigating the role of lipids and substrate recognition motifs in the function of aspartyl intramembrane proteases

Dissertation
zum Erwerb des Doktorgrades der Naturwissenschaften
an der Medizinischen Fakultät
der Ludwig-Maximilians-Universität zu München

vorgelegt von
Lukas Peter Feilen

aus
Saarlouis

2023

Mit Genehmigung der Medizinischen Fakultät
der Universität München

Erstgutachter:	Prof. Dr. rer. nat. Harald Steiner
Zweitgutachter:	Prof. Dr. rer. nat. Christian Behrends
Dekan:	Prof. Dr. med. Thomas Gudermann
Tag der mündlichen Prüfung:	29. August 2023

Eidesstattliche Versicherung

Ich erkläre hiermit an Eides statt, dass ich die vorliegende Dissertation mit dem Titel:

Investigating the role of lipids and substrate recognition motifs in the function of aspartyl intramembrane proteases

selbständig verfasst, mich außer der angegebenen keiner weiteren Hilfsmittel bedient und alle Erkenntnisse, die aus dem Schrifttum ganz oder annähernd übernommen sind, als solche kenntlich gemacht und nach ihrer Herkunft unter Bezeichnung der Fundstelle einzeln nachgewiesen habe.
Ich erkläre des Weiteren, dass die hier vorgelegte Dissertation nicht in gleicher oder in ähnlicher Form bei einer anderen Stelle zur Erlangung eines akademischen Grades eingereicht wurde.

Kopenhagen, den 02.01.2023

Lukas Peter Feilen

Erst wenn die Mutigen klug und die Klugen mutig geworden sind, wird das zu spüren sein, was irrtümlicherweise schon oft festgestellt wurde: ein Fortschritt der Menschheit.

Erich Kästner

Man merkt nie, was schon getan wurde, man sieht immer nur, was noch zu tun bleibt.

Marie Curie

Teilweise wurden die Ergebnisse der vorliegenden Dissertation bereits in folgenden Publiaktionen veröffenlicht:

Feilen, LP, Chen, SY, Fukumori, A, Feederle, R, Zacharias, M, Steiner, H (2022). Active site geometry stabilization of a presenilin homolog by the lipid bilayer promotes intramembrane proteolysis. *eLife*. doi:10.7554/eLife.76090

Chen, SY, **Feilen, LP**, Chávez-Gutiérrez, L, Steiner, H, Zacharias, M (2023). Enzyme-substrate hybrid β-sheet controls geometry and water access to the γ-secretase active site. *Communications Biology*. doi:10.1038/s42003-023-05039-y

Contents

List of Figures

List of Tables

Summary

Intramembrane proteases (IMPs) are interesting proteolytic enzymes since they are able to perform the water-requiring hydrolysis reaction in the water-excluding lipid membrane. IMPs are involved in various crucial cellular processes like development or cell signalling but also play a role in the onset and progression of diseases such as Alzheimer's disease (AD) or certain cancers. The human aspartyl IMP γ-secretase is directly involved in the onset of AD, since it cleaves the C-terminal fragment β (CTFβ) of the β-amyloid precursor protein (APP) releasing amyloid β (Aβ) peptides of which the longer forms like $A\beta_{42}$ aggregate into oligomers and plaques which is thought to be causative for AD. γ-Secretase is a multiprotein complex composed of four subunits. The catalytically active subunit is presenilin (PS) which exists in two homologs (PS1 and PS2). PS also has homologs in other organisms like the presenilin/SPP homolog (PSH) found in an archaeabacterium. Like PS, PSH is able to cleave APP-based substrates resulting in the release of an APP intracellular domain (AICD) and Aβ species of various lengths. The Aβ species are released from the substrate in a stepwise cleavage mechanism (processive cleavage). In contrast to PS, the activity of PSH is not dependent on the formation of a complex with accessory proteins and therefore allows to study PS function independent of complex formation.

The activity of IMPs is strongly dependent on their environment and can be modulated by several factors like the surrounding pH, the composition of the lipid bilayer or the thickness of the membrane. But little is known about the mechanism underling this modulatory effect of the lipid membrane on IMPs and how the lipid membrane influences the structural dynamics of IMPs. Furthermore, it is also unknown whether – at least – aspartyl IMPs share structural motifs for substrate recognition/binding and what role these motifs might play for their activity.

The first part of this study focusses on how the lipid environment modulates the activity of PSH and tries to unravel the underlying mechanism. It was shown that PSH produces longer Aβ peptides when its activity was assessed in a DDM micelle environment. This attenuated processive cleavage was enhanced when PSH was reconstituted into a POPC bilayer and shorter Aβ species were generated. Homology model building could reveal that PSH shares substrate recognition/binding mo-

tifs with γ-secretase, namely a small additional helix called transmembrane domain (TMD)6a C-terminal of TMD6 and a cytosolic hybrid β-sheet formed by β-strands from PSH and the APP-based C83 substrate. Mutational analysis could confirm the existence of these elements and their importance for the PSH activity. MD simulations based on this model suggest that the active site geometry is destabilized in the detergent environment compared to the lipid environment and this was validated by performing inhibitor affinity precipitation experiments. Taken together, these results show that PSH share key structural elements with γ-secretease and that the lipid environment is crucial for the correct formation of the active site geometry and promotes the processive cleavage.

The second part of this study focused on the hybrid β-sheet of the γ-secretase–C83 complex. To this end, mutational analysis of one of the PS1 β-strands (β2) and of the C83 β-strand (β3) were performed. These mutations were designed to disrupt the β-sheet and all mutations studied here strongly reduced the total activity of γ-secretase. Furthermore, most of the mutations also decreased the processive cleavage resulting in the release of longer Aβ peptides and they also shifted the site of the first γ-secretase cleavage, determining which Aβ product line is used. In addition, the β2-strand mutations also reduced the endoproteolysis of PS1 into an N-terminal fragment (NTF) and a CTF. Taken together, the hybrid β-strand is an important structural element of the γ-secretase–substrate complex which influences the total activity as well as the processive cleavage.

The results of this study help to explain how the lipid bilayer can modulate the activity of IMPs by influencing the structural dynamics of the enzymes, especially of important structural elements. One very important structural element of aspartyl IMPs is the hybrid β-sheet formed in the enzyme–substrate complex which influences the total activity as well as the processive cleavage since it is needed to correctly position the scissile bond between the two catalytic aspartates and to drain out excess water molecules from the active site.

Zusammenfassung

Intramembranproteasen (IMPs) sind faszinierende Proteasen, die in der Lage sind die wasserabhängie Hydrolysereaktion innerhalb der Lipidmembran durchzuführen. IMPs spielen eine Rolle bei verschiedensten Prozessen wie der zellulären Entwicklung oder auch der Signalweitergabe, sind aber auch an der Entstehung und dem Fortschreiten von Krankheiten, wie der Alzheimer Erkrankung (AD) oder bei verschiedenen Krebsarten beteiligt. Eine dieser IMPs, ist die γ-Sekretase, eine humane Aspartyl-Intramembranprotease, die direkt an der Entstehung von AD beteiligt ist. Dabei spaltet diese Protease das C-terminale Fragment β (CTFβ) des Amyloidvorläuferproteins (APP) und setzt β-Amyloid-Peptide (Aβ) frei. Von diesen Peptiden lagern sich die längeren Formen wie $A\beta_{42}$ zu Oligomeren und Plaques zusammen, was als ursächlich für Alzheimer angesehen wird. Die γ-Sekretase ist ein Multiproteinkomplex, der aus vier Untereinheiten besteht. Die katalytisch aktive Untereinheit ist Präsenilin (PS), das in zwei Homologen (PS1 und PS2) vorliegt. PS hat auch Homologe in anderen Organismen, wie das Präsenilin/SPP-Homolog (PSH), das aus einem Archaeon stammt. Ähnlich dem PS, kann PSH auch APP-basierte Substrate spalten, was zur Freisetzung einer intrazellulären APP-Domäne (AICD) und Aβ-Spezies unterschiedlicher Längen führt. Die Aβ-Spezies werden dabei schrittweise vom Substrat abgespalten (sogenannte prozessive Spaltung). Diese Aktivität ist bei PSH unabhängig von der Bildung eines Komplexes mit anderen Proteinen, so wie es bei PS und der γ-Sekretase notwendig ist. Daher ist es mit PSH möglich PS-Funktionen unabhängig einer Komplexbildung zu untersuchen.
Verschiedenste äußere Faktoren können die Aktivität von IMPs beeinflussen, wie zum Beispiel der pH-Wert der Umgebung oder die Zusammensetzung der Lipidmembran. Der zugrunde liegende Mechanismus des modulatorischen Effektes der Lipidmembran auf IMPs ist noch wenig verstanden, insbesondere der Einfluss der Lipidmembran auf die strukturelle Dynamik von IMPs. Darüber hinaus ist es noch weitgehend unverstanden welche Rolle strukturelle Motive für die Substraterkennung/-bindung für die Aktivität von Aspartyl-Intramembranproteasen spielen und ob solche Motive von verschiedenen Aspartyl-IMPs geteilt werden.
Der erste Teil der hier vorliegenden Studie geht der Frage nach, wie die Lipidumgebung die Aktivität von PSH moduliert und versucht den zugrunde liegenden Mech-

anismus zu entschlüsseln. Dabei konnte gezeigt werden, dass PSH in einer reinen DDM-Mizellenumgebung länger Aβ-Peptide produziert. Wurde die Aktivität von PSH hingegen in einer POPC-Lipiddoppelschicht untersucht, so wurde die prozessive Spaltung verstärkt und kürzere Aβ-Spezies erzeugt. Um den zugrunde liegenden Mechanismus dafür zu verstehen, wurde ein Homologiemodel erstellt, welches zeigen konnte, dass PSH Substraterkennungs-/Bindungsmotive mit der γ-Sekretase teilt: C-terminal der Transmembrandomäne (TMD) 6 eine kleine zusätzliche Helix (TMD6a) und auf der zytosolisches Seite ein hybrides β-Faltblatt, das durch β-Stränge von PSH und dem APP-basierten C83-Substrat gebildet wird. Mittels biochemischer Mutationsanalysen konnte gezeigt werden, dass diese Motive für die Aktivität von PSH von entscheidender Bedeutung sind. Basierend auf diesem Homologiemodel wurden Molekulardynamik-Simulationen durchgeführt, die darauf hindeuten, dass die Geometrie des aktiven Zentrums in der Detergenzumgebung im Vergleich zur Lipidumgebung destabilisiert ist, was durch die Durchführung von Inhibitorbindestudien bestätigt werden konnte. Diese Ergebnisse zeigen zusammenfassen, dass PSH wichtige Strukturelemente mit der γ-Sekretase teilt und dass die Lipidumgebung für die korrekte Ausbildung der Geometrie des aktiven Zentrums entscheidend ist.
Der zweite Teil dieser Studie konzentrierte sich auf das hybride β-Faltblatt des γ-Sekretase–C83-Komplexes. Zu diesem Zweck wurde eine Mutationsanalyse des PS1-β-Stranges und des C83-β-Stranges (β3) durchgeführt und die Mutationen so gewählt, dass die Ausbildung des β-Faltblattes verhindert wird. Alle untersuchten Mutationen verringerten die Gesamtaktivität der γ-Sekretase stark, beeinflussten darüber hinaus meist auch die prozessive Spaltung von APP, sodass längere Aβ-Peptide freigesetzt wurden und verschoben ebenfalls die Stelle der ersten γ-Sekretase-Spaltung. Darüber hinaus reduzierten die Mutationen im β2-Strang auch die Endoproteolyse von PS1 in ein N- und ein C-terminales Fragment. Somit konnte das hybride β-Faltblatt als ein wichtiges Strukturelement des γ-Sekretase–Substrat-Komplexes etabliert werden, das sowohl die Gesamtaktivität als auch die prozessive Spaltung beeinflusst.
Die Ergebnisse dieser Studie helfen zu erklären, wie die Lipiddoppelschicht die strukturelle Dynamik der Enzyme, insbesondere wichtiger Strukturelemente, beeinflusst und damit letzten Endes die Aktivität von IMPs modulieren kann. Darüber hinaus konnte gezeigt werden, dass das hybride β-Faltblatt ein sehr wichtiges Strukturelement von substratgebundenen Aspartyl-IMPs ist. Dieses β-Faltblatt beeinflusst sowohl die Gesamtaktivität als auch die prozessive Spaltung, da es für die korrekte Positionierung der Schnittstelle zwischen den beiden katalytischen Aspartaten und für das Abfließen überschüssiger Wassermoleküle aus dem aktiven Zentrum erforderlich ist.

1 Introduction

1.1 Proteases and proteolysis

Proteases - or more precisely called peptidases - are catalytic enzymes found in all kingdoms of life which cleave proteins by addition of a water molecule to a peptide bond (Bond, 2019). Currently, the peptidase database MEROPS (Rawlings *et al.*, 2018) lists more than 850 known and putative human proteases. Proteases fulfill important cellular functions and are therefore crucial in health and disease (Bond, 2019).
Protease are proteins with a highly specialized active site (also called catalytic site). This active site is a three-dimensional cleft which binds the substrate and provides the amino acid (aa) residues for the hydrolysis reaction (these residues are also often called catalytic group) (Copeland, 2000). The substrate is bound by weak – but also highly specific – interaction forces to the active site. Furthermore, the cleft generates a specific microenvironment which is important for the enzymatic reaction. Nevertheless, the active site is only a small portion of the whole enzyme. Proteases contain also other important domains for their regulation and/or localization, like autoinhibitory prodomains or sorting signals (López-Otín & Bond, 2008). For some proteases, also so called exosites were reported (Klein *et al.*, 2018). These are substrate binding sites different from the active site. It is assumed that these exosites are initial substrate binding or docking sites which might perform already a first specificity check before the substrate is handed over to the active site.

1.1.1 Classes of proteases

When the first proteases where discovered they were classified by the cleavage site(s) within their respective substrates (Brix & Stöcker, 2013; Klein *et al.*, 2018). Endopeptidases cleave peptide bonds within the substrate. Exopeptidases – in contrast – act on the termini of their substrates and cleave off few aa from these ends. They are further divided into aminopeptidases which act on the N-terminus of proteins and carboxypeptidases which act on the C-terminus.

Advances in biochemical and biophysical techniques led to an increased understanding of proteases and their cleavage mechanisms and resulted in a new classification of proteases by their active site (Brix & Stöcker, 2013; Klein *et al.*, 2018). Today, six families of proteases are distinguished by their catalytic site: metalloproteases, aspartic proteases, glutamic proteases, serine proteases, threonine proteases and cysteine proteases.
As all other proteins, proteases are either soluble (such as pepsin or proteasome), membrane-bound/anchored (such as ADAM10 or BACE1) or membrane-embedded proteins (such as rhomboids or γ-secretase). The latter ones – also termed intramembrane proteases – are a very special class of proteases since they are able to cleave their substrate with in the rather hydrophobic membrane environment (Wolfe (2009), discussed in detail in 1.1.5).

1.1.2 Proteolysis mechanisms

Proteases cleave peptide bonds within their respective protein substrate by the addition of a water to these peptide bonds. This hydrolysis of a peptide bond is in principle a thermodynamically favoured but also a very slow process with a half-life time of over 100 years (Berg *et al.*, 2009). The slow reaction is a result of the planar form of the peptide bond which forms a partial double bond. The C-atom of the carbonyl group is less electrophilic and therefore less accessible for a nucleophilic attack. Proteases help to overcome the long half-life time by increasing the electrophilicity of the C-atom and by reducing the distance between the substrate and the nucleophile. Roughly, the cleavage mechanisms of the six protease families can be divided into two basic subtypes: a single addition-elimination reaction or a double addition-elimination reaction (Sterchi & Stöcker, 1999). In the single addition-elimination reaction a water molecule directly attacks the carbonyl C-atom of the substrate peptide bond leading to the formation of a tetrahedral intermediate. This intermediate is subsequently resolved by the hydrolysis of the attacked peptide bond. This reaction mechanisms is carried out by metallo-, aspartic- and glutamic proteases (Sterchi & Stöcker, 1999; Klein *et al.*, 2018). The double addition-elimination reaction is carried out by the cysteine, serine and threonine proteases. Here, the catalytic aa residue directly acts as the nucleophile and attacks the carbonyl C-atom resulting in a covalent acyl-enzyme intermediate and a free amino product. The intermediate is then resolved by the nucleophilic attack of a water molecule and the second product is released (Sterchi & Stöcker, 1999; Klein *et al.*, 2018).

1.1.3 Regulation of proteases

Since proteases execute an irreversible reaction and due to their important participation in diverse cellular pathways, their activity needs to be tightly regulated (López-Otín & Bond, 2008). This regulation can happen on various cellular levels. The first layer of protease regulation is gene expression (Twining, 1994). In response to an injury or an inflammation reaction but also during development and ageing the expression of certain proteases can be up- or downregulated to imitate a protease response to a certain stimulus. After gene expression and translation, the protease itself can also be regulated on various levels. A lot of proteases are expressed as inactive zymogens which are either activated by autocatalytic cleavage events or by the cleavage by another protease (Khan & James, 1998). The expression of proteases as zymogens allows the storage of proteases in an inactive form. The fully active form of a protease can also be regulated by various mechanisms like posttranslational modifications, localization or inhibitors (Twining, 1994; López-Otín & Bond, 2008). Posttranslational modification can for example influence the conformation of the active site, reduce the substrate binding or (in case of glycosylations) influence the localization. Proteases can further be sequestered into vesicles to avoid cleavage of proteins in the cytosol or localized to the membrane to specifically act on membrane-associated substrates (Twining, 1994). Active proteases can be inhibited by endogenous protease inhibitors which tightly bind to the protease (Bode & Huber, 2000; Turk, 2006; López-Otín & Bond, 2008). These protease inhibitors can even bind directly to the active site and poison the catalytic activity. Other inhibitors bind to a site different from the active site and thereby allosterically regulate protease activity by inducing conformational changes within the protease. So far, all known endogenous protease inhibitors are proteins. Known classes of these inhibitors are serpins (inhibit serine proteases), cystatins (inhibit cysteine protesease) or tissue inhibitors of metalloproteases (TIMPS) (Twining, 1994).

1.1.4 Proteases in health and disease

Proteases are crucial for life (López-Otín & Bond, 2008). They are involved in many cellular processes and misregulation in proteolytic cleavage events can result in severe diseases (Klein *et al.*, 2018). Proteases are for example involved in the maturation of proteins, in the degradation of (misfolded) proteins, in the activation of inactive proteins, in the shedding of ectodomains (cleavage of ectodomains), in the regulation of signaling cascades, in apoptosis and cell death or in immunity responses. Besides their important physiological functions, proteases are also in

involved several diseases, like cancer (Song *et al.*, 2021), cardiometabolic diseases (Hua & Nair, 2015), Alzheimer's disease (AD, De Strooper (2010)) or viral infections (Sharma & Gupta, 2017). There, they can be either directly involved in disease onset and/or progression but also in disease control. Therefore, proteases are interesting targets for therapeutical interventions but their broad functional spectrum makes it challenging to tackle specific protease functions.

1.1.5 Intramembrane proteases

At a first glance, intramembrane proteases (IMPs) seem to be quite unusual proteases since they perform the water-requiring hydrolysis reaction within the hydrophobic membrane environment. But since the first discovery of an IMP in 1997 (Rawson *et al.*, 1997), several IMPs belonging to the different catalytic classes were identified. So far, metallo-, aspartyl, glutamyl and serine IMPs are known (Kühnle *et al.*, 2019). These IMPs have in common that they are multipass intramembrane proteins which adopt a cup-shaped or a horseshoe-like structure (Beard *et al.*, 2019) and form a hydrophilic cavity in which water molecules can enter the catalytic site. Structural investigations could show that water is indeed able to bind at least in close proximity to the active site (Wang *et al.*, 2006b; Manolaridis *et al.*, 2013; Cho *et al.*, 2019).
IMPs play an important role in cell signalling and in the cellular response to environmental changes. Since they are able to cleave within the membrane plane, they can liberate a cytosolic fragment which can function as a signalling molecule within the cell. The cleavage of substrates by IMPs can thereby influence various cellular processes like cell differentiation, lipid metabolism or cellular stress response (Jurisch-Yaksi *et al.*, 2013; Beard *et al.*, 2019; Kühnle *et al.*, 2019).

1.1.5.1 Classes of IMPs

The first discovered IMP was the site-2 protease (S2P, Rawson *et al.* (1997)), which belongs to the class of metalloproteases and is conserved throughout all kingdoms of life except for budding *Saccharomyces cerevisiae* (Kühnle *et al.*, 2019). Structural analysis of an archeal S2P protease showed that the catalytic zinc ion is embedded in a bundle of six transmembrane domains (TMDs) and coordinated by the highly conserved two His and one Asp aa side chains (Feng *et al.*, 2007). In humans, S2P is located in the lipid bilayer of the Golgi apparatus and involved in the regulation of cholesterol production by liberating the signalling competent N-terminal part from the sterol regulatory element binding proteins (SREBPs, Rawson (2013)). Another

known human zinc metalloprotease is the ER-located protease ZMPSTE24. ZMPSTE4 is composed of 7 TMDs which form a water-filled capped barrel within the membrane in which the catalytic site is located (Pryor *et al.*, 2013; Quigley *et al.*, 2013). Interestingly, the so far known canonical substrates are peripheral membrane proteins and not integral membrane proteins. ZMPSTE4 cleaves proteins that clog the translocon and thereby helps to restore the translocon activity (Ast *et al.*, 2016; Kayatekin *et al.*, 2018). The cleavage of these substrates occurs at the membrane-embedded catalytic site (Kühnle *et al.*, 2019).

The largest group of IMPs is the family of rhomboid serine proteases (Lastun *et al.*, 2016). These proteases have been identified in all (sequenced) organisms and come in two general topologies: either with 6 TMDs or with an additional TMD C- or N-terminal of the protease core (7 TMDs in total). Besides the active proteases, also inactive pseudoproteases, the so-called iRhoms are known. In mammals, five rhomboid proteases have been identified RHBDL1-4 (rhomboid-like) and PARL (presenilin-associated rhomboid-like); only for three of them (RHBDL2, RHBDL4 and PARL) the respective substrates and functions have been described (Kühnle *et al.*, 2019). The mammalian rhomboid proteases are found in the lipid bilayer of all cellular compartments, RHBL1 is located in the Golgi apparatus, RHBL2 in the plasma membrane, RHBL3 in the late endosome, RHBL4 in the ER and PARL in the mitochondria. Rhomboids cleave type I TMD proteins close to the luminal site but there are also few reports for non-canonical cleavage outside of the membrane. The human rhomboid proteases are involved in several cellular functions and processes like wound healing and angiogenesis (RHBL2), ER-associated degradation (ERAD, RHBL4) or mitophagy (PARL) (Lastun *et al.*, 2016; Beard *et al.*, 2019; Kühnle *et al.*, 2019).

In humans, two members of the aspartyl IMP family are known: the presenilins and the signal peptide peptidase (SPP)/SPP-like (SPPL) family (Kühnle *et al.*, 2019). The presenilin family is composed of two homologs, PS1 and PS2 and will be discussed in more detail in 1.4.1.1. The SPP/SPPL family is composed of the five members SPP, SPPL2a-c and SPPL3 (Kühnle *et al.*, 2019; Mentrup *et al.*, 2020). Presenilins and SPPs share a common structural fold with 9 TMDs but are oriented inversely in the cellular membrane. While presenilins have their N-terminus in the cytosol, the N-terminus of SPPs is located in the lumen. Both belong to the family of GxGD-type aspartyl IMPs, and have their catalytic aspartes within the highly conserved YD and GxGD motifs located in TMD6 and 7, respectively. Furthermore, they also share the conserved PAL motif in TMD9 (Friedmann *et al.*, 2004). In contrast to presenilins, SPPs can function without accessory protein and without undergoing endoproteolysis. As already indicated by their inversed topology, SPPs cleave type II TMD proteins and a growing number of substrates have been identi-

fied for these proteases (Mentrup *et al.*, 2020). For SPP, SPPL2a and b it was shown that they cleave substrates within their TMD after ectodomain shedding, e.g. the cleavage of TNFα by SPPL2a and b. In contrast, SPPL3 does not seem to require ectodomain shedding and substrates are directly cleaved by SPPL3 (like for rhomboid proteases). SPP and SPPL2c are able to cleave tail-anchored proteins with a type II TMD orientation (Mentrup *et al.*, 2020). The various SPPLs are differently located within the cell, SPPL2a is found in late endosomes/lysosomes, SPPL2b in the plasma membrane, SPP and SPPL2c in the ER and SPPL3 in the Golgi apparatus (Kühnle *et al.*, 2019). They are involved in different cellular processes like signal transduction, membrane trafficking or protein glycosylation (Mentrup *et al.*, 2020).
For the family of of glutamyl IMPs only one member has been identified so far, the the Ras-converting enzmye 1 (RCE1) in *S. cerevisiae* (Boyartchuk *et al.*, 1997; Manolaridis *et al.*, 2013) and no membrane protein as substrate is known but the active site was found to be located within the membrane.

1.1.5.2 Substrate requirements & cleavage mechanism of IMPs

Whereas soluble proteases have a more or less clear substrate consensus (mainly due to the primary aa sequence), the substrate recognition motif(s) of IMPs are mainly unclear. Nevertheless, they show a high substrate specificity and a few principle substrate requirements are known (Langosch *et al.*, 2015). IMPs have a preference for the orientation of their respective substrate(s), some preferring type I TMD substrates (N-terminus oriented towards the extracellular space) other type II TMD substrates (N-terminus oriented towards the cytosol) (Beard *et al.*, 2019). Recently, it was reported that IMPs might also be able to cleave a TMD or in close vicinity of a TMD in a multipass membrane protein, whereas the exact mechanism of this cleavage process is still mainly unclear (Grieve *et al.*, 2021; Restrepo *et al.*, 2022). The cleavage of substrates by metallo- and aspartyl IMPs normally requires a prior cleavage step by another protease within the ectodomain (Beard *et al.*, 2019). The remaining membrane-bound fragment is then the actual substrate of the IMP. For bacterial rhomboid proteases also a recognition motif in the substrate around the cleavage site is reported (Akiyama & Maegawa, 2007; Strisovsky *et al.*, 2009) but so far such a consensus motif is not reported for other IMPs. Furthermore, it is suggested that IMPs can recognize and/or cleave only certain conformations of the substrate's TMD (Langosch *et al.*, 2015).
The principle catalytic mechanisms of IMPs are the same as for all other proteases (see also 1.1.2) but there are some additional challenges (Wolfe, 2009). As already

discussed above, water needs to access the catalytic site which is embedded in the hydrophobic membrane environment. Furthermore, the α-helical structure of the substrates is an unfavoured conformation for cleavage since the aa side chains sterically hinder the access of water to the protein backbone (Wolfe, 2009). Therefore, TMD substrates needs to unwind around the scissile bond to make the peptide bond available for cleavage. Several studies including structural analysis of protease-substrate complexes (Brown *et al.*, 2018; Clemente *et al.*, 2018; Cho *et al.*, 2019; Yang *et al.*, 2019; Zhou *et al.*, 2019) could show for different IMPs and substrates that the substrate TMD indeed undergoes conformational changes at and around the scissile bond when bound at the active site. These conformational changes result in an unwinding of the α-helix and make the peptide bond available for the cleavage.
In contrast to soluble protease, the cleavage of substrates by intramembrane proteases is a very slow process (Dickey *et al.*, 2013; Kamp *et al.*, 2015; Naing *et al.*, 2015; Bolduc *et al.*, 2016a; Naing *et al.*, 2018). IMPs were found to be (several) thousandfold slower than soluble proteases of the same catalytic class, cleaving only round about 6 (Kamp *et al.*, 2015) to 22 (Dickey *et al.*, 2013) substrate molecules within one hour within the cellular context. Interesting, while the turn-over rate was similar for the proteases reconstituted into proteoliposomes, it was 10-fold higher in a detergent system (Dickey *et al.*, 2013). The factors which make the cleavage process so slow are not understood yet. Maybe a prior substrate selection at an exosite, the substrate handling within the protease and/or the necessary substrate unwinding slows down the cleavage process (Dickey *et al.*, 2013; Kamp *et al.*, 2015).

1.1.5.3 Regulation of IMPs

As for all other classes of proteases, IMPs can be regulated on several cellular levels, like transcription, translation or localization. In addition, also the lipid bilayer can regulate the activity of IMPs even though little is known about the details of this mechanism so far. An *in vitro* study on rhomboid cleavage could show that different membrane phospholipid environments differentially modulate the activity of several rhomboid IMPs (Urban & Wolfe, 2005) but the mechanism behind this observation remains elusive. Furthermore, the cleavage site within the substrate Spitz by the rhomboid IMP GlpG differed from the natural cleavage site in *E. coli* when assessed in DDM (Moin & Urban, 2012). The natural cleavage site was restored in the *in vitro* system upon reconstitution of GlpG into proteoliposomes with various lipid compositions. The modulation of IMP activity by the composition of the membrane environment is not limited to rhomboid IMPs but was also observed for γ-secretase (Urban & Wolfe, 2005; Osenkowski *et al.*, 2008) where also cholesterol was found as an important modulator for γ-secretase activity. Cholesterol decreases $A\beta_{40}$

levels and increases $A\beta_{42}$ levels resuling in an increased $A\beta_{42}/A\beta_{40}$ ratio (Osenkowski *et al.*, 2008). Furthermore, not only the composition of the (lipid) environment can regulate the activity of IMPs but also the thickness of the membrane bilayer as it was observed for γ-secretase (Holmes *et al.*, 2012; Winkler *et al.*, 2012). Thicker membranes result in a decreased $A\beta_{42/43}/A\beta_{\text{total}}$ ratio and an increased $A\beta_{40}/A\beta_{\text{total}}$ ratio and $A\beta_{38}/A\beta_{\text{total}}$ ratio, respectively (Winkler *et al.*, 2012).
Whether the effects of membrane composition and membrane properties on IMP activity is solely a bulk effect or whether this involves also direct lipid-protease interactions remains elusive. The available cryo-EM structures of γ-secretase provide evidences for a direct lipid-protease interactions since they showed phospholipid and cholesterol molecules directly bound to the protease (Bai *et al.*, 2015b; Yang *et al.*, 2019; Zhou *et al.*, 2019). Such a lipid-protease interaction was previously also found in two crystal structures of rhomboid proteases (Ben-Shem *et al.*, 2007; Lemieux *et al.*, 2007). But for non of these lipid molecules a direct functional role in rhomboid and/or γ-secretase activity was described.

1.2 Alzheimer's disease

One disease in which proteases play an important role – especially the IMP γ-secretase – is AD (De Strooper, 2010). AD is the most common form of dementia worldwide representing 60-80% of all dementia cases (Barker *et al.*, 2002; Alzheimer's Association, 2020). Dementias are an increasing burden in an ageing society. Currently, more than 50 million people worldwide are suffering from any form of dementia and this number steadily increases and is expected to reach 152 million people in 2050 (Alzheimer's Disease International, 2020). The increasing number of dementia patients and their high care needs pose major (financial) challenges for the healthcare system. Therefore, the understanding of disease mechanisms and the development of effective therapeutics is crucial (Alzheimer's Disease International, 2015; Winblad *et al.*, 2016).
AD is a progressive neurodegenerative disease which was first described by Alois Alzheimer at the beginning of the previous century. In 1906, Alzheimer reported the case of his patient Auguste Deter (Alzheimer, 1907, 1911), a woman which was suffering from disorientation, forgetfulness and the inability to perform simple verbal and written tasks. When her brain was examined, profound brain atrophy (neurodegeneration) and extra- and intracellular deposits were found. The extracellular amyloid plaques and the intracellular neurofibrillary tangles (NFTs) are until today the pathological hallmarks of AD and necessary for its unambiguous diagnosis

(Hyman *et al.*, 2012). The NFTs are deposits of hyperphosphorylated tau (Grundke-Iqbal *et al.*, 1986; Kosik *et al.*, 1986; Goedert *et al.*, 1988; Wischik *et al.*, 1988a,b; Köpke *et al.*, 1993). Tau normally binds to microtubles and stabilizes them but it gets hyperphosphorylated during disease progression, disassembles from the microtubles and aggregates into tangles (Wang & Mandelkow, 2016). The deposition of tau is also a hallmark of other neurodegenerative diseases – the so called tauopathies (Arendt *et al.*, 2016). The amyloid plaques are composed of aggregated, fibrillar Aβ (Glenner & Wong, 1984; Masters *et al.*, 1985) which is derived from amyloid precursor protein (APP) processing (Estus *et al.* (1992); Haass *et al.* (1992b); Golde *et al.* (1992); Busciglio *et al.* (1993); Haass *et al.* (2012), see also 1.3.1 and 1.4.4). Mainly longer Aβ peptides like $A\beta_{42}$ but also $A\beta_{43}$ are found in these plaques (Iwatsubo *et al.*, 1994).
The exact pathological mechanism of AD is still not well understood but it is currently widely accepted that AD onset and progression is best described by the amyloid hypothesis or amyloid cascade hypothesis (Hardy & Higgins, 1992; Selkoe & Hardy, 2016). The disease starts with increased levels of Aβ and/or relatively increased levels of longer Aβ species. These can aggregate into plaques and induce synaptic dysfunctions. In a process not yet understood, this leads to the hyperphosphorylation of tau and to its aggregation into NFTs. These pathological processes result in an increased neurodegeneration leading ultimately to dementia.

1.2.1 Sporadic and familial AD

Most of the AD cases are sporadic forms of the disease (sporadic AD, SAD) with a late onset (LOAD, late onset AD), typically at the age of 65 and older. What exactly drives the accumulation of Aβ in SAD is still elusive and it is proposed that reduced clearance/depletion of Aβ drive the Aβ accumulation. But several genetic risk factors were found to contribute to AD. In the recent years, analysis of such risk factors could show that the innate immune system and especially the brain resident microglia cells can contribute to AD. Exposure of microglia with Aβ (plaques) induced changes in cellular processes and "reprogrammed" microglia. These cells can then not respond properly to pathological changes and might therefore contribute to disease onset and/or progression (Jay *et al.*, 2017; Keren-Shaul *et al.*, 2017; Krasemann *et al.*, 2017; Gratuze *et al.*, 2018; Henstridge *et al.*, 2019). The main risk factor for sAD is the Apolipoprotein E (ApoE) which comes in three different variants ε2, ε3 and ε4 (Holtzman *et al.*, 2011; Liu *et al.*, 2013). While ε2 seems to be a protective ApoE variant, ε4 is associated with a 20-fold increased risk in sAD onset (Corder *et al.*, 1993; Strittmatter *et al.*, 1993; Verghese *et al.*, 2011). Interestingly, in 2019 a

protective ApoE ε3 mutant was found (Arboleda-Velasquez *et al.*, 2019). So far, the exact mechanism how the ApoE variants contribute to AD onset and progression is not fully understood but they differentially influence the aggregation and removal of Aβ (Kim *et al.*, 2009; Castellano *et al.*, 2011; Verghese *et al.*, 2011; Hashimoto *et al.*, 2012).

Only a minor proportion of AD cases is linked to mutations within genes directly involved in disease onset. In these familial forms of AD (familial AD, FAD) autosomal dominant mutations within the APP (Chartier-Harlin *et al.*, 1991; Goate *et al.*, 1991; Murrell *et al.*, 1991), PS1 (Sherrington *et al.*, 1995) or PS2 (Levy-Lahad *et al.*, 1995; Rogaev *et al.*, 1995) gene are causative for the disease. The Alzfroum mutation database currently reports mutations at more than 235 aa positions of PS1, more than 10 aa positions of PS2 and more than 20 aa positions of APP related to AD. At several of these aa potions more than one AD causing mutation is known, resulting in a large number of AD related mutations within these genes. The PS mutations secrete longer Aβ species, especially $A\beta_{42}$ and $A\beta_{43}$, resulting in an increased $A\beta_{42/43}/A\beta_{40}$ ratio (Borchelt *et al.*, 1996; Scheuner *et al.*, 1996; Citron *et al.*, 1997; Saito *et al.*, 2011). Furthermore, longer Aβ species can also accumulate intracellularly which might also contribute to the disease (Sannerud *et al.*, 2016). The main reason for the production of longer Aβ species is the decreased processivity of γ-secretase, especially the reduced γ-cleavage from $A\beta_{42}$ to $A\beta_{38}$ and $A\beta_{43}$ to $A\beta_{40}$, respectively (Chávez-Gutiérrez *et al.*, 2012; Okochi *et al.*, 2013; Fernandez *et al.*, 2014; Szaruga *et al.*, 2015; Devkota *et al.*, 2021). The mutations destabilize the interaction between γ-secretase and $A\beta_{42/43}$ which makes it easier for these peptides to dissociate from the protease (Okochi *et al.*, 2013; Szaruga *et al.*, 2017). Furthermore, several studies could show that PS mutations also influence the conformation of the active site (Chau *et al.*, 2012) and thereby alter the binding/positioning of the substrate to γ-secretase's active site region (Fukumori & Steiner, 2016; Trambauer *et al.*, 2020) as well as binding of active site directed inhibitors (Xia *et al.*, 2000; Ikeuchi *et al.*, 2003; Czirr *et al.*, 2007). For some FAD mutants a reduced total γ-secretase activity was observed which did not correlate with the increased $A\beta_{42}/A\beta_{40}$ ratio (Moehlmann *et al.*, 2002; Quintero-Monzon *et al.*, 2011). Most of the reported APP mutations are located within the APP C-terminal fragment β (CTFβ) which is the direct γ-secretase substrate. One of the identified mutations (A2T, Icelandic mutation, Aβ numbering) was found to be protective (Jonsson *et al.*, 2012; Benilova *et al.*, 2014; Hashimoto & Matsuoka, 2014; Murray *et al.*, 2016). The other mutations within the APP CTFβ were identified as pathogenic. The Swedish mutation (KM670/671NL) is located at the β-secretase cleavage site resulting in increased levels of CTFβ and consequently also higher levels of Aβ (Citron *et al.*, 1992; Mullan *et al.*, 1992; Haass *et al.*, 1995; Kimura *et al.*, 2016). The other APP

mutations are located either at the γ-secretase cleavage sites or within the Aβ domain and therefore either shift the production of Aβ to longer and more aggregation prone forms (Iwatsubo *et al.*, 1994; Tamaoka *et al.*, 1994; Weggen & Beher, 2012) or the mutation itself changes the aggregation behavior of the secreted Aβ species (Nilsberth *et al.*, 2001; Hori *et al.*, 2007; Hatami *et al.*, 2017). Both, more Aβ and/or more aggregation prone Aβ can be causative for AD.

1.2.2 Lipids in AD

Several studies could link fatty acids, lipids and lipid metabolism to AD (Yin, 2022) and genome-wide association studies (GWAS) in AD patients identified several misregulated genes linked to lipid metabolic pathways like apolipoproteins, cholesterol transporters or lipid receptors (Pimenova *et al.*, 2018; Vogrinc *et al.*, 2021). Furthermore, it was shown that nearly all lipid classes play a role in AD pathogenesis (Di Paolo & Kim, 2011; Kao *et al.*, 2020).
The cholesterol level is positively correlated with AD. Lower cholesterol levels abolish the activity of β- and γ-secretase, whereas high cholesterol levels enhance the activity of both proteases, resulting in an increased Aβ production (Simons *et al.*, 1998; Wahrle *et al.*, 2002; Fassbender *et al.*, 2001; Kalvodova *et al.*, 2005; Osenkowski *et al.*, 2008; Cheng *et al.*, 2014). High levels of sphingomyelin – a sphingolipid – can decrease γ-secretase activity (Grimm *et al.*, 2005) and it is suggested that sphingolipids in general are able to modulate γ-secretase activity (Sawamura *et al.*, 2004). β-Secretase and γ-secretase both are more directed to lipid rafts – specialized membrane subdomains rich of cholesterol and sphingolipids – further supporting the important role of these lipids in AD (Di Paolo & Kim, 2011). But not only cholesterol and sphingolipids play a role in AD and APP processing but also phospholipids. A decrease in phosphatidylinositol-4,5-bisphosphate (PtdIns(4,5)P_2) results in elevated Aβ_{42} levels (Landman *et al.*, 2006). Furthermore, PtdIns(4,5)P_2 reduces γ-secretase activity *in vitro* and it was suggested that PtdIns(4,5)P_2 and the APP compete for γ-secretase binding (Osawa *et al.*, 2008).
Lipids do not only influence the production of Aβ but can also contribute (indirectly) to Aβ depostion and/or aggregation (Di Paolo & Kim, 2011). Furthermore, Aβ can also influence lipid metabolism and homeostasis resulting in a complex interplay between APP trafficking and processing, Aβ production and accumulation and lipid homeostasis (Di Paolo & Kim, 2011). Since alterations in lipid levels were observed in post mortem AD brains, lipids and lipid metabolism are considered as potential AD therapeutics (Grimm *et al.*, 2017). But the complex regulation of these metabolic processes and the systemic effects of these treatment strategies makes it

difficult to fine tune the therapeutical effect (Grimm *et al.*, 2017; Chew *et al.*, 2020). Nevertheless, it might be still possible to use the alterations in lipid compositions during AD as biomarkers for diagnosis or disease progression (Di Paolo & Kim, 2011; Chew *et al.*, 2020).

1.2.3 AD therapeutics

Since disease-modifying therapeutics were missing until recently, AD patients were so far only treated symptomatically (Long & Holtzman, 2019). Since Aβ seems to be the driving molecule in AD onset, it was also the primary target in the development of disease-modifying therapies, either by reducing its production or by increasing its degradation. However, most of the approaches targeting Aβ failed, be it the inhibition of proteases involved in the generation of Aβ (Nie *et al.* (2020); Cho *et al.* (2022), discussed also in 1.4.5.1) or the active immunisation of patients with aggregated $A\beta_{42}$ (Jäkel *et al.*, 2019; Nicoll *et al.*, 2019). The passive immunisation with biotechnological produced monoclonal antibodies targeting Aβ like Aducanumab (Sevigny *et al.*, 2016) or Gantenerumab (Ostrowitzki *et al.*, 2017) showed a decrease in the Aβ accumulation in the patients' brains. Nevertheless, the patients within the clinical studies showed no or only mild cognitive improvements which in the first place resulted in early discontinuation of these studies. Detailed analysis of data from clinical studies performed with Aducanumab could show – according to Biogen, which is owing Aducanumab – a slight cognitive improvement of patients (Knopman *et al.*, 2021) and led to the approval of this monoclonal antibody for AD therapy in the United States (US) by the US Food and Drug Administration (FDA) (Nisticò & Borg, 2021). Since summer 2021, Aducanumab is now available under the brand name Aduhelm for treatment of AD patients in the US. The European regulatory authorities have decided – based on the poor data on cognitive improvements – not to admit Aduhelm for clinical use in Europe (Pawlowski & Warnecke, 2022). In autumn 2022, Eiasi and Biogen announced that their Aβ-targeting antibody Lecanemab slowed cognitive decline in a phase 3 study (Rogers, 2022; van Dyck *et al.*, 2022).

1.3 The β-amyloid precursor protein (APP)

APP is an ubiquitously expressed protein with a single pass TMD, a large ectodomain and a small intracellular domain (Dyrks *et al.*, 1988). It belongs to the APP family of proteins and has two homologs APLP1 and APLP2 in humans (Müller *et al.*,

2017). The highly glycosylated ectodomain is mainly composed of the two folded domains E1 and E2 which are separated by the unfolded acidic domain (figure 1.3.1). The E1 is composed of two subdomains, the growth factor-like domain (GFLD) and the copper binding domain (CuBD) (Müller & Zheng, 2012). The GFLD is able to bind heparin with a highly positively charged patch. This heparin binding facilitates the dimerization of APP in *cis* or *trans* (Hoefgen *et al.*, 2014). The homodimerization in *cis* is supported and strengthened by a GxxxG dimerization motif in the TMD (Munter *et al.*, 2007; Kaden *et al.*, 2008). In addition, this motif also functions as a cholesterol binding site for APP (Barrett *et al.*, 2012). The Aβ domain contains parts of the TMD as well as the N-terminal juxtamembrane domain. The APP intracellular domain (AICD) contains a YENPTY internalization motif and can be phosphorylated at several sites (Lai *et al.*, 1995; Marquez-Sterling *et al.*, 1997; Bukhari *et al.*, 2017).

As a result of alternative splicing events, APP exists in three isoforms, APP_{695}, APP_{751} and APP_{770} (Müller *et al.*, 2017). APP_{770} contains in addition a Kunitz-like protease inhibitor domain (KPI) and a short Ox-2 antigen domain between the acidic domain and domain E2, APP_{751} only contains the KPI (figure 1.3.1).

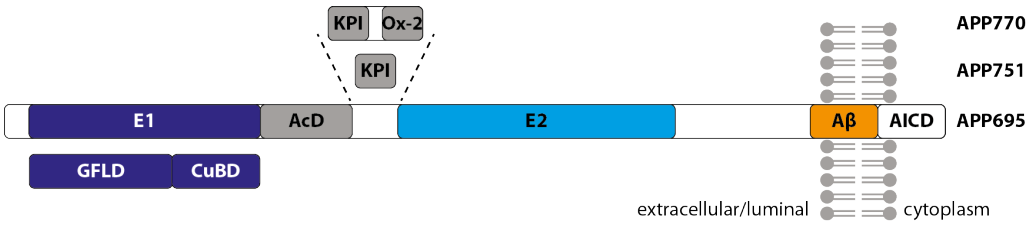

Figure 1.3.1: Schematic representation of APP. The domain organization of the three different APP isoforms is shown.

1.3.1 Processing of APP

APP is proteolytically cleaved by various proteases resulting in different cleavage products with diverse physiological functions. In general, canonical and non-canonical processing pathways are distinguished (Müller *et al.*, 2017). After its synthesis in the endoplasmatic reticulum (ER), APP is maturing in the secretory pathway and transported to the cell surface (Haass *et al.*, 2012). From the cell surface, APP can then be re-internalized by clathrin-mediated endocytosis into the endosomal system where it is either degraded in the lysosomes or recycled to the cell surface (Haass *et al.*, 1992a; Nordstedt *et al.*, 1993; Koo & Squazzo, 1994; Yamazaki *et al.*, 1996).

The canonical processing of APP is divided into a non-amyloidogenic and an amyloidogenic pathway which are both constitutively active (Haass & Selkoe, 1993) and

both canonical pathways involve a first cleavage of APP in its ectodomain (Esch *et al.*, 1990; Sisodia *et al.*, 1990; Haass & Selkoe, 1993). In the non-amyloidogenic pathway (figure 1.3.2), APP is first cleaved at the cell surface in its ectodomain by α-secretases which are metalloproteases of the ADAM family (Buxbaum *et al.*, 1998; Lammich *et al.*, 1999). The physiological most relevant α-secretase is ADAM10 (Kuhn *et al.*, 2010; Hitschler & Lang, 2022). The α-secretase cleavage between aa K16 and L17 (Aβ numbering, K687 and L689 APP_{770} numbering, (figure 1.3.3)) results in the release of a soluble fragment (sAPPα). The remaining 83 aa long C-terminal fragment (CTFα, C83) is then further processed by γ-secretase resulting in the release of AICD and p3 fragments (Haass *et al.* (1993), discussed in detail in 1.4.4).

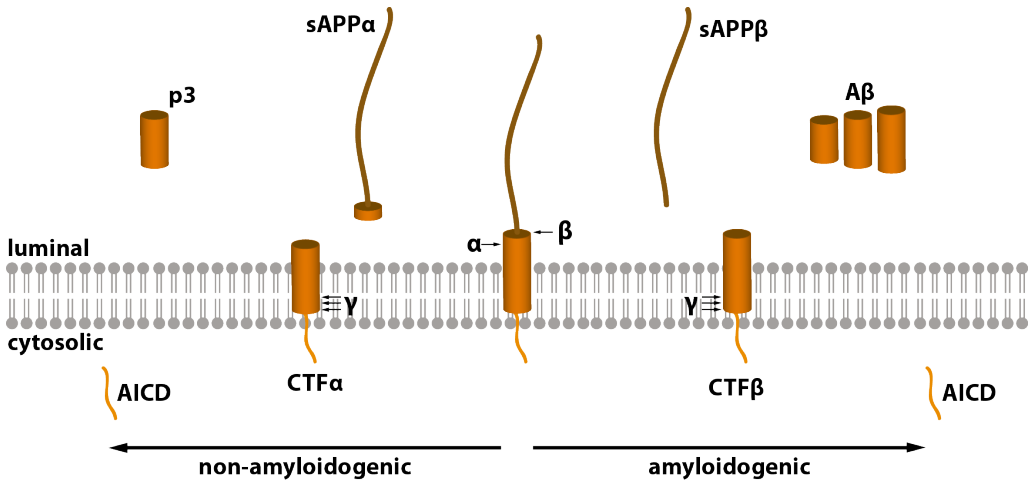

Figure 1.3.2: APP processing. APP is either cleaved in a non-amyloidogenic or an amyloidogenic pathway. First APP ectodomain is shedded by either α- or β-secrtease resulting in the CTFα or CTFβ, respectively. The CTFs are further cleaved by γ-secretase into AICD and p3 or AICD and Aβ, respectively.

In the amyloidogenic pathway (figure 1.3.2), APP is first cleaved by the β-secretase BACE1 in the ectodomain between aa M671 and D672 (APP_{770} numbering, before D1, Aβ numbering) resulting in the release of the soluble sAPPβ (Sinha *et al.*, 1999; Vassar *et al.*, 1999; Yan *et al.*, 1999). As for the CTFα, the remaining 99 aa long CTFβ (C99) is processed by γ-secretase releasing an AICD and Aβ peptides (Haass & Selkoe (1993), discussed in detail in 1.4.4). BACE1 can also cleave APP between aa Y10 and E11 (Aβ numbering, (figure 1.3.3)) resulting in shorter CTFβ' and N-terminal shorter $Aβ_{11\text{-}x}$ peptides (Haass *et al.*, 1992b; Vassar *et al.*, 1999).
APP can also be cleaved by other proteases than α- or β-secretase in different non-canonical pathways (Müller *et al.*, 2017). The asparagine endopeptidase (AEP or δ-secretase) cleaves between aa N373 and E374 or between aa N660 and I661 in the ectodomain of APP (Zhang *et al.*, 2015b). The fragment generated by the cleavage between N373 and E374 is again substrate for a second δ-cleavage between N660 and

I661. The resulting CTFδ is then further processed by β-secretase and γ-secretase resulting in the release of AICD and Aβ peptides (Zhang *et al.*, 2015b; Andrew *et al.*, 2016). Meprin-β cleaves the APP ecotdomain at different sites among others one aa C-terminal of β-secretase resulting in a one aa shorter CTFβ* (C98, (figure 1.3.3)), which is further processed by γ-secretase to Aβ* (Bien *et al.*, 2012). These $Aβ^*_{2\text{-}x}$ peptides tend to aggregate faster than Aβ peptides derived from β-secretase cleavage (Schönherr *et al.*, 2016). Another protease which cleaves APP ectodomain is the Θ-secretase BACE2, a BACE1 homolog. BACE2 cleaves APP between aa F19 and F20 (figure 1.3.3) and the resulting CTF is further processed into Aβ-like fragments which might be non-amyloidogenic (Sun *et al.*, 2006). APP can also be cleaved my matrix metalloproteases (η-secretase) N-terminal of the α-/β-secretase cleavage sites. The resulting CTFη is further processed by α- or β-secretase releasing small Aη-α and Aη-β peptides (Willem *et al.*, 2015). Caspases 3, 6 and 8 can cleave APP or CTFα/β within the AICD between aa D68 and A69 resulting in two AICD fragments: AICD31 (A69 to C-terminus) and AICD-Jcasp (released by γ-secretease cleavage) (Lu *et al.*, 2000; Bertrand *et al.*, 2001; Dumanchin-Njock *et al.*, 2001). Both of these fragments are implicated in apoptosis.

Figure 1.3.3: Schematic representation of the Aβ domain. The Aβ domain (orange) as well as parts of the neighbouring sequence are shown including the Aβ and APP_{770} numbering. The arrows indicate the cleavage sites of α-, β-secretases and meprin-β within the APP ectodomain as well as the cleavage sites (ε, ζ, γ) of γ-secretase within the TMD (gray).

1.3.2 Physiological functions of APP and Aβ

APP and its cleavage products can conduct a versatile set of physiological functions. While APP_{695} is mainly expressed in the brain (Kang *et al.*, 1987), APP_{751} and APP_{770} are mainly expressed outside the brain (Oltersdorf *et al.*, 1989; van Nostrand *et al.*, 1991). These longer isoforms are associated with blood coagulation. The shorter APP isoform plays a role in synaptic plasticity, memory and learning (Roch *et al.*, 1994; Dawson *et al.*, 1999; Seabrook *et al.*, 1999; Ring *et al.*, 2007; Nikolaev *et al.*, 2009). These effects are mainly mediated by the ability of APP to form *cis* and *trans* dimers (Müller *et al.*, 2017). Together with adaptor proteins,

APP can also transduce signals to downstream signalling cascades.
Furthermore, the proteolytic fragments of APP have several functions, even though their detailed role is still unclear. sAPPα seems to play a main role for the synaptic activity, in learning and memory. It stimulates the growth of synapses and regulates synapse plasticity as well as spine density (Roch *et al.*, 1994; Furukawa *et al.*, 1996; Ring *et al.*, 2007; Richter *et al.*, 2018; Rice *et al.*, 2019). In contrast, the only 16 aa longer sAPPβ does not convey the same function and its physiological role is still elusiv (Richter *et al.*, 2018). An-α and An-β were shown to impair the long term potentiation (LTP) *ex vivo* and *in vivo* and to impair neuronal activity (Willem *et al.*, 2015; Mensch *et al.*, 2021). The functions of the AICD are still highly debated (Bukhari *et al.*, 2017). While several *in vitro* studies could show that the AICD can – in complex with binding partners – function as a transcription factor (Cao & Südhof, 2001; Cupers *et al.*, 2001; Kimberly *et al.*, 2001) the results of *in vivo* studies were not convincingly showing the same effect (Hébert *et al.*, 2006; Waldron *et al.*, 2008). The highly labile AICD is stabilized by its binding partner – e.g. FE65 – and can thereby enter the cell nucleus where it can convey its potential function (Kimberly *et al.*, 2001). A transport of the AICD on its own into the nucleus seems not to be possible (Bukhari *et al.*, 2017).
Despite its extensively studied and well established role in AD, Aβ is proposed to have also important (beneficial) roles in physiological processes like antimicrobial defence, tumor suppression, blood-brain barrier (BBB) integrity or regulation of synaptic functions (Brothers *et al.*, 2018). It is still unclear which form of Aβ is conveying which function in the brain. In principle Aβ is found in three different forms: as monomers, as oligomers or as fibrils. Monomeric or oligomeric Aβ is neurotoxic, reduces LTP (long-term potentiation) and leads to degeneration of dendrites (Yankner *et al.*, 1990; Lacor *et al.*, 2007; Shankar *et al.*, 2008; Li *et al.*, 2009). Nevertheless, there seems to be a complex regulation of beneficial and detrimental roles of Aβ. The role of the total amount of Aβ and the role of the ratio between the different Aβ species in this process are not yet well understood. Even though, the role of Aβ in AD is well established, it is still unclear which Aβ species and which Aβ forms are important in disease onset and progression. An important factor in this process is the aggregation potential of Aβ (Shankar *et al.*, 2008; Esparza *et al.*, 2013; Selkoe & Hardy, 2016). While longer Aβ species, like $A\beta_{42}$ or $A\beta_{43}$, are highly aggregation prone (Jarrett *et al.*, 1993; Jarrett & Lansbury, 1993; Mucke *et al.*, 2000; Saito *et al.*, 2011), shorter species, like $A\beta_{40}$, might decrease the aggregation of the longer species (Kim *et al.*, 2007; Yan & Wang, 2007; Moore *et al.*, 2018). Therefore, the ratio between longer and shorter species is important for disease onset (Kuperstein *et al.*, 2010; Petit *et al.*, 2022) and higher levels of $A\beta_{38}$ correlate with a slower cognitive decline in AD patients (Cullen *et al.*, 2022). A recent study could further

show that the $A\beta_{37}/A\beta_{42}$ ratio improves the discrimination between AD patients and cognitively not impaired persons (Liu *et al.*, 2022) . Nevertheless, it is still under debate which form of Aβ is neurotoxic. Increasing evidences indicate that soluble oligomeric forms of Aβ are toxic and disturb synaptic functions (Shankar *et al.*, 2008; Koffie *et al.*, 2009; Esparza *et al.*, 2013).
The role of the non-amyloidogenic Aβ counterpart p3 is not known yet and so far no pathological effects of this peptide are reported.

1.4 The intramembrane protease γ-secretease

γ-Secretase is an integral membrane protein complex composed of four subunits (figure 1.4.1): presenilin (PS), nicastrin (NCT), presenilin enhancer 2 (PEN-2) and anterior pharynx defective 1 (APH-1) (Edbauer *et al.*, 2003; Kimberly *et al.*, 2003; Takasugi *et al.*, 2003) with PS being the catalytic subunit of the protease (Steiner *et al.*, 1999a; Wolfe *et al.*, 1999; Esler *et al.*, 2000; Kimberly *et al.*, 2000; Li *et al.*, 2000; Steiner *et al.*, 2000). Both, PS and APH-1 exist as two homologs, PS1 and PS2 as well as APH-1a and APH-1b. Therefore, γ-secretase can assemble in at least four distinct complexes in the cell (Hébert *et al.*, 2004; Shirotani *et al.*, 2004b). This complexity is increased by alternative splicing events of APH-1a (Lee *et al.*, 2002; Gu *et al.*, 2003). The four subunits are found in a 1:1:1:1 ratio in the complex (figure 1.4.1) and are necessary and sufficient for the catalytic activity of the protease (Sato *et al.*, 2007). The four subunits are arranged in a horseshoe-like shape and are made of 19 TMDs from which PEN-2 TMD1 adopts a hairpin-like structure (Bai *et al.*, 2015b).

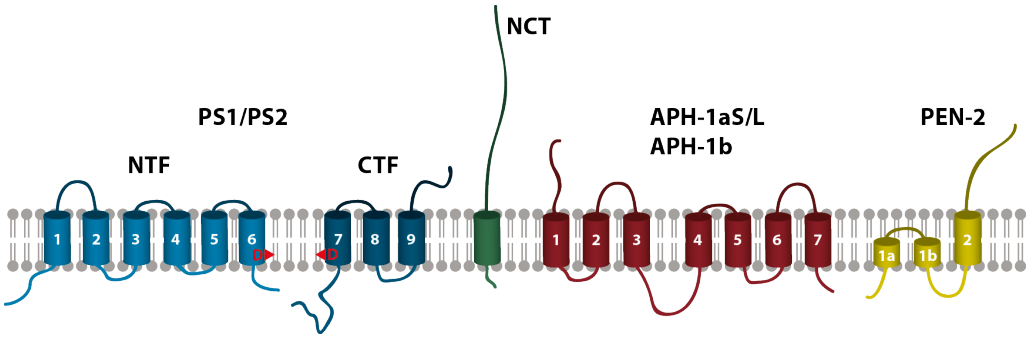

Figure 1.4.1: Schematic representation of the γ-secretase complex. The subunits of γ-secretase are shown: PS NTF (blue), PS CTF (darkblue), NCT (green), APH-1 (red), PEN-2 (yellow). The catalytic aspartates in TMD 6 and 7 are represented as red arrow heads.

1.4.1 Structure and assembly of the γ-secretase complex

1.4.1.1 Presenilin (PS)

Presenilin is a polytopic membrane protein made of 9 TMDs, with the N-terminus located in the cytosol and the C-terminus in the lumen (Kaether *et al.*, 2004; Henricson *et al.*, 2005; Laudon *et al.*, 2005; Oh & Turner, 2005a,b; Spasic *et al.*, 2006). PS1 is composed of 467 aa and PS2 of 448 aa and the two human PS homologs share a sequence identity of 66%. PS is the catalytic subunit of the γ-secretase complex with the two conserved catalytic aspartates D257 and D385 in case of PS1 and D263 and D366 in case of PS2 are located in TMD6 and 7 (Steiner *et al.*, 1999a; Wolfe *et al.*, 1999; Kimberly *et al.*, 2000). The aspartate residues are found in the two highly conserved YD (TMD76) and GxGD (TMD7) motifs (Steiner *et al.*, 2000; Ponting *et al.*, 2002; Torres-Arancivia *et al.*, 2010). Studies have shown that the two conserved glycine residues of this motif (G382, G384) are important for substrate cleavage and only tolerate the mutation to an alanine residue indicating that small amino acid site chains are needed at these positions (Steiner *et al.*, 2000; Pérez-Revuelta *et al.*, 2010). Nevertheless, the mutations G382A and G384A lead to an increased $A\beta_{42}/A\beta_{40}$. At the position between the two conserved glycine residues (x383) more aa residues are tolerated and it seems that this position guides the substrate selectivity (Yamasaki *et al.*, 2006; Kretner *et al.*, 2013). Another important motif within PS is the PAL motif (aa 433-435, PS1) which is located in TMD9. It is part of the active site and stabilize its conformation (Wang *et al.*, 2004, 2006a; Sato *et al.*, 2008; Tolia *et al.*, 2008). Recent structural investigations also imply a role of the PAL motif in stabilizing the enyzme–substrate interaction at the active site (Yang *et al.*, 2019; Zhou *et al.*, 2019).
During the maturation of the γ-secretase complex, presenilin is autocatalytically cleaved in the large cytosolic loop between TMD6 and 7 (Thinakaran *et al.*, 1996; Wolfe *et al.*, 1999; Edbauer *et al.*, 2003; Fukumori *et al.*, 2010). This endoproteolysis between T291 and A299 (PS1) is a stepwise/processive cleavage mechanism (Fukumori *et al.*, 2010) and results in the formation of a 30 kDa NTF (N-terminal fragment) with 6 TMDs and a 20 kDa CTF (C-terminal fragment) with 3 TMDs (Thinakaran *et al.*, 1996; Podlisny *et al.*, 1997; Beher *et al.*, 2001; Campbell *et al.*, 2002). These fragments remain tightly bound in the complex. Mutations in the PS gene can reduce or even prevent this endoproteolysis step. The mutation PS1 M292D at the cleavage site in the loop completely abolish the endoproteolysis but does not change the activity of the γ-secretase complex (Steiner *et al.*, 1999b). Similarly, the double mutation M298D/V299A at the endoptoreolysis site of PS2 did not change the total activity but influenced the processive cleavage (Jacobsen *et al.*,

1999). In contrast, other mutations like PS1 R278I (Saito *et al.*, 2011) strongly reduce endoproteolyis and as well the activity of the protease.

1.4.1.2 Nicastrin (NCT)

NCT is a type I TMD protein and with 110 kDa (709 aa) the largest member of the γ-secretase complex (Yu *et al.*, 2000). It has a large stable ectodomain (Fluhrer *et al.*, 2011) which undergoes extensive N- and O-glycosylations during the transport of the complex through the secretory pathway (Edbauer *et al.*, 2002; Leem *et al.*, 2002; Capell *et al.*, 2005). This glycosylation is – as the endoproteolysis of PS – a marker for the maturation of the complex (Kaether *et al.*, 2002). Nevertheless, the role and importance of the gylcosylation for the protease maturation and activity is still debated. Most studies so far suggest that the glycosylation does not influence the activity of γ-secretase (Yang *et al.*, 2002; Herreman *et al.*, 2003; Dries & Yu, 2008; López *et al.*, 2015) but another study came to an opposite result (Moniruzzaman *et al.*, 2018).
NCT is proposed to be the substrate receptor of the γ-secretase complex (Shah *et al.*, 2005). NCT consists of a so called DAP domain (DYGIS and peptidase domain) composed of round about 200 aa (Fagan *et al.*, 2001). Within this domain two important motifs were identified, the DYGIS motif and aa E333. The DYGIS motif is important for the interaction with PS and mutations reduce this interaction resulting in decreased activity (Yu *et al.*, 2000; Chen *et al.*, 2001). E333 seems to be important for NCT's function as substrate receptor (Shah *et al.*, 2005). E333 is proposed to recognize the free N-terminus of substrates via ionic interactions (Shah *et al.*, 2005; Dries *et al.*, 2009). But mutation studies could show that this residue is also important for the complex maturation and not only for substrate recognition (Shirotani *et al.*, 2004a; Chávez-Gutiérrez *et al.*, 2008). Furthermore, the high-resolution structures of γ-secretase in complex with its substrates did not show any interaction of the substrate with this specific residue (Yang *et al.*, 2019; Zhou *et al.*, 2019). The view on the receptor role of NCT has therefore changed and it is thought that nicastrin strerically exclude substrates with large ectodomains (Bolduc *et al.*, 2016a). Furthermore, in a recent study a new substrate interaction site was shown. Residues I241 and N242 of NCT form an interface which is interacting with the TMD flanking aa K28 of APP and controls the length of the produced Aβ species (Petit *et al.*, 2019).

1.4.1.3 PEN-2

PEN-2 is the smallest component of the γ-secretase complex (101 aa) with a molecular weight of 12 kDa. For long time it was assumed that PEN-2 forms two TMDs with both termini located in the lumen (Crystal *et al.*, 2003). But further biochemical and structural investigations revealed that TMD1 is forming two half TMDs which do not completely span the lipid bilayer and are arranged in a hairpin-like structure (Bai *et al.*, 2015b; Zhang *et al.*, 2015a). Upon its binding to the ternary complex composed of NCT, PS and APH-1, PS endoproteolysis is induced (Luo *et al.*, 2003; Takasugi *et al.*, 2003). Its C-terminus stabilizes the whole γ-secretase complex after endoproteolysis (Hasegawa *et al.*, 2004; Prokop *et al.*, 2004, 2005). In addition, it seems possible that PEN-2 influences the structure of the active site and therefore also the activity of the complex (Shiraishi *et al.*, 2004; Isoo *et al.*, 2007).

1.4.1.4 APH-1

APH-1 is composed of 7 TMDs and small extracellular elements (Fortna *et al.*, 2004). It seems to be kind of a scaffolding protein for the γ-secretase complex since it is important for its stability and correct structural arrangement (Francis *et al.*, 2002; Goutte *et al.*, 2002; Lee *et al.*, 2002). In humans two homologs are known APH-1a (29 kDa, 265 aa) and APH-1b (28.5 kDa, 257 aa) (Francis *et al.*, 2002; Gu *et al.*, 2003). Due to alternative splicing events APH-1a additionally exists in a large (APH-1aL) or a small (APH-1aS) isoform (Lee *et al.*, 2002; Gu *et al.*, 2003). As for PS, only one of the APH-1 isoforms is found in the γ-secretase complex (Shirotani *et al.*, 2004b). Therefore, the assembly of six different γ-secretase complexes is in principle possible.

1.4.1.5 Complex assembly, maturation and localization

All components of the γ-secretase complex are co-translationally translocated into the ER and there also rapidly degraded in their uncomplexed form (Escamilla-Ayala *et al.*, 2020). The assembly of the complex is occurring in a stepwise process and is happening in pre-Golgi compartments or during the transport between these compartments. This requires the release of the single components from the ER by packing into vesicles. A recent study (Wouters *et al.*, 2021) could shed new light on the assembly of the γ-secretase complex. Each complex component is independently from the other components packed into COPII vesicles and NCT and PS1 are preferentially sorted to different COPII vesicles. NCT prefers Sec24C/D coated vesicles

whereas PS1 prefers Sec24A coated vesicles (Wouters *et al.*, 2021). In line with previous data (Gu *et al.*, 2003; LaVoie *et al.*, 2003; Morais *et al.*, 2003), it was shown that NCT and APH-1 form a subcomplex dimer in the ER. Furthermore, also PS1 and PEN-2 are forming a subcomplex dimer at this site (Wouters *et al.*, 2021). Most likely in the ER-Golgi intermediate compartment these two heterodimeric subcomplexes assemble together to the tetrameric γ-secretase complex. How this assembly of the two subcomplex dimers works is not clear so far. The preferential sorting of the complex components into different Sec24 vesicles might be a way to prevent early complex assembly in the ER (Wouters *et al.*, 2021). It also still remains elusive what sorts the NCT/APH-1 dimer into their respective vesicles since they are lacking a clear cargo protein motif. Maybe the interaction with cargo molecules like Rer1p (Retrieval of ER protein) might facilitate sorting. Other studies showed that Rer1p interacts with immature NCT and might thereby prevent its assembly with APH-1 (Spasic *et al.*, 2007). Furthermore, it was suggested that Rer1p is capable to bind uncomplexed PEN-2 to stabilize this subunit until it is assembled in the γ-secretase complex (Kaether *et al.*, 2007). After complex assembly, it is further maturated, especially by the glycosylation of NCT (Herreman *et al.*, 2003) and by the endoproteolyis of PS into NTF and CTF (Luo *et al.*, 2003). In addition, NCT and PS can be post-translationally modified by phosphorylation, myristoylation and ubiquitination which regulate the cellular turnover of the protease (Escamilla-Ayala *et al.*, 2020).

After complex assembly and maturation the γ-secretase complexes are sorted to their cellular compartments. Thereby, the localization of the complexes is mainly dependent on the PS variant within the respective complex. While PS1 complexes are mainly localized at the cell surface and within the secretory pathway (Kaether *et al.*, 2002; Chyung *et al.*, 2005; Meckler & Checler, 2016), PS2 complexes are exclusively localized at late endosomes and lysosomes (Meckler & Checler, 2016; Sannerud *et al.*, 2016). Due to their rather strict intracellular localization, PS2–γ-secretase complexes are mainly responsible for the production of intracellular Aβ. This intracellular Aβ is normally produced in the more toxic $A\beta_{42}$ form and might therefore contribute to AD pathogenesis (Kanatsu *et al.*, 2014; Sannerud *et al.*, 2016). Within the respective cellular membrane γ-secretase is not randomly distributed but rather confined in specific detergent-resistant subdomains like lipid rafts or tetraspanin-enriched microdomains (Wahrle *et al.*, 2002; Vetrivel *et al.*, 2004; Hur *et al.*, 2008; Wakabayashi *et al.*, 2009). The lipid composition of these subdomains, especially their cholesterol and sphingolipid content, influence the activity of γ-secretease (Ehehalt *et al.*, 2003; Osenkowski *et al.*, 2008; Vetrivel & Thinakaran, 2010).

1.4.1.6 Structure and dynamics of γ-secretase

In the last decade enormous work has been done to unravel the structure of the γ-secretase complex. In 2006, first structural data at a resolution of 15 Å were obtained based on negative stained samples analyzed by electron microscopy (EM) (Lazarov *et al.*, 2006). These low resolution data showed an aqueous chamber and two pores in the complex. A central aqueous pore was further identified in in two independent studies (Renzi *et al.*, 2011; Li *et al.*, 2014). In addition, also a lateral cleft was identified which was proposed to be an initial substrate binding site (Li *et al.*, 2014). Sampling different conformations of γ-secretase revealed that the protease complex can exist in extended, intermediate and compact conformations (Elad *et al.*, 2015). Interestingly, the binding of a γ-secretase inhibitor seems to induce the compact γ-secretase conformation (Elad *et al.*, 2015). Already these early studies could show that γ-secretase can by highly dynamic.
First deeper insights into the structural arrangement of γ-secretase came around the same time by higher resolution cryo-EM studies (Lu *et al.*, 2014; Bai *et al.*, 2015b). Already in a structure of 4.5 Å resolution the general assembly of γ-secretase (NCT/Pen-2/PS1/APH-1a) with 19 TMDs in a horseshoe-shaped structure was observed but the low resolution especially in the loop regions made it impossible to assign the individual TMDs to the components of the complex (Lu *et al.*, 2014). Nevertheless, the ectodomain of NCT could be identified unambiguously and was shown to fold directly above the TMDs. The atomic structure of the same complex at an average resolution of 3.4 Å allowed then the assignment of the TMDs to the components of the complex (figure 1.4.2, (Bai *et al.*, 2015b)). Most of the TMDs were well resolved and only TMD2 and 6 of PS1 were less well resolved which indicates a great flexibility of these two TMDs. The increased resolution of the structure also allowed to identify the position of the two catalytic aspartates (figure 1.4.2). Interestingly, these are located at the convex side of the horseshoe-shaped complex. In addition, this study also revealed that TMD1 of PEN-2 is forming a hairpin-like structure with two half-TMDs and not a single membrane-spanning TMD (figure 1.4.2). Advances in filtering and classification techniques subsequentially led to the identification of three distinct conformations of PS1 in the γ-secretase complex (Bai *et al.*, 2015a), underscoring the flexibility of the protease.
Even though the low resolution areas within the γ-secretase structures are indicative for higher protein flexibility, the structures only represent a static snapshot and do not provide information about the dynamics of the complex. Molecular dynamics (MD) simulations based on the available structures can shed a light on this topic (Hitzenberger *et al.*, 2020). Several studies using different simulation approaches could show that the ectodomain of NCT is the most mobile subunit of the whole

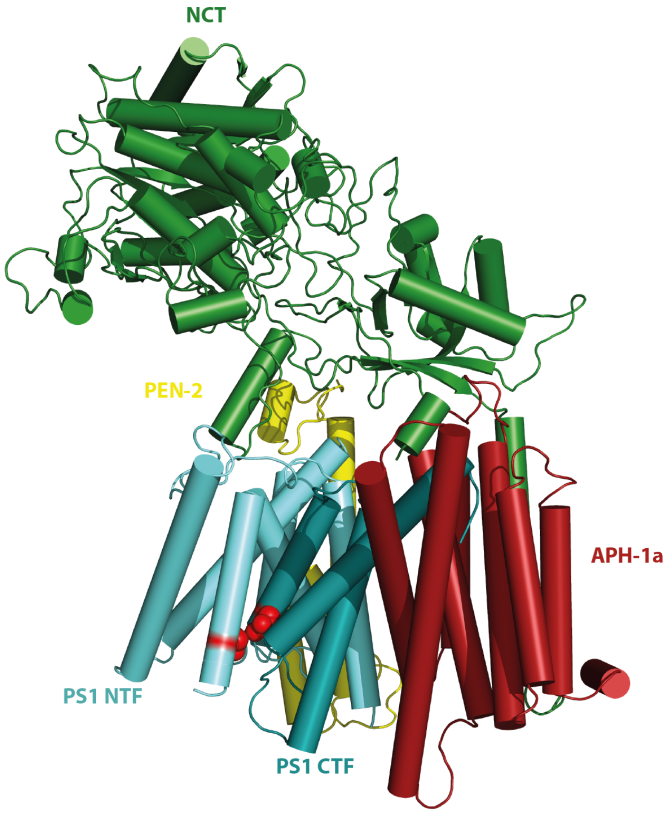

Figure 1.4.2: Structure of γ-secretase. Cartoon representation of γ-secretase cryo-EM strcuture (PDB 5FN3). NCT (green), PS1 NTF (cyan), PS1 CTF (darkcyan), APH-1a (red), PEN-2 (yellow), catalytic aspartates D257 and D385 (red spheres).

complex: it moves up and down relative to the PS1 TMDs, it rotates to the left and right and in itself it is composed of a small and large lobe which move independently from each other (Aguayo-Ortiz *et al.*, 2017; Lee *et al.*, 2017; Hitzenberger & Zacharias, 2019a). These movements and the different possible conformational states of NCT do not influence the conformation and dynamics of PS1. Simulations could further show that PS1 undergoes large TMD rearrangements when it shifts from an inactive to an active state, especially in TMDs1, 6, 7, 8 and 9 (Aguayo-Ortiz *et al.*, 2017; Hitzenberger & Zacharias, 2019a). The simulation studies can provide further interesting new hypothesise on the flexibility and structural arrangements of γ-secretase which can be tested in future structural and biochemical experiments (Hitzenberger *et al.*, 2020).

1.4.1.7 γ-Secretase interacting proteins

Even though it was shown that the four components of γ-secretase are necessary and sufficient for its activity (Edbauer *et al.*, 2003), more than 40 interacting proteins

have been identified that are able to influence the assembly, localization and/or activity of the complex (Escamilla-Ayala *et al.*, 2020). The role of these interacting proteins is still largely controversial. CD147 (or also called Basigin) – for example – is suggest to be a negative regulator of γ-secretase and its knockdown increases the production of Aβ (Zhou *et al.*, 2005). But the direct interaction between CD147 and γ-secretase could was not shown so far (Vetrivel *et al.*, 2008; Winkler *et al.*, 2009) and it is suggested that CD147 rather plays a role in the degradation of Aβ than in its production (Vetrivel *et al.*, 2008). In contrast, the γ-secretase-activating protein (GSAP) is a positive regulator of the complex and its knockdown results in a decreased Aβ production (He *et al.*, 2010). In another study this effect was not reproduced and the role of GSAP for the γ-secretase activity remains uncertain (Hussain *et al.*, 2013). Recently, a novel interactor was identified, the innate immunity protein IFITM3 (interferon-induced transmembrane protein 3) which directly binds to γ-secretase (Hur *et al.*, 2020). Upon an inflammatory stimulus, the expression of IFITM3 is increased and results into an increased activity of the protease.
Besides the interaction with modulating proteins, it was described that γ-secretase can also form a super-complex with either ADAM10 (Chen *et al.*, 2015) or BACE1 (Liu *et al.*, 2019). It is suggested, that ADAM10 or BACE1 are not directly interacting with the γ-secretase but that this interaction is rather mediated by tetraspanines. A ternary complex composed of all three secretase has been described in one study (Wang & Pei, 2018) but not seen in others (Chen *et al.*, 2015; Liu *et al.*, 2019). Since the experiments on these super-complexes were performed in a detergent environment, it is unclear whether they really exist in cells (Escamilla-Ayala *et al.*, 2020).

1.4.2 γ-Secretase substrates

Up to date, more than 140 substrates for γ-secretase have been identified (Güner & Lichtenthaler, 2020) but specific factors for the substrate selectivity are mainly elusive so far. Nevertheless, all the substrates have to fulfill two criteria to make them γ-secretase substrates (Güner & Lichtenthaler, 2020). First, the γ-secretase substrates all have a type I TMD orientation. Second, the ectodomains of these substrates have to be either naturally short or have to be shortened by the cleavage through sheddases, like ADAM10 or BACE1. γ-Secretase can tolerate substrates with a ectodomain shorter than 300 aa but efficient cleavage was observed for substrates with ectodomians shorter than 50 aa(Struhl & Adachi, 2000). Typically the length of substrate ectodomains is 10 to 30 aa (Güner & Lichtenthaler, 2020). Well known and studied substrates are for example members of the Notch (De Strooper

et al., 1999; Saxena *et al.*, 2001) and APP family (De Strooper *et al.*, 1998; Scheinfeld *et al.*, 2002), Trem2 (Triggering receptor expressed on myeloid cells-2, Wunderlich *et al.* (2013)), Neuregulin-1 (Bao *et al.*, 2003) or E- and N-cadherin (Marambaud *et al.*, 2002, 2003). There seems to be some putative substrates which do not fulfill the criteria of having a type I TMD orientation like neuregulin-1 type III (NRG1). It is a membrane protein with two TMDs. However, these TMDs first undergo shedding in their connecting loop resulting in two single pass TMDs. One of these TMDs is in type I orientation and subsequently a γ-secretase substrate (Fleck *et al.*, 2016). Recently, it was reported that γ-secretase is able to cleave the C-terminus of Frizzled2 (Fz2) in *Drosophila* which is a receptor composed of 7 TMDs (Restrepo *et al.*, 2022). Nevertheless, the exact mechanism of this cleavage and whether γ-secretase directly cleaves the polytopic membrane protein remains elusive.
The cleavage of the substrate by γ-secretease liberates an intracellular domain (ICD) from the respective substrate into the cytosol which is – in most of the cases – rather labile and rapidly degraded. Nevertheless, for some substrates like Notch1 (De Strooper *et al.*, 1999) or N-cadherin (Marambaud *et al.*, 2003) a transcriptional activity of these ICDs was shown. Furthermore, substrate cleavage can not only promote signalling but also terminate signalling like it is observed for a substrate called deleted in colorectal cancer (DCC, Parent *et al.* (2005); Jurisch-Yaksi *et al.* (2013)). All in all, the versatile set of γ-secretase substrates and their partition in diverse cellular pathways make γ-secretase a crucial protease in various physiological processes like synaptogenesis, cellular differentiation and immune response. Therefore, γ-secretase is also implicated to play important roles in several diseases like AD, cancer or cardiovascular disease (Jurisch-Yaksi *et al.*, 2013).

1.4.3 Substrate recognition

Within the last years, several studies gave new insights in the substrate recognition process by γ-secretase. Of note, most of the studies on substrate recognition were performed with the APP substrate. Despite the large and versatile set of substrates, the active site of γ-secretase plays an important role for substrate recognition. In addition to the above discussed GxGD motif in TMD7 of PS (see also 1.4.1.1), three binding pockets have been identified in the active site (Bolduc *et al.*, 2016b; Hitzenberger & Zacharias, 2019c), a small pocket flanked by two large pockets. The aa side chains of the substrate are able to accommodate within these pockets, whereas the small size of the middle pocket excludes mainly large aromatic aa side chains. Mutations of these substrate side chains resulted in a $A\beta_{42}/A\beta_{40}$ ratio shift (Bolduc *et al.*, 2016b).

The role of the γ-secretase subunit NCT in substrate recognition has been established by several studies. A study with the APP-derived, His-tagged recombinant substrate APP C100-His_6 (referred to as C99) has shown that specific residues in the N-terminal part of C99 directly interact with NCT (Fukumori & Steiner, 2016), especially C99 H6. Furthermore in another study it was shown that NCT functions as a sterical hindrance for large substrate ectodomains (Bolduc *et al.*, 2016a) which might explain why substrates need to be shedded (or have a naturally short ectodomain) before undergoing γ-secretase cleavage.

The afore mentioned study by Fukumori and Steiner was the first extensive study to elucidate the participation of the C99 aa in substrate recognition. By introducing 68 single aa substitutions to the photocrosslinkable unnatural aa *p*-benzoyl-L-phenylalanine (Bpa) it was possible to map which substrate aa is in contact with the enzyme and which subunit is interacting with the substrate (Fukumori & Steiner, 2016). C99-Bpa was mainly interacting with PS1 NTF (more than 40 residues of C99), most prominently residues at and around the cleavage sites (V44, T48 and L49). Some more prominent interactions were also found for residues at and around the cleavage sites with PS1 CTF (L51 and M52), indicating the important role of PS1 (and especially PS1 NTF) as substrate recognition site. Interestingly, also more distant residues in the extracellular part of the substrate were interacting with PS1 NTF as well, here most prominently C99 E3. In addition to the interaction with NCT, PS1 NTF and CTF, also some interactions with PEN-2 were found (most prominently C99 A30). Overall the interactions distant from the cleavage sites were less prominent, indicating the PS1 NTF, NCT and PEN-2 might provide exosites for initial substrate binding. This finding was supported by an accumulation of substrate at these sites when the active site of γ-secretase was blocked with the active site directed inhibitor L-685,458. Taken all these findings together, a stepwise substrate recognition was proposed in which the exosite(s) play(s) in concert with the active site: first the substrate is recognized at (an) exosite(s) at NCT and/or PEN-2; then handed over to (an) exosite(s) in PS1 NTF before it enters the active site of γ-secretase (Fukumori & Steiner, 2016).

Recent cryo-EM structural data on γ-secretase in complex with two of its substrates (Yang *et al.*, 2019; Zhou *et al.*, 2019) could confirm some of the biochemical data on substrate recognition. In these studies the Notch1-derived Notch100 substrate and the APP-derived APP C83 substrate were used and covalently bound with a disulfide bridge to the large PS1 extracellular loop 1 (between TMD1 and TMD2). The structures for both substrates were highly similar and differences mainly arose from the differences in the primary sequence of the substrate. In the following, the findings will be discussed based on C83 (Zhou *et al.*, 2019). The substrate is buried in a hydrophobic cavity composed of TMD2, TMD3, TMD5, TMD6 and

TMD7 of PS1 (figure 1.4.3A). The short N-terminal part protrudes into a cavity made of NCT, supporting its role in substrate recognition. At its C-terminus the α-helical TMD of the substrate unwinds at the initial cleavage sites between T48/L49 and L49/V50 followed by a newly formed, four aa long β-strand (M51-K54, β3). This β-strand is embedded in an antiparallel hybrid β-sheet composed two more

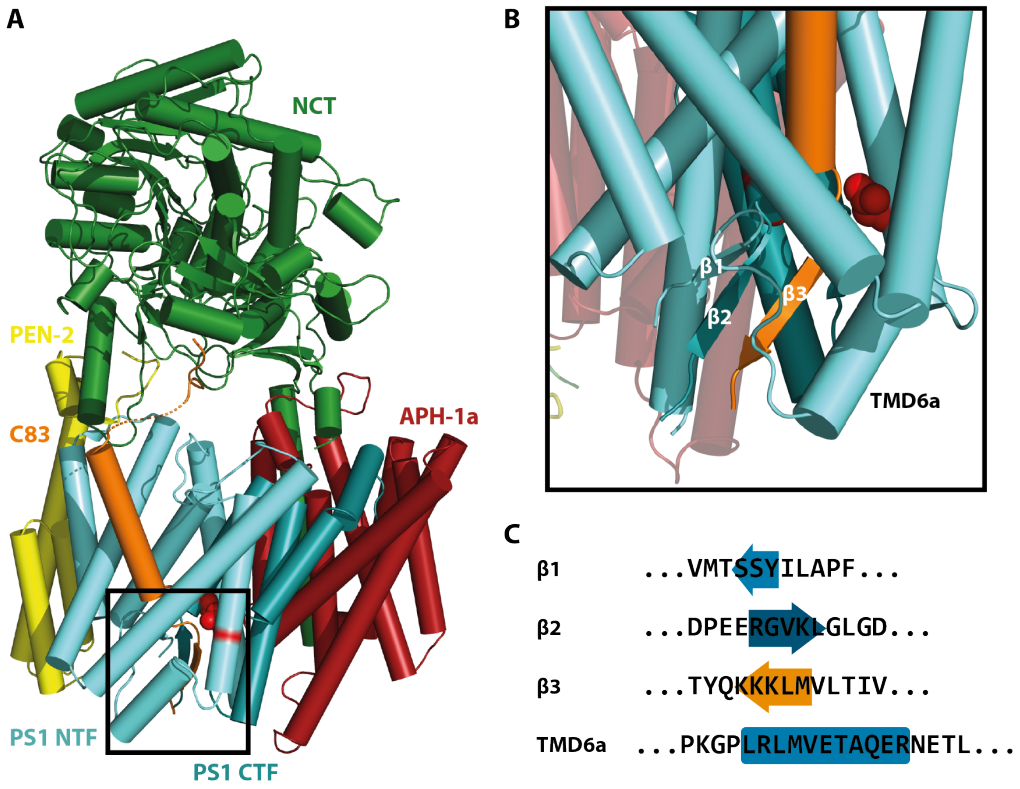

Figure 1.4.3: Structure of γ-secretase with APP C83. (A) Cartoon representation of the cryo-EM structure of γ-secretase in complex with APP C83 substrate (PDB 6IYC). NCT (green), PS1 NTF (cyan), PS1 CTF (darkcyan), APH-1a (red), PEN-2 (yellow), C83 (orange), catalytic aspartates D257 and D385 (red spheres). (B) Close up on the area around the active site (marked in (A)) with the unwound substrate and the newly formed hybrid β-sheet between PS1 and substrate as well as PS1 TMD6a. (C) Schematic representation of hybrid β-sheet and TMD6a including the respective sequences.

β-strands coming from PS1 NTF (Y288-S290, β1) and PS1 CTF (R377-L381, β2) (1.4.3B and C). Main-chain H-bond interactions between substrate and PS1 L432 (preceding the PAL motif) further stabilize the substrate positioning. Deletion of these newly identified substrate recognition motifs resulted in the complete abolishing of γ-secretase activity (Zhou *et al.*, 2019) pointing towards an essential role of these motifs. Furthermore, the C-terminus of TMD6 undergoes a conformational rearrangement resulting in the formation of a small additional helix called TMD6a (L267-R278) which also seems to be important for the correct positioning and unfolding of the substrate (Zhou *et al.*, 2019). In good agreement with the biochemical data (Fukumori & Steiner, 2016), V44 is in the structure directly interacting with W165 located in PS1 TMD3 and embedded in a groove between PS1 TMD2 and

3 comprised of aa residues M146, L150, W165 and S169 (Zhou *et al.*, 2019). It is important to keep in mind that both methods, the structural investigations as well as the biochemical cross-linking experiments have certain limitations. The introduction of the Bpa-mutation in the substrate might already induce a different substrate recognition compared to the wild-type substrate (Fukumori & Steiner, 2016). For the structural investigations, the covalent binding of the substrate to PS might have induced a non-natural enzyme-substrate interaction. In addition, γ-secretease activity was abolished by mutation of the catalytic aspartate D385 to alanine which might also influence the substrate binding at the active site (Yang *et al.*, 2019; Zhou *et al.*, 2019).

1.4.4 Cleavage mechanism

The cleavage mechanism of γ-secretase is a very interesting mechanism since it is not only performing an endopeptidase cleavage to liberate an ICD from its respective substrate but also shortens the remaining membrane bound stub in a sequential carboxypeptidase mechanism by 6 to 12 aa. So far, the detailed cleavage mechanism has only been reported for the APP CTFβ (and APP CTFα, Funamoto *et al.* (2020)) but it is likely that this mechanism is also found for other substrates like Notch1 (Okochi *et al.*, 2006; Ran *et al.*, 2017; Funamoto *et al.*, 2020).
In a first cleavage step, γ-secretase cleaves CTFβ after L49 and also to a smaller amount after T48. This cleavage step is called ε-cleavage and liberates two AICD species, AICD50 and AICD51 respectively, into the cytosol (Gu *et al.*, 2001; Sastre *et al.*, 2001; Yu *et al.*, 2001; Weidemann *et al.*, 2002). The membrane remnant fragments $A\beta_{49}$ and $A\beta_{48}$ are then further processed to $A\beta_{38}$ and $A\beta_{42}$ or $A\beta_{40}$, respectively (Takami *et al.*, 2009; Matsumura *et al.*, 2014). Thereby, γ-secretase cleaves in a stepwise manner, mainly liberating tri-peptides from the substrate. $A\beta_{49}$ is further processed to $A\beta_{46}$ (ζ-cleavage), followed by $A\beta_{43}$ and resulting in $A\beta_{40}$ (γ-cleavage). In small amounts $A\beta_{40}$ is further cleaved to $A\beta_{37}$ (Zhao *et al.*, 2004; Qi-Takahara *et al.*, 2005; Zhao *et al.*, 2005; Yagishita *et al.*, 2006). Similar, $A\beta_{48}$ is first processed to $A\beta_{45}$ and then to $A\beta_{42}$ (Yagishita *et al.*, 2006). The release of the tetrapeptide VVIA from $A\beta_{42}$ results into $A\beta_{38}$. $A\beta_{38}$ can also be produced by the liberation of the pentapeptide VVIAT from $A\beta_{43}$ (Takami *et al.*, 2009). The liberation of VVIA and VVIAT resulting in $A\beta_{38}$ is thereby equally important in cells (Okochi *et al.*, 2013). The production of Aβ species is therefore possible by two product lines, the $A\beta_{40}$ product line starting with $A\beta_{49}$ and the $A\beta_{42}$ product line starting with $A\beta_{48}$. Aβ is mainly produced by the $A\beta_{40}$ product, with $A\beta_{40}$ accounting for 80-90% off all secreted Aβ species. Further studies could show that –

depending on the condition – not only tri- and tetrapeptides from these two product lines are released but γ-secretase is also able to release other tri-, tetra-, penta- and even hexapeptides (Matsumura *et al.*, 2014; Olsson *et al.*, 2014). These cleavage events result in additional Aβ-species and additional switches between the product lines. The released peptides - also called γ-byproducts - are not secreted and might serve as another marker for γ-secretase activity than Aβ secretion (Funamoto *et al.*, 2020). Similarly, for the endoporteolysis of PS also a step-wise cleavage in a three amino acid spacing was observed but no direct measurement of tripeptide release was performed (Fukumori *et al.*, 2010).

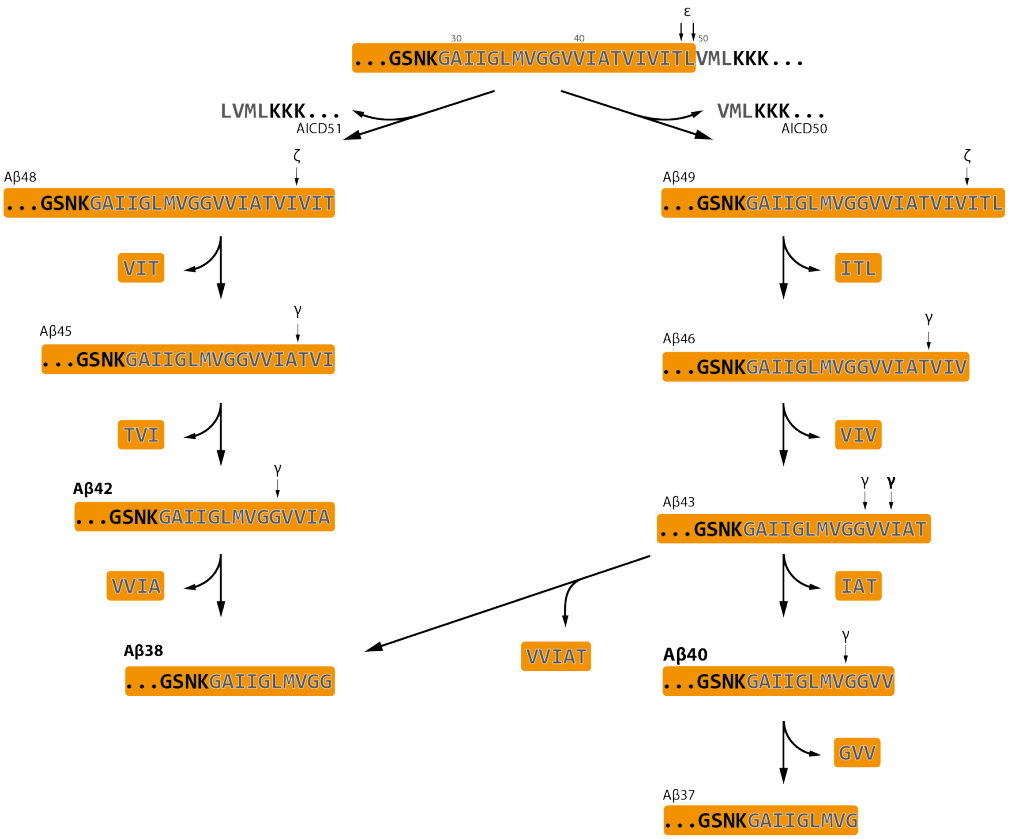

Figure 1.4.4: Schematic representation of the Aβ product lines. In the $Aβ_{40}$ product line (right side), $Aβ_{49}$ is cleaved to $Aβ_{46}$, then to $Aβ_{43}$ resulting in $Aβ_{40}$ and to minor amount further cleaved into $Aβ_{37}$. In the $Aβ_{42}$ product line (left side), $Aβ_{48}$ is cleaved to $Aβ_{45}$, then to $Aβ_{42}$ and further to $Aβ_{38}$. Some $Aβ_{38}$ is also directly produced from $Aβ_{43}$.

A recent study (Bhattarai *et al.*, 2022) could show by MD simulations that the ξ-cleavage from $Aβ_{49}$ to $Aβ_{46}$ requires conformational rearrangements in the γ-secretase–substrate complexes including the downward movement of L49 by roughly 5 Å and the unwinding of the substrate helix from T43 to I45. These structural rearrangements are only possible if the N-terminal positively charged AICD remained bound to the γ-secretase (Bhattarai *et al.*, 2022). An experimental validation of these findings is still missing.

One of the determinants in regulating the processive cleavage of APP is the N-terminal TMD anchoring aa lysine (K28, Aβ-numbering). Several mutational studies (Ren *et al.*, 2007; Page *et al.*, 2010; Kukar *et al.*, 2011; Ousson *et al.*, 2013; Jung *et al.*, 2014; Petit *et al.*, 2019) confirmed the important role of this residue in APP cleavage and especially APP processing. Replacing the charged aa lysine by the uncharged aa alanine (K28A) resulted in a strongly increased processivity and the production of (very) short Aβ species like $A\beta_{33}$, $A\beta_{34}$ and even shorter $A\beta_{27}$ (Kukar *et al.*, 2011; Jung *et al.*, 2014). Aβ species longer than $A\beta_{34}$ have not been reported for this mutation so far. The K28A mutation does not only influence the processivity but also shifts the ε-cleavage site preference towards cleavage at ε49 releasing AICD50 (Kukar *et al.*, 2011). Another mutation which increases the processivity is the replacement of lysine by the negatively charged glutamate (K28E, Page *et al.* (2010); Ousson *et al.* (2013); Jung *et al.* (2014); Petit *et al.* (2019)). This mutation results in Aβ species between $A\beta_{32}$ and $A\beta_{40}$ with $A\beta_{37}$ being the main species generated (Page *et al.*, 2010; Ousson *et al.*, 2013; Jung *et al.*, 2014). In contrast to K28A, K28E did not change the specificity for the ε-cleavage site (Jung *et al.*, 2014).
More recent biochemical (Petit *et al.*, 2019) and MD simualtion studies (Hitzenberger & Zacharias, 2019b) could shed more light on the role of K28 in the APP processing. On the one hand K28 seems to be not only a membrane anchor for the TMD but also anchors the substrate to NCT by direct interaction with NCT I214 (Petit *et al.*, 2019) and might therefore stabilize the enzyme-substrate interaction. On the other hand, K28 needs to slide vertically through the lipid bilayer during the processive cleavage (Hitzenberger & Zacharias, 2019b). Thereby, the charged lysine is pulled into the hydrophobic membrane environment which is energetically unfavoured and therefore only possible until a certain point. The energetical barrier becomes too high when $A\beta_{43}$ is becoming substrate for γ-secretase and this might explain why the APP processing mainly stops at $A\beta_{40}$ (Hitzenberger & Zacharias, 2019b).

1.4.5 Pharmacological treatment of γ-secretase

Since γ-secretase is involved in the onset/progression of AD it is a valuable target for pharmacological treatment of this disease and therefore, several attempts were made to design molecules that either inhibit or modulate γ-secretase (Nie *et al.*, 2020).

1.4.5.1 γ-Secretase inhibitors (GSIs)

γ-Secretase inhibitors (GSIs) were the first class of molecules that were designed to specifically target the protease (Golde *et al.*, 2013). These GSIs can be in principle divided in two classes, the transition state analogues (TSAs) and the non-transition state analogues (non-TSAs). The inhibitors L-685,458 (also termed Merck A, Shearman *et al.* (2000)) and III-31C (Esler *et al.*, 2002) belong to the class of TSAs (figure 1.4.5A and B). L-685,458 contains an hydroxyethylene dipeptide isostere which is the functional transition state mimic and the inhibitor shows a high potency to inhibit the cleavage of APP by γ-secretase (Shearman *et al.*, 2000). III-31C is a hydroxyethylurea peptidomimetic (Esler *et al.*, 2002) and also very potent in inhibition of γ-secretase cleavage (Kornilova *et al.*, 2003). Chemical derivatives of these TSAs were used to study the biochemistry of γ-secretease. A biotinylated version of L-685,458 (Merck C, L-685,458-bt, Beher *et al.* (2003), figure 1.4.5C) is able to precipitate active γ-secretase and precipitation experiments could show that only a small portion of γ-secretase complexes in cells is in an active conformation. Furthermore, photoaffinity labeling experiments with TSAs specifically labeled PS NTF and CTF (Esler *et al.*, 2000; Kimberly *et al.*, 2000; Li *et al.*, 2000) confirming that PS is the catalytic subunit of γ-secretase. Interestingly, several studies with TSAs could further show that the substrate is still able to bind to γ-secretase when a TSA is bound indicating additional substrate binding/docking sites that are spatially separated from the active site (Esler *et al.*, 2002; Beher *et al.*, 2003; Kornilova *et al.*, 2003; Berezovska *et al.*, 2003; Ramdya *et al.*, 2003; Kornilova *et al.*, 2005).

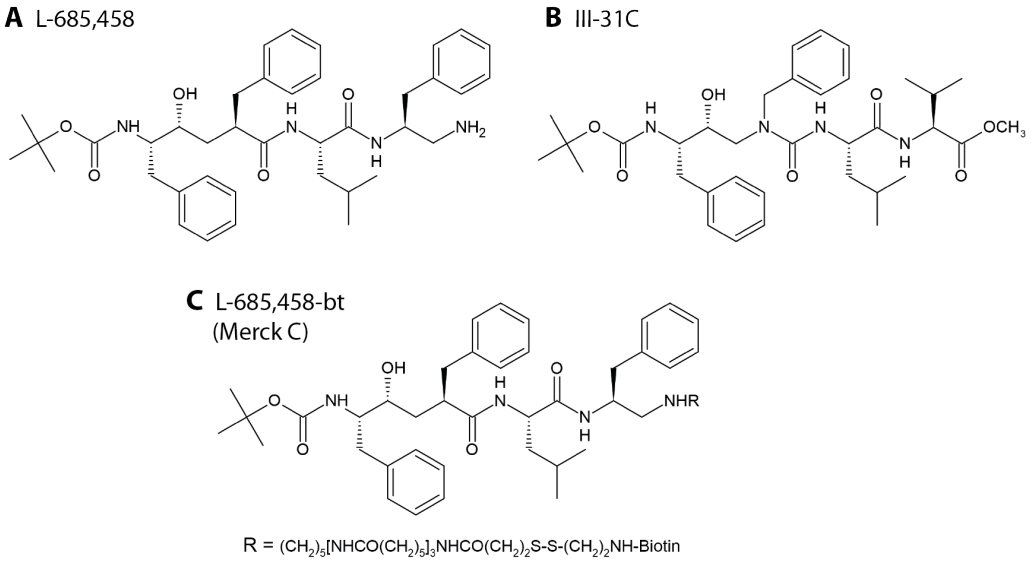

Figure 1.4.5: Chemical structures of TSA GSIs. (A) L-685,458 (Merck A). (B) III-31C. (C) L-685,456-biotin (Merck C).

Another class of GSIs that was developed to potently and specifically inhibit γ-secretase are the non-TSAs. DAPT (Dovey *et al.*, 2001), LY411575 (Lanz *et al.*, 2004), Begacestat (Mayer *et al.*, 2008), MRK-560 (Best *et al.*, 2006), Semagacestat (Henley *et al.*, 2009) and Avagacestat (Gillman *et al.*, 2010) belong to this class of GSIs (figure 1.4.6 A-F). These inhibitors belong to different chemical classes. DAPT for example is a dipeptidic GSI (Dovey *et al.*, 2001) and Semagacestat and LY411575 arebenzazepine-derivatives as further developments of these dipeptidic GSIs (Henley *et al.*, 2009; Lanz *et al.*, 2004). Begacestat and Avagacestat belong

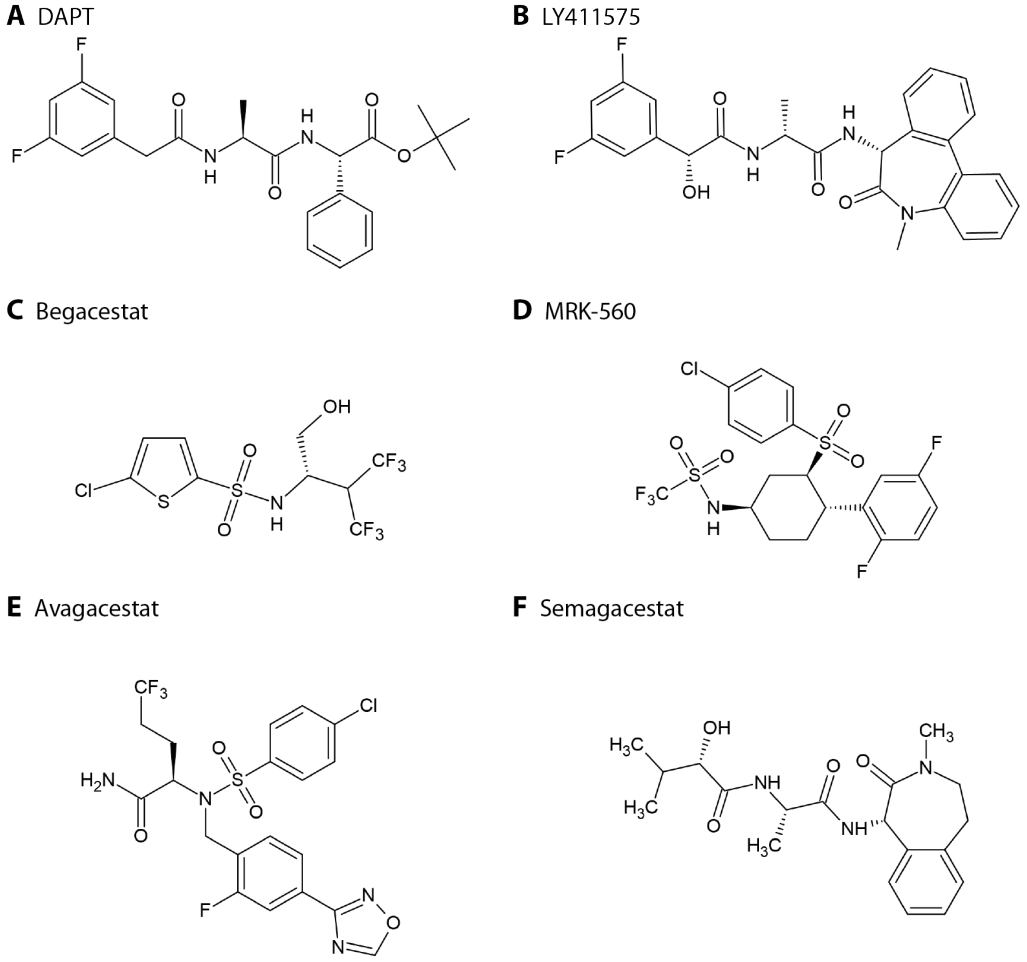

Figure 1.4.6: Chemical structures of non-TSA GSIs. (A) DAPT. (B) LY411575. (C) Begacestat. (D) MRK-560. (E) Avagacestat. (F) Semagacetat.

to the class of sulfonamides and were designed as so-called "Notch-sparing" GSIs (Mayer *et al.*, 2008; Gillman *et al.*, 2010). These GSIs were designed to specifically inhibit the cleavage of APP by γ-secretase but not the cleavage of Notch. The reason for the development of the Notch-sparing GSIs were side effects observed in clinical studies with other GSIs. In a phase III trial with Semagacestat, inhibitor-treated patients cognitively declined faster than patients that received a placebo control. Furthermore, the risk for developing severe skin cancer was increased in patients administered with Semagacestat. This finally led to the termination of the

clinical trial (Doody *et al.*, 2013). One of the reasons for the observed side effects might be the APP-unspecific inhibition of γ-secretase by Semagacestat, especially the inhibition of Notch cleavage but possibly also of other γ-secretase substrates. Nevertheless, whether the Notch-sparing GSIs are truly Notch-sparing and could prevent from these side effects is still under debate (Chávez-Gutiérrez *et al.*, 2012; Crump *et al.*, 2012). Recently, also another mechanism was suggested for the side effects observed for non-TSA GSIs. Contradictory to what would be expected, the treatment of cells with non-TSA GSIs resulted in an increased intracellular accumulation of γ-byproducts and in the same line also of longer Aβ-species, like $A\beta_{45}$ or $A\beta_{46}$ (Tagami *et al.*, 2017). These byproducts as well as the longer Aβ species might contribute to the side effects. Therefore, non-TSAs like Semagacestat might be not true GSIs but pseudo-GSIs. Due to their Notch inhibitory effects, some GSIs are currently repurposed for the treatment of several Notch-dependent cancer types (Golde *et al.*, 2013; Habets *et al.*, 2019; Ghanbari-Movahed *et al.*, 2021).
Recent structural investigations by cryo-EM could reveal how L-685,458 and Semagacestat as well as Avagacestat are bound to γ-secretase (Yang *et al.*, 2021). Interestingly, all three inhibitors occupy the position of the β-strand of the γ-secretase substrate (figure 1.4.7). As expected from its chemistry, TSA L-685,458 protrudes into a cleft above the catalytic aspartates and the transition state mimic is placed between the two catalytic aspartates (figure 1.4.7A). Both L-685,458 and the non-

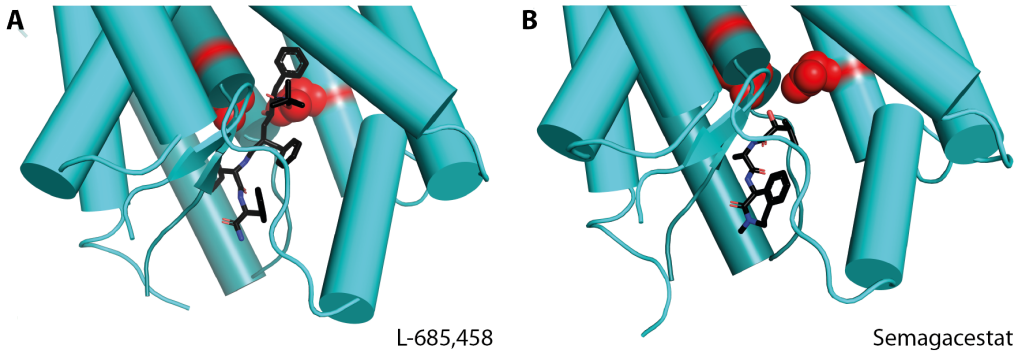

Figure 1.4.7: Structure of γ-secretase with bound GSIs. Close up into active site of γ-secretase with (A) bound L-685,458 (black, PDB 7C9I) and (B) bound Semagacestat (black, PDB 6LR4). Only PS (cyan) and the bound GSIs are shown, red spheres show the side chains of the catalytic aspartates.

TSA GSIs occupy the space of the β3-strand from the substrate but the non-TSAs form fewer interactions with the protease than L-685,458 (Yang *et al.*, 2021). The structure might help to explain why non-TSAs might be pseudo-GSIs. It might be possible that due to the fewer interactions with the protease, non-TSA GSIs might not completely out-compete the substrate from the enzyme compared to TSA GSIs. Therefore it might be possible that non-TSA GSIs are only able to bind to γ-secretase after the first cleavage steps of γ-secretase resulting in the generation of

the first γ-byproducts and longer Aβ species.

1.4.5.2 γ-secretase modulators (GSMs)

To overcome the issues resulting from the inhibition of γ-secretase another therapeutic approach came into focus: the modulation of γ-secretase activity by GSMs (Golde *et al.*, 2013). Even though the detailed mechanism how GSMs act on γ-secretase is not well understood, it is clear that these compounds are able to shift the production of Aβ species towards shorter species without affecting the actual cleavage of substrates. GSMs act thereby after the ε-cleavage but do not change the efficiency as well as the position of this cleavage (Ebke *et al.*, 2011; Chávez-Gutiérrez *et al.*, 2012; Dimitrov *et al.*, 2013). Like this, important cleavage products, like NICD, are still released and can fulfill their (signaling) functions (Crump *et al.*, 2013). The modulators promote the cleavage from from $A\beta_{42}$ or $A\beta_{43}$ to shorter species by by stabilizing the substrate–protease interaction resulting in an increased residence time of the substrate during the cleavage process (Chávez-Gutiérrez *et al.*, 2012; Okochi *et al.*, 2013; Szaruga *et al.*, 2017).
The first molecules discovered to modulate γ-secretase were the non-steroidal anti-inflammatory agents (NSAIDs) like ibuprofen, indomethacin or sulindac sulfide (Oehlrich *et al.*, 2011) which have an acidic group that is important for the modulatory effect of these molecules (Weggen *et al.*, 2001; Zall *et al.*, 2011). Structurally related molecules lacking this acidic group increased the level of $A\beta_{42}$ and were referred to as inverse GSMs (iGSMs) (Kukar *et al.*, 2005). The discovery of molecules that are able to modulate γ-secretase led to further developments of GSMs. Thereby one can discriminate between two main developments lines: the further development of the acidic GSMs and the search for NSAID-independent GSMs (Luo & Li, 2022). The second generation of acidic GSMs improved the potency of modulation, the pharamacokinetics and the brain penetrance. One example for these GSMs is GSM-1, an acidic piperidine developed by Merck (Page *et al.*, 2008). The search for NSAID-independent GSMs resulted in one basic chemical scaffold: the heterocyclic GSMs. These GSMs are typically composed of four connected (hetero)aromatic rings from which the central ring system is normally in a planar conformation (Mekala *et al.*, 2020). Interestingly, these new class of GSMs does not only act on $A\beta_{42}$ but also reduce $A\beta_{40}$ and increase $A\beta_{37}$ (Mekala *et al.*, 2020; Luo & Li, 2022).

1.5 PSH - a model protease for γ-secretase?

The presenilin/SPP homolog PSH, also termed MCMJR1 (Torres-Arancivia *et al.*, 2010) or mIAP (Naing *et al.*, 2018), is an aspartyl intramembrane protease which was identified in the archeaon *Methanoculleus marisnigri* JR1 (Torres-Arancivia *et al.*, 2010). Sequence analysis and alignment revealed that it is a multipass transmembrane protein which shares the well conserved GxGD and YD motifs with other aspartyl intramembrane proteases like PS and SPP.

1.5.1 Structure and topology of PSH

The bioinformatic analysis of the PSH sequence suggested that it is composed of 8 TMDs with the catalytic aspartates D162 and D210 located in TMD5 and 6 (Torres-Arancivia *et al.*, 2010). Subsequent structural studies on PSH could then reveal that PSH is composed of 9 TMDs and that the catalytic aspartates are located in TMD6 and 7 (figure 1.5.1) (Li *et al.*, 2013), as it is known also from PS and SPPs. Since all studies carried out so far were performed with overexpressed and solubilized PSH in non-natural environments, it still remains elusive how PSH is orientated in the membrane of *M. marisnigri*. Since PSH is able to cleave type I TMD proteins *in vitro* it might have the same orientation than PS. PSH adopts a protein fold – the so called presenilin fold: TMD1 to 6 form a horseshoe-shaped structure which is surrounding TMD7 to 9. The side chains of the two catalytic aspartates in TMD6

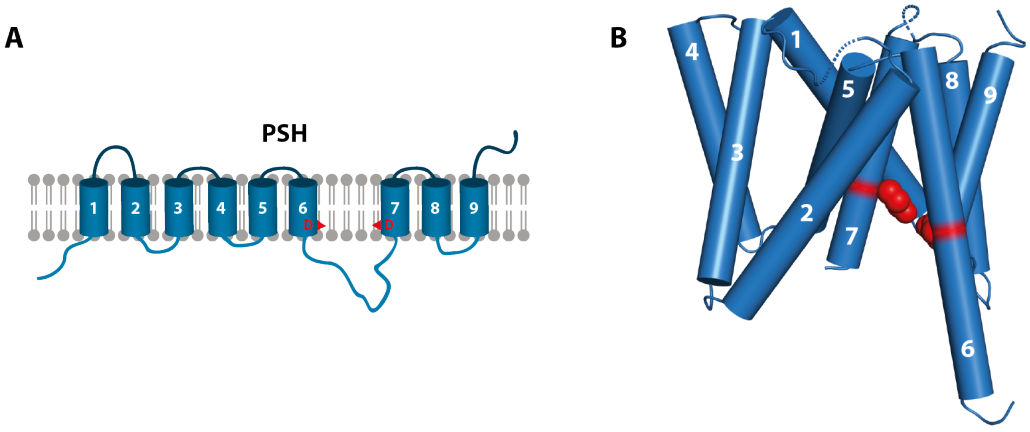

Figure 1.5.1: Topology and structure of PSH. (A) Topological representation of PSH with its 9 TMDs. The catalytic aspartates in TMD6 and 7 are indicated with red arrow heads. (B) Crystal structure of PSH (PDB 4HYG). The red spheres show the side chains of the catalytic aspartates D162 and D210.

and 7 are separated by 6.7 Å which most likely reflects an inactive state of the protease (Li *et al.*, 2013). It might be possible that upon substrate binding, PSH

adopts another conformation which is more favorable for cleavage. In contrast to PS and SPP, no clear PAL motif was identified for PSH. Based on sequence alignment, the sequence PPL (aa 276-278) located in TMD9 is suggested to be the PAL motif; but experimental proof for this hypothesis is missing (Torres-Arancivia *et al.*, 2010). Furthermore, there is no evidence that PSH undergoes endoproteolysis as PS. As a result of the experimental procedure in which PSH was treated with V8 protease to remove the loop between TMD6 and 7 for crystallization purposes, PSH is shown as an NTF and a CTF in the crystal structure (Li *et al.*, 2013) but whether this has any functional consequences for PSH is not clear.

1.5.2 Cleavage mechanism of PSH

Several studies could show that PSH is indeed a fully functional aspartyl intramembrane proteases which is able to cleave type I transmembrane proteins (Torres-Arancivia *et al.*, 2010; Dang *et al.*, 2015; Naing *et al.*, 2015) within their respective TMD. This cleavage seems also to be independent of any accessory protein as it is known for PS. The mutation of the two putative catalytic aspartates to alanines abolished the cleavage (Torres-Arancivia *et al.*, 2010; Li *et al.*, 2013) proving that D162 and D220 are indeed the catalytic residues. Interestingly, PSH is able to cleave APP-based substrates (Li *et al.*, 2013; Dang *et al.*, 2015) resulting in the release of AICD and different Aβ species, indicating that the cleavage mechanism of PSH is similar to γ-secretase's cleavage mechanism and might also include processive trimming of the substrate's TMD. This is further supported by the observation that TSA GSIs are able to abolish the cleavage (Torres-Arancivia *et al.*, 2010; Dang *et al.*, 2015; Naing *et al.*, 2015) and the observation that GSMs are able to modulate PSH (Dang *et al.*, 2015) even though rather high concentrations of the GSM are needed for PSH modulation. Of note, the several studies on PSH cleavage used different model substrates and different experimental conditions which makes it difficult to compare them and to draw clear conclusions on the cleavage mechanism. In addition, so far no natural PSH substrate from *M. marisnigri* is known. It might be possible that natural substrates of PSH undergo a different cleavage mechanism.
As already reported for other intramembrane proteases, PSH is also a slow enzyme with a low k_{cat} rate (Naing *et al.*, 2015, 2018). Nevertheless, a direct comparison with the catalytic rates of γ-secretase is difficult, especially since different substrates were used for the various studies. The PSH studies used either a Renin-based FRET-substrate (Naing *et al.*, 2015) or an APP-TMD FRET-subtrate (Naing *et al.*, 2018) whereas for γ-secretase APP C99 was used as substrate (Kamp *et al.*, 2015).
Since so far no studies with PSH were performed in its natural context or with a

natural substrate the exact function of PSH and its role within *M. marisnigri* are completely unclear. Based on our knowledge about other intramembrane proteases one can deduce that PSH might also fulfill signalling functions. Despite its ability to cleave type I transmembrane proteins one study also showed that PSH – *in vitro* – has also a cation channel activity which is linked to its protease activity (Kuo *et al.*, 2015) which might extend its function in the archeaon.

1.6 Objectives of study

The aim of this study is to increase the understanding of how the activity of IMPs is modulated by their environment and to elucidate how structural elements of the enzyme–substrate complex influence the cleavage by IMPs.
The first part of this study investigates how the lipid environment influences the activity of the archaeal IMP PSH. It is known that the lipid environment influences the activity if IMPs (Urban & Wolfe, 2005; Osenkowski *et al.*, 2008; Holmes *et al.*, 2012; Moin & Urban, 2012; Winkler *et al.*, 2012) but little is known on the mechanism underlying these lipid-dependent modulatory effects. Therefore, this study will not only analyze how a lipid bilayer compared to a detergent micelle will influence the activity of PSH but also the structural dynamics and the active site geometry. Since γ-secretease is not active in a detergent environment without the addition of lipids (Fraering *et al.*, 2004; Wrigley *et al.*, 2005; Zhou *et al.*, 2010), this study is restricted to PSH.
The second part will investigate how the hybrid β-sheet and the TMD6a of the enzyme–substrate complexes influence the activity of the respective enzymes. This will be analyzed for PSH as well as γ-secretase. For the γ-secretase previous studies already showed that the hybrid β-sheet is important for its activity (Yang *et al.*, 2019; Zhou *et al.*, 2019) but more detailed analysis are missing. This study investigates how mutations and deletions within the hybrid β-sheet of PSH and γ-secretase influence the enzymes' activity and processive cleavage mechanism. Furthermore, mutational analyzes on PSH TMD6a will reveal the role of this structural element in PSH activity.

2 Materials & Methods

2.1 Materials

2.1.1 Devices and consumables

All devices and consumables used in this study are listed with their respective manufacturer in the following table.

Instrumentation or consumable	Manufacturer
4800 MALDI TOF/TOF Analyzer	Applied Biosystems
96 well plate (96 Maxisorb)	Thermo Scientific
Aβ Peptide Panel 1 Kit	Meso Scale Discovery (MSD)
Blotting paper (MN 218 B)	Macherey-Nagel
Cell culture dish (12 wells, single dish 10 cm diameter)	Thermo Scientific
Cell scraper	Costar
Centrifuges and rotors	
Mini centrifuge (Mini Star Silverline)	VWR International
Ultracentrifuge (Optima MAX-XP), rotor TLA-55	Beckman
Ultracentrifuge (L7-55), rotor Ti 70	Beckman
Tabletop centrifuge for Eppendorf tubes	Eppendorf
Tabletop centrifuge with cooling (PerfectSpin 24R Refrigated centrifuge)	PQELAB
Cooling centrifuge (Megafuge 40R)	Thermo Scientific
Large cooling centrifuge (Avanti J-20XP)	Beckman
Rotors JA10 and JA25.50	Beckman
Centrifugation tubes (for 70 Ti, 30 ml)	Beckman
CO_2 incubator	Heraeus, Kendro
Combitips advanced	Eppendorf
Cuvettes (disposable)	Sarstedt
Developing solutions	
Developer G153 A & B	Agfa

Rapid fixer G354	Agfa
Eppendorf Multipette 4780	Eppendorf
Eppendorf tubes (0.2 ml, 0.5 ml, 1.5 ml, 2 ml)	Eppendorf
Eppendorf tubes for ultracentrifugation (1.5 ml)	Beckman
Falcon tubes (15 ml, 50 ml)	Sarstedt
Film developer(CP1000)	Agfa
Films (Super RX)	Fuji
Fluoroscan Asket FI	Labsystems
Freezer -20 °C	Elektrolux, Liebherr
Freezer -80 °C	Heraeus
Fridge 4 °C	Elektrolux, Siemens
Gas burner	W_LD Tec
Gel electrophoresis chamber (Mighty small II Hoefer)	Hoefer
Gel electrophoresis chamber (Mini PROTEAN 3)	Bio-Rad
Gel electrophoresis chamber X Cell Sure Lock mini	Invitrogen
Gel casting apparatus	Bio-Rad, Hoefer
Glass bottles, flasks and cylinders	VWR International
Hamilton glass pipette	Hamilton
Heating blocks (37, 42, 65, 96 °C)	Liebisch
Incubators 37 and 56 °C	Heraeus, Kendro
Inoculation loop	Sarstedt
Isopropanol boxes (Nalgene Mr. Frosty Cryo 1 °C)	Thermo Scientific
Magnet stirrer	IKA Labortechnik
Membranes	
Nitrocellulose membrane 0.45 and 0.2 µm (Protran)	GE Healthcare
PVDF membrane (Immobilion-P)	Millipore
Microwave	Sharp
Microscope	Helmut Hund GmbH
Multichannel pipette	Eppendorf
N_2 tank (Chronos)	Messer Griesheim
Nanodrop (NanoPhotometer)	Implen
Needles (Sterican 21 and 27 G)	B. Braun
NucleoBond Xtra Midi kit	Macherey-Nagel
NucleoSpin Plasmid, mini kit for plasmid DNA	Macherey-Nagel
Parafilm	Bemis
Pasteur pipettes	Sarstedt

PCR machines (Mastercycler Nexus)	Eppendorf
pH Electrode (InLab Expert Pro)	Mettler Toledo
pH Meter (FiveEasy™ FE20)	Mettler Toledo
Photometer	
for cuvettes: SmartSpec™Plus	Bio-Rad
for 96 well plates	BioTek
Pipettes (P2, P10, P20, P100, P200, P1000)	Gilson
Pipettes with filters, steril	Sarstedt
(2 ml, 5 ml, 10 ml, 25 ml)	
Pipette tips (for Gilson pipettes)	Sarstedt
Pipette boy (Accu-Jet)	Brand
Power pack (power pac 300)	Bio-Rad
Power pack (EPS 3501 XC, EPS 1001) for Hoefer systems	GE Healthcare
Quantifier (LAS-4000, ImageQuant 800)	Fuji/Amersham
rapifleX MALDI Tissuetyper	Bruker
Rotator (Rotator Genie™)	Scientific Industries
Scales	
analytical (0.0001 - 200 g)	Sartorius
standard (0.001 - 200 g)	Sartorius
Scalpel	B. Braun
Scanner	Epson
Shaking incubator (Multitron)	Infors HT
Shaker (KS-2)	Edmund Bühler GmbH
Sonifier (W-250D) with large and small tip	Branson
Syringes (1 ml, 5 ml)	B. Braun
Thermoshaker (ThermoMixer C)	Eppendorf
UV lamp (8 W, 230 V, 50 Hz, 0.16 Amps)	UVP
Vortexer (Vortex Genie 2)	Scientic Industries
Water deionization (Milli-Q)	Millipore

2.1.2 Reagents

If not otherwise stated chemicals and reagents had the purity level p.a. (*pro analysis*).

Reagent	Manufacturer
Acetic acid	Merck
Acetonitrile (HPLC grade)	Roth
Acryl-/bisacrylamide solution 19:1 (40%)	Bio-Rad
Acryl-/bisacrylamide solution 37.5:1 (40%)	Serva
Ampicillin sodium salt	Roth
Ammonium peroxodisulfate (APS)	Roth
Bacto agar	BD
Bacto trypton	BD
Bacto yeast extract	BD
Begacestat	F. Hoffmann- La Roche Ltd.
Bicine, 2-(Bis(2-hydroxyethyl)amino)acetic acid	Sigma
Bisacrylamide, N,N'-Methylenebisacrylamide	Serva
Bis-tris methane, 2-[Bis(2-hydroxyethyl)amino]- 2-(hydroxymethyl)propane-1,3-diol	Sigma
Bromophenol blue	Fluka
Bovine serum albumin (BSA)	Sigma
$CaCl_2$	Merck
Calbiosorb adsorbent beads	Calbiochem
CHAPSO, 3-[(3-Cholamidopropyl)dimethyl- ammonio]-1-propanesulfonate	Biomol
Chloramphenicol	Sigma
Citric acid monohydrate	Merck
α-Cyano-4-hydroxycinnamic acid	Sigma
DAPT	Boehringer-Ingelheim
DDM, *n*-Dodecyl-β-D-maltopyranoside	Calbiochem
Dimethyl sulfoxide (DMSO)	Sigma
Dithiothreitol (DTT)	Biomol
DMEM GlutaMAX™-I (Dulbecco's modified Eagle's medium)	Gibco
ECL immunoblot detection kit	GE Healthcare
Ethylenediaminetetraacetic acid (EDTA)	Sigma

Ethanol (80%)	Merck
Fetal bovine serum (FBS)	Sigma
G418 (Geniticin)	Invitrogen
Glycerine	Roth
Glycine	Applichem
I-Block	Tropix
Hydrochloric acid	Sigma
III-31C	Sigma
Imidazole	Sigma
Isopropyl β-D-1-thiogalactopyranoside (IPTG)	Roth
KCl	Merck
KH_2PO_4	Merck
L-685,458 (Inhibitor X, MerckA)	Merck
Lipofectamine 2000	Invitrogen
LY-411,575	F. Hoffmann-La Roche Ltd.
β-Mercaptoethanol	Roth
Merck C (L-685,458-biotin)	TAROS
$MgCl_2$	Merck
MRK-560	F. Hoffmann-La Roche Ltd.
NaCl	Roth
$Na_2HPO_4 \times 2H_2O$	Merck
NaOH	Roth
4-16% Novex NativePAGE	Invitrogen
Ni-NTA Agarose	Qiagen
Octyl-β-D-glucopyranoside	Sigma
Opti-MEM Reduced Serum Media	Gibco
Penicillin/Streptomycin (Pen/Strep)	PAA
L-α-Phosphatidylcholine, Typ XVI-E	Sigma
PIPES, piperazine-N,N'-bis(2-ethanesulfonic acid)	Sigma
Ponceau S	Sigma
2-Propanol (Isopropanol)	Merck
Protease inhibitor cOmplete	Roche
Protease inhibitor cOmplete, EDTA-free	Roche
Protein A Sepharose	GE Healthcare
Protein G Sepharose	GE Healthcare
Puromycin	Invitrogen
Rhodamine-DHPE	Invitrogen

Sodium azide	Merck
Sodium dodecyl sulfate (SDS)	Serva
SeeBlue Plus2 Pre-stained Protein Standard	Invitrogen
Sephacryl S-200 HR	Pharmacia
Tri-sodium citrate dihydrate	Sigma
Streptavidin Sepharose	GE Healthcare
Sulphuric acid	Honeywell
TEMED, N,N,N',N'-Tetramethylethane-1,2-diamine	Roth
Tetracycline hydrochloride	Sigma
Tricin, N-(Tri(hydroxymethyl)methyl)glycine	Biomol
Trifluoroacetic acid (TFA, HPLC grade)	Sigma
Tris, Tris(hydroxymethyl)aminomethane	Applichem
10-20% Tris-Tricine-Gels	Invitrogen
Triton X-100	Merck
Trypsin/EDTA	Invitrogen
Tween-20 (Polysorbate 20)	Merck
Urea	Serva
Urea BioUltra	Sigma
Zeocin	Invitrogen

2.1.3 Antibodies

All antibodies used in this studies are listed in the following table. All mouse and rat primary antibodies are monoclonal antibodies, all rabbit primary antibodies are polyclonal antibodies unless otherwise stated.

antibody	epitope	species	IB	IP	source
6F4	PSH aa 192-204	rat	3 µg/ml	-	Feilen *et al.* (2022)
2D8	Aβ aa 1-16	rat	3 µg/ml	-	Shirotani *et al.* (2007)
4G8	Aβ aa 17-24	mouse	-	4 µg/ml	BioLegend (800702)
Aβ22-35	Aβ aa 22-35	rabbit	1:1000	-	Sigma (A3356)
22C11	APP aa 66-81	mouse	1:5000	3 µg/ml	Merck (MAB348)
Y188[1,2]	APP-CTF	rabbit	1:5000	-	Abcam (ab32136)
6687	APP695 aa 675-695	rabbit	-	1:3000	Steiner *et al.* (2000)
N1660	NCT aa 1693-1709	rabbit	1 µg/ml	-	Sigma (N1660)
2G7	PS1 NTF aa 39-52	rat	3 µg/ml	-	Trambauer *et al.* (2020)
Penta-His	His_5 peptide	mouse	1:2000	-	Qiagen (34660)
α-mouse HRP	mouse IgG	goat	1:5000	-	Promega (W402B)
α-rabbit HRP	rabbit IgG	goat	1:5000	-	Promega (W401B)
α-rat HRP	rat IgG	goat	1:3000	-	Merck Millipore (AP136P)

aa: amino acid, **IB**:immunoblot, **IP**: immunoprecipitation; [1]exact epitope proprietary to manufacturer; [2]monoclonal antibody

2.1.4 Primers

Primers used to generate mutant constructs are listed with their respective sequence in the following table.

alias	primer	sequence
prLF129	mutPSH_D162A_fw	CTGGCAGTGTATGCTGCTATTTCTGTTTACC
prLF130	mutPSH_D162A_rev	GGTAAACAGAAATAGCAGCATACACTGCCAG
prLF131	mutPSH_D219A_fw	GGGCATGGGTGCTCTGATTATGCCG
prLF132	mutPSH_D219A_rev	CGGCATAATCAGAGCACCCATGCCC
prLF157	PS1_d377-381_fw	GGTGAAGACCCAGAGGAAGGATTGGGAGATTTCATTTTCTACAG
prLF158	PS1_d377-381_rev	CTGTAGAAAATGAAATCTCCCAATCCTTCCTCTGGGTCTTCACC
prLF239	PS1_K380P_fw	GAAAGGGGAGTACCACTTGGATTGGGAGATTTC
prLF240	PS1_K380P_rev	GAAATCTCCCAATCCAAGTGGTACTCCCCTTTC
prLF259	mutC100_L52P_fw	CCTTGGTGATGCCGAAGAAGAAACAGTACACATCC
prLF260	mutC100_L52P_rev	GGATGTGTACTGTTTCTTCTTCGGCATCACCAAGG
prLF263	mutC100_M51P_fw	CATCACCTTGGTGCCGCTGAAGAAGAAACAGTAC
prLF264	mutC100_M51P_rev	GTACTGTTTCTTCTTCAGCGGCACCAAGGTGATG
prLF265	PSH_d213-216_fw	GGCGAAGAACGCGGTGGCATGGGTGATCTG
prLF266	PSH_d213-216_rev	CAGATCACCCATGCCACCGCGTTCTTCGCC
prLF267	PSH_d213-217_fw2	GGCGAAGAACGCGGTATGGGTGATCTG
prLF268	PSH_d213-217_rev2	CAGATCACCCATACCGCGTTCTTCGCC
prLF274	mutPSH_M172K_fw	GTACCAAACACAAGATCACGCTGGCAG
prLF275	mutPSH_M172K_rev	CTGCCAGCGTGATCTTGTGTTTGGTAC
prLF278	mutPSH_I173K_fw	GTACCAAACACATGAAAACGCTGGCAG
prLF279	mutPSH_I173K_rev	CTGCCAGCGTTTTCATGTGTTTGGTAC
prLF282	mutPSH_L175K_fw	CATGATCACGAAAGCAGAAGGCGTGC
prLF283	mutPSH_L175K_rev	GCACGCCTTCTGCTTTCGTGATCATG
prLF286	mutPSH_A176K_fw	CATGATCACGCTGAAGGAAGGCGTGC
prLF287	mutPSH_A176K_rev	GCACGCCTTCCTTCAGCGTGATCATG
prLF288	mutPSH_A213P_fw	GAACGCGGTCCATTCGTTATGGGCATGGG
prLF289	mutPSH_A213P_rev	CCCATGCCCATAACGAATGGACCGCGTTC
prLF290	mutPSH_F214P_fw	GAACGCGGTGCACCCGTTATGGGCATGGG
prLF291	mutPSH_F214P_rev	CCCATGCCCATAACGGGTGCACCGCGTTC
prLF292	mutPSH_V215P_fw	GAACGCGGTGCATTCCCTATGGGCATGGG
prLF293	mutPSH_V215P_rev	CCCATGCCCATAGGGAATGCACCGCGTTC

2.1.5 Plasmids

Plasmids used and generated in this study are listed with their respective source in the following table.

name	backbone	resistance	source
PSH wt	pET-21b	amp	Li *et al.* (2013)
mutPSH_D162A	pET-21b	amp	this study
mutPSH_D220A	pET-21b	amp	this study
mutPSH_D162/220A	pET-21b	amp	this study
mutPSH_M172K	pET-21b	amp	this study
mutPSH_I173K	pET-21b	amp	this study
mutPSH_L175K	pET-21b	amp	this study
mutPSH_A176K	pET-21b	amp	this study
mutPSH_A213P	pET-21b	amp	this study
mutPSH_F214P	pET-21b	amp	this study
mutPSH_V275P	pET-21b	amp	this study
mutPSH_d213-216	pET-21b	amp	this study
mutPSH_d213-217	pET-21b	amp	this study
PS1	pcDNA3.1 zeo(+)	amp	Loetscher *et al.* (1997)
PS1_d377-381	pcDNA3.1 zeo(+)	amp	this study
PS1_K380P	pcDNA3.1 zeo(+)	amp	this study
PS1_M292D	pcDNA3.1 zeo(+)	amp	Steiner *et al.* (1999b)
APP-C100	pQE60	amp	Edbauer *et al.* (2003)
APP-C100_L52P	pQE60	amp	this study
APP-C100_M51P	pQE60	amp	this study
APP-C83	pQE60	amp	Akio

amp: ampicillin, **tet**: tetracycline

2.1.6 Cell lines

Cell lines used and generated in this study are listed with their respective source in the following table.

cell line	clone no	resistance	transgene	source
HEK293	-	-	-	Selkoe *et al.* (1988)
HEK293/sw	-	G	APPsw	Citron *et al.* (1996)
HEK293/sw PS1/2 dKO	2	G, Z	APPsw	this study[1]
HEK293/sw PS1/2 dKO wtPS1	3	G, Z	APPsw, PS1	provided by Johannes Trambauer
HEK293/sw PS1/2 dKO PS1 M292D	9	G, Z	APPsw PS1 M292D	this study
HEK293/sw PS1/2 dKO PS1 K380P	8	G, Z	APPsw PS1 K380P	this study
HEK293/sw PS1/2 dKO PS1 Δ377-381	3	G, Z	APPsw PS1 Δ377-381	this study

G: G418 (Geniticin) **Z**: Zeocin; [1] original cell stocks were provided by Masayasu Okochi (Tagami *et al.*, 2017); a new single cell clone was generated from these stocks.

2.1.7 γ-Secretase inhibitors

GSIs used in this study are listed with their respective IC_{50} for $A\beta_{40}$ in the following table. The IC_{50} values were determined in cells if not otherwise stated.

substance	IC_{50} for $A\beta_{40}$	reference
L-685,458	113 nM	Shearman *et al.* (2000)
III-31C	200 nM	Kornilova *et al.* (2003)
DAPT	20 nM	Dovey *et al.* (2001)
LY-411575	0.085 nM	Wong *et al.* (2004)
Begacestat	14.8 nM	Martone *et al.* (2009)
MRK-560	0.65 nM	Best *et al.* (2006)
Merck C (L-685,458-bt)	13.7 nM[1]	Beher *et al.* (2003)

[1] IC_{50} value of Merck C was not determined but of a derivative lacking the biotin moiety (Merck B); also, value was determined in an *in vitro* assay and not in cells.

2.2 Methods

2.2.1 Molecular biology methods

2.2.1.1 Site-directed mutagenesis

To introduce specific mutations into plasmid DNA, site-directed mutagenesis was performed via polymerase chain reaction (PCR). Therefore, specific primers (listed in 2.1.4) were designed. In these primers, the mutating bases in the middle were flanked by round about 15 bases on both sites, the primers always ended with a G or C at both ends and had a melting temperature between 60 to 70 °C. The lyophilized primers (Thermo Scientific) were reconstituted with H_2O to a final concentration of 100 pmol/ µl.
The PCR approach was the following:

template DNA	10 ng
forward primer	1 µl
reverse primer	1 µl
dNTP mix (10 mm, Roche)	0.5 µl
10× reaction buffer	2 µl
Pfu DNA polymerase (1 U/ µl, PeqLab)	1 µl
H_2O	ad 20 µl

As control the same approach was pipetted without polymerase (replaced by H_2O). The reaction was incuabted in a thermocycler follwowing this protocol. The annealing temperature was adjusted to the melting temperature of the primers (normally -5 °C of the melting temperature).

step	time	temperature	number of cycles
initial denaturation	5 min	95 °C	1
denaturation	0.5 min	-	15-20
primer annealing	1 min	annealing temperature 55-65 °C	
elongation	2 min per kB of fragment	72 °C	
final elongation	15 min	72 °C	1

After the amplification, 1 µl DpnI was added and incubated for 1 to 2 h at 37 °C to digest the parental plasmid. Half of the reaction mix was then transformed into chemical competent *Escherichia coli* DH5α cells (described in 2.2.1.3). From

the grown colonies, single colonies were picked (3 to 8 colonies per construct) and plasmid preparations were performed (described in 2.2.1.4). The purified plasmids were send for sequencing to check for mutagenesis (described in 2.2.1.6).

2.2.1.2 Generation of chemical competent *E. coli* cells

LB medium	1% Bacto Tryptone, 0.5% yeast extract, 17.25 mM NaCl, autoclaved at 120 °C and 1.2 bar for 20 min
transformation buffer	10 mM PIPES (pH 6.6), 50 mM $CaCl_2$, 15% glycerol

A 10 ml LB pre-culture of *E. coli* DH5α or BL21(DE3)RIL cells was grown at 37 °C over night. The next day, 200 ml culture was inoculated to OD_{600} of 0.05 and cells were grown at 37 °C until OD_{600} of 0.2 to 0.3. Cells were chilled on ice for 10 min and then pelleted by centrifugation at 5000 rpm and 4 °C for 10 min. Cells were resuspended in 100 ml transformation buffer and incubated on ice for further 20 min. After another round of centrifugation, cells were resuspended in 1 ml transformation buffer and aliquoted. Aliquots were flash frozen in liquid nitrogen and cells were stored at -80 °C until usage.

2.2.1.3 Transformation of DNA into competent *E. coli* cells

Competent cells were thawed on ice. To 50 µl of competent cells 5 to 10 µl of plasmid were added and cells were incubated on ice for 1 h. Then cells were heat shocked at 42 °C for 45 s and cooled down on ice for 2 min. After addition of 500 µl LB medium without antibiotics cells recovered by shaking at 37 °C for 1 h. Cells were plated onto LB agar plates with respective selection antibiotics and incubated over night at 37 °C.

2.2.1.4 Plasmid preparation

LB medium	1% Bacto Tryptone, 0.5% yeast extract, 17.25 mM NaCl, autoclaved at 120 °C and 1.2 bar for 20 min
ampicillin 1000× stock	100 mg/ml in 70% ethanol
kanamycin 1000× stock	30 mg/ml in 50% glycerol
chloramphenicol 1000× stock	34 mg/ml in 70% ethanol
tetracycline 1000× stock	10 mg/ml in 70% ethanol

Small scale preparation of plasmid DNA was performed with the NucleoSpin Plasmid Kit following the manufacturer's protocol. 5 to 7 ml LB medium containing the respective antibiotics were inoculated with a single *E. coli* DH5α colony and grown at 37 °C. The plasmid was eluted from the column with 30 to 50 µl H_2O.

Larger preparation of plasmid DNA was performed with the NucleoBond Xtra Midi Kit following the manufacturer's protocol and using 200 ml LB cultures (as described above). The resulting DNA pellet was desolved in 100 µl water and the final DNA concentration was adjusted to 1 µg/µl.

2.2.1.5 Measurement of DNA concentration

The concentration of DNA was determined by measurement of the absorption at 260 nm using a Nanophotometer (Nanodrop). Simultaneously, the absorption at 280 nm was measure to determine potential contaminations with proteins. The ration A_{260nm}/A_{280nm} should thereby be at least 1.8.

2.2.1.6 Plasmid sequencing

Plasmid DNA was Sanger sequenced with GATC Biotech / Eurofins following the recommendations of the company.

2.2.2 Tissue culture methods

2.2.2.1 Culturing HEK293 cells

Penicillin/Streptomycin (Pen/Strep)	100 U/ml/100 µg/ml, PAA
G418 (Geneticine)	200 µg/ml, Invitrogen
Zeocin	200 µg/ml, Invitrogen

All cell lines were cultured in DMEM with addition of 10% FBS and Pen/Strep at 37 °C in the presence of 5% CO_2. Cell line specific (see 2.1.6) selection antibiotics were used for stable expression of cell line specific proteins. To split cells into a new dish, a confluent dish of cells was washed with 2 to 4 ml PBS and cells were detached by incubating with 1 ml Trypsin/EDTA for up to 5 min at 37 °C. Detached cells were transferred to 3 ml medium with selection antibiotics, pelleted at 1000×g for 5 min, resuspended in medium and then distributed into new dishes with respective medium.
For cryopreservation pelleted cells were resuspended in freezing medium (FBS containing 10% DMSO) and frozen in an isopropanol freezing box at -80 °C.

2.2.2.2 Transfection of HEK293 cells

DNA	16 µg in 1.5 ml OptiMEM
Lipofectamine 2000	40 µl in 1.5 ml OptiMEM

To generate stable cell lines, cells were seeded in antibiotic free medium the day before transfection so that the dish was 75% confluent at day of transfection. Lipofectamine and DNA solution were mixed together and incubated for 20 min at room temperature and then added to the cells. The next day, cells were splitted and seeded in different dilutions (1:10 to 1:1000) and cells were grown until single cell clones appeared. Cell clones were transferred to 12 well plates and further grown until they were analyzed.

2.2.3 Biochemical methods

2.2.3.1 Purification of C100-His_6 & C83-His_6 substrates from *E. coli* cells

TE buffer	20 mM Tris-HCl (pH 7.5), 1 mM EDTA
urea buffer	20 mM Tris-HCl (pH 8.5), 6 M urea, 1% Triton X-100, 1% SDS, 1 mM $CaCl_2$, 100 mM NaCl
dilution buffer	20 mM Tris-HCl (pH 8.5), 150 mM NaCl
Triton X-100 wash buffer	20 mM Tris-HCl (pH 8.5), 300 mM NaCl, 1% Triton X-100
SDS wash buffer	20 mM Tris-HCl (pH 8.5), 300 mM NaCl, 0.2% SDS
imidazole wash buffer	20 mM Tris-HCl (pH 8.5), 300 mM NaCl, 0.2% SDS, 20 mm imidazole
elution buffer	20 mM Tris-HCl (pH 8.5), 300 mM NaCl, 0.2% SDS, 100 mm imidazole
final elution buffer	20 mM Tris-HCl (pH 8.5), 300 mM NaCl, 0.2% SDS, 500 mm imidazole

A 50 ml LB pre-culture with chloramphenicol and ampicillin was inoculated with BL21(DE3)RIL cells harbouring the pQE60 vector encoding the C100-His_6 or C83-His_6 substrate respectively and grown over night at 37 °C. The next day, 500 ml LB culture with the same antibiotics was inoculated and cells were grown until OD_{600} of 0.6. Expression of the protein was induced by addition of 1 mM IPTG (final concentration) and cells were grown further for 4 to 5 h. Cells were pelleted, resuspended in ice cold TE buffer with PI complete (10 ml per g cell pellet) and opened up by sonification on ice (30 s on, 30 s off, 50% duty cycle, total sonication time: 5 min). After centrifugation (12000 rpm, 4 °C, 15 min), the pellet was resuspended in the same volume of TE buffer and the procedure was repeated. The final pellet was resuspended in urea buffer with PI complete (4 ml per g of cell pellet) and solubilised by shaking in the cold over night.

To remove non-solubilzed particles, the urea solution was centrifuged (12000 rpm, 4 °C, 15 min) and the protein concentration of the supernatant was determined by BCA. The supernatant was diluted 1:5 with dilution buffer, Ni-NTA agarose was added (1 ml Ni-NTA agarose per 40 mg protein) and incubated at room temperature by shaking for 2 h. The beads were transferred to an empty plastic column and washed with 5 bead volumes (BV) Triton X-100 wash buffer and 5 BV SDS wash buffer followed by 3 BV imidazole wash buffer. Protein was eluted into 5×1 BV elution buffer and 1 BV final elution buffer.
The purification was controlled by SDS-PAGE followed by Comassie staining or immunoblotting. Fractions with the highest amount of purified protein were pooled, protein concentration was determined and aliquots were stored at -20 °C.

2.2.3.2 Precipitation of flAPP from HEK293 cells

lysis buffer	50 mM Tris-HCl (pH 8.0), 100 mM NaCl, 1 mM EDTA, 1% CHAPSO
wash buffer	50 mM Tris-HCl (pH 8.0), 100 mM NaCl, 1 mM EDTA
elution buffer	20 mM Tris-HCl (pH 8.5), 300 mM NaCl, 1% SDS
dilution buffer	20 mM Tris-HCl (pH 8.5), 300 mM NaCl

The precipitation of flAPP was adapted from Vieira *et al.* (2010). One dish of HEK293 cells expressing full-length Swedish APP (flAPP/sw) was lysed in 1 ml lysis buffer containing PI complete for 30 min on ice followed by centrifugation (13000×g, 4 °C, 15 min) to remove cell debris. The supernatant was pre-cleared by incubation with 25 µl protein A sepharose (PAS) for 1 h at 4 °C and PAS beads were removed by centrifugation at 1500× g and 4 °C for 1 min. To precipitate flAPP/sw, the pre-cleared supernatant was incubated with APP-specific antibody 22C11 and PAS over night at 4 °C. flAPP was eluted from the beads by incubation with 25 µl elution buffer containing PI complete for 1 h at room temperature. Protein was diluted to 0.2% SDS with dilution buffer and stored at 4 °C.

2.2.3.3 Purification of PSH from *E. coli* cells

resuspension buffer	25 mM Tris-HCl (pH 8.0), 150 mM NaCl
solubilisation buffer	25 mM Tris-HCl (pH 8.0), 150 mM NaCl, 2% DDM
wash buffer	25 mM Tris-HCl (pH 8.0), 150 mM NaCl, 20 mM imidazole, 0.6% DDM
elution buffer	25 mM Tris-HCl (pH 8.0), 150 mM NaCl, 250 mM imidazole, 0.6% DDM

The protocol was adapted from Li *et al.* (2013). A 50 ml LB pre-culture with ampicillin and chloramphenicol was inoculated with *E. coli* BL21(DE3)RIL cells

transformed with pET-21b vector encoding the N-terminal His_8-tagged PSH construct and grown at 37 °C over night. For expression of the protein, 500 ml LB culture were inoculated with the pre-culture and grown at 37 °C to OD_{600} of 1.5. After induction with 0.2 mM IPTG, cells were grown over night at 22 °C; cells were harvested and resuspended in resuspension buffer (10 ml per g cell pellet). Cells were sonified (30 s on, 30 s off, 50% duty cycle, total sonication time: 5 min) and cell suspension was pre-cleared by centrifugation (23000×g, 4 °C, 10 min). The supernatant was ultracentrifuged (150000×g, 4 °C, 1 h) and the pellet was resuspended in solubilisation buffer (7 ml per g cell pellet) and solubilised by rocking in the cold for 1 h. After removing the insoluble particles by ultracentrifugation (150000×g, 4 °C, 30 min), supernatant was incubated with 100 to 200 µl Ni-NTA slurry for 2 h at room temperature. Ni-NTA beads were subjected to an empty plastic column and washed with 6 BV wash buffer. Protein was eluted from the beads with 4×1 BV elution buffer. Purification was checked by SDS-PAGE followed by Comassie staining and immunoblotting.

2.2.3.4 Reconstitution of PSH into POPC SUVs

reconstitution buffer 5 mM Na citrate (pH 6.4), 3.5 % glycerol, 30 mM DTT

Preparation of POPC SUVs. L-α-phosphatidylcholine (POPC) was hydrated in water (10 mg/ml) and sonicated in pulsed mode until clarity. The small unilamellar vesicles (SUVs) were diluted into reconstituion buffer to a final concentration of 3.45 mg/ml (5×POPC) and stored at -20 °C until further use.

Reconstitution of PSH into vesicles. 5×POPC were diluted with reconstitution buffer to 2×POPC. For reconstitution of PSH into POPC SUVs, 1 volume of purified PSH was incubated with 4 volumes of the 2×POPC vesicle preparation. An excess of Calbiosorb adsorbent beads was added and the solution was incubated by shaking at 4 °C for 30 min. Then the adsorbent beads were replaced by fresh beads and the solution was further incubated over night by shaking at 4 °C.

Verification of reconstitution. To check proper reconstitution of PSH into POPC vesicles, POPC was reconstituted into POPC vesicles containing the fluorescent lipid rhodamine-DHPE (1000:1 molar ratio) following the protocol described above. A small gel filtration column was packed with 250 µl Sephacryl S-200 HR and equilibrated with reconstitution buffer. The PSH-containing liposomes were subjected to this column and small fractions (20 µl) were collected. Fractions were analyzed for fluorescent vesicles (λ_{ex} 530 nm, λ_{em} 590 nm) with fluorometer Fluoroscan Asket Fl and for PSH by immunoblotting (2.2.3.14).

2.2.3.5 PSH *in vitro* assay

To test the activity of PSH, *in vitro* assays were performed with the C100-His_6, C83-His_6 or flAPP substrate, respectively. 0.5 µM of the substrate were incubated with 1 to 2 µM PSH, either DDM-solubilized or reconstituted in POPC SUVs, in a master buffer (20 mm Bicine, 20 mm HEPES, 20 mm MES) over night at 37 °C. For the DDM-solubilized PSH the final DDM concentration in the assay was 0.02% and for the PSH in POPC SUVs DDM was added to a final concentration of 0.008%. To test the influence of the pH the master buffer was adjusted to different pH values between 5.5 and 9.0. Later, the *in vitro* assay was performed at pH 7.0 if not otherwise stated. To control for cleavage specificity GSI L-685,458 was added to a final concentration of 20 µM. Depending on the following analysis the reaction was stopped by addition of Tris-Bicine urea sample buffer (2.2.3.14) or IP-MS buffer (2.2.3.9).

2.2.3.6 Preparation of HEK293 cell lysates

STEN lysis buffer 50 mM Tris-HCl (pH 7.6), 150 mM NaCl, 2 mM EDTA, 1% NP-40

Harvesting of HEK293 cells. Confluent dishes of HEK293 cells were washed with ice cold PBS and scrapped in 1 ml PBS per dish. Cells were pelleted by centrifugation (1500×g, 4 °C, 5 min), flash frozen in liquid nitrogen and stored at -20 °C.

Cell lysis. Cells were resuspended in 500 µl STEN lysis buffer supplemented with 1×PI complete and incubated for 30 min on ice. Then the cell suspension was centrifuged (160000×g, 4 °C, 20 min) and the supernatant was transferred to a fresh reaction tube.

2.2.3.7 Preparation of HEK293 membrane fractions

hypotonic buffer 15 mM Na citrate (pH 6.4), 10 mM KCl

Harvesting of HEK293 cells. Confluent dishes of HEK293 cells were washed with ice cold PBS and scrapped in 1 ml PBS per dish. Cells were pelleted by centrifugation (1500×g, 4 °C, 5 min), flash frozen in liquid nitrogen and stored at -20 °C.

Cell lysis and membrane preparation. Cells were resuspended in hypotonic buffer supplemented with 1×PI complete (1 ml per 1 dish of cells) and OD_{600} was

adjusted to 2. Cell suspension was flash frozen in liquid nitrogen, thawed on ice and needled with a 23 gauge needle. The cell suspension was pre-cleared by centrifugation (1000×g, 4 °C, 15 min) and the supernatant was aliquoted (one aliquot corresponds to dish of cells) and centrifuged at 16000×g rpm and 4 °C for 45 min. Membrane pellets were stored at -80 °C until usage.

2.2.3.8 γ-Secetrase *in vitro* assay

citrate buffer	150 mM Na citrate (pH 6.4)
2× assay buffer	150 mM Na citrate (pH 6.4), 1 mg/ml PC, 20 mM DTT, 0.2 mg/ml BSA

Membrane lysate. A membrane pellet from one dish of cells (see 2.2.3.7) was resuspended in 100 µl citrate buffer containing 1% CHAPSO and PI complete and incubated on ice for 20 min. The lysate was centrifuged at 100000×g and 4 °C for 30 min and the supernatant was either directly used for activity assays or flash frozen in liquid nitrogen and stored at -80 °C.

Activity assay. For each reaction 5 µl of membrane lysate was used. This was diluted with 5 µl citrate buffer (without CHAPSO) and 10 µl freshly prepared 2× assay buffer resulting in a final CHAPSO concentration of 0.25%. For the assay buffer, PC was freshly sonified from a stock solution. 0.5 µM C100-His_6 substrate were added (final SDS concentration below 0.008%) and reaction was incubated over night at 37 °C. To control cleavage specificity the assay was performed in the presence of 1 to 2 µM GSI L-685,458. The reaction was stopped by addition of Tris-Bicine urea sample buffer (2.2.3.14) or IP-MS buffer (2.2.3.9).

Activity assay with purified γ-secretase. Purified γ-secretase was provided by Lucía Chávez-Gutiérrez. The activity assay was based on the activity assay for γ-secretase from HEK293 membrane lysates. 0.15 ng purified γ-secretase were incubated with 0.5 µM C100-His_6 substrate over night at 37 °C in assay buffer. To control cleavage specificity the assay was performed in the presence of 1 to 2 µM GSI L-685,458. The reaction was stopped by addition of Tris-Bicine urea sample buffer (2.2.3.14) or IP-MS buffer (2.2.3.9)

2.2.3.9 Mass spectrometry analyis

Tris-EDTA solution	750 mM Tris-HCl (pH 8.0), 125 mM EDTA
20× IP-MS buffer	200 mM Tris-HCl (pH 8.0), 2.8 M NaCl, 100 mM NaCl, 2% Octyl β-D-glucopyranoside
MS matrix	TFA:water:acetonitril (1:20:20), saturated with α-Cyano-4-hydroxycinnamic acid

In vitro assays with either PSH or γ-secretase were diluted with 1 ml IP-MS buffer. To precipitate Aβ species, 4 µl Aβ-specific antibody 4G8 and 12 µl protein G sepharose (PGS) were added to the diluted assay. To precipitate AICD species, 15 µl of PAS preloaded with 4 µl antibody 6687 were added. Immunoprecipitation was performed over night in the cold room by shaking. For precipitation of Aβ species from medium of cells, 5 ml of medium incubated over night on a confluent dish of HEK293 cells were centrifuged (5000 rpm, 4 °C, 5 min) to remove cell debris. The cleared medium was neutralized with 1:25 Tris-EDTA solution. Aβ species were precipitated as described above. After precipitation, PGS or PAS beads were washed with 3×1 ml IP-MS buffer and 3×1 ml water and beads were completely dried with a syringe.
Aβ and AICD species were eluted from the beads by addition of 10 µl matrix. The matrix solution was then spotted 3×0.4 µl onto the sample plate. MS-samples were analyzed on a 4800 MALDI TOF/TOF Analyzer or rapifleX MALDI Tissuetyper instrument in linear mode. Data were vizualized with GraphPad Prism and for comparison of different spectra the intensity of the highest peak was set to 100%.

2.2.3.10 Electrochemiluminescence immunoassay

Electrochemiluminescence immunoassay (ECL-IA) with samples from PSH *in vitro* assays was performed following the manufacturers protocol using the Aβ Peptide Panel 1 Kit (MSD) with SULFO-tagged anti-Aβ antibody (4G8). Antibody was diluted 1:50 in Diluent 100. Briefly, samples were centrifuged at 21000×g for 30 min and supernatant was diluted 1:25 in Diluent 35. 4-spot MULTI-SPOT® plates were blocked with Diluent 35 for 1 h at room temperature then washed with MSD Wash Buffer. Samples (or calibrators) and SULFO-tagged antibody 4G8 were added to each well (in technical duplicates) and incubated for 2 h at room temperature. After another round of washing, Read Buffer T was added and light emission at 620 nm was measured.

2.2.3.11 Inhibitor affinity precipitation

MES buffer	50 mM MES (pH 6.0), 500 mM NaCl, 5 mM $MgCl_2$
Blocking buffer	1% I-Block (Tropix) in PBS

The protocol for the inhibitor affinity precipitation was adopted from Beher *et al.* (2003).

Preparation of streptavidin sepharose beads. Beads were washed three times with PBS and then blocked with blocking buffer over night at 4 °C. The next day, beads were additionally blocked for 30 min at room temperature with fresh blocking buffer.

PSH. PSH (DDM-solubilised or POPC-reconstituted) was diluted with MES buffer to 1 to 2 µM protein. As for the *in vitro* assay, the final DDM concentration in the case of DDM-solubilised PSH was 0.02% and in the case of reconstituted PSH DDM was added to a final concentration of 0.008%. The diluted protein solution was incubated for 30 min at 4 °C with streptavidin sepharose beads to preclear the solution and then incubated with 10 µ GSI inhibitor Merck C (L-685,458-biotin) in the presence of fresh streptavidin beads for 2 h at room temperature. Non-specific binding was analyzed either by omitting Merck C or by competition with 100-fold molar excess of the unbiotinylated (parental) compound L-685,458. Samples were eluted from the beads with 1.5× Laemmli urea sample buffer containing 4 mM biotin and then analyzed by SDS-PAGE (see 2.2.3.14).

2.2.3.12 Nano differential scanning fluorimetry (nanoDSF)

For nanoDSF, 10 µl of WT and mutant PSH (25 µM) were loaded into NanoTemper Tycho NT.6 capillaries and analyzed on the Tycho NT.6 system. The data is automatically analyzed by the Tycho software and calculates the inflection temperatures (T_i). T_i is a measure for the protein unfolding temperature.

2.2.3.13 Dynamic light scattering (DLS)

To prepare protein samples, 60 µl of WT and mutant PSH (25 µM) were ultracentifuged (100000×g and 4 °C) for 30 min. DLS measurements were performed on a Malvern Instruments High Performance Particle Sizer using a Hellma Analytics High Precision Cell.

2.2.3.14 SDS-PAGE

Depending on the analysed proteins different gel systems were used. Total sAPP, APP, AICD and Aβ were normally analysed by separating them on Tris-Tricine gels. Single cell clones were analysed on 10% Urea Tris-Glycine gels to separate PS1-NTF and Nicastrin. 10% Urea Tris-Glycine gels were also used to analyse PSH except of PSH purification which was analysed via 15% Tris-Glycine gels. Aβ species were separated via Tris-Bicine urea gels.
Samples were prepared with the respective sample buffers and denatured at 65 °C for 5 min. For analysing Aβ species, samples were denatured at 95 °C for 10 min.

Tris-Tricine gels from Invitrogen

10× Tris-Tricine running buffer	1 M Tris-HCl, 1 M Tricine, 1% SDS
3× Laemmli urea sample buffer	188 mM Tris-HCl (pH 6.8), 6% SDS, 30% glycerol, 7.5% β-mercaptoethanol, 6 M urea, spatula tip bromophenol blue

The samples were separated in a X Cell Sure Lock mini gelelectrophoresis chamber first at 80 V to focus samples in the running front and then at 120 V until full separation.

Tris-Tricine gels according to Schaegger

Schaegger gel buffer	3 M Tris-HCl (pH 8,45), 0.3% SDS
10× Tris-Tricine running buffer	1 M Tris-HCl, 1M Tricine, 1% SDS
5× Schaegger gel anode buffer	1 M Tris-HCl (pH 8.9)
3× Laemmli urea sample buffer	188 mM Tris-HCl (pH 6.8), 6% SDS, 30% glycerol, 7.5% β-mercaptoethanol, 6 M urea, spatula tip bromophenol blue

The Tris-Tricine gels according to Schaegger represent an alternative to the commercial Tris-Tricine gels from Invitrogen. They were mainly used to analyse purification of C100-His_6 substrates and pre-experiments. The recipe is for two gels with 1.5 mm thickness. Samples were analysed analogous to the commercial gels described above in a mini-Protean 3 gel electrophoresis chamber except that two different running buffers (Tris-Tricine running buffer for the cathode and Schaegger gel anode buffer) were used.
Separation and spacer gels were polymerized and poured at the same time. 5 ml of the separation gel solution is overlayed carefully with 2.5 ml spacer gel solution. After complete polymerisation of this layer, the stacking gel was polymerised on top.

	16% separation gel	9% spacer gel 2.7 cm	4% stacking gel 1.7 cm
H_2O	-	3.5 ml	4.2 ml
glycerol (32%)	3.5 ml	-	-
gel buffer	3.5 ml	2.5 ml	1.55 ml
acryl-/bisacrylamide (32:1, 49.5%)	3.5 ml	1.5 ml	0.5 ml
APS (10%)	65 µl	70 µl	100 µl
TEMED	6.5 µl	8 µl	15 µl

Urea Tris-Glyicine gels

4× stacking gel buffer	0.5 M Tris-HCl (pH 6.8), 0.4% SDS
4× separating gel buffer	1.5 M Tris-HCl (pH 8.8), 0.4% SDS
Tris-Glycine running buffer	25 mM Tris-HCl, 200 mM glycine, 0.1% SDS
3× Laemmli urea sample buffer	188 mM Tris-HCl (pH 6.8), 6% SDS, 30% glycerol, 7.5% β-mercaptoethanol, 6 M urea, spatula tip bromophenol blue

The recipe is for two gels with 1.5 mm thickness.

	10% separation gel	12% separation gel	stacking gel
urea (8 M)	5.25 ml	5.25 ml	5 ml
H_2O	2.25 ml	1.5 ml	1.825 ml
stacking gel buffer	-	-	2.5 ml
separation gel buffer	3.75 ml	4.5	-
acryl-/bisacrylamide (37.5:1, 40%)	3.5 ml	1.5 ml	0.5 ml
APS (10%)	70 µl	70 µl	50 µl
TEMED	70 µl	70 µl	50 µl

8 M urea solution was prepared freshly each time. Separation and stacking gel were polymerized and poured after each other. The samples were separated in a mini-Protean 3 gel electrophoresis chamber with Tris-Glycine running buffer at constant 40 mA.

Tris-Glyicine gels

4× stacking gel buffer	0.5 M Tris-HCl (pH 6.8), 0.4% SDS
4× separating gel buffer	1.5 M Tris-HCl (pH 8.8), 0.4% SDS
Tris-Glycine running buffer	25 mM Tris-HCl, 200 mM Glycine, 0.1% SDS
4× Laemmli sample buffer	250 mM Tris-HCl (pH 6.8), 8% SDS, 40% glycerol, 10% β-mercaptoethanol, spatula tip bromophenol blue

The recipe is for two gels with 1.5 mm thickness. Preparation and sample separation was performed as for Urea Tris-Glycine gels with the exception that no urea was used in the gels and the Laemmli sample buffer was used for sample preparation.

	12% separation gel	15% separation gel	stacking gel
H_2O	2.25 ml	1.5 ml	1.825 ml
stacking gel buffer	-	-	2.5 ml
separation gel buffer	3.75 ml	4.5	-
acryl-/bisacrylamide (37.5:1, 40%)	3.5 ml	1.5 ml	0.5 ml
APS (10%)	70 µl	70 µl	50 µl
TEMED	70 µl	70 µl	50 µl

Tris-Bicine urea gels according to Wiltfang

stacking gel buffer	0.72 M Bis-Tris, 0.32 M Bicine
spacer gel buffer	0.8 M Bis-Tris, 0.2 M H_2SO_4
separating gel buffer	1.6 M Tris, 0.4 M H_2SO_4
cathode buffer	0.2 M Bicine, 0.1 M NaOH, 0.25% SDS
anode buffer	0.2 M Tris, 0.05 M H_2SO_4
3× Tris-Bicine urea sample buffer	0.72 M Bis-Tris, 0.72 M Bicine, 2% SDS, 45% saccherose, 7.5% β-mercaptoethanol, spatula tip bromophenol blue

The Tris-Bicine urea gel described here is adopted from Wiltfang and used to separate the different Aβ species. The recipe is for two gels with 1.5 mm thickness.

	11% separation gel	6% spacer 1.2 cm	9.14% stacking gel 1.1 cm
urea	9.6 g	-	-
H_2O	2 ml	1.36 ml	0.74 ml
stacking gel buffer	-	-	1.5 ml
spacer gel buffer	-	2 ml	-
separation gel buffer	5 ml	-	-
SDS (20%)	100 µl	20 µl	15 µl
acryl-/bisacrylamide (37.5:1, 40%)	5.5 ml	0.6 ml	0.675 ml
APS (10%)	80 µl	16 µl	18 µl
TEMED	10 µl	4 µl	18 µl

For the separation gel urea was dissolved in H_2O and separation gel buffer and heated until complete dissolution of the urea. The three layers were polymerized and poured one after the other in between 8×9 cm Hoefer gel plates and normally used directly the following day. Samples were separated in a Mighty small II Hoefer

gel electrophoresis chamber with the respective cathode and anode buffer. Samples were collected in the running front at 80 V and then separated at 30 mA (per gel) at a maximum of 150 V.

2.2.3.15 Blue Native (BN)-PAGE

Dark blue cathode buffer	50 mM Tricine, 15 mM Bis-Tris, 0.02% Comassie Blue G-250
Light blue cathode buffer	50 mM Tricine, 15 mM Bis-Tris, 0.002% Comassie Blue G-250
Anode buffer	50 mM Tricine, 15 mM Bis-Tris
3× BN sample buffer	150 mM Bis-Tris, 200 mM ε-aminocaproic acid, 20% glycerol
Tris-Glycine running buffer	25 mM Tris-HCl, 200 mM glycine, 0.1% SDS

To analyze the aggregation of WT and mutant PSH, protein samples were separated on 4-16% Bis-Tris gels. Samples were prepared in BN sample buffer with the addition of Comassie to 1/4 of the detergent concentration. Samples were separated at constant 150 V and after 1/3 of sample separation, the dark blue cathode buffer was exchanged by the light blue cathode buffer. Before immunoblotting, the gel was soaked for 15 min in Tris-Glycine running buffer and immunoblotting was performed as described in 2.2.3.16 with the exception that proteins were transferred at constant 40 V for 60 min.

2.2.3.16 Immunoblotting

10× Tris-Glycine blotting buffer	250 mM Tris-HCl, 2M Glycin
10× TBS/Tween	100 mM Tris-HCl pH 7.4, 1.5 M NaCl, 1% Tween-20
Blocking solution	0.2% I-Block (Tropix), 0.1% Tween-20, in PBS
10× PBS	1.4 M NaCl, 100 mM $Na_2HPO_4 \times 2H_2O$, 17.5 mM KH_2PO_4, 27 mM KCl, pH 7.4

Transfer of proteins. After SDS-PAGE, separated proteins were transferred onto membranes for specific protein detection. PSH was blotted onto PVDF membranes, all other proteins onto nitrocellulose membranes. For proteins below 15 kDa, nitrocellulose membrane with a pore size of 0.2 µm was used, for larger proteins nitrocellulose membrane with a pore size of 0.45 µm was used. PVDF membrane was hydrated in isopropanol for some minutes and then washed with H_2O. All membranes were equilibrated in blotting buffer.
Gel and membrane were placed into a blotting cassette (Bio-Rad) together with a sponge and 4 sheets of filter paper on each sites. The gel was placed in direction of the cathode, the membrane in the direction of the anode. The transfer took place in a mini trans-blot transfer chamber filled with blotting buffer and an ice pack at 400 mA for 60 min. For smaller proteins and peptides the transfer time was

reduced to 50 min. When necessary, nitrocellulose membrane was cooked in PBS after transfer for 5 min allowing the antibody epitope to expose.

Blocking and incubation with primary antibody. After blotting, membranes were incubated in blocking solution at room temperature for at least 1 h. This step blocks unspecific binding sites on the membrane. Then the primary antibody diluted in blocking solution was added and incubated by gently shaking over night in the cold room .

Washing and incubation with secondary antibody. Blots were washed 3×10 min with TBS/Tween and then membrane was incubated with secondary antibody diluted in blocking solution for 1 h at room temperature.

Washing and detection. After incubation with secondary antibody, blots were washed again 3×10 min with TBS/Tween. Then membranes were quickly pulled through H_2O and incubated for 2 min with the ECL substrate. After this films were exposed to visualize protein bands. For quantification membranes were exposed in the LAS-4000 or ImageQuant 800 image reader.

2.2.4 Computational methods

2.2.4.1 Homology model building & molecular dynamics simulations

The homology model building as well as the molecular dynamics (MD) simulations were performed by Shu-Yu Chen and Martin Zacharias from the Technical University Munich. Details on these methods can be found in Feilen *et al.* (2022).

2.2.4.2 Structure predictions using AlphaFold

To predict the structures of PSH–C83 and PSH–C99 complexes AlphaFold-Multimer (Jumper *et al.*, 2021; Evans *et al.*, 2022) coupled to Google Colaboratory was used. The prediction of the enzyme–substrate complexes is based on the aa sequences of PSH, C83 and C99 and was performed with the default AlphaFold-Multimer settings.

3 Results

3.1 Basic biochemical characteristics of PSH

3.1.1 Monoclonal specific PSH antibodies

So far, no specific antibodies against PSH are available and the detection of PSH in immunoblotting relies on tags added to the protein. In collaboration with the Monoclonal Antibody Core Facility at the Helmholtz Center Munich, monoclonal PSH-specific antibodies were generated. To this end, three epitopes (PSH1-3) were chosen, two (PSH1 and 2) – partially overlapping – in the loop between TMD6 and 7 and one (PSH3) in the loop between TMD8 and 9 (figure 3.1.1A).

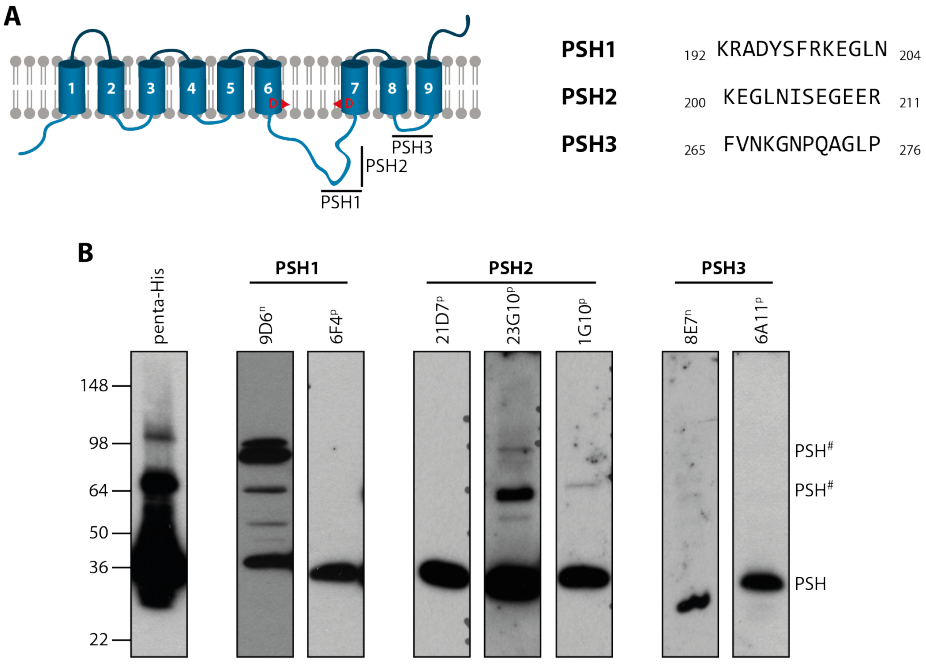

Figure 3.1.1: Screening for PSH-specific antibodies. (A) Schematic representation of PSH with indicated epitopes PSH1-3 (left) and the sequences of the epitopes (right). (B) Immunoblotting for PSH with different PSH-specific antibodies using nitrocellulose (n) or PVDF (p) membranes. The hash sign mark PSH multimers.

Antibodies were raised in Wistar rats against the respective peptides. In total, 27 primary supernatants against all three epitopes were tested in immunoblotting using nitrocellulose and PVDF membranes. From these, 7 antibodies were able to detect PSH, two against epitope PSH1, three against epitope PSH2 and two against epitope PSH3 (figure 3.1.1B) and these were then monoclonalized. Some of the antibodies, like 9D7 or 23G10, not only detected the monomeric form of PSH but also multimeric PSH. The antibody 6F4 against PSH1 is used in this study for PSH detection.

3.1.2 PSH purification

PSH was purified based on the previous published protocol by (Li *et al.*, 2013) after expression in *E.coli* BL21(RE3)RIL. Membranes were solubilized in DDM and the His-tagged PSH was bound to Ni-NTA beads. After column washing, PSH was eluted from the column in a buffer containing 0.6% DDM. The analysis of the purity by Coomassie Blue staining after separation by SDS-PAGE revealed that the samples still contained some impurities, but monomeric PSH was the most prominent band in the elution fractions (figure 3.1.2). Elution fractions containing more monomeric PSH (e.g. E2) also showed more multimeric/aggregate PSH. The identity of the bands on the Coomassie Blue-stained gel were confirmed by immunoblotting using the PSH-specific antibody 6F4 (figure 3.1.2). Furthermore, the immunoblotting also revealed smaller PSH fragments in the elution fractions. These will be discussed further in 3.1.3.

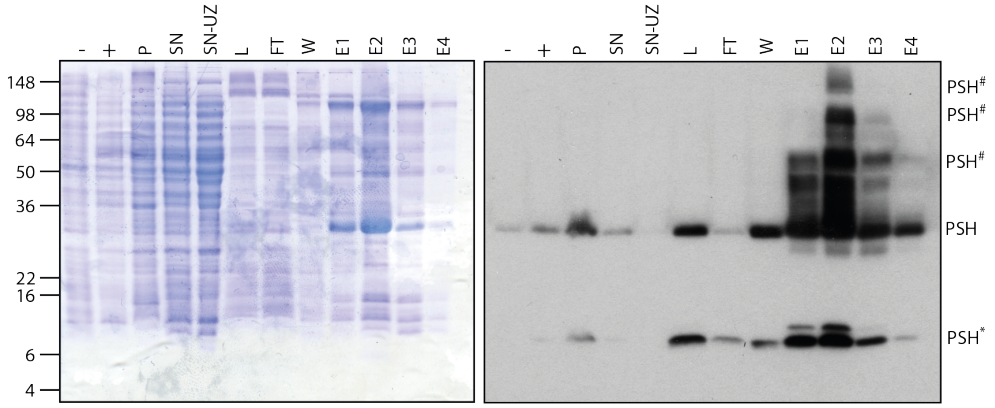

Figure 3.1.2: Analysis of PSH purification. Analysis of PSH purification by Coomassie Blue staining (left) and immunoblotting with PSH-specific antibody 6F4 (right). Equal volumnia from each sample were loaded. The hash sign marks PSH multimers, the asterisk marks PSH fragments. -: before induction of expression, +: after induction of expression, P: pellet, SN: supernatant, SN-UZ: supernatant after ultracentrifugation, L. load, FT: flow-through, W: wash, E: elution.

3.1.3 PSH endoproteolysis

Whether PSH undergoes endoproteolyis like PS is not clear and has not been studied in detail yet. Therefore, catalytic dead mutants PSH D162A, PSH D220A and PSH D162/220A were generated, expressed and purified. Purified wild type (WT) and mutant PSH were incubated over night at 37 °C and then analyzed by immunoblotting using PSH-specific antibody 6F4.
For all PSH constructs, a band was detected at the expected size of PSH at round about 32 kDa (figure 3.1.3). Furthermore, additional bands were detected below this PSH band at different sizes. Most prominent were bands at roughly 17 kDa and 14 kDa. Additionally also a band at roughly 10 kDa was observed for all PSH constructs but most prominently for WT and D220A PSH (figure 3.1.3). Since all of these bands were visible for all constructs, they are independent from PSH activity and might result from degradation or cleavage by another protease.
Therefore, PSH is not endoproteolysed as γ-secretase and the endoproteolysis is not a prerequisite for PSH activity. In this aspect PSH resembles more the SPP IMPs than γ-secretase.

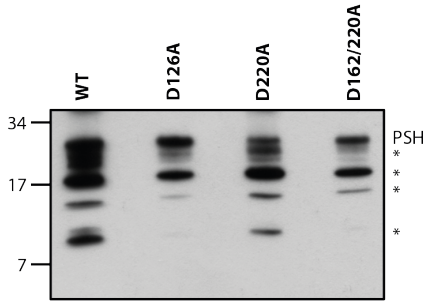

Figure 3.1.3: Analysis of PSH endoproteolysis. Immunoblotting for PSH (6F4) of WT and mutant PSH (D162A, D220A and D162/220A) after incubation at 37 °C over night and separation by Tris-Tricine SDS-PAGE. The asterisks mark PSH degradation bands

3.1.4 Cleavage of C99 by PSH

Several studies were already carried out to investigate the cleavage mechanism of PSH (Dang *et al.*, 2015; Naing *et al.*, 2018). Due to experimental variations within these studies, the data on PSH cleavage are not conclusive. One study suggested that the Aβ species produced are similar than the ones produced by γ-secretase (Dang *et al.*, 2015) whereas another study showed that preferably longer Aβ species are produced (Naing *et al.*, 2018). Therefore, the cleavage of purified PSH was evaluated in an *in vitro* assay with DDM. As reported, PSH is able to cleave C99-based

APP C100-His$_6$ substrate into AICD and Aβ (figure 3.1.4A). This cleavage was inhibited by the TSA GSI L-685,458. In contrast to the inhibition of γ-secretase, a 10-fold higher molar concentration was needed for a proper inhibition of PSH. The Aβ species were further analyzed by Tris-Bicine urea SDS-PAGE (figure 3.1.4B) and MALDI-TOF mass spectrometry (figure 3.1.4C). The profiles of the Aβ species revealed that PSH is mainly producing Aβ$_{40}$ and Aβ$_{42}$ with a clear preference for Aβ$_{42}$. Moreover, also longer Aβ species, like Aβ$_{46}$, were detected. These data indicate that besides its ability to cleave C99, PSH is under these experimental conditions impaired in its processive cleavage mechanism and preferably produces longer Aβ species.

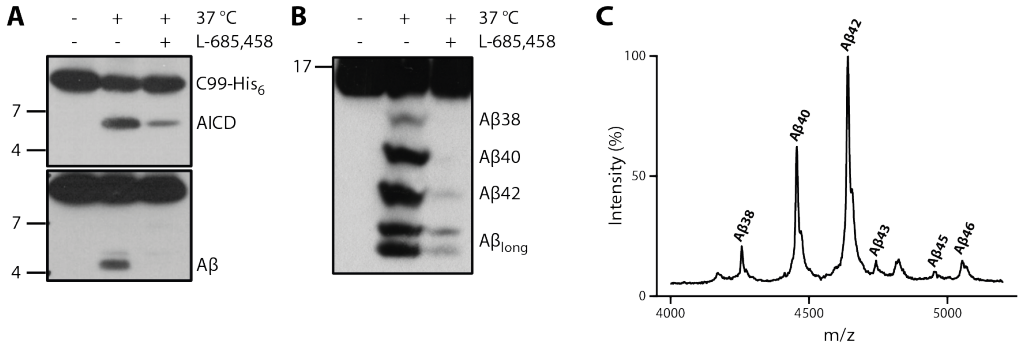

Figure 3.1.4: Cleavage of APP C99 by PSH. (A) Immunoblotting for AICD (Y188) and Aβ (2D8) after incubation of C100-His$_6$ with PSH in DDM micelles at 37 °C over night. (B) Immunoblotting for Aβ species (2D8) produced by PSH from C100-His$_6$ separated by Tris-Bicine urea SDS-PAGE. (C) MALDI-TOF analysis of Aβ species produced by PSH in DDM micelles (adapted from Feilen *et al.* (2022)).

3.1.5 Protein quality control

Throughout this study several mutants of PSH and their ability to cleave APP-derived substrates will be analyzed. The introduction of mutants can change the folding of a protein resulting in severe misfolding and/or even aggregation of the protein. To rule out these possibilities for the PSH mutations introduced here, the aggregation and folding of WT and mutant PSH was analyzed by dynamic light scattering (DLS), Blue Native (BN)-PAGE and nano differential scanning fluorimetry (nanoDSF).

In DLS experiemts an average particle size (Z-Ave) above 100 nm is indicative of protein aggregates. For WT and mutant PSH, the observed average particle size was always below 100 nm, indicating that non of the PSH constructs is aggregated in solution (figure 3.1.5A). This is further supported by BN-PAGE immunoblot analysis; WT and mutant PSH only showed two bands, one for monomeric PSH and another

one for dimeric PSH. Larger protein aggregates were not observed (figure 3.1.5B). All the analyzed constructs also behaved similar in nanoDSF experiments and showed an inflection temperature (T_i) of round about 72.5 °C (figure 3.1.5C) which correspond to an unfolding of the protein at his temperature. The combination of these three protein quality control analysis show that the introduction of a single point mutation or the deletion of four to five aa within PSH do not alter the folding, thermal stability and aggregation of the protein.

A

PSH	Z-Ave (nm)
WT	47.93
M172K	10.68
I173K	34.42
L175K	20.91
A176A	29.07
A213P	13.47
F214P	13.49
V215P	19.41
Δ213-216	52.59
Δ213-217	11.10

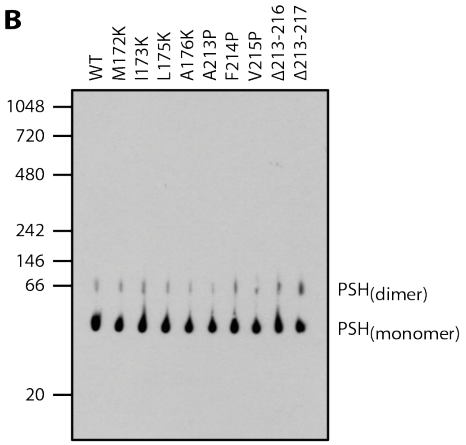

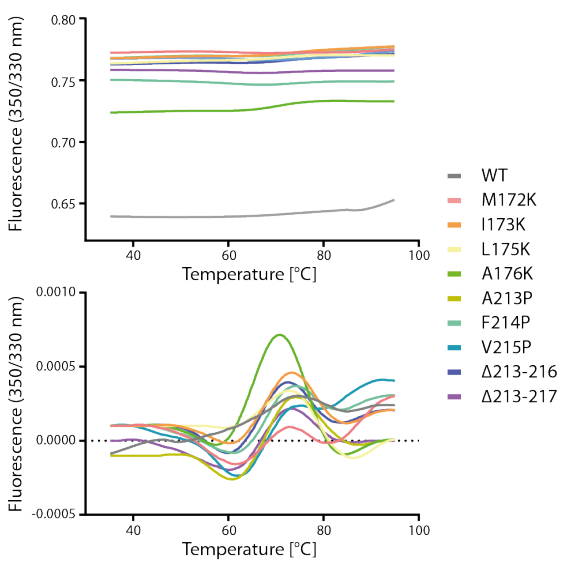

PSH	T_i [°C]
WT	74.225
M172K	72.293
I173K	73.440
L175K	73.440
A176K	70.573

PSH	T_i [°C]
A213P	73.923
F214P	73.198
V215P	73.319
Δ213-216	71.987
Δ213-217	72.745

Figure 3.1.5: PSH quality control. (A) Z-Ave values of WT and mutant PSH as measured by DLS. (B) Immunoblotting for PSH (6F4) after separating of WT and mutant PSH by BN-PAGE. (C) Fluorescence signals (upper panel) and T_i values (lower panel) of WT and mutant PSH as measured by nanoDSF (adapted from Feilen *et al.* (2022)).

3.2 Influence of lipid environment on PSH activity and structure

3.2.1 PSH reconstituion

To test whether and how a bilayer environment influences PSH activity, PSH was reconstituted into POPC SUVs. To check proper incorporation of PSH into SUVs, POPC SUVs were prepared containing the fluorescent marker lipid rhodamine-DHPE (1:1000 molar ratio) and PSH was reconstituted into these vesicles. Following gel filtration via a small size Sephacryl S200 HR column (200 µl), fractions were analyzed fluorometrically and via immunoblotting for PSH. Fluorescently labeled vesicles eluted in one single peak (fractions 3 to 6) and immunoblotting could confirm that these vesicles also contained PSH. Some PSH was not properly incorporated into vesicles and eluted in later fractions (fractions 7 to 10) but most of the PSH was properly reconstituted into POPC SUVs (figure 3.2.1).

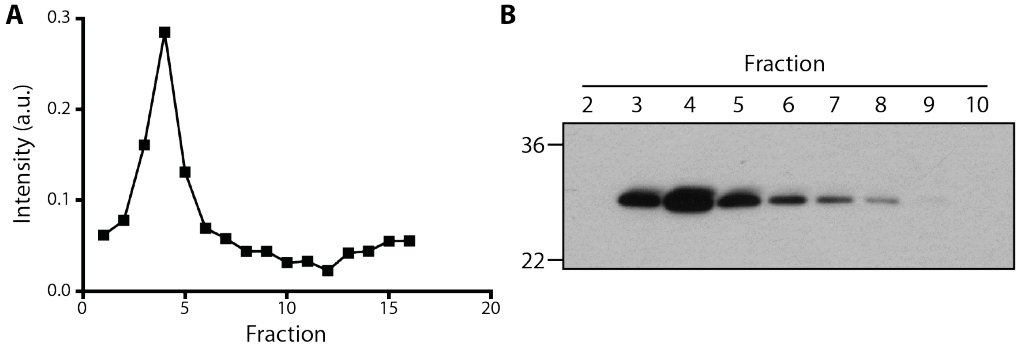

Figure 3.2.1: Check for PSH reconstitution into POPC SUVs. (A) Representative graph of fluorometric analysis of fractions after gel filtration of PSH-containing POPC vesicles with rhodamine-DHPE as fluorescent marker lipid. (B) Immunoblotting for PSH (6F4) in the gel filtration fractions (adapted from Feilen *et al.* (2022)).

3.2.2 Environmental dependent cleavage

Previous studies on γ-secretase (Quintero-Monzon *et al.*, 2011) or rhomboid proteases (Moin & Urban, 2012) showed that the assay condition (pH, salt concentration) and the lipid environment can influence the cleavage by IMPs. Since the processive cleavage of C99 by PSH in DDM micelles was decreased, several *in vitro* assay conditions were tested for their potency to modulate PSH (processive) cleavage.

To asses whether and how the assay condition influence PSH, the cleavage of C99 by PSH was analyzed over a broad range of different pH values (from pH 5.5 to pH 9.0) and in two different environments, DDM micelles and POPC bilayer. PSH was active in both environments and produced AICD and Aβ from C99 and showed its highest activity at pH 7.0 to 7.5 (figure 3.2.2A).

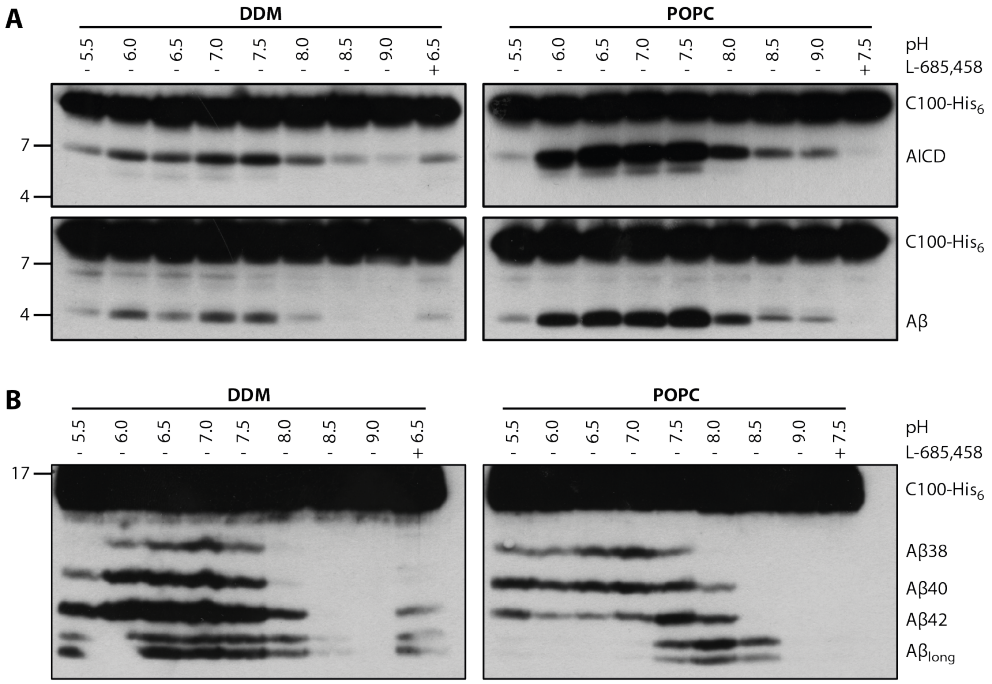

Figure 3.2.2: Cleavage of PSH in DDM micelles and POPC vesicles. (A) Immunoblotting for AICD (Y188) and Aβ (2D8) after incubation of C100-His_6 with PSH in DDM micelles and POPC vesicles at 37 °C over night. (B) Immunoblotting for Aβ species (2D8) produced by PSH from C100-His_6 in DDM micelles and POPC vesicles separated by Tris-Bicine SDS-PAGE (adapted from Feilen *et al.* (2022)).

Beyond its pH optimum, the activity of PSH sharply dropped at more alkaline pH. The reconstitution of PSH into a POPC bilayer strongly increased its processivity. This drop in total activity was accompanied by a decrease in processive cleavage as evident by the increase in longer Aβ-sepecies ($Aβ_{42}$ and longer, figure 3.2.2B). Compared to PSH in DDM micelles, POPC-reconstituted PSH showed an increase in the shorter Aβ species $Aβ_{38}$ and $Aβ_{40}$ and a reduction in longer Aβ species (figure 3.2.2B). The processivity of PSH in DDM and POPC environments was further analyzed by direct comparison of Aβ profiles at pH 7.0 by MALDI TOF mass spectrometry. In line with the observations from the immunoblot, POPC increased the processivity of PSH, resulting in the production of shorter Aβ species (figure 3.2.3A).
In principle, the increases in shorter Aβ species, especially $Aβ_{38}$, might also have arisen from a preferred usage of the $Aβ_{42}$ over the $Aβ_{40}$ product line. To elucidate on this possibility, the AICD species generated from C99 by PSH in DDM and POPC environment were compared by MALDI TOF mass spectrometry. In both

conditions, C99 is cleaved at both ε-cleavage sites (ε48 and ε49) releasing the two distinct AICD species AICD51 and AICD50 (figure 3.2.3B).

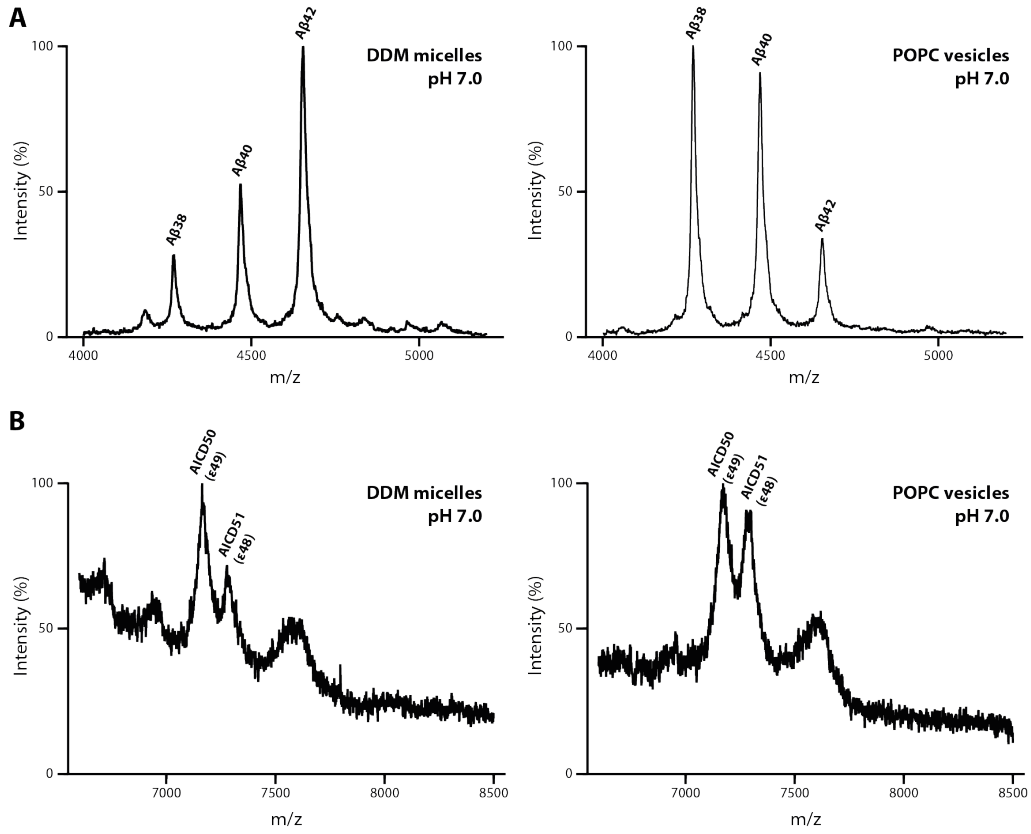

Figure 3.2.3: Mass spectrometry analysis of PSH cleavage. (A) MALDI-TOF analysis of Aβ species produced by PSH in DDM micelles and POPC vesicles at pH 7.0. (B) MALDI-TOF analysis of AICD species produced by PSH in DDM micelles and POPC vesicles at pH 7.0 (adapted from Feilen *et al.* (2022))

Taken these data together, POPC is able to modulate PSH activity and to increase its processivity resulting in the generation of shorter Aβ species.

3.2.3 Activity of PSH in brain lipid environment

Since PSH might serve as a surrogate protease to study the activity of PS independent of the other proteins of the γ-secretase complex, PSH activity should be assessed in a natural γ-secretase environment. To mimic this environment, PSH was reconstituted into brain lipid vesicles and the cleavage of C99 by PSH was analyzed at pH 7.0.

PSH was also active in the brain lipid environment, resulting in the release of AICD and Aβ (figure 3.2.4A). Strikingly, the brain lipid environment increased the processivity of PSH even more than the POPC environment and short Aβ species like $Aβ_{38}$ and $Aβ_{37}$ were mainly released (figure 3.2.4B, C).

The PSH processive cleavage is not only modulated by reconstitution of PSH into a lipid bilayer but also by the composition of this lipid bilayer.

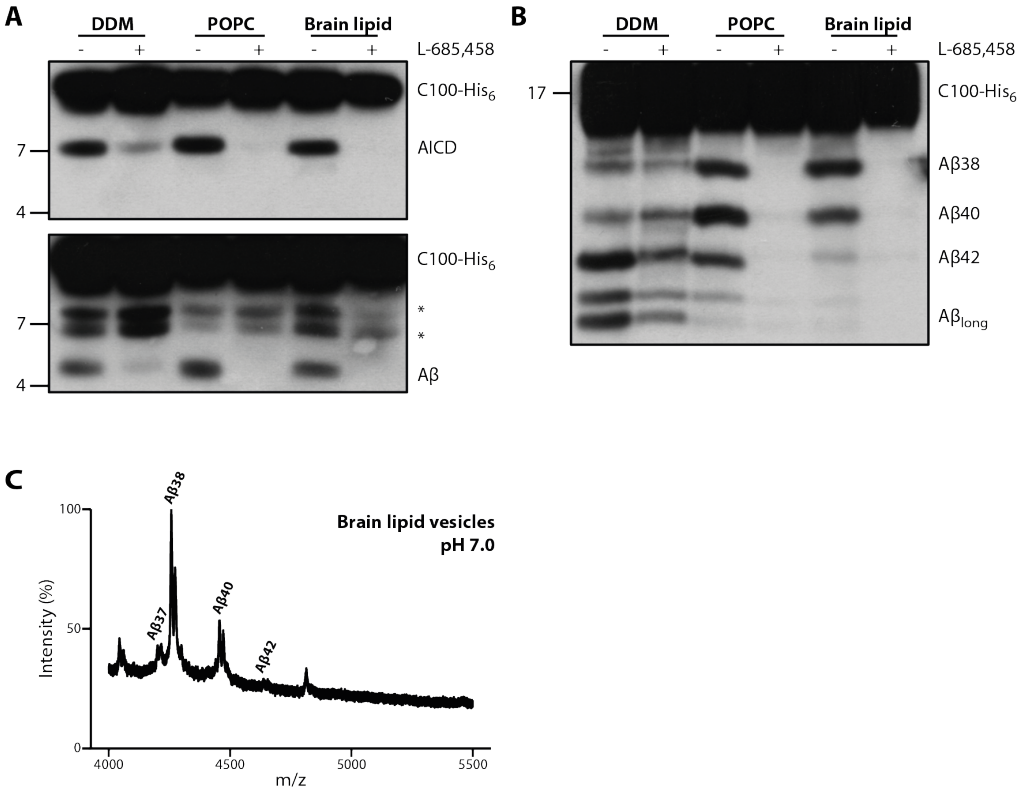

Figure 3.2.4: Cleavage of PSH in brain lipid vesicles (A) Immunoblotting for AICD (Y188) and Aβ (2D8) after incubation of C100-His_6 with PSH in DDM micelles, POPC vesicles and brain lipid vesicles at 37 °C over night. (B) Immunoblotting for Aβ species (2D8) produced by PSH from C100-His_6 in DDM micelles, POPC vesicles and brain lipid vesicles separated by Tris-Bicine SDS-PAGE. (C) MALDI-TOF analysis of Aβ species produced by PSH in brain lipid vesicles vesicles at pH 7.0 (adapted from Feilen *et al.* (2022))

3.2.4 Cleavage of APP C83

Another APP-based substrate is C83 which derives from APP by α-secretase cleavage and it is N-terminally 16 aa shorter than C99. Studies could show that C83 is the better substrate compared to C99 for γ-secretase (Funamoto *et al.*, 2013) resulting in an increased production of AICD. It is elusive whether C83 is also a substrate for PSH and whether the changes observed in the processivity of C99 are also observed for C83.

Therefore, the cleavage of C83 by PSH in DDM and POPC environment was analysed at pH 7.0. PSH was able to cleave C83 in both environments resulting in the release of AICD and p3 (figure 3.2.5A). Immunoblotting with the penta-His antibody to detect the AICD indicate that C83 is cleaved more efficiently than C99 by

PSH in both environments. In contrast, the immunoblotting for p3 and Aβ, respectively, with antibody Aβ22-35 indicate that C99 is cleaved more efficiently. It might be possible that the epitope of the antibody Aβ22-35 is differently recognized for p3 and Aβ and this might result in these observed differences. As already observed for C99 (figure 3.2.5C), the bilayer environment again increased the processivity resulting in an increased $p3_{40}/p3_{42}$ ratio in the POPC environment compared to the DDM environment (figure 3.2.5B). Due to technical limitations it was not possible to detect $p3_{38}$ in the ECL-IA and to detect p3 species by mass spectrometry.
Taken together C83 is another (non-)natural substrate of PSH, which is cleaved in a similar manner than C99 and also showed an increased processive cleavage in the POPC bilayer. Therefore, the observed differences in the processive cleavage seem to be independent of the substrate and solely dependent on the protease environment.

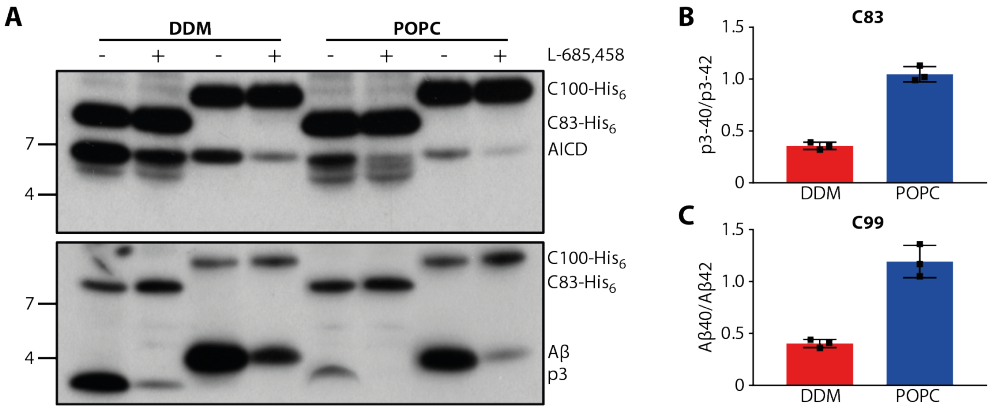

Figure 3.2.5: Cleavage of APP C83 by PSH. (A) Immunoblotting for AICD and Aβ and p3 (Aβ22-35) after incubation of $C100\text{-}His_6$ and $C83\text{-}His_6$ with PSH in DDM micelles and POPC vesicles at 37 °C over night. (B, C) $p3_{40}/p3_{42}$ ratio (B) and $Aβ_{40}/Aβ_{42}$ ratio (C) produced from $100\text{-}His_6$ and $C83\text{-}His_6$ by PSH respectively analyzed by ECL-IA. Data are represented as mean ± SD (n = 3 biological replicates, adapted from Feilen *et al.* (2022)).

3.2.5 PSH inhibtion by GSIs

It was shown that PSH is inhibited by TSA GSI L-685,458 even though rather high concentrations are needed to achieve proper inhibition. Furthermore, several studies utilized different other GSIs to inhibit PSH cleavage (Li *et al.*, 2013; Dang *et al.*, 2015; Naing *et al.*, 2015) but a systematic analysis of the inhibition profile is missing so far.
First, the inhibition profile of L-685,458 and of its biotinylated derivative Merck C was assessed in DDM micelles and POPC bilayer. Both GSIs were able to inhibit PSH in both conditions but for L-685,458 lower molecular concentrations were

needed than for Merck C (figure 3.2.6). Furthermore, the inhibition of PSH by both inhibitors was weaker in DDM micelles than in the POPC bilayer, indicating that the inhibitor binding site is less well formed in DDM micelles.

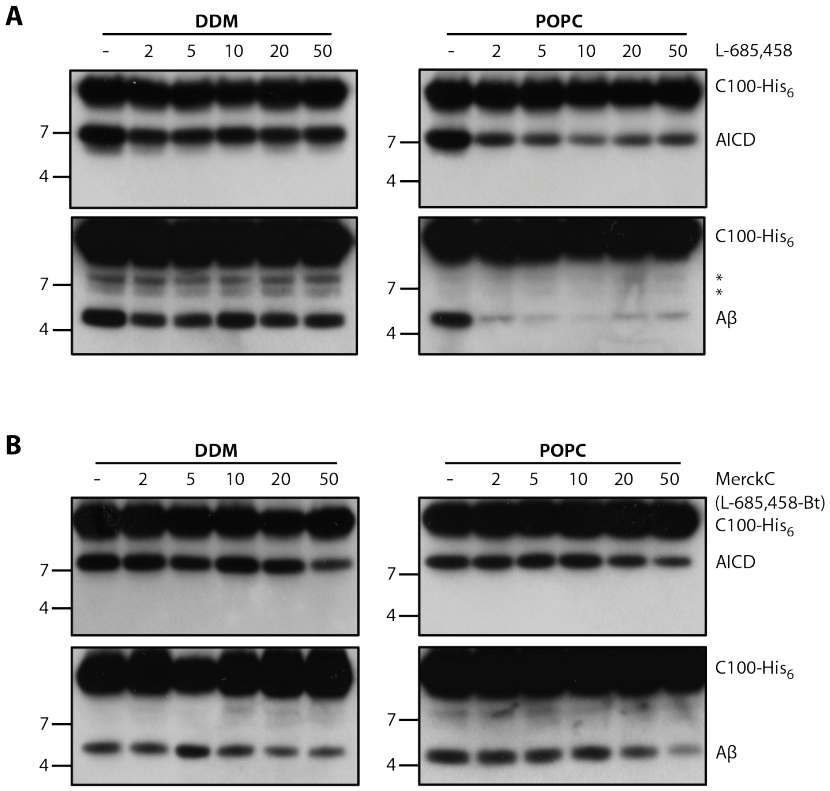

Figure 3.2.6: PSH inhibition profiles. Inhibition of PSH cleavage in DDM micelles and POPC vesicles by increasing concentrations of L-685,458 (A) and Merck C (B) analysed by immunoblotting for AICD (Y188) and Aβ (2D8) after incubation with C100-His_6 at 37 °C over night. The asterisks mark two PSH-independent substrate degradation bands (adapted from Feilen *et al.* (2022)).

In addition, the capability of different TSA and non-TSA GSIs to inhibit PSH was evaluated in the POPC bilayer at pH 7.0. The two TSA GSIs L-685,458 and III-31C inhibited PSH activity at high molar concentrations (20 μM). In contrast all four tested non-TSAs (DAPT, LY411575, Begacestat and MRK-560) did not inhibit PSH at the same high concentration (figure 3.2.7). The low potency of TSAs to inhibit PSH indicate that the binding site of TSA within PSH might be somewhat different than in γ-secretase and maybe important interactions are missing. The inability of non-TSAs in inhibiting PSH indicate further that the binding sites for non-TSAs are not existing in PSH or the interactions are very weak and non-TSAs might only transiently bind to PSH.

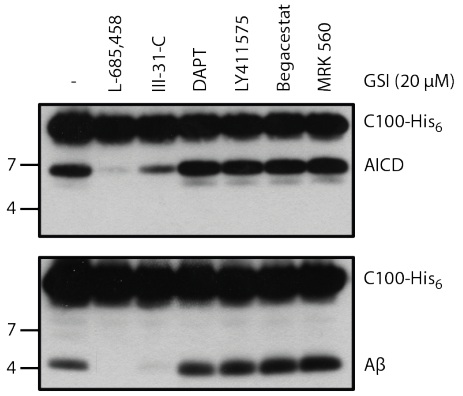

Figure 3.2.7: PSH inhibition by TSAs and non-TSAs. Inhibition of PSH cleavage in POPC vesicles by TSA and non-TSA GSIs assessed by immunoblotting for AICD (Y188) and Aβ (2D8) after incubation with C100-His$_6$ at 37 °C over night (adapted from Feilen *et al.* (2022)).

3.2.6 Inhibitor affinity precipitation

The increased processivity of PSH in a bilayer environment is indicative of a more stable enzyme–substrate interaction and a stabilized PSH conformation under this condition. Additionally, the lower potency of TSAs in DDM micelles further indicate that the active site might be destabilized in the micelles. To test whether and how the POPC bilayer might influence the conformation of the PSH active site, inhibitor affinity precipitation with Merck C was performed. Merck C captured PSH in DDM and POPC environment. This specific binding of Merck C to PSH was competed by the parental compund L-685,458 and the competition of Merck C binding in the DDM environment by the parental compound was less effective than in the POPC bilayer. In the POPC environment ∼10-fold more PSH was specifically captured by Merck C compared to the DDM environment (∼0.74% versus ∼0.05%).

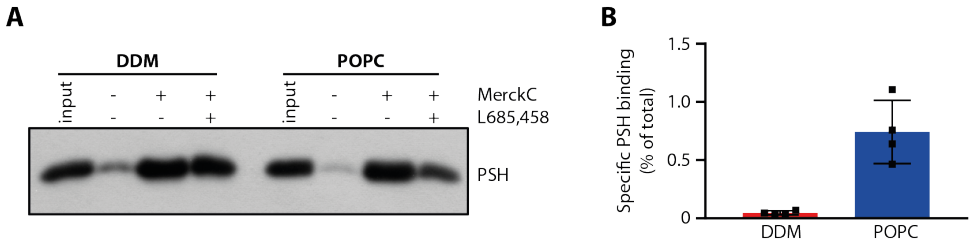

Figure 3.2.8: PSH inhibitor affinity precipitation. (A) Immunoblotting for PSH (6F4) after inhibitor affinity precipitation of PSH in DDM micelles and POPC bilayer with Merck C. Specificity of Merck C binding was controlled by competition with the parental compound L-685,458. The input represents 2.5% of total PSH. (B) Quantitation of specific PSH binding in DDM micelles (red) and POPC bilayer (blue). Data are represented as mean ± SD (n = 4 biological replicates, adapted from Feilen *et al.* (2022)).

Therefore, together with the inhibition profile data for L-685,458 and Merck C, these data show that POPC seems to stabilize the geometry of the active site resulting in the increased processivity observed in this environment (figure 3.2.8).

3.2.7 Molecular dynamics simulation of PSH in DDM and POPC environment

The biochemical data on PSH in a POPC bilayer indicate that the active site of PSH is stabilized and that most likely the whole PSH structure might be stabilized resulting in increased processivity. In a collaborative approach, Shu-Yu Chen and Martin Zacharias from the Technical University Munich, performed MD simulations on a PSH homology model to investigate how DDM and POPC influence the structural dynamics of PSH (and its active site).
Since structural information on the PSH–substrate complex are missing, an homology model way built based on the available cryo-EM structure of γ-secretase in complex with C83 (PDB 6iyc, (Zhou *et al.*, 2019)). The PSH model showed structural features which were also found in the γ-secretase–C83 complex but not in the substrate-free (apo) PSH structure (figure 3.2.9A). C-terminal of PSH TMD6 a conformation transition was observed, resulting in the formation of an additional small TMD formed by residues H171-E177, called TMD6a. Furthermore, residues preceding the catalytic aspartate in TMD7 (A213-G217) form a β-strand called β2. This β-strand is part of a small anti-parallel β-sheet with a β-strand (β3, V50-K54) formed C-terminal of the ε-cleavage sites in C83 (figure 3.2.9B). Backbone interactions with residue Q272 preceding TMD9 stabilizes this β-sheet. The positioning of TMD6a in the homology model is stabilized by a salt bridge between R70 in TMD3 and E181 in THD6a (figure 3.2.9C). This salt bridge replaces the hydrogen interaction between Y159 in TMD3 and R278 in TMD6a in the γ-secretase–C83 structure (figure 3.2.9D).
Molecular dynamics simulations performed with the substrate-bound (holo) PSH model in DDM and POPC environment revealed differences in the geometry of the active site. In the POPC bilayer, PSH was sampled more frequently in a hydrolysis-compatible conformation, meaning a Cγ-Cγ distance between the catalytic aspartates D162 and D220 below 7 Å (figure 3.2.10A). The shorter Cγ-Cγ distance not only brings the two catalytic aspartates closer together and closer to the substrate but also allows the positioning of one water molecule between the catalytic aspartates and C83 (figure 3.2.10C).

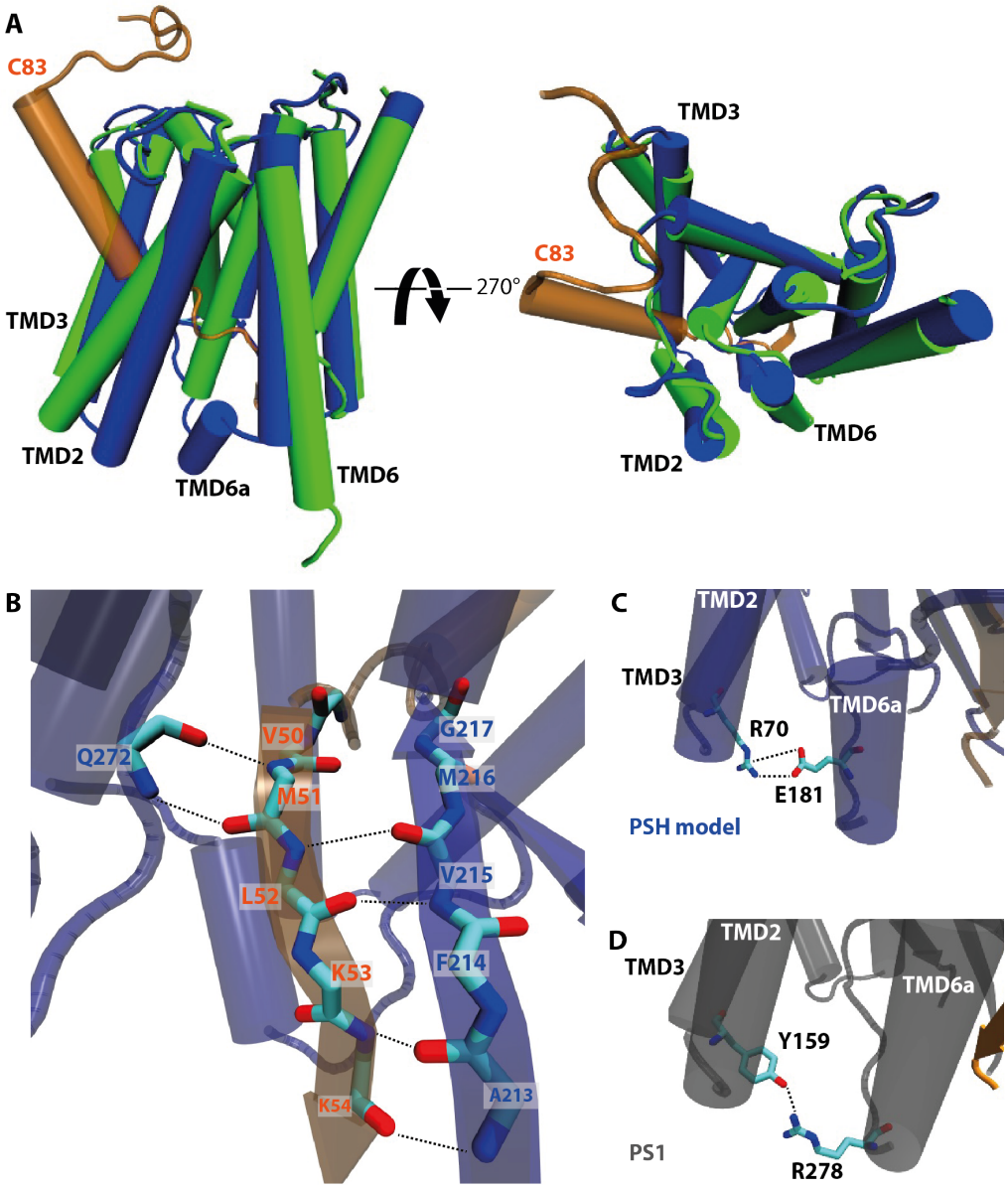

Figure 3.2.9: PSH homology model. (A) Side (left panel) and top (right panel) view of the PSH homology model (blue) aligned with the crystal structure of PSH (PDB 4HYG) in the apo form. The APP C83 substrate is shown in orange. (B) Enlarged view on the hybrid β-sheet formed between C83 (orange) and PSH (blue) in the homology model. (C) Interaction between R70 in TMD3 and E181 in TMD6a in the C83-bound PSH model. (D) Interaction between Y159 in TMD3 and R278 in TMD6a in C83-bound γ-secretase cryo-EM structure (PDB 6IYC) (adapted from Feilen *et al.* (2022)).

The larger Cγ-Cγ distance in the DDM environment results in the drainage of more than one water molecule from the cytosol into the gap between the catalytic aspartates which disturbs the catalytic mechanism (figure 3.2.10B). The differences in the Cγ-Cγ distance between the two environments observed in the MD simulations is in the line with the experimental data on inhibitor potency and PSH affinity precipitation in both environment. The biochemical data already suggested that DDM alters the geometry of the active site (see 3.2.5 and 3.2.6).

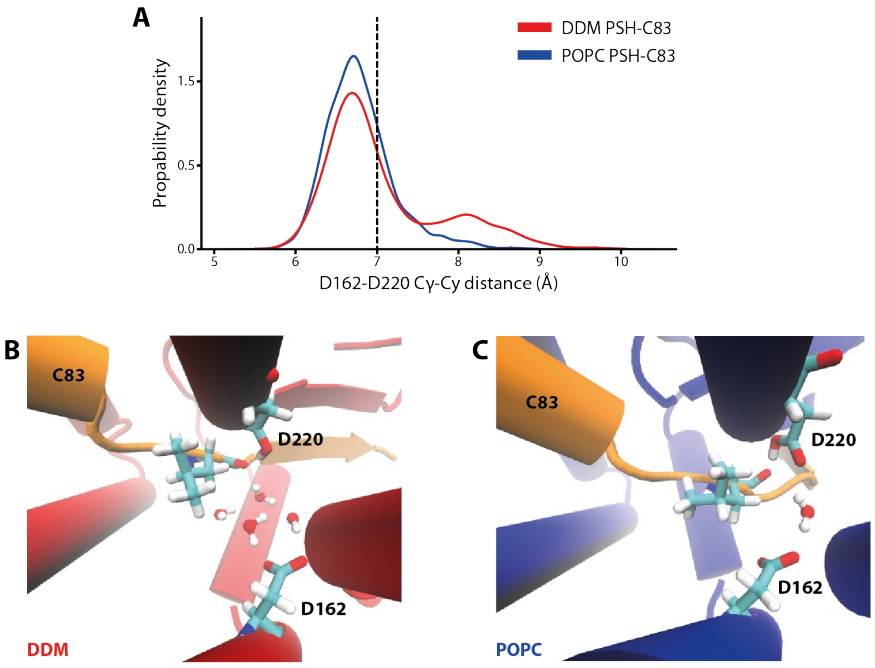

Figure 3.2.10: PSH active site geometry. (A) Histogram of Cγ-Cγ distances between PSH D162 and D220 sampled in DDM micelles (red) and POPC bilayer (blue). Snapshot of the active site of PSH in DDM (B) and POPC (C) environment with water molecules accessing this cavity (adapted from Feilen *et al.* (2022)).

3.2.8 Structural elements of the PSH–substrate complex

Sequence alignments of PSH with PS1 and the PSH homology model suggest that PSH residues A213 to G217 form a β-strand (β2) and residues H171 to E177 C-terminal of TMD6 form the small helix TMD6a. These were previously already identified as structural important features in the γ-secretase–substrate complexes (Yang *et al.*, 2019; Zhou *et al.*, 2019). To investigate whether these putative structural elements exist in PSH and have a functional role, mutational analysis were performed and the activity of the mutant PSH was compared to the WT PSH in DDM and POPC environments.

For the β2-strand, residues A213, F214 and V215 were each mutated to prolines and the β-strand was deleted from A213 to M216 and from A213 to G217, respectively. In both environments, the single proline mutations as well as the β-strand deletions strongly decreased the cleavage of C99 by PSH. Only in the POPC environment some activity for A213P was observed. Since A213 is located at the beginning of the putative β-strand, a mutation at this position might influence the PSH activity to a lesser extend than proline mutations within the β-strand.

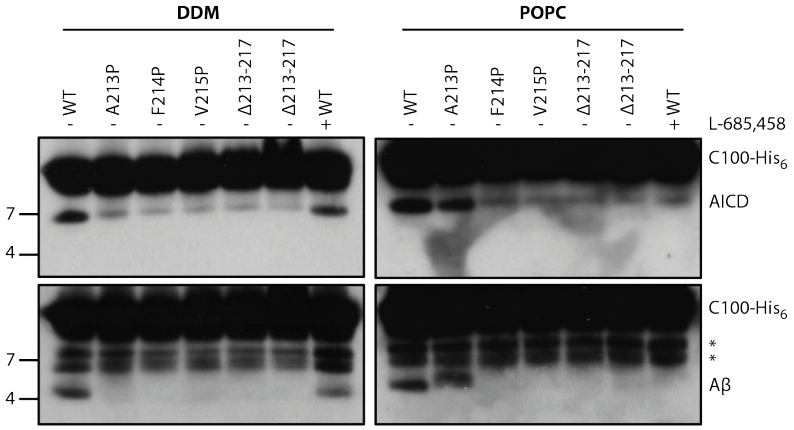

Figure 3.2.11: Activity of PSH β2-strand mutants. Immunoblotting for AICD (Y188) and Aβ (2D8) after incubation of C100-His_6 with WT and mutant PSH in DDM micelles and POPC vesicles at 37 °C over night. The asterisks mark two PSH-independent substrate degradation bands (adapted from Feilen *et al.* (2022)).

Four residues of TMD6a (M172, I173, L175 and A176) form a hydrophobic patch which is in contact with substrate residues at the ε-cleavage site region. To test whether these residues are also functional important, they were mutated to the charged aa lysine to disrupt the hydrophobic patch and the activity of mutated PSH was assesses in DDM and POPC environment. All four lysine mutants showed a completely abolished activity towards C99 in DDM micelles and the POPC bilayer.

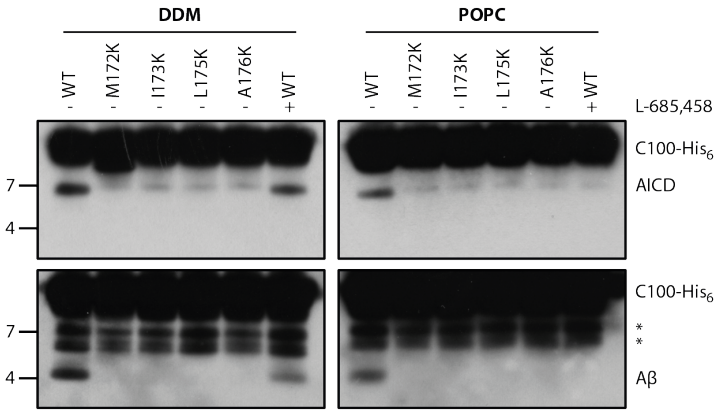

Figure 3.2.12: Activity of PSH TMD6 mutants. Immunoblotting for AICD (Y188) and Aβ (2D8) after incubation of C100-His_6 with WT and mutant PSH in DDM micelles and POPC vesicles at 37 °C over night. The asterisks mark two PSH-independent substrate degradation bands (adapted from Feilen *et al.* (2022)).

These results show that the aa residues of the β2-strand as well as of TMD6a are of functional importance. Furthermore, this strongly suggest that these two structural elements are indeed formed in the PSH–substrate complex and of functional relevance there.

3.2.9 Cleavage of full-length APP

The cleavage of APP by γ-secretase requires its previous shedding by either α- or β-seretase to fit under the large Nct ectodomain of the γ-secretase complex. Since PSH is not forming a complex with any accessory protein, no "lid" might hinder the cleavage of full-length (fl) APP (bearing the Swedish mutation). To test this hypothesis, flAPP was incubated with DDM-solubilized and POPC-reconstituted PSH. Interestingly, PSH differentially cleaved flAPP depending on the environment. In DDM micelles, PSH was not able to cleave flAPP and no cleavage products (AICD and Aβ) were detected (figure 3.2.13). In the POPC bilayer, flAPP was cleaved by PSH resulting in the release of a fragment which corresponds to an APP CTF. This cleavage was not inhibited by L-685,458 but by the PSH aspartate mutant D162/220A. The inhibition of this cleavage by the aspartate mutants indicates that the cleavage is dependent on the catalytic activity of PSH. It is expected that the inhibitor L-685,458 should also show an inhibition of this cleavage but this is not observed here. The reason for this needs to be elucidated further. Furthermore, the production of AICD and Aβ-peptides was observed which presumably arise from the generated CTF (figure 3.2.13). One should note that the presumable cleavage site within the APP ectodomain and the active site of PSH are far away from each other and on opposite sites of the lipid bilayer. The exact cleavage site for the CTF generation and the exact mechanism of this cleavage needs to be elucidated in future.

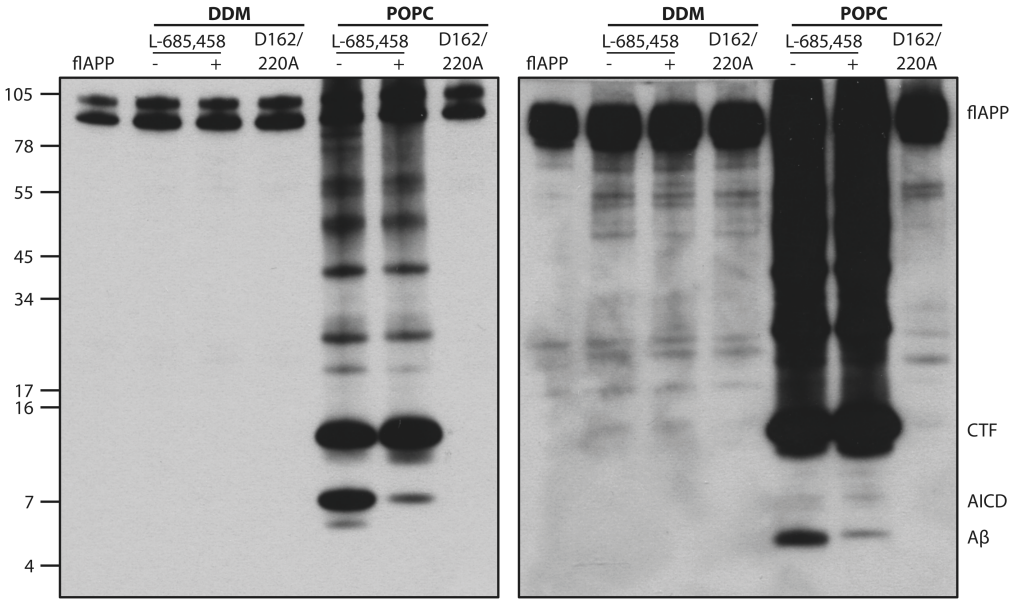

Figure 3.2.13: Cleavage of flAPP by PSH. Immunoblotting for AICD (Y188) and Aβ (2D8) after incubation of flAPP with PSH in DDM micelles and POPC vesicles at 37 °C over night.

3.2.10 Structure prediction of PSH–substrate complexes

The structure information on the PSH-C83 complex used in this study, rely on the building of an homology model. Model building strongly relies on the quality of the input data and is therefore also prone to misinterpretation. But the biochemical validation of the two important structural elements TMD6a and β2 strongly support that the homology model presented here might be true (see 3.2.8). The AI system AlphaFold is a tool which can predict the 3D structure of proteins based on their aa sequence (Jumper *et al.*, 2021; Tunyasuvunakool *et al.*, 2021; Varadi *et al.*, 2022) and its latest development AlphaFold-Multimer allows now also the prediction of 3D structures of protein complexes (Evans *et al.*, 2022). Therefore, AlphaFold-Multimer was used to predict the structure of PSH in complex with C83 or C99 based on the fl aa sequences of PSH, C83 and C99.

In both predicted PSH–substrate complexes, the respective substrate is located in between TMD2 and 3 and protudes into the catalytic cleft in between the two catalytic aspartates D162 and D220 (figure 3.2.14). Furthermore, for both enzyme–substrate complexes an additional small TMD6a, C-terminal of TMD6, is predicted and also an antiparallel β-sheet formed by two β-strands from PSH at is cytosolic site. AlphaFold also estimates the prediction confidence for each residue (pLDDT). For the PSH predictions, most regions had a pLDDT value above 70 (figure 3.2.14C, D), meaning that these regions are at least well predicted. The regions which were less well predicted ($50 \leq$ pLTDD ≤ 70) correspond mainly to the loop regions of PSH. For parts of the large loop connecting TMD6 and 7 the pLDDT value was even below 50 which indicates that these regions are disordered. For the C83 and C99 predictions the pLDDT value was mainly for all residues below 50 (figure 3.2.14C, D) making an interpretation of these predictions difficult.

Even though the pLDDT value for the substrate predictions was low, the general features of both enzyme–substrate complexes will still be described. In comparison to the PSH–C83 homology model, several differences are observed. While in both predicted structures two β-strands for PSH are observed (β1 – M187-P191 and β2 – A213-G217), only β2 was found in the homology model. Interestingly, aa that form this β-strand were the same in the predicted structures as well as in the homology model (A213-G217, table 3.2.1). Furthermore, the predicted structures did not show a β-strand within the respective substrate which was found in the homology model (β3, V50-K54). In the predicted structures, residues H171-T182 form TMD6a and similarly, residues H171-E177 in the homology model form the small helix TMD6a (table 3.2.1). The homology model and the structure predictions largely differ in the position at which the unwinding of the substrate helix starts. In the model, the helix unwinds after V46, in the predictions the helix unwinds after Y57 (C83) or

T58 (C99), respectively (table 3.2.1).

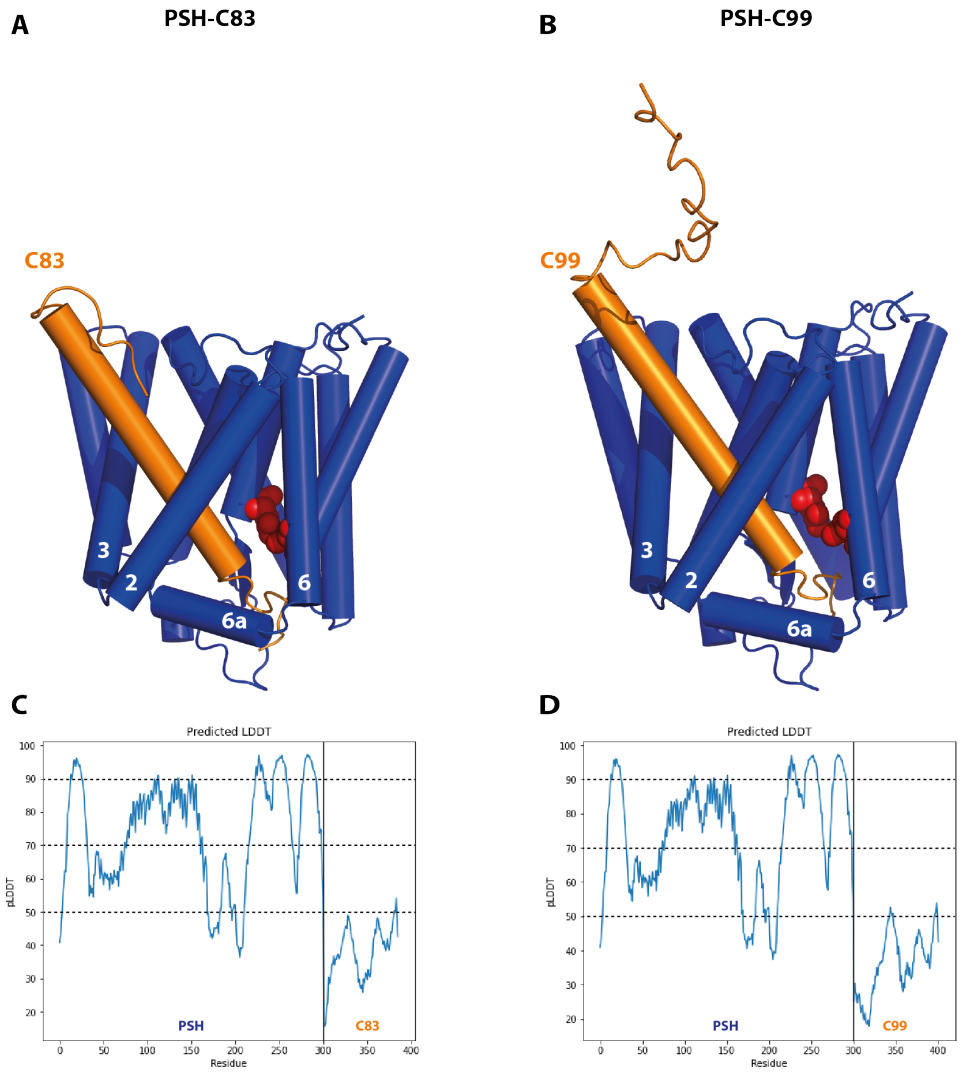

Figure 3.2.14: Prediction of PSH–substrate complexes. AlphaFold-Multimer prediction of PSH–C83 (A) and PSH–C99 (B) complexes. PSH is depicted in blue and the substrates (C83/C99) are depicted in orange. Only C-terminal truncated substrates are shown (C83: L17-V66, C99: D1-V66). The red spheres show the catalytic aspartates. pLDDT values for each residue of the predicted PSH–C83 (C) and PSH–C99 (D) structures. The dotted horizontal lines represent pLDDT values of 90, 70 and 50, respectively and the vertical line mark the end of PSH residues.

The predicted PSH–substrate structures reveal show similar structural features as the homology model and might in addition to this homology model help to guide new experiments like further mutational analysis. This is especially interesting for the PSH–C99 complex which can not be modeled by homology modeling because of missing structural information on the first 16 N-terminal aa residues.

Table 3.2.1: Position of structural elements. Amino acid positions of structural elements β1, β2, β3 and TMD6a as well as beginning of substrate helix unwinding of predicted PSH–substrate complexes and homology model.

	PSH–C83	PSH–C99	homology model
β1	M187-P191	M187-P191	–
β2	A213-G217	A213-G217	A213-G217
β3	–	–	V50-K54
TMD6a	H171-T182	H171-T182	H171-E177
unwinding	Y57	T58	V46

3.3 The hybrid β-sheet of γ-secretase–substrate complex

The structural investigations of γ-secretease with two of its substrates identified a newly formed hybrid β-sheet at the cytosolic site of the complex, composed of two β-strands (β1 (Y288-S290) and β2 (R377-L381)) from γ-secretase and one β-strand (β3) from the respective substrate (Yang *et al.*, 2019; Zhou *et al.*, 2019). The subsequent functional analysis revealed that – at least – the β-strands formed in the γ-secretase are of functional importance (Yang *et al.*, 2019; Zhou *et al.*, 2019).

3.3.1 The β2-strand of γ-secretase

The afore mentioned studies investigated the functional importance of the γ-secretase β-strands by deleting the respective aa. Since a deletion of several aa within a protein might result into larger structural changes, the role of β2-strand was investigated here by additionally mutating K380 to proline which should disrupt the β-strand and the hydrogen bonds within the hybrid β-sheet.
First PS1 K380P and PS1 Δ377-381 were analysed in HEK293 cells. To this end, PS1 K380P and PS1 Δ377-381 as well as WT PS1 and PS1 M292D, a mutant PS1 which is not endoproteolysed but processes APP CTFs like WT PS1 (Steiner *et al.*, 1999b), were stably expressed in HEK293 cells stably overexpressing Swedish (sw) mutant APP and lacking endogenous PS1 and 2 (HEK293/sw PS1/2 dKO). When assessed for γ-secretase complex assembly and PS1 endoproteolysis, PS1 K380P and PS1 Δ377-381 showed a normal complex assembly and normal maturation of NCT (figure 3.3.1A). But both mutants were defective in their endoproteolysis. While PS1 Δ377-381 was not endoproteolysed at all, PS1 K380P showed some residual endoproteolysis but most of the PS1 remained uncleaved (figure 3.3.1A). Next, the processing of APP CTFs by these mutants was analysed. PS1 K380P

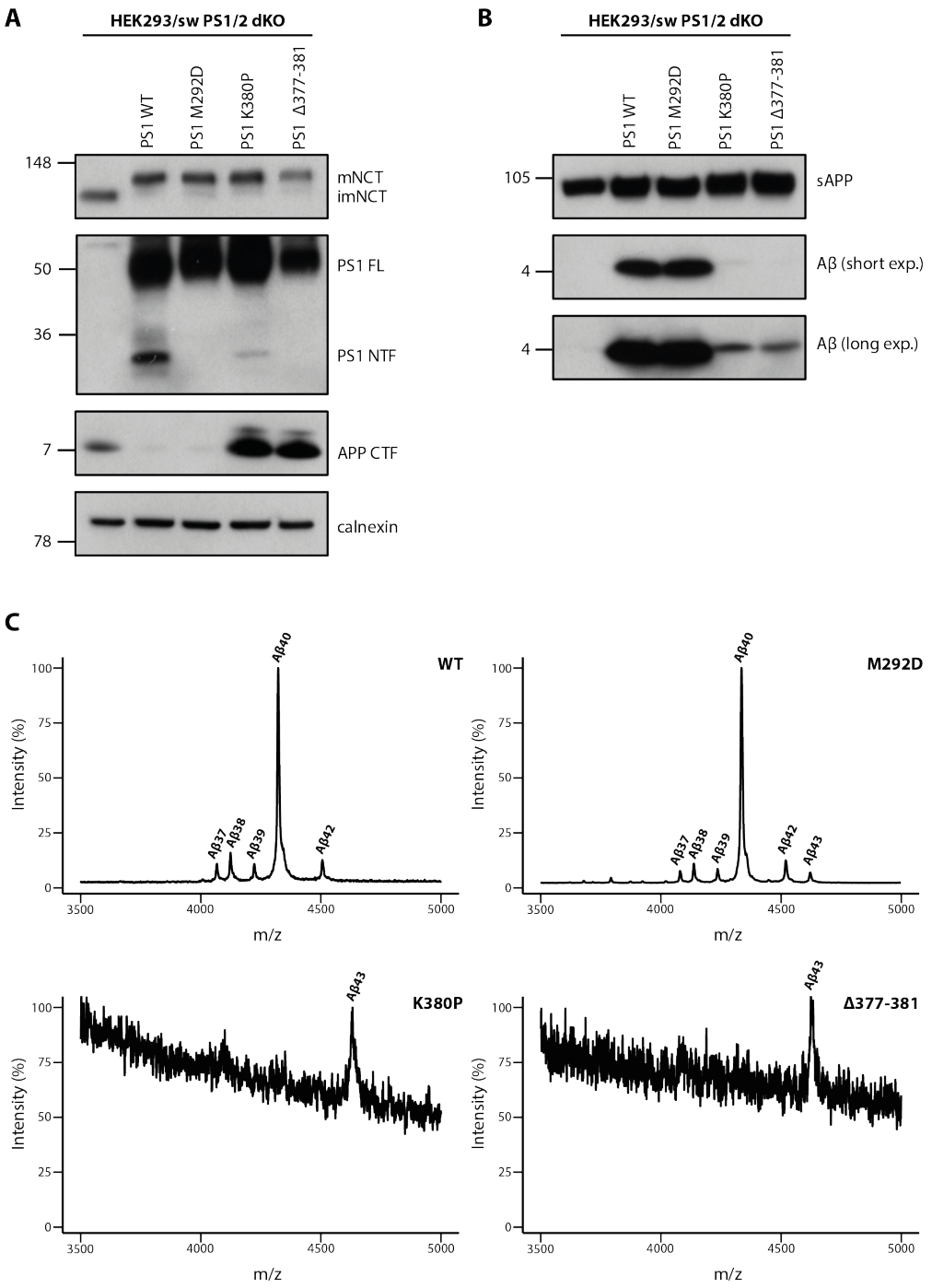

Figure 3.3.1: Analysis of endoproteolysis and APP processing of PS1 mutants. (A) PS1 endoproteolysis and NCT maturation of mutant PS1 analyzed by immunoblotting. WT and mutant PS1 were overexpressed in HEK293/sw PS1/2 dKO cells. (B) Secretion of sAPP and Aβ from HEK293/sw PS1/2 dKO cells overexpressing WT and mutant PS1 into the medium analyzed by immunoblotting. The lower panel shows a longer exposure of the Aβ immunoblot. (C) MALID-TOF analysis of immunoprecipitated Aβ species from conditioned media of HEK293/sw PS1/2 dKO cells overexpressing WT and mutant PS1.

and PS1 Δ377-381 showed an accumulation of APP CTFs in the cell lysates (figure 3.3.1B), indicative of impaired cleavage by these PS mutants. In line, both mutants showed a strongly reduced secretion of Aβ into the medium of the cells (fig-

ure 3.3.1B). But in contrast to previously published results on cleavage of C99 by PS1 Δ377-381 in an cell-free assay approach (Zhou *et al.*, 2019), PS1 Δ377-381 is at least partially active in cells. The secreted Aβ was further analysed by IP-MS MALDI-TOF. In both mutants the secretion of $Aβ_{43}$ was observed (figure 3.3.1C). The impaired endoproteolysis as well as the impaired APP cleavage and secretion of $Aβ_{43}$ resemble the strong, $Aβ_{43}$-producing loss-of-function FAD PS1 mutants (Kretner *et al.*, 2016; Trambauer *et al.*, 2020).

The discrepancy in the activity of PS1 Δ377-381 towards APP between this study and previous published data (Zhou *et al.*, 2019) might arise from the different experimental setup. To rule out this possibility, cell-free assays were performed with PS1 K380P and PS1 Δ377-381. C99-based recombinant C100-His_6 substrate was incubated with CHAPSO-solubilized HEK293/sw PS1/2 dKO membranes (expressing the respective PS1 variant) over night at 37 °C. As already observed in the cellular system, both mutants were strongly impaired in cleavage of C100-His_6 and for PS1 Δ377-381 no activity could be detected by immunoblotting, at least for Aβ production (figure 3.3.2A). A faint AICD band for the Δ377-381 mutation might indicate that this mutation also has a strongly decreased activity. It is possible that the reduced activity of PS1 Δ377-381 is only hardly assessable with the methods used here or that in the cell-free system the reduction is stronger than in the cellular system. Strikingly, PS1 K380P was not inhibited by L-685,458 at the same concentration (2 µM) used for the other PS1 constructs. It might be possible that the binding of L-685,458 to PS1 K380P is reduced since this residue stabilizes the interaction with the GSI by two backbone hydrogen bonds (Yang *et al.*, 2021). Furthermore,

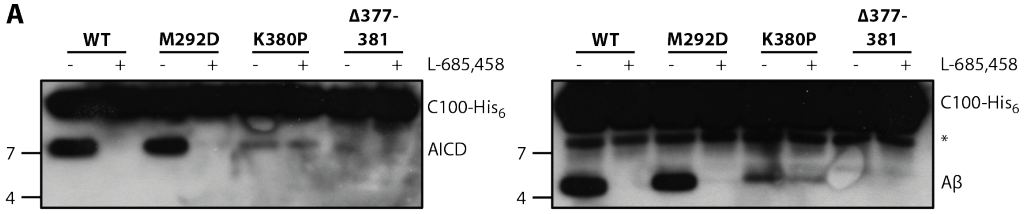

Figure 3.3.2: Activity of PS1 β2-strand mutations *in vitro*. Immunoblotting for AICD (penta-His) and Aβ (2D8) after incubation of C100-His_6 with CHAPSO-solubilized γ-secretase complexes containing WT and mutant PS1 at 37 °C over night. The lower panels show a longer exposure.

the AICD species generated by these mutants were analysed by MALDI-TOF. No AICD was detected for PS1 Δ377-381 but for PS1 K380P. PS1 K380P exclusively cleaves after L49 (ε49), releasing AICD50 (figure 3.3.3). This shows that PS1 K380P is not only impaired in the processivity but also preferentially cleaves in the $Aβ_{40}$ product line.

Taken together, the β2-strand of γ-secretase is important for the endoproteolysis of PS and for the cleavage of γ-secretase substrates. Thereby it is not only affecting

the processive cleavage but also the Aβ product line preference.

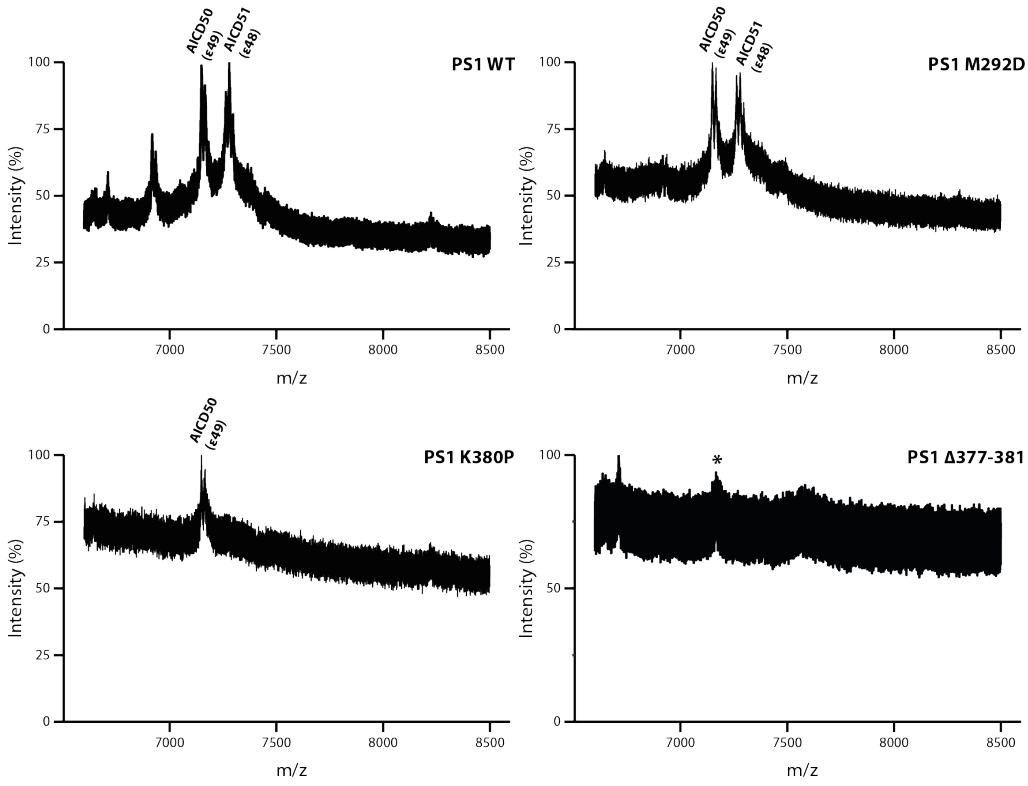

Figure 3.3.3: AICD generation by PS1 β2-strand mutations *in vitro*. MALDI-TOF analysis of immunoprecipitated AICD species generated produced by CHAPSO-solubilized γ-secretase complexes containing WT and mutant PS1 *in vitro*. The asterisk marks a peak that was also found in the inhibitor control.

3.3.2 The β-strand of APP

Another part of the hybrid β-sheet in the γ-secretase–substrate complex is the β3-strand formed C-terminal of the cleavage site of the substrate, which is involved in the helical unfolding at the scissile bond. The influence of this β-strand on APP cleavage was assessed in an cell-free approach. To this end, cleavage of mutant C100-His_6 bearing proline mutations at aa M51 and L52 was compared to cleavage of WT substrate by CHAPSO-solubilized γ-secretase. For M51P no AICD and Aβ fragments were detected figure 3.3.4A) indicating that APP M51P is not cleaved at all by γ-secretase under these conditions. In contrast, for L52P Aβ and AICD fragments were detected but no inhibition of the AICD cleavage was observed (figure 3.3.4A). This indicates that L52P is not only cleaved by γ-secretase but also by another protease. To analyse this, the cell-free assay was additionally performed with CHAPSO-solubilized membranes from HEK293 PS1/2 dKO cells and for L52P again a cleavage fragment corresponding to AICD was identified (figure 3.3.4A). This shows that L52P is not only cleaved by γ-secretase but also by (an)other – so far not

identified – protease(s), perhaps a rhomboid IMP which also cleaves type I TMD proteins. To further elucidate on the cleavage of WT and mutant APP, the cell-free assay was additionally performed with purified γ-secretase coomplex composed of PS1, NCT, APH-1a and PEN-2 (provided by Lucía Chávez-Gutiérrez). All three APP constructs were cleaved by the purified γ-secretase complex with WT being the most efficiently cleaved followed by L52P and M51P (figure 3.3.4B). In contrast to the cell-free assay performed with CHAPSO-solubilized membranes, also cleavage fragments for M51P were observed but with a very low abundance. Since this cleavage assay is performed in a pure system, only γ-secretase-dependent cleavage fragments were observed. Analysis of Aβ species by Tris-Bicine urea SDS-PAGE (figure 3.3.4C) did not show large differences between the Aβ species generated by from WT and L52P.

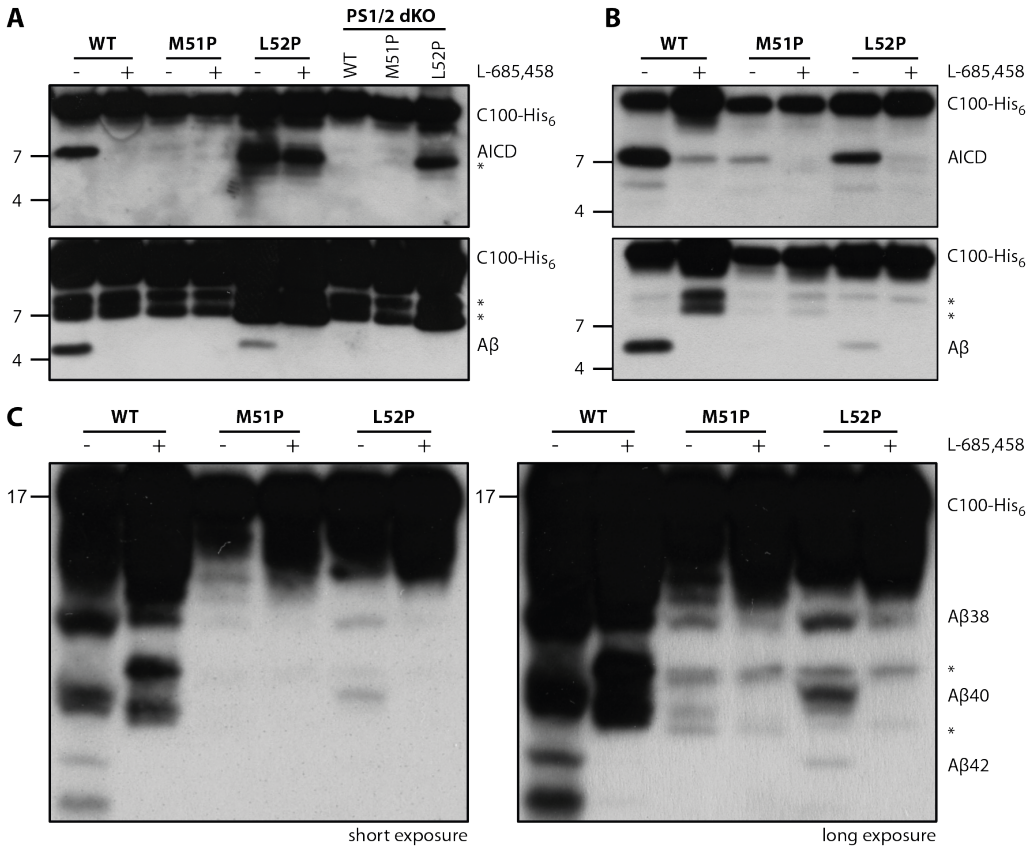

Figure 3.3.4: Cleavage of APP β3-strand mutants. (A) Immunoblotting for AICD (penta-His) and Aβ (2D8) after incubation of WT and mutant C100-His_6 with CHAPSO-solubilized γ-secretase at 37 °C over night. The asterisks mark two γ-secretase-independent substrate degradation bands. (B) Immunoblotting for AICD (penta-His) and Aβ (2D8) after incubation of WT and mutant C100-His_6 with purified γ-secretase at 37 °C over night. The asterisks mark two γ-secretase-independent substrate degradation bands. (C) Immunoblotting for Aβ species (2D8) produced by purified γ-secretase from WT and mutant C100-His_6 in short (left) and long (right) exposure.

AICD species were analyzed from cell-free assays performed with purified γ-secretase. Due to the low abundance of cleavage fragments of M51P it was not possible to detect AICD species in mass spectrometry experiments. For the WT the two expected AICD species AICD50 and AICD51 were identified, corresponding to cleavage at ε49 and ε48 (figure 3.3.5). L52P is exclusively cleaved after T48 (ε48) releasing AICD51 (figure 3.3.5) which has already been previously reported for this well-known FAD mutation (L723P, (Dimitrov *et al.*, 2013)).

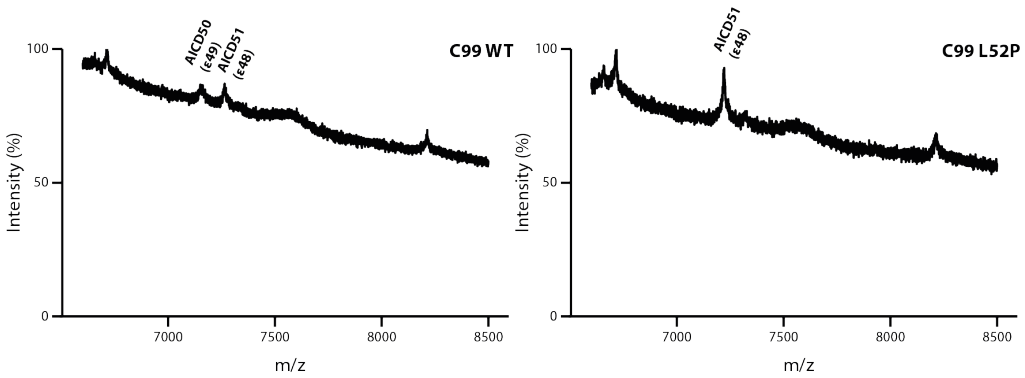

Figure 3.3.5: AICD generation from APP β3-strand mutants. MALDI-TOF analysis of immunoprecipitated AICD species generated produced by purified γ-secretase from WT C100-His_6 and C100-His_6 L52P

4 Discussion

This dissertation focuses on two presenilin IMPs, the archaeal presenilin homolog PSH and the human γ-secretase. In the first part, the influence of a detergent environment versus a lipid bilayer on the activity and active site geometry of PSH were investigated. This was accompanied by studies on the importance of two structural elements of the PSH–substrate complex (β2-strand and TMD6a). The second part focused on the structurally and functionally important hybrid β-sheet in the γ-secretase–substrate complex.

4.1 PSH as a model protease for γ-secretase

The discovery of PSH in 2010 (Torres-Arancivia *et al.*, 2010) offered new possibilities to study the activity of presenilin IMPs since PSH is in – contrast to PS – active without accessory proteins. And even though the cleavage of APP-derived substrates by PSH was analysed in several studies (Dang *et al.*, 2015; Clemente *et al.*, 2018; Naing *et al.*, 2018), the results on the cleavage differed dependent of the experimental designs of these studies. Dang *et al.* (2015) used a C99 construct with an N-terminal MBP-fusion and a C-terminal octa-His tag and could show that PSH processes C99 in a similar manner than γ-secretase. In contrast, Naing *et al.* (2018) used a C100FRET construct and short C99 TMD-based constructs N-terminally fused to MBP and C-terminal to a SUMO-tag. These experiments showed a preferred cleavage at $A\beta_{42}$ over $A\beta_{40}$. This already indicates that the experimental set-up can strongly influence the cleavage by PSH. Furthermore, little is known about some basic characteristics of PSH. No study so far revealed whether PSH is endoproteolysed as PS or what topology it might have in its natural environment. Therefore it might still be possible that the natural PSH substrates are of type II topology and the cleavage of APP-based type I TMD substrates is an artefact of the *in vitro* system in which PSH can adopt both possible topologies.
This present study did also not focus largely on the basic characteristics of PSH since this would include studies in *M. marisnigri* and also the identification of natural PSH substrates. Nevertheless, inactivating the catalytic activity by alanine

mutants showed that PSH is – in contrast to PS – not endoproteolysed and in this aspect more reflecting the SPP proteases. In addition, the cleavage of the APP-based C99 substrate by PSH was confirmed in DDM micelles. Compared to γ-secretase the processivity of PSH towards C99 was reduced and longer Aβ species were generated as it was also observed in previous studies (Naing *et al.*, 2018). This study here could also show that PSH is not only able to cleave C99 but also another APP-based substrate C83 also in a similar manner than γ-secretase, making C83 another authentic but non-natural PSH substrate. Interestingly, the cleavage could be inhibited by TSA GSIs, inhibitors specifically designed to inhibit γ-secretase but higher concentrations were needed than for a proper inhibition of γ-secretase. Dang *et al.* (2015) already reported a high IC_{50} for PSH inhibition by another TSA GSI III-31C (10 µM). Furthermore, non-TSA GSIs were at the same high molecular concentration not able to inhibit PSH cleavage. This indicates that the binding sites for GSIs is structurally somewhat different and that potential interaction points might not exist in PSH. As it was shown for γ-secretase, both TSA and non-TSA inhibitors occupy a similar binding site at the active site of the enzyme, but TSA GSIs additionally protrude into the catalytic cleft (Yang *et al.*, 2021). Assuming that both types of GSIs bind in a similar way to PSH as they bind to γ-secretase, this further supports the hypothesis that inhibitor binding sites are missing within PSH resulting in the reduced activity of TSA GSIs and the complete abolished activity of non-TSA GSIs towards PSH. This is further supported by the observation that L-685,458 is less potently inhibiting PSH in the DDM micelles than in the POPC bilayer. The destabilized active site geometry in the detergent environment therefore not only weakens the enzyme–substrate interaction but also the enzyme–GSI interaction. This also helps to understand why the Merck C binding was less well competed by the parental compound L-685,458 in the DDM micelles in addition to a higher unspecific PSH binding to the strepativdin beads.

Even though PSH is able to cleave type I TMD proteins in the *in vitro* system and the cleavage of C83 and C99 strongly resembles the cleavage by γ-secretase, one can not rule out the possibility that PSH might be more SPP-like than PS-like. PSH is not endoproteolysed like PS and resembles more SPP in this aspect. Furthermore, a higher sequence conservation between PSH and SPP compared to PS1 and an evolutionary closer relation between PSH and SPP is reported (Raut *et al.*, 2021). Theoretically, it might also be possible that PSH is found in both topologies within the membrane of *M. marisnigri* and therefore might cleave type I and type II TMD proteins. Future studies on PSH in its natural environment and the identification of natural substrates are necessary to shed light on this. Nevertheless, the rather authentic cleavage of APP-based substrates by PSH releasing Aβ, p3 and AICD still makes PSH an interesting surrogate for γ-secretase cleavage, especially to study PS

functions in the absence of accessory proteins.

4.2 Effects of detergent and lipid environments on intramembrane proteolysis

Previous studies could already show that the lipid environment (Osenkowski *et al.*, 2008; Moin & Urban, 2012; Winkler *et al.*, 2012) and also the condition of the *in vitro* assay (Quintero-Monzon *et al.*, 2011) can strongly influence the activity of IMPs. Moin & Urban (2012) could show that the *E. coli* rhomboid IMP GlpG cleaves at different cleavage sites within its substrates depending on the *in vitro* assay system. Reconstituted in proteoliposomes, the cleavage sites were the same than the ones in *E. coli*. In contrast, GlpG cleaved its substrates at different cleavage sites when the cleavage was analysed in DDM micelles (Moin & Urban, 2012). Studies performed on γ-secretease cleavage in lipid membranes of various compositions (Osenkowski *et al.*, 2008) and different membrane thickness (Winkler *et al.*, 2012) showed a complex modulation of enzyme activity by the lipid environment. Not only the total activity of γ-secretase but also the processivity strongly depends on membrane lipid composition and thickness. But little did these studies reveal about the mechanism underlying the modulation of IMP activity by the lipid environment. The membrane environment seem to restrict the helical conformation of the substrate which is only opened when the substrate enters the active site of the enzyme. In contrast, the helical conformation is less strict in a detergent micelles which might explain the difference in cleavage site usage in GlpG (Moin & Urban, 2012).
PSH activity is dependent on the pH, showing an optimum at around pH 7.0-7.5 in DDM and POPC environment and a sharp drop in total activity at higher pH. The drop in total activity is accompanied by a decreased processvity and the generation of longer Aβ species. This was similarly observed for γ-secretease which is impaired in total activity as well as processivity at more alkaline pH (Quintero-Monzon *et al.*, 2011). Interestingly – in contradiction to the observed impaired processivity – $A\beta_{38}$ increased at alkaline pH for γ-secretase (Quintero-Monzon *et al.*, 2011).
Since the lipid environment can influence IMP activity, the influence of such an environment on PSH was also assessed. The experiments were all performed in POPC environment, the most abundant phospholipid in humans. Importantly, the POPC environment does not reflect the natural membrane environment of PSH, of which nothing is also known so far. In general, the backbone of archaeal phospholipids is glycerol-1-phosphate to which highly methylated isoprenoid chains are ether-linked which makes archaeal membranes quite thermally stable (Caforio & Driessen, 2017).

Since these lipids are commercially not available, it was not possible to perform experiments in an natural PSH environment. Therefore, the experiments were restricted to POPC vesicles. For both APP-based substrates C99 and C83 the lipid environment greatly enhanced the processivity of PSH compared to DDM micelles resulting in the release of shorter Aβ and p3 species, respectively. PSH was also active when reconstituted into vesicles composed of brain lipids and this environment enhanced the processive cleavage even more than the POPC environment. These data do not only show that the lipid environment per se is important for the activity of aspartyl intramembrane proteases but also the specific composition of this lipid environment can modulate the IMP activity.

Whether the lipid environment effect is mediated as a bulk effect or whether it involves direct protein–lipid interactions remains unclear. Structural investigations on different IMPs already revealed lipid molecules bound to the respective protease (Ben-Shem *et al.*, 2007; Lemieux *et al.*, 2007; Bai *et al.*, 2015b; Yang *et al.*, 2019; Zhou *et al.*, 2019). Since these lipid molecules were still bound after extensive purification of the proteases, it might be possible that these lipid molecules tightly interact with the respective protease. Especially for γ-secretase one lipid molecule was found to be located in between the TMD of NCT and several TMDs of APH-1 (Bai *et al.*, 2015b), further supporting a strong binding of some lipid molecules to the protease. Nevertheless, non of these studies investigated these protease–lipid interactions in depth nor biochemically identified a lipid binding site. It might be possible that the conformational stabilization of the enzyme–substrate complex (E-S) by the lipid environment is more related to a lipid bulk effect and that the interaction with specific lipids might fine tune the activity of the protease. Future studies are needed to unravel the protein–lipid interaction and its role in modulating IMP activity. In depth inspections of the MD simulations performed on the PSH–substrate complex (Feilen *et al.*, 2022) could already reveal some potential POPC binding sites – e.g. in the gap between the N-terminal part of the TMD of C83 and the C-terminal part of TMD3 – and these might be a good starting point for future investigations.

The remarkably increase in processivity in the POPC environment was supported by an increased stability of the active site geometry of POPC-reconstituted PSH. Already in the MD simulations a Cγ-Cγ distance shorter than 7 Å – which is here defined as a measure for a proteolyis-compatible active site geometry – was more frequently sampled in the POPC bilayer than in the DDM micelle. The larger Cγ-Cγ distance in the DDM environment results in a drainage of water molecules from the cytosol to the active site which disrupt important hydrogen-bond interactions. In contrast, the shorter Cγ-Cγ distance in the POPC bilayer squeezes out excess water molecules from the active site leaving only the one water molecule which is necessary for the hydrolysis reaction between the catalytic aspartates and the substrate. The

inhibitor affinity precipitation experiments using Merck C, a biotinylated derivative of the GSI L-685,458, could confirm the observations from the MD simulations. In the POPC bilayer, more PSH was precipitated by Merck C, indicating a stronger binding of Merck C to PSH in this environment. Since Merck C (and L-685,458) is directed to the active site of PSH the stronger binding reflects a more stabilized active site geometry in POPC.
Previous experiments with γ-secretase already observed cleavage differences in a micelle environment compared to a lipid raft-like membrane environment (Szaruga *et al.*, 2017). The lipid environment promoted the processive cleavage of γ-secretase by stabilizing the enzyme–substrate complex and facilitates the binding of shorter Aβ species to γ-secretase. The biochemical experiments in combination with the MD simulations in the present study now can explain these observation in more detail: the lipid bilayer stabilizes the conformation of the E-S and reduces conformational flexibility resulting in an increased processive cleavage.
In general, this study further supports the notion that the lipid environment is important for the activity of IMPs in general by stabilizing the active site geometry.

4.3 Cleavage of flAPP by PSH

For γ-secretase, it is known that substrates require a short ectodomain to fit under the NCT ectodomain and to be cleaved by γ-secretase. Since no such "lid" is knwon for PSH, it might be able to also directly cleave substrates with large ectodomains. For both environments – DDM micelles and POPC bilayer – no direct cleavage of flAPP into AICD and Aβ was observed. But unexpectedly, flAPP is shed by PSH in the POPC environment. The resulting CTF is then substrate for the canonical PSH cleavage. The exact mechanism of this non-canonical cleavage remains elusive especially since the APP cleavage site and the PSH active site are distantly located at opposite sites of the membrane plane. It might be possible that two PSH molecules that are differentially oriented act here together. First, flAPP is shed by PSH in a "SPP-like topology" resulting in the formation of a CTF. This CTF is then cleaved in by PSH which is inversely oriented ("PS-like topology") in the canonical way (figure 4.3.1). This combination of non-canonical shedding and canonical cleavage might be an artefact of the *in vitro* assay, in which both – the substrate and the enyzme – are found in both orientations. Interestingly, the non-canonical shedding was only observed in the POPC environment but not in DDM micelles. It might be that the stabilized active site geometry facilitates the shedding or that the conformation of the substrate is different in the POPC bilayer than in the DDM micelle. Such an influence of the substrate conformation on shedding was already previously

observed for the non-canonical shedding of TNFα by SPPL2a (Spitz *et al.*, 2020). Besides SPPL2a also SPPL3 can directly shed full-length substrates (Mentrup *et al.*, 2020) and also for γ-secretase a direct cleavage of APLP1 without prior ecotodomain shedding by either α- or β-secretase was reported (Schauenburg *et al.*, 2018) without further mechanistic explanation.

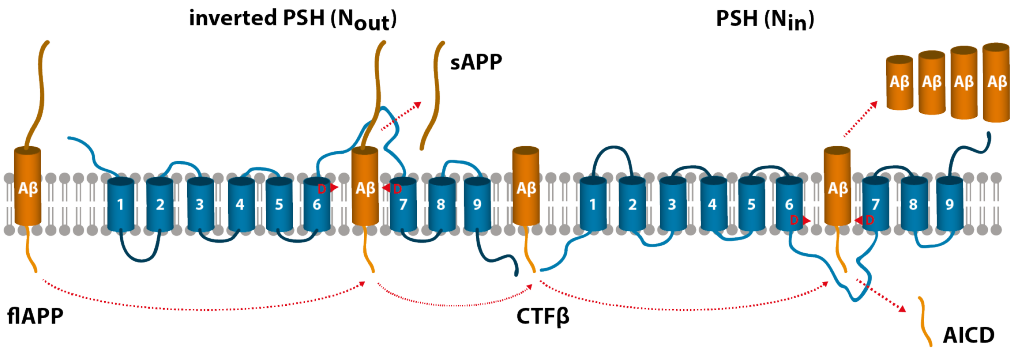

Figure 4.3.1: Model of APP shedding and cleavage by PSH. flAPP is first shed by PSH resulting in a CTF. This CTF is then further cleaved by a second PSH in an inverse topology releasing AICD and Aβ.

It might also be possible that the shedding and cleavage of flAPP does not require PSH in two orientations. The elution of flAPP from the beads after immunoprecipitation was performed in a buffer containing 1% SDS which might have resulted in the unfolding of the large APP ectodomain. As a consequence, this ecotodomain may also be able to fold into the active site of PSH and might be cleaved resulting in the CTF which is further cleaved by PSH.
It remains elusive why the non-canonical shedding by PSH is not inhibited by the GSI L-685,458 and it might be possible that the "SPP-like oriented" PSH molecules are also in a slightly different conformation. This conformation still allows the cleavage of APP but it impairs the inhibitor binding similar to the decreased inhibition of PSH in DDM micelles. Another possibility is that flAPP has a greater binding affinity for PSH than APP CTFs and/or L-685,458 and L-685,458 cannot compete with the flAPP binding. After the shedding, L-685,458 might then be able to compete with the resulting CTF. In this case, increased GSI concentrations might inhibit the non-canonical cleavage.
In a previous study by Dang *et al.* (2015) it was already shown that PSH is able to directly cleave a C99-based substrate with an N-terminal MBP-fusion in a DDM micelle. For this MBP-C99 cleavage no shedding of the substrate resulting in a CTF was reported and investigated. Maybe the afore mentioned unfolding of the APP ecotdomain might facilitate or allow the APP ectodomain shedding by PSH and maybe under certain experimental conditions APP can be directly cleaved by PSH

withoud prior shedding. Further work on this non-canonical cleavage is needed to understand if, how and under which conditions this mechanism takes place.

4.4 The substrate recognition/binding motifs of PSH

The work on PSH furthermore revealed that within the PSH–C83 complex also structural elements are found that have been previously reported for the γ-secretease–substrate complexes, namely TMD6a C-terminal of TMD6 and a hybrid β-sheet composed of β-strands from the enzyme and the substrate (Yang *et al.*, 2019; Zhou *et al.*, 2019). In contrast to the hybrid β-sheet of γ-secretease–C83, the hybrid β-sheet of PSH–C83 is only composed of two β-strands, one from the enzyme (β2) and one from the substrate (β3), in the homology model. Since the available PSH structures used as templates for model building are lacking parts of the loop regions (Li *et al.*, 2013; Dang *et al.*, 2015), the homology model is lacking 17 aa in the loop between TMD6 and 7. This also results in two fragments in the homology model, an NTF and a CTF. Therefore, there is a possibility that not all β-strands are present in this model. Interestingly, the predicted structures by AlphaFold contained two β-strands within PSH but not one within the substrate and the two PSH β-strands correspond to those of PS. Keeping in mind that the predictive power of the substrates was low (pLDDT < 50) it might be possible that this particular β-strand was just not predicted. Both methods – the homology model building and the structure predictions – have their weaknesses, future structural investigations of the PSH–substrate complex might help to unravel the details of the structural elements involved in substrate recognition/binding. It might be possible that these structural investigations on the PSH–substrate complex would reveal a hybrid β-sheet with three β-strands, one from the substrate and two from the enzyme, as it is known for γ-secretase (Yang *et al.*, 2019; Zhou *et al.*, 2019). Nevertheless, the homology model here served as a good starting point for further biochemical experiments, since it suggests that an hybrid β-strand as well as a TMD6a are involved in this process.
The mutational analysis in β2 and TMD6a revealed that these residues in PSH are important for PSH activity since they all (nearly) completely abolished the activity. Of course, the introduction of mutants into a protein can not only change the properties of the exchanged aa, but also lead to protein misfolding or even aggregation. However, this could be excluded by various quality control experiments for the corresponding mutants in the structural motifs. The role of the β2-strand is discussed in more detail later (see 4.5) and only the role of TMD6a is discussed

here. The four aa M172, I173, L175 and A176 create an hydrophobic patch which accommodates two aa of the substrate (V50 and L52) that are part of the substrate β-strand (β3). Introduction of charged aa residues into this patch abolished the PSH activity because they unfold TMD6a. The unfolded TMD6a is not able to stabilize the enzyme–substrate interaction and to facilitate the unwinding of the substrate and/or the correct positioning of the cleavage sites at the active site. This hydrophobic patch formed by the four aa in TMD6a can also be found in PS1 (Yang *et al.*, 2019; Zhou *et al.*, 2019) and might fulfil there the same function as for PSH. Future mutational analysis of this structural element in PS can shed more light on the role of TMD6a in γ-secretase.

4.5 The hydrid β-sheet in presenilin IMPs

For both IMPs investigated in this present study, it was shown that the hybrid β-sheet is important for the cleavage of the C99 substrate and disruptions of this β-sheet can result in a decreased or even completely abolished activity.
The previous structural investigations on the γ-secretase–substrate complexes already reported an abolished cleavage of Notch and APP-based substrates, respectively upon the deletion of β2 (Δ377-381), showing the importance of this structural motif (Yang *et al.*, 2019; Zhou *et al.*, 2019). The present study could shed more light on the role of this β-strand as well as the complete hybrid β-sheet formed between enzyme and substrate in PSH and γ-secretase. For both enzymes, mutations within the β2-strand impaired or even completely abolished the enzyme activity (for PSH). Interestingly, for γ-secretase, the mutation of β2 (PS1 K380P) or the deletion of β2 did not completely abolish the activity when expressed in HEK293 cells. Both mutations strongly reduced the secretion of Aβ and only $A\beta_{43}$ was found in the medium of these cells. Interestingly, both PS1 mutations were also impaired in their endoproteolysis which has not been reported before. Therefore, these mutations resemble the loss of function phenotype of strong PS1 FAD mutations (Kretner *et al.*, 2016; Trambauer *et al.*, 2020). Of note, the afore mentioned studies investigated the activity of PS1 Δ377-381 only in an *in vitro* system (Yang *et al.*, 2019; Zhou *et al.*, 2019) and might therefore have missed these observations. This is supported by findings in this study which also showed a completely abolished activity for PS1 Δ377-381 *in vitro*. Interestingly, mutating or deleting the β2-strand in PSH always completely abolished the activity, except for PSH A213P in the POPC environment. This exception might be explained by the fact that this mutation is located directly

at the border of the β-strand and is not always part of it in the MD simulations. Nevertheless, it remains elusive why all the proline mutation within the PSH β2-strand completely abolish the activity and not only reduce it like K380P in presenilin. It might be possible that the enzyme–substrate interaction within the PSH–substrate complex is lower than in the γ-secretase–substrate complex. Furthermore, the other components of the γ-secretease complex might reduce the functional consequences of the β2-strand mutations in PS in comparison to the uncomplexed PSH. NCT and PEN-2 are also involved in substrate binding (Fukumori & Steiner, 2016) and might facilitate the γ-secretase–substrate interaction even if PS is mutated. Additionally, APH-1 stabilizes the γ-secretase complex (Lee *et al.*, 2002; Niimura *et al.*, 2005). Therefore, disrupting such a structurally important element involved in substrate binding/positioning within PS1 might have reduced functional consequences compared to mutations within the same structural element in PSH.

Strikingly, PS1 K380P was less well inhibited by GSI L-685,458 than WT PS1 or PS1 M292 in the *in vitro* system. It was shown previously that K380 forms a stable backbone hydrogen bond to L-685,458 (Hitzenberger & Zacharias, 2019c; Yang *et al.*, 2021) and seems to be needed for the binding/positioning of this GSI at the active site. The mutation K380P disrupts this hydrogen bond and therefore might reduce/weaken the binding of L-685,458 to γ-secretase which might result in the reduced potency.

Not only the disruption of β2 in the γ-secretase–substrate complex impaired cleavage but also mutations in the APP β-strand (β3). Both mutations studied here – M51P and L52P – impaired the cleavage especially M51P which nearly completely abolished the cleavage. The L52P mutation strongly impaired the cleavage *in vitro*, resulting in the decreased production of AICD and Aβ as it was previously also shown in cells (Hecimovic *et al.*, 2004). Furthermore, APP L52P was also cleaved by another IMP in the CHAPSO-solubilized membrane assay, most likely a rhomboid IMP. Interestingly, single aa proline mutations in the N-terminal part of the APP TMD (e.g. postion 4, 7 or 8) also convert the γ-secretase substrate into a rhomboid substrate by increasing the TMD dynamics (Moin & Urban, 2012). Changing the TMD dynamics seem to allow the conversion of substrates into nearly non-substrates or into substrates for different IMPs. In the future, this observation might help to better understand what determines a γ-secretase substrate or non-substrate. In line with previous published data (Dimitrov *et al.*, 2013), L52P was preferentially cleaved at ε48. Structural studies on this particular mutation could show that it locally unfolds the APP TMD and makes the ε48 cleavage site more accessible than the ε49 cleavage site (Bocharov *et al.*, 2019). The afore mentioned study by Dimitrov *et al.* (2013) could not show any alterations in the processive cleavage whereas cellular studies reported an increased $A\beta_{42}/A\beta_{40}$ ratio (Kwok *et al.*, 2000; Hecimovic *et al.*,

2004). In this study, also no alterations on the processive cleavage of the L52P mutants were shown in the *in vitro* system. This suggest that this particular mutation is more severe *in vivo*. Since the mutations is located C-terminal the ε-cleavage site and released after this cleavage, it might probably not affect the processive cleavage directly but rather the cellular localization of the substrate and thereby also which γ-secretase complex cleaves the mutant APP. This could then translate in the release of longer Aβ species observed in cells and might explain the pathomechanisms of this FAD mutation.

Furthermore, the hybrid β-sheet is not only important for the processive cleavage but also for the choice of the Aβ product line. Both mutations studied here in this hybrid β-sheet shifted the ε-site cleavage preference, PS1 K380P to ε49 cleavage ($A\beta_{40}$ product line) and APP L52P to ε48 cleavage ($A\beta_{42}$ product line). A previous study on (artificial) APP mutations already showed that mutations within the APP cleavage site region and especially also within the region of the β3-strand can direct the ε-cleavage and decide which Aβ product line will be preferred (Bolduc *et al.*, 2016b). These mutations were designed to either enlarge or reduce the size of the aa side chain but no proline mutation was assessed. Bolduc *et al.* (2016b) show that the size of the aa of the substrate determines into which binding pocket within the enzyme the respective aa binds. Therefore, there are two determinants which define the activity of the enzyme–substrate complex, the ability to form a hybrid β-sheet and how the substrate β-strand is positioned based on the (size of the) side chains of the aa within the substrate β-strand.

Interesting, the hybrid β-sheet is a hotspot for AD-causing FAD mutations in PS1 and in total 8 of the 12 aa involved in this β-sheet are known mutation sites (Zhou *et al.*, 2019). For some of these FAD mutations like R377W (Sun *et al.*, 2017) or L381V (Ikeuchi *et al.*, 2008; Sun *et al.*, 2017) a reduced total activity as well as an increased $A\beta_{42}/A\beta_{40}$ ratio was reported. For the PS1 L381V mutation also elevated $A\beta_{43}$ levels (Kakuda *et al.*, 2021) and an impaired endoproteolysis (Ikeuchi *et al.*, 2008) were reported, similar to the PS1 K380P mutation analyzed in this study. Of note, non of these FAD mutations in this region substitutes an aa with a proline so they might influence the formation of the hybrid β-sheet to a lower extend than the PS1 K380P mutation. Nevertheless, the mutation there and their functional consequences further underpin the importance of this hybrid β-sheet for the activity of γ-secretase.

Such a hybrid β-sheet might be a general feature of aspartyl IMPs and not restricted to presenilin aspartyl IMPs. The predicted structures of the SPPL2a, SPPL2b, SPPL2c and SPPL3 IMPs in the AlphaFold database (Jumper *et al.*, 2021; Varadi *et al.*, 2022) also show a β-sheet formed between two β-strands of the respective IMP even in substrate-free state. These β-strands are similar located as the two β-

strands of PS1 one C-terminal of TMD6 and one directly preceding the GxGD motif in TMD7. Whether this β-sheet is really formed in the substrate-free form of SPPLs as suggested from the predictions or whether it only exists in a hybrid β-sheet in the substrate-bound state needs to be shown in the future by determining the structures of E-S. Given the high similarity between PS and SPP, it is not unlikely that SPPLs – at least in the substrate-bound form – also form such a hybrid β-sheet.

4.6 The hybrid β-sheet zipper model

The biochemical studies on the hybrid β-sheet showed that this structural element is important for PSH and PS1 activity (ε-cleavage and processive cleavage). Complementary MD simulations performed by Shu-Yu Chen and Martin Zacharias (data not shown) helped to explain these findings and a zipper model for the hybrid β-sheet is proposed: A proper formed hybrid β-sheet brings the two catalytic aspartates and the substrate's scissile bond in the correct position and is able to squeeze out excess water molecules from the active site. In contrast, the disruption of this β-sheet by a mutation or shortening results in an increased drainage of water molecules from the cytosol to the active site thereby disrupting the hydrogen bonding network at this particular site (figure 4.6.1).

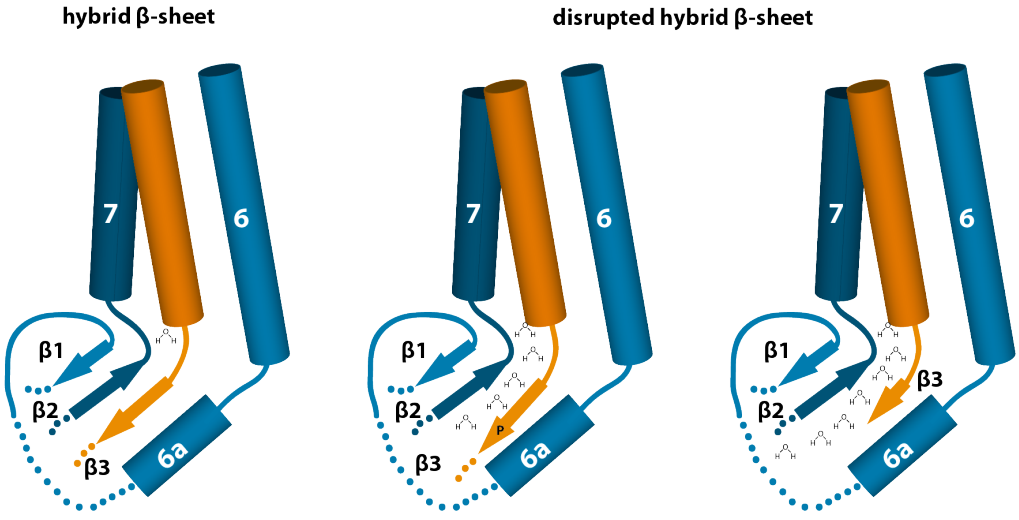

Figure 4.6.1: Zipper model of the hybrid β-sheet. The correct formed hybrid β-sheet squeezes out excess water from the active site (left). A disruption of the hybrid β-sheet results in a drainage of water molecules to the active site (right).

4.7 Outlook

To better understand how the lipid environment influences the activity of IMPs, it would be advantageous to identify lipid binding sites within the respective proteases. To this end, crosslinkable lipid molecules could be used in combination with mass spectrometry analysis (Peng *et al.*, 2014; Korn *et al.*, 2022). Especially bifunctional lipid molecules could facilitate such studies (Peng *et al.*, 2014). The identified lipid interaction sites could then be further validated my mutational analysis. Applying different types of crosslinkable lipids would also allow to see whether different lipid types/classes have distinguished interaction/binding sites. This would not only help to understand how the lipid effect might be mediated but also how and which specific lipid types mediate certain effects.
Furthermore, it would be interesting to see whether aspartyl IMPs are able to locally thin/distort their surrounding lipid membrane as it is described for serine rhomboid intramembrane(pseudo)proteases (Urban, 2010; Kreutzberger *et al.*, 2019; Lemberg & Strisovsky, 2021; Engberg *et al.*, 2022). In depth investigations of MD simulations of aspartyl IMPs in a lipid bilayer might already give a first hint. Structural investigations combined with biochemical experiments, e.g. mutational analysis of lipid anchor regions, could elucidate further on this. Answering this question might help to understand how aspartyl IMPs engage their substrates within the membrane plane. Something similar has already been reported for rhomboid proteases, which can diffuse faster within the lipid membrane due to the local thinning of the membrane which might allow the engagement of substrates that are restricted in their movement (Kreutzberger *et al.*, 2019).
Another interesting aspect for future studies would be how mutations (FAD mutations or artificial mutations like K380P) influence the geometry of the active site. Especially the investigation of the FAD mutations located in the two PS1 β-strands would be very interesting since they might strongly influence the geometry of the active site. This could be further studied by using the inhibitor affinity precipitation with Merck C and might help to broader describe the phenotypes of such mutations. Furthermore, it would be interesting to understand more the role of the hybrid β-sheet in the processive cleavage mechanism. So far, it is unclear whether such a β-sheet is also formed in the subsequent cleavage steps after the ε-cleavage. In a recent MD simulation study, no β-sheet formation for the cleavage of $A\beta_{49}$ to $A\beta_{46}$ was observed (Bhattarai *et al.*, 2022). Using Aβ peptides – like $A\beta_{49}$ or $A\beta_{49}$ – as substrates for γ-secretase bearing the PS1 K380P mutation might allow to investigate this further. If the hybrid β-sheet formation is needed for every γ-secretase cleavage step than also the cleavage of Aβ peptides should be impaired by PS1 K380P and not only the cleavage of APP CTF (APP C99).

All the future studies suggested here, should not be restricted to PSH but, due to its low complexity (in comparison to γ-secretase) and its rather easy accessibility (heterologous expression in *E. coli*), PSH might be a good starting point for such studies. The technical developments based on PSH studies, as well as the generated knowledge can be transferred to γ-secretase and maybe also other aspartyl IMPs like SPP an SPPLs.

Bibliography

Aguayo-Ortiz, R, Chávez-García, C, Straub, JE, Dominguez, L (2017). Characterizing the structural ensemble of γ-secretase using a multiscale molecular dynamics approach. *Chemical Science*, **8**(8): 5576–5584. doi:10.1039/c7sc00980a.

Akiyama, Y, Maegawa, S (2007). Sequence features of substrates required for cleavage by GlpG, an Escherichia coli rhomboid protease. *Molecular Microbiology*, **64**(4): 1028–1037. doi:10.1111/j.1365-2958.2007.05715.x.

Alzheimer, A (1907). Über einge eigenartige Erkrankung der Hirnrinde. *Allgemeine Zeitschrift für Psychiatrie und psychisch-gerichtliche Medicin*, **64**(1-2): 146–148.

Alzheimer, A (1911). Über eigenartige Krankheitsfälle des späten Alters. *Zeitschrift für die Gesamte Neurologie und Psychiatrie*, **4**(1): 356–385.

Alzheimer's Association (2020). 2020 Alzheimer's disease facts and figures. doi:10.1002/alz.12068.

Alzheimer's Disease International (2015). The World Alzheimer Report 2015 provides an update on ADI's global dementia data, as well as a systematic review around prevalence and incidence of dementia over time.

Alzheimer's Disease International (2020). Numbers of people with dementia worldwide: An update to the estimates in the World Alzheimer Report 2015.

Andrew, RJ, Kellett, KAB, Thinakaran, G, Hooper, NM (2016). A greek tragedy: The growing complexity of Alzheimer amyloid precursor protein proteolysis. *Journal of Biological Chemistry*, **291**(37): 19235–19244. doi:10.1074/jbc.R116.746032.

Arboleda-Velasquez, JF, Lopera, F, O'Hare, M, Delgado-Tirado, S, Marino, C, Chmielewska, N, Saez-Torres, KL, Amarnani, D, Schultz, AP, Sperling, RA, Leyton-Cifuentes, D, Chen, K, Baena, A, Aguillon, D, Rios-Romenets, S, Giraldo, M, Guzmán-Vélez, E, Norton, DJ, Pardilla-Delgado, E, Artola, A, Sanchez, JS, Acosta-Uribe, J, Lalli, M, Kosik, KS, Huentelman, MJ, Zetterberg, H, Blennow, K, Reiman, RA, Luo, J, Chen, Y, Thiyyagura, P, Su, Y, Jun, GR, Naymik, M, Gai, X, Bootwalla, M, Ji, J, Shen, L, Miller, JB, Kim, LA, Tariot, PN, Johnson, KA,

Reiman, EM, Quiroz, YT (2019). Resistance to autosomal dominant Alzheimer's disease in an APOE3 Christchurch homozygote: A case report. *Nature Medicine*, **25**(11): 1680–1683. doi:10.1038/s41591-019-0611-3.

Arendt, T, Stieler, JT, Holzer, M (2016). Tau and tauopathies. *Brain Research Bulletin*, **126**(Pt 3): 238–292. doi:10.1016/j.brainresbull.2016.08.018.

Ast, T, Michaelis, S, Schuldiner, M (2016). The protease Ste24 clears clogged translocons. *Cell*, **164**(1): 103–114. doi:10.1016/j.cell.2015.11.053.

Bai, XC, Rajendra, E, Yang, G, Shi, Y, Scheres, SH (2015a). Sampling the conformational space of the catalytic subunit of human γ-secretase. *eLife*, **4**: e11182. doi:10.7554/eLife.11182.

Bai, Xc, Yan, C, Yang, G, Lu, P, Ma, D, Sun, L, Zhou, R, Scheres, SHW, Shi, Y (2015b). An atomic structure of human γ-secretase. *Nature*, **525**(7568): 212–217. doi:10.1038/nature14892.

Bao, J, Wolpowitz, D, Role, LW, Talmage, DA (2003). Back signaling by the Nrg-1 intracellular domain. *Journal of Cell Biology*, **161**(6): 1133–1141. doi:10.1083/jcb.200212085.

Barker, WW, Luis, CA, Kashuba, A, Luis, M, Harwood, DG, Loewenstein, D, Waters, C, Jimison, P, Shepherd, E, Sevush, S, Graff-Radford, N, Newland, D, Todd, M, Miller, B, Gold, M, Heilman, K, Doty, L, Goodman, I, Robinson, B, Pearl, G, Dickson, D, Duara, R (2002). Relative frequencies of Alzheimer disease, Lewy body, vascular and frontotemporal dementia, and hippocampal sclerosis in the State of Florida Brain Bank. *Alzheimer Disease and Associated Disorders*, **16**(4): 203–212. doi:10.1097/00002093-200210000-00001.

Barrett, PJ, Song, Y, Van Horn, WD, Hustedt, EJ, Schafer, JM, Hadziselimovic, A, Beel, AJ, Sanders, CR (2012). The amyloid precursor protein has a flexible transmembrane domain and binds cholesterol. *Science*, **336**(6085): 1168–1171. doi:10.1126/science.1219988.

Beard, H, Barniol-Xicota, M, Yang, J, Verhelst, SHL (2019). Discovery of cellular roles of intramembrane proteases. *ACS Chemical Biology*, **14**(11): 2372–2388. doi:10.1021/acschembio.9b00404.

Beher, D, Fricker, M, Nadin, A, Clarke, EE, Wrigley, JDJ, Li, YM, Culvenor, JG, Masters, CL, Harrison, T, Shearman, MS (2003). In vitro characterization of the presenilin-dependent γ-secretase complex using a novel affinity ligand. *Biochemistry*, **42**(27): 8133–8142. doi:10.1021/bi034045z.

Beher, D, Wrigley, JD, Nadin, A, Evin, G, Masters, CL, Harrison, T, Castro, JL, Shearman, MS (2001). Pharmacological knock-down of the presenilin 1 heterodimer by a novel γ-secretase inhibitor: Implications for presenilin biology. *Journal of Biological Chemistry*, **276**(48): 45394–45402. doi:10.1074/jbc.M103075200.

Ben-Shem, A, Fass, D, Bibi, E (2007). Structural basis for intramembrane proteolysis by rhomboid serine proteases. *Proceedings of the National Academy of Sciences of the United States of America*, **104**(2): 462–466. doi:10.1073/pnas.0609773104.

Benilova, I, Gallardo, R, Ungureanu, AA, Cano, VC, Snellinx, A, Ramakers, M, Bartic, C, Rousseau, F, Schymkowitz, J, De Strooper, B (2014). The Alzheimer disease protective mutation A2T modulates kinetic and thermodynamic properties of amyloid-β (Aβ) aggregation. *Journal of Biological Chemistry*, **289**(45): 30977–30989. doi:10.1074/jbc.M114.599027.

Berezovska, O, Ramdya, P, Skoch, J, Wolfe, MS, Bacskai, BJ, Hyman, BT (2003). Amyloid precursor protein associates with a nicastrin-dependent docking site on the presenilin 1–γ-secretase complex in cells demonstrated by fluorescence lifetime imaging. *Journal of Neuroscience*, **23**(11): 4560–4566. doi:10.1523/jneurosci.23-11-04560.2003.

Berg, JM, Tymoczko, JL, Stryer, L (2009). *Stryer Biochemie*. Spektrum Akademischer Verlag, Heidelberg, Germany.

Bertrand, E, Brouillet, E, Caillé, I, Bouillot, C, Cole, GM, Prochiantz, A, Allinquant, B (2001). A short cytoplasmic domain of the amyloid precursor protein induces apoptosis in vitro and in vivo. *Molecular and Cellular Neuroscience*, **18**(5): 503–511. doi:10.1006/mcne.2001.1030.

Best, JD, Jay, MT, Otu, F, Churcher, I, Reilly, M, Morentin-Gutierrez, P, Pattison, C, Harrison, T, Shearman, MS, Atack, JR (2006). In vivo characterization of Aβ(40) changes in brain and cerebrospinal fluid using the novel γ-secretase inhibitor N-[cis-4-[(4-Chlorophenyl)sulfonyl]-4-(2,5-difluorophenyl)cyclohexyl]-1,1,1-trifluoromethanesulfonamide (MRK-560) in the rat. *Journal of Pharmacology and Experimental Therapeutics*, **317**(2): 786–790. doi:10.1124/jpet.105.100271.

Bhattarai, A, Devkota, S, Do, HN, Wang, J, Bhattarai, S, Wolfe, MS, Miao, Y (2022). Mechanism of tripeptide trimming of amyloid β-peptide 49 by γ-secretase. *Journal of the American Chemical Society*, **144**(14): 6215–6226. doi:10.1021/jacs.1c10533.

Bien, J, Jefferson, T, Causević, M, Jumpertz, T, Munter, L, Multhaup, G, Weggen, S, Becker-Pauly, C, Pietrzik, CU (2012). The metalloprotease meprin β generates amino terminal-truncated amyloid β peptide species. *Journal of Biological Chemistry*, **287**(40): 33304–33313. doi:10.1074/jbc.M112.395608.

Bocharov, EV, Nadezhdin, KD, Urban, AS, Volynsky, PE, Pavlov, KV, Efremov, RG, Arseniev, AS, Bocharova, OV (2019). Familial L723P mutation can shift the distribution between the alternative APP transmembrane domain cleavage cascades by local unfolding of the ε-cleavage site suggesting a straightforward mechanism of Alzheimer's disease pathogenesis. *ACS Chemical Biology*, **14**(7): 1573–1582. doi:10.1021/acschembio.9b00309.

Bode, W, Huber, R (2000). Structural basis of the endoproteinase–protein inhibitor interaction. *Biochimica et Biophysica Acta (BBA) - Protein Structure and Molecular Enzymology*, **1477**(1): 241–252. doi:10.1016/s0167-4838(99)00276-9.

Bolduc, DM, Montagna, DR, Gu, Y, Selkoe, DJ, Wolfe, MS (2016a). Nicastrin functions to sterically hinder γ-secretase–substrate interactions driven by substrate transmembrane domain. *Proceedings of the National Academy of Sciences of the United States of America*, **113**(5): E509–E518. doi:10.1073/pnas.1512952113.

Bolduc, DM, Montagna, DR, Seghers, MC, Wolfe, MS, Selkoe, DJ (2016b). The amyloid-β forming tripeptide cleavage mechanism of γ-secretase. *eLife*, **5**: e17578. doi:10.7554/eLife.17578.

Bond, JS (2019). Proteases: History, discovery, and roles in health and disease. *Journal of Biological Chemistry*, **294**(5): 1643–1651. doi:10.1074/jbc.TM118.004156.

Borchelt, DR, Thinakaran, G, Eckman, CB, Lee, MK, Davenport, F, Ratovitsky, T, Prada, CM, Kim, G, Seekins, S, Yager, D, Slunt, HH, Wang, R, Seeger, M, Levey, AI, Gandy, SE, Copeland, NG, Jenkins, NA, Price, DL, Younkin, SG, Sisodia, SS (1996). Familial Alzheimer's disease-linked presenilin 1 variants elevate Aβ1-42/1-40 ratio in vitro and in vivo. *Neuron*, **17**(5): 1005–1013. doi:10.1016/s0896-6273(00)80230-5.

Boyartchuk, VL, Ashby, MN, Rine, J (1997). Modulation of Ras and a-Factor function by carboxyl-terminal proteolysis. *Science*, **275**(5307): 1796–1800. doi:10.1126/science.275.5307.1796.

Brix, K, Stöcker, W (2013). *Proteases: Structure and function*. Springer, Vienna, Wien, Austria. doi:10.1007/978-3-7091-0885-7.

Brothers, HM, Gosztyla, ML, Robinson, SR (2018). The physiological roles of amyloid-β peptide hint at new ways to treat Alzheimer's disease. *Frontiers in Aging Neuroscience*, **10**(118). doi:10.3389/fnagi.2018.00118.

Brown, MC, Abdine, A, Chavez, J, Schaffner, A, Torres-Arancivia, C, Lada, B, JiJi, RD, Osman, R, Cooley, JW, Ubarretxena-Belandia, I (2018). Unwinding of the substrate transmembrane helix in intramembrane proteolysis. *Biophysical Journal*, **114**(7): 1579–1589. doi:10.1016/j.bpj.2018.01.043.

Bukhari, H, Glotzbach, A, Kolbe, K, Leonhardt, G, Loosse, C, Müller, T (2017). Small things matter: Implications of APP intracellular domain AICD nuclear signaling in the progression and pathogenesis of Alzheimer's disease. *Progress in Neurobiology*, **156**: 189–213. doi:10.1016/j.pneurobio.2017.05.005.

Busciglio, J, Gabuzda, DH, Matsudaira, P, Yankner, BA (1993). Generation of β-amyloid in the secretory pathway in neuronal and nonneuronal cells. *Proceedings of the National Academy of Sciences of the United States of America*, **90**(5): 2092–2096. doi:10.1073/pnas.90.5.2092.

Buxbaum, JD, Liu, KN, Luo, Y, Slack, JL, Stocking, KL, Peschon, JJ, Johnson, RS, Castner, BJ, Cerretti, DP, Black, RA (1998). Evidence that tumor necrosis factor α converting enzyme is involved in regulated α-secretase cleavage of the Alzheimer amyloid protein precursor. *Journal of Biological Chemistry*, **273**(43): 27765–27767. doi:10.1074/jbc.273.43.27765.

Caforio, A, Driessen, AJM (2017). Archaeal phospholipids: Structural properties and biosynthesis. *Biochimica et Biophysica Acta (BBA) - Molecular and Cell Biology of Lipids*, **1862**(11): 1325–1339. doi:10.1016/j.bbalip.2016.12.006.

Campbell, WA, Iskandar, MK, Reed, MLO, Xia, W (2002). Endoproteolysis of presenilin in vitro: Inhibition by γ-secretase inhibitors. *Biochemistry*, **41**(10): 3372–3379. doi:10.1021/bi015810h.

Cao, X, Südhof, TC (2001). A transcriptionally [correction of transcriptively] active complex of APP with Fe65 and histone acetyltransferase Tip60. *Science*, **293**(5527): 115–120. doi:10.1126/science.1058783.

Capell, A, Beher, D, Prokop, S, Steiner, H, Kaether, C, Shearman, MS, Haass, C (2005). γ-Secretase complex assembly within the early secretory pathway. *Journal of Biological Chemistry*, **280**(8): 6471–6478. doi:10.1074/jbc.M409106200.

Castellano, JM, Kim, J, Stewart, FR, Jiang, H, DeMattos, RB, Patterson, BW, Fagan, AM, Morris, JC, Mawuenyega, KG, Cruchaga, C, Goate, AM, Bales, KR,

Paul, SM, Bateman, RJ, Holtzman, DM (2011). Human ApoE isoforms differentially regulate brain amyloid-β peptide clearance. *Science Translational Medicine*, **3**(89): 89ra57. doi:10.1126/scitranslmed.3002156.

Chartier-Harlin, MC, Crawford, F, Houlden, H, Warren, A, Hughes, D, Fidani, L, Goate, A, Rossor, M, Roques, P, J Hardy, , et al. (1991). Early-onset Alzheimer's disease caused by mutations at codon 717 of the β-amyloid precursor protein gene. *Nature*, **353**(6347): 844–846. doi:10.1038/353844a0.

Chau, DM, Crump, CJ, Villa, JC, Scheinberg, DA, Li, YM (2012). Familial Alzheimer disease presenilin-1 mutations alter the active site conformation of γ-secretase. *Journal of Biological Chemistry*, **287**(21): 17288–17296. doi:10.1074/jbc.M111.300483.

Chen, AC, Kim, S, Shepardson, N, Patel, S, Hong, S, Selkoe, DJ (2015). Physical and functional interaction between the α- and γ-secretases: A new model of regulated intramembrane proteolysis. *Journal of Cell Biology*, **211**(6): 1157–1176. doi:10.1083/jcb.201502001.

Chen, F, Yu, G, Arawaka, S, Nishimura, M, Kawarai, T, Yu, H, Tandon, A, Supala, A, Song, YQ, Rogaeva, E, Milman, P, Sato, C, Yu, C, Janus, C, Lee, J, Song, L, Zhang, L, Fraser, PE, George-Hyslop, PHS (2001). Nicastrin binds to membrane-tethered Notch. *Nature Cell Biology*, **3**(8): 751–754. doi:10.1038/35087069.

Cheng, F, Cappai, R, Lidfeldt, J, Belting, M, Fransson, LA, Mani, K (2014). Amyloid precursor protein (APP)/APP-like protein 2 (APLP2) expression is required to initiate endosome-nucleus-autophagosome trafficking of glypican-1-derived heparan sulfate. *Journal of Biological Chemistry*, **289**(30): 20871–20878. doi:10.1074/jbc.M114.552810.

Chew, H, Solomon, VA, Fonteh, AN (2020). Involvement of lipids in Alzheimer's disease pathology and potential therapies. *Frontiers in Physiology*, **11**(589). doi:10.3389/fphys.2020.00598.

Cho, S, Baker, RP, Ji, M, Urban, S (2019). Ten catalytic snapshots of rhomboid intramembrane proteolysis from gate opening to peptide release. *Nature Structural & Molecular Biology*, **26**(10): 910–918. doi:10.1038/s41594-019-0296-9.

Cho, Y, Bae, HG, Okun, E, Arumugam, TV, Jo, DG (2022). Physiology and pharmacology of amyloid precursor protein. *Pharmacology & Therapeutics*, **235**: 108122. doi:10.1016/j.pharmthera.2022.108122.

Chyung, JH, Raper, DM, Selkoe, DJ (2005). γ-Secretase exists on the plasma membrane as an intact complex that accepts substrates and effects intramembrane cleavage. *Journal of Biological Chemistry*, **280**(6): 4383–4392. doi: 10.1074/jbc.M409272200.

Chávez-Gutiérrez, L, Bammens, L, Benilova, I, Vandersteen, A, Benurwar, M, Borgers, M, Lismont, S, Zhou, L, Van Cleynenbreugel, S, Esselmann, H, Wiltfang, J, Serneels, L, Karran, E, Gijsen, H, Schymkowitz, J, Rousseau, F, Broersen, K, De Strooper, B (2012). The mechanism of γ-secretase dysfunction in familial Alzheimer disease. *The EMBO Journal*, **31**(10): 2261–2274. doi: 10.1038/emboj.2012.79.

Chávez-Gutiérrez, L, Tolia, A, Maes, E, Li, T, Wong, PC, de Strooper, B (2008). Glu(332) in the Nicastrin ectodomain is essential for γ-secretase complex maturation but not for its activity. *Journal of Biological Chemistry*, **283**(29): 20096–20105. doi:10.1074/jbc.M803040200.

Citron, M, Diehl, TS, Capell, A, Haass, C, Teplow, DB, Selkoe, DJ (1996). Inhibition of amyloid β-protein production in neural cells by the serine protease inhibitor AEBSF. *Neuron*, **17**(1): 171–179. doi:10.1016/s0896-6273(00)80290-1.

Citron, M, Oltersdorf, T, Haass, C, McConlogue, L, Hung, AY, Seubert, P, Vigo-Pelfrey, C, Lieberburg, I, Selkoe, DJ (1992). Mutation of the β-amyloid precursor protein in familial Alzheimer's disease increases β-protein production. *Nature*, **360**(6405): 672–674. doi:10.1038/360672a0.

Citron, M, Westaway, D, Xia, W, Carlson, G, Diehl, T, Levesque, G, Johnson-Wood, K, Lee, M, Seubert, P, Davis, A, Kholodenko, D, Motter, R, Sherrington, R, Perry, B, Yao, H, Strome, R, Lieberburg, I, Rommens, J, Kim, S, Schenk, D, Fraser, P, Hyslop, PSG, Selkoe, DJ (1997). Mutant presenilins of Alzheimer's disease increase production of 42-residue amyloid β-protein in both transfected cells and transgenic mice. *Nature Medicine*, **3**(1): 67–72. doi:10.1038/nm0197-67.

Clemente, N, Abdine, A, Ubarretxena-Belandia, I, Wang, C (2018). Coupled transmembrane substrate docking and helical unwinding in intramembrane proteolysis of amyloid precursor protein. *Scientific Reports*, **8**(1): 12411. doi: 10.1038/s41598-018-30015-6.

Copeland, RA (2000). *Enzymes: a practical introduction to structure, mechanism, and data analysis, 2nd Edition*. Wiley, Chichester, England, UK.

Corder, EH, Saunders, AM, Strittmatter, WJ, Schmechel, DE, Gaskell, PC, Small, GW, Roses, AD, Haines, JL, Pericak-Vance, MA (1993). Gene dose of apolipoprotein E type 4 allele and the risk of Alzheimer's disease in late onset families. *Science*, **261**(5123): 921–923. doi:10.1126/science.8346443.

Crump, CJ, Castro, SV, Wang, F, Pozdnyakov, N, Ballard, TE, Sisodia, SS, Bales, KR, Johnson, DS, Li, YM (2012). BMS-708,163 targets presenilin and lacks Notch-sparing activity. *Biochemistry*, **51**(37): 7209–7211. doi:10.1021/bi301137h.

Crump, CJ, Johnson, DS, Li, YM (2013). Development and mechanism of γ-secretase modulators for Alzheimer's disease. *Biochemistry*, **52**(19): 3197–3216. doi:10.1021/bi400377p.

Crystal, AS, Morais, VA, Pierson, TC, Pijak, DS, Carlin, D, Lee, VMY, Doms, RW (2003). Membrane topology of γ-secretase component PEN-2. *Journal of Biological Chemistry*, **278**(22): 20117–20123. doi:10.1074/jbc.M213107200.

Cullen, N, Janelidze, S, Palmqvist, S, Stomrud, E, Mattsson-Carlgren, N, Hansson, O, Initiative, ADN (2022). Association of CSF Aβ 38 levels with risk of Alzheimer disease-related decline. *Neurology*, **98**(9): 958–967. doi:10.1212/wnl.0000000000013228.

Cupers, P, Orlans, I, Craessaerts, K, Annaert, W, De Strooper, B (2001). The amyloid precursor protein (APP)-cytoplasmic fragment generated by γ-secretase is rapidly degraded but distributes partially in a nuclear fraction of neurones in culture. *Journal of Neurochemistry*, **78**(5): 1168–1178. doi:10.1046/j.1471-4159.2001.00516.x.

Czirr, E, Leuchtenberger, S, Dorner-Ciossek, C, Schneider, A, Jucker, M, Koo, EH, Pietrzik, CU, Baumann, K, Weggen, S (2007). Insensitivity to Aβ42-lowering nonsteroidal anti-inflammatory drugs and γ-secretase inhibitors is common among aggressive presenilin-1 mutations. *Journal of Biological Chemistry*, **282**(34): 24504–24513. doi:10.1074/jbc.M700618200.

Dang, S, Wu, S, Wang, J, Li, H, Huang, M, He, W, Li, YM, Wong, CCL, Shi, Y (2015). Cleavage of amyloid precursor protein by an archaeal presenilin homologue PSH. *Proceedings of the National Academy of Sciences of the United States of America*, **112**(11): 3344–3349. doi:10.1073/pnas.1502150112.

Dawson, GR, Seabrook, GR, Zheng, H, Smith, DW, Graham, S, O'Dowd, G, Bowery, BJ, Boyce, S, Trumbauer, ME, Chen, HY, Van der Ploeg, LH, Sirinathsinghji, DJ (1999). Age-related cognitive deficits, impaired long-term potentiation and

reduction in synaptic marker density in mice lacking the β-amyloid precursor protein. *Neuroscience*, **90**(1): 1–13. doi:10.1016/s0306-4522(98)00410-2.

De Strooper, B (2010). Proteases and proteolysis in Alzheimer disease: A multifactorial view on the disease process. *Physiological Reviews*, **90**(2): 465–494.

De Strooper, B, Annaert, W, Cupers, P, Saftig, P, Craessaerts, K, Mumm, JS, Schroeter, EH, Schrijvers, V, Wolfe, MS, Ray, WJ, Goate, A, Kopan, R (1999). A presenilin-1-dependent γ-secretase-like protease mediates release of Notch intracellular domain. *Nature*, **398**(6727): 518–522. doi:10.1038/19083.

De Strooper, B, Saftig, P, Craessaerts, K, Vanderstichele, H, Guhde, G, Annaert, W, Von Figura, K, Van Leuven, F (1998). Deficiency of presenilin-1 inhibits the normal cleavage of amyloid precursor protein. *Nature*, **391**(6665): 387–390. doi:10.1038/34910.

Devkota, S, Williams, TD, Wolfe, MS (2021). Familial Alzheimer's disease mutations in amyloid protein precursor alter proteolysis by γ-secretase to increase amyloid β-peptides of >45 residues. *Journal of Biological Chemistry*, **296**(100281). doi:10.1016/j.jbc.2021.100281.

Di Paolo, G, Kim, TW (2011). Linking lipids to Alzheimer's disease: Cholesterol and beyond. *Nature Reviews Neuroscience*, **12**(5): 284–296. doi:10.1038/nrn3012.

Dickey, SW, Baker, RP, Cho, S, Urban, S (2013). Proteolysis inside the membrane is a rate-governed reaction not driven by substrate affinity. *Cell*, **155**(6): 1270–1281. doi:10.1016/j.cell.2013.10.053.

Dimitrov, M, Alattia, JR, Lemmin, T, Lehal, R, Fligier, A, Houacine, J, Hussain, I, Radtke, F, Dal Peraro, M, Beher, D, Fraering, PC (2013). Alzheimer's disease mutations in APP but not γ-secretase modulators affect ε-cleavage-dependent AICD production. *Nature Communications*, **4**(2246): 1–10. doi:10.1038/ncomms3246.

Doody, RS, Raman, R, Farlow, M, Iwatsubo, T, Vellas, B, Joffe, S, Kieburtz, K, He, F, Sun, X, Thomas, RG, Aisen, PS, Alzheimer's Disease Cooperative Study Steering Committee, Siemers, E, Sethuraman, G, Mohs, R, Semagacestat Study Group (2013). A phase 3 trial of semagacestat for treatment of Alzheimer's disease. *New England Journal of Medicine*, **369**(4): 341–350. doi:10.1056/NEJMoa1210951.

Dovey, HF, John, V, Anderson, JP, Chen, LZ, De Saint Andrieu, P, Fang, LY, Freedman, SB, Folmer, B, Goldbach, E, Holsztynska, EJ, Hu, KL, Johnson-Wood, KL, Kennedy, SL, Kholodenko, D, Knops, JE, Latimer, LH, Lee, M, Liao, Z, Lieberburg, IM, Motter, RN, Mutter, LC, Nietz, J, Quinn, KP, Sacchi, KL, Seubert, PA,

Shopp, GM, Thorsett, ED, Tung, JS, Wu, J, Yang, S, Yin, CT, Schenk, DB, May, PC, Altstiel, LD, Bender, MH, Boggs, LN, Britton, TC, Clemens, JC, Czilli, DL, Dieckman-McGinty, DK, Droste, JJ, Fuson, KS, Gitter, BD, Hyslop, PA, Johnstone, EM, Li, WY, Little, SP, Mabry, TE, Miller, FD, Ni, B, Nissen, JS, Porter, WJ, Potts, BD, Reel, JK, Stephenson, D, Su, Y, Shipley, LA, Whitesitt, CA, Yin, T, Audia, JE (2001). Functional γ-secretase inhibitors reduce β-amyloid peptide levels in brain. *Journal of Neurochemistry*, **76**(1): 173–181. doi:10.1046/j.1471-4159.2001.00012.x.

Dries, DR, Shah, S, Han, YH, Yu, C, Yu, S, Shearman, MS, Yu, G (2009). Glu-333 of nicastrin directly participates in γ-secretase activity. *Journal of Biological Chemistry*, **284**(43): 29714–29724. doi:10.1074/jbc.M109.038737.

Dries, DR, Yu, G (2008). Assembly, maturation, and trafficking of the γ-secretase complex in Alzheimer's disease. *Current Alzheimer Research*, **5**(2): 132–146. doi:10.2174/156720508783954695.

Dumanchin-Njock, C, Da Costa, CA, Mercken, L, Pradier, L, Checler, F (2001). The caspase-derived C-terminal fragment of βAPP induces caspase-independent toxicity and triggers selective increase of Aβ42 in mammalian cells. *Journal of Neurochemistry*, **78**(5): 1153–1161. doi:10.1046/j.1471-4159.2001.00513.x.

Dyrks, T, Weidemann, A, Multhaup, G, Salbaum, JM, Lemaire, HG, Kang, J, Müller-Hill, B, Masters, CL, Beyreuther, K (1988). Identification, transmembrane orientation and biogenesis of the amyloid A4 precursor of Alzheimer's disease. *The EMBO Journal*, **7**(4): 949–957. doi:10.1002/j.1460-2075.1988.tb02900.x.

Ebke, A, Luebbers, T, Fukumori, A, Shirotani, K, Haass, C, Baumann, K, Steiner, H (2011). Novel γ-secretase enzyme modulators directly target presenilin protein. *Journal of Biological Chemistry*, **286**(43): 37181–37186. doi:10.1074/jbc.C111.276972.

Edbauer, D, Winkler, E, Haass, C, Steiner, H (2002). Presenilin and nicastrin regulate each other and determine amyloid β-peptide production via complex formation. *Proceedings of the National Academy of Sciences of the United States of America*, **99**(13): 8666–8671. doi:10.1073/pnas.132277899.

Edbauer, D, Winkler, E, Regula, JT, Pesold, B, Steiner, H, Haass, C (2003). Reconstitution of γ-secretase activity. *Nature Cell Biology*, **5**(5): 486–488. doi:10.1038/ncb960.

Ehehalt, R, Keller, P, Haass, C, Thiele, C, Simons, K (2003). Amyloidogenic processing of the Alzheimer β-amyloid precursor protein depends on lipid rafts. *Journal of Cell Biology*, **160**(1): 113–123. doi:10.1083/jcb.200207113.

Elad, N, De Strooper, B, Lismont, S, Hagen, W, Veugelen, S, Arimon, M, Horré, K, Berezovska, O, Sachse, C, Chávez-Gutiérrez, L (2015). The dynamic conformational landscape of γ-secretase. *Journal of Cell Science*, **128**(3): 589–598. doi:10.1242/jcs.164384.

Engberg, O, Ulbricht, D, Döbel, V, Siebert, V, Frie, C, Penk, A, Lemberg, MK, Huster, D (2022). Rhomboid-catalyzed intramembrane proteolysis requires hydrophobic matching with the surrounding lipid bilayer. *Science Advances*, **8**(38): eabq8303. doi:10.1126/sciadv.abq8303.

Escamilla-Ayala, A, Wouters, R, Sannerud, R, Annaert, W (2020). Contribution of the presenilins in the cell biology, structure and function of γ-secretase. *Seminars in Cell and Developmental Biology*, **105**: 12–26. doi:10.1016/j.semcdb.2020.02.005.

Esch, FS, Keim, PS, Beattie, EC, Blacher, RW, Culwell, AR, Oltersdorf, T, McClure, D, Ward, PJ (1990). Cleavage of amyloid β peptide during constitutive processing of its precursor. *Science*, **248**(4959): 1122–1124. doi:10.1126/science.2111583.

Esler, WP, Kimberly, WT, Ostaszewski, BL, Diehl, TS, Moore, CL, Tsai, JY, Rahmati, T, Xia, W, Selkoe, DJ, Wolfe, MS (2000). Transition-state analogue inhibitors of γ-secretase bind directly to presenilin-1. *Nature Cell Biology*, **2**(7): 428–434. doi:10.1038/35017062.

Esler, WP, Kimberly, WT, Ostaszewski, BL, Ye, W, Diehl, TS, Selkoe, DJ, Wolfe, MS (2002). Activity-dependent isolation of the presenilin–γ-secretase complex reveals nicastrin and a γ substrate. *Proceedings of the National Academy of Sciences of the United States of America*, **99**(5): 2720–2725. doi:10.1073/pnas.052436599.

Esparza, TJ, Zhao, H, Cirrito, JR, Cairns, NJ, Bateman, RJ, Holtzman, DM, Brody, DL (2013). Amyloid-β oligomerization in Alzheimer dementia versus high-pathology controls. *Annals of Neurology*, **73**(1): 104–119. doi:10.1002/ana.23748.

Estus, S, Golde, TE, Kunishita, T, Blades, D, Lowery, D, Eisen, M, Usiak, M, Qu, XM, Tabira, T, B D. Greenberg, , et al. (1992). Potentially amyloidogenic, carboxyl-terminal derivatives of the amyloid protein precursor. *Science*, **255**(5045): 726–728. doi:10.1126/science.1738846.

Evans, R, O'Neill, M, Pritzel, A, Antropova, N, Senior, A, Green, T, Žídek, A, Bates, R, Blackwell, S, Yim, J, Ronneberger, O, Bodenstein, S, Zielinski, M, Bridgland, A, Potapenko, A, Cowie, A, Tunyasuvunakool, K, Jain, R, Clancy, E, Kohli, P, Jumper, J, Hassabis, D (2022). Protein complex prediction with AlphaFold-Multimer. *bioRxiv*. doi:2021.10.04.463034.

Fagan, R, Swindells, M, Overington, J, Weir, M (2001). Nicastrin, a presenilin-interacting protein, contains an aminopeptidase/transferrin receptor superfamily domain. *Trends in Biochemical Sciences*, **26**(4): 213–214. doi:10.1016/s0968-0004(01)01789-3.

Fassbender, K, Simons, M, Bergmann, C, Stroick, M, Lutjohann, D, Keller, P, Runz, H, Kuhl, S, Bertsch, T, von Bergmann, K, Hennerici, M, Beyreuther, K, Hartmann, T (2001). Simvastatin strongly reduces levels of Alzheimer's disease β-amyloid peptides Aβ 42 and Aβ 40 in vitro and in vivo. *Proceedings of the National Academy of Sciences of the United States of America*, **98**(10): 5856–5861. doi:10.1073/pnas.081620098.

Feilen, LP, Chen, SY, Fukumori, A, Feederle, R, Zacharias, M, Steiner, H (2022). Active site geometry stabilization of a presenilin homolog by the lipid bilayer promotes intramembrane proteolysis. *eLife*, **11**: e76090. doi:10.7554/eLife.76090.

Feng, L, Yan, H, Wu, Z, Yan, N, Wang, Z, Jeffrey, PD, Shi, Y (2007). Structure of a site-2 protease family intramembrane metalloprotease. *Science*, **318**(5856): 1608–1612. doi:10.1126/science.1150755.

Fernandez, MA, Klutkowski, JA, Freret, T, Wolfe, MS (2014). Alzheimer presenilin-1 mutations dramatically reduce trimming of long amyloid β-peptides (Aβ) by γ-secretase to increase 42-to-40-residue Aβ. *Journal of Biological Chemistry*, **289**(45): 31043–31052. doi:10.1074/jbc.M114.581165.

Fleck, D, Voss, M, Brankatschk, B, Giudici, C, Hampel, H, Schwenk, B, Edbauer, D, Fukumori, A, Steiner, H, Kremmer, E, Haug-Kröper, M, Rossner, MJ, Fluhrer, R, Willem, M, Haass, C (2016). Proteolytic processing of Neuregulin 1 type III by three intramembrane-cleaving proteases. *Journal of Biological Chemistry*, **291**(1): 318–333. doi:10.1074/jbc.M115.697995.

Fluhrer, R, Kamp, F, Grammer, G, Nuscher, B, Steiner, H, Beyer, K, Haass, C (2011). The nicastrin ectodomain adopts a highly thermostable structure. *De Gruyter*, **392**(11): 995–1001. doi:10.1515/bc.2011.169.

Fortna, RR, Crystal, AS, Morais, VA, Pijak, DS, Lee, VMY, Doms, RW (2004). Membrane topology and nicastrin-enhanced endoproteolysis of APH-1, a component of the γ-secretase complex. *Journal of Biological Chemistry*, **279**(5): 3685–3693. doi:10.1074/jbc.M310505200.

Fraering, PC, Ye, W, Strub, JM, Dolios, G, LaVoie, MJ, Ostaszewski, BL, van Dorsselaer, A, Wang, R, Selkoe, DJ, Wolfe, MS (2004). Purification and characterization of the human γ-secretase complex. *Biochemistry*, **43**(30): 9774–9789. doi:10.1021/bi0494976.

Francis, R, McGrath, G, Zhang, J, Ruddy, DA, Sym, M, Apfeld, J, Nicoll, M, Maxwell, M, Hai, B, Ellis, MC, Parks, AL, Xu, W, Li, J, Gurney, M, Myers, RL, Himes, CS, Hiebsch, R, Ruble, C, Nye, JS, Curtis, D (2002). Aph-1 and pen-2 are required for Notch pathway signaling, γ-secretase cleavage of βAPP, and presenilin protein accumulation. *Developmental Cell*, **3**(1): 85–97. doi:10.1016/s1534-5807(02)00189-2.

Friedmann, E, Lemberg, MK, Weihofen, A, Dev, KK, Dengler, U, Rovelli, G, Martoglio, B (2004). Consensus analysis of signal peptide peptidase and homologous human aspartic proteases reveals opposite topology of catalytic domains compared with presenilins. *Journal of Biological Chemistry*, **279**(49): 50790–50798. doi:10.1074/jbc.M407898200.

Fukumori, A, Fluhrer, R, Steiner, H, Haass, C (2010). Three-amino acid spacing of presenilin endoproteolysis suggests a general stepwise cleavage of γ-secretase-mediated intramembrane proteolysis. *Journal of Neuroscience*, **30**(23): 7853–7862. doi:10.1523/jneurosci.1443-10.2010.

Fukumori, A, Steiner, H (2016). Substrate recruitment of γ-secretase and mechanism of clinical presenilin mutations revealed by photoaffinity mapping. *The EMBO Journal*, **35**(15): 1628–1643. doi:10.15252/embj.201694151.

Funamoto, S, Sasaki, T, Ishihara, S, Nobuhara, M, Nakano, M, Watanabe-Takahashi, M, Saito, T, Kakuda, N, Miyasaka, T, Nishikawa, K, Saido, TC, Ihara, Y (2013). Substrate ectodomain is critical for substrate preference and inhibition of γ-secretase. *Nature Communications*, **4**(2529): 1–12. doi:10.1038/ncomms3529.

Funamoto, S, Tagami, S, Okochi, M, Morishima-Kawashima, M (2020). Successive cleavage of β-amyloid precursor protein by γ-secretase. *Seminars in Cell and Developmental Biology*, **105**: 64–74. doi:10.1016/j.semcdb.2020.04.002.

Furukawa, K, Sopher, BL, Rydel, RE, Begley, JG, Pham, DG, Martin, GM, Fox, M, Mattson, MP (1996). Increased activity-regulating and neuroprotective efficacy of

α-secretase-derived secreted amyloid precursor protein conferred by a C-terminal heparin-binding domain. *Journal of Neurochemistry*, **67**(5): 1882–1896. doi: 10.1046/j.1471-4159.1996.67051882.x.

Ghanbari-Movahed, M, Ghanbari-Movahed, Z, Momtaz, S, Kilpatrick, KL, Farzaei, MH, Bishayee, A (2021). Unlocking the secrets of cancer stem cells with γ-secretase inhibitors: A novel anticancer strategy. *Molecules*, **26**(4): 972. doi:10.3390/ molecules26040972.

Gillman, KW, Starrett, JE, Parker, MF, Xie, K, Bronson, JJ, Marcin, LR, McElhone, KE, Bergstrom, CP, Mate, RA, Williams, R, Meredith, JE, Burton, CR, Barten, DM, Toyn, JH, Roberts, SB, Lentz, KA, Houston, JG, Zaczek, R, Albright, CF, Decicco, CP, Macor, JE, Olson, RE (2010). Discovery and evaluation of BMS-708163, a potent, selective and orally bioavailable γ-secretase inhibitor. *ACS Medicinal Chemistry Letters*, **1**(3): 120–124. doi:10.1021/ml1000239.

Glenner, GG, Wong, CW (1984). Alzheimer's disease and Down's syndrome: Sharing of a unique cerebrovascular amyloid fibril protein. *Biochemical and Biophysical Research Communications*, **122**(3): 1131–1135. doi:10.1016/0006-291x(84) 91209-9.

Goate, A, Chartier-Harlin, MC, Mullan, M, Brown, J, Crawford, F, Fidani, L, Giuffra, L, Haynes, A, Irving, N, L James, , et al. (1991). Segregation of a missense mutation in the amyloid precursor protein gene with familial Alzheimer's disease. *Nature*, **349**(6311): 704–706. doi:10.1038/349704a0.

Goedert, M, Wischik, CM, Crowther, RA, Walker, JE, Klug, A (1988). Cloning and sequencing of the cDNA encoding a core protein of the paired helical filament of Alzheimer disease: Identification as the microtubule-associated protein tau. *Proceedings of the National Academy of Sciences of the United States of America*, **85**(11): 4051–4055. doi:10.1073/pnas.85.11.4051.

Golde, TE, Estus, S, Younkin, LH, Selkoe, DJ, Younkin, SG (1992). Processing of the amyloid protein precursor to potentially amyloidogenic derivatives. *Science*, **255**(5045): 728–730. doi:10.1126/science.1738847.

Golde, TE, Koo, EH, Felsenstein, KM, Osborne, BA, Miele, L (2013). γ-Secretase inhibitors and modulators. *Biochimica et Biophysica Acta (BBA) - Biomembranes*, **1828**(12): 2898–2907. doi:10.1016/j.bbamem.2013.06.005.

Goutte, C, Tsunozaki, M, Hale, VA, Priess, JR (2002). APH-1 is a multipass membrane protein essential for the Notch signaling pathway in Caenorhabditis elegans

embryos. *Proceedings of the National Academy of Sciences of the United States of America*, **99**(2): 775–779. doi:10.1073/pnas.022523499.

Gratuze, M, Leyns, CEG, Holtzman, DM (2018). New insights into the role of TREM2 in Alzheimer's disease. *Molecular Neurodegeneration*, **13**(1): 66. doi:10.1186/s13024-018-0298-9.

Grieve, AG, Yeh, YC, Chang, YF, Huang, HY, Zarcone, L, Breuning, J, Johnson, N, Stříšovský, K, Brown, MH, Parekh, AB, Freeman, M (2021). Conformational surveillance of Orai1 by a rhomboid intramembrane protease prevents inappropriate CRAC channel activation. *Molecular Cell*, **81**(23): 4784–4789.e7. doi:10.1016/j.molcel.2021.10.025.

Grimm, MOW, Grimm, HS, Pätzold, AJ, Zinser, EG, Halonen, R, Duering, M, Tschäpe, JA, De Strooper, B, Müller, U, Shen, J, Hartmann, T (2005). Regulation of cholesterol and sphingomyelin metabolism by amyloid-β and presenilin. *Nature Cell Biology*, **7**(11): 1118–1123. doi:10.1038/ncb1313.

Grimm, MOW, Michaelson, DM, Hartmann, T (2017). Omega-3 fatty acids, lipids, and apoE lipidation in Alzheimer's disease: A rationale for multi-nutrient dementia prevention. *Journal of Lipid Research*, **58**(11): 2083–2101. doi:10.1194/jlr.R076331.

Grundke-Iqbal, I, Iqbal, K, Quinlan, M, Tung, YC, Zaidi, MS, Wisniewski, HM (1986). Microtubule-associated protein tau. A component of Alzheimer paired helical filaments. *Journal of Biological Chemistry*, **261**(13): 6084–6089.

Gu, Y, Chen, F, Sanjo, N, Kawarai, T, Hasegawa, H, Duthie, M, Li, W, Ruan, X, Luthra, A, Mount, HTJ, Tandon, A, Fraser, PE, George-Hyslop, PS (2003). APH-1 interacts with mature and immature forms of presenilins and nicastrin and may play a role in maturation of presenilin-nicastrin complexes. *Journal of Biological Chemistry*, **278**(9): 7374–7380. doi:10.1074/jbc.M209499200.

Gu, Y, Misonou, H, Sato, T, Dohmae, N, Takio, K, Ihara, Y (2001). Distinct intramembrane cleavage of the β-amyloid precursor protein family resembling γ-secretase-like cleavage of Notch. *Journal of Biological Chemistry*, **276**(38): 35235–35238. doi:10.1074/jbc.C100357200.

Güner, G, Lichtenthaler, SF (2020). The substrate repertoire of γ-secretase/presenilin. *Seminars in Cellular and Developmental Biology*, **105**: 27–42. doi:10.1016/j.semcdb.2020.05.019.

Haass, C, Capell, A, Citron, M, Teplow, DB, Selkoe, DJ (1995). The vacuolar H+-ATPase inhibitor bafilomycin A1 differentially affects proteolytic processing of mutant and wild-type β-amyloid precursor protein. *Journal of Biological Chemistry*, **270**(11): 6186–6192. doi:10.1074/jbc.270.11.6186.

Haass, C, Hung, AY, Schlossmacher, MG, Teplow, DB, Selkoe, DJ (1993). β-Amyloid peptide and a 3-kDa fragment are derived by distinct cellular mechanisms. *Journal of Biological Chemistry*, **268**(5): 3021–3024. doi:10.1016/s0021-9258(18)53650-4.

Haass, C, Kaether, C, Thinakaran, G, Sisodia, S (2012). Trafficking and proteolytic processing of APP. *Cold Spring Harbor Perspectives in Medicine*, **2**(5): a006270. doi:10.1101/cshperspect.a006270.

Haass, C, Koo, EH, Mellon, A, Hung, AY, Selkoe, DJ (1992a). Targeting of cell-surface β-amyloid precursor protein to lysosomes: Alternative processing into amyloid-bearing fragments. *Nature*, **357**(6378): 500–503. doi:10.1038/357500a0.

Haass, C, Schlossmacher, MG, Hung, AY, Vigo-Pelfrey, C, Mellon, A, Ostaszewski, BL, Lieberburg, I, Koo, EH, Schenk, D, Teplow, DB, Selkoe, DJ (1992b). Amyloid β-peptide is produced by cultured cells during normal metabolism. *Nature*, **359**(6393): 322–325. doi:10.1038/359322a0.

Haass, C, Selkoe, DJ (1993). Cellular processing of β-amyloid precursor protein and the genesis of amyloid β-peptide. *Cell*, **75**(6): 1039–1042. doi:10.1016/0092-8674(93)90312-e.

Habets, RA, de Bock, CE, Serneels, L, Lodewijckx, I, Verbeke, D, Nittner, D, Narlawar, R, Demeyer, S, Dooley, J, Liston, A, Taghon, T, Cools, J, de Strooper, B (2019). Safe targeting of T cell acute lymphoblastic leukemia by pathology-specific NOTCH inhibition. *Science Translational Medicine*, **11**(494): eaau6246. doi:10.1126/scitranslmed.aau6246.

Hardy, JA, Higgins, GA (1992). Alzheimer's disease: The amyloid cascade hypothesis. *Science*, **256**(5054): 184–185. doi:10.1126/science.1566067.

Hasegawa, H, Sanjo, N, Chen, F, Gu, YJ, Shier, C, Petit, A, Kawarai, T, Katayama, T, Schmidt, SD, Mathews, PM, Schmitt-Ulms, G, Fraser, PE, George-Hyslop, PS (2004). Both the sequence and length of the C terminus of PEN-2 are critical for intermolecular interactions and function of presenilin complexes. *Journal of Biological Chemistry*, **279**(45): 46455–46463. doi:10.1074/jbc.M406289200.

Hashimoto, T, Serrano-Pozo, A, Hori, Y, Adams, KW, Takeda, S, Banerji, AO, Mitani, A, Joyner, D, Thyssen, DH, Bacskai, BJ, Frosch, MP, Spires-Jones, TL,

Finn, MB, Holtzman, DM, Hyman, BT (2012). Apolipoprotein E, especially apolipoprotein E4, increases the oligomerization of amyloid β peptide. *Journal of Neuroscience*, **32**(43): 15181–15192. doi:10.1523/jneurosci.1542-12.2012.

Hashimoto, Y, Matsuoka, M (2014). A mutation protective against Alzheimer's disease renders amyloid β precursor protein incapable of mediating neurotoxicity. *Journal of Neurochemistry*, **130**(2): 291–300. doi:10.1111/jnc.12717.

Hatami, A, Monjazeb, S, Milton, S, Glabe, CG (2017). Familial Alzheimer's Disease mutations within the amyloid precursor protein alter the aggregation and conformation of the amyloid-β peptide. *Journal of Biological Chemistry*, **292**(8): 3172–3185. doi:10.1074/jbc.M116.755264.

He, G, Luo, W, Li, P, Remmers, C, Netzer, WJ, Hendrick, J, Bettayeb, K, Flajolet, M, Gorelick, F, Wennogle, LP, Greengard, P (2010). γ-Secretase activating protein is a therapeutic target for Alzheimer's disease. *Nature*, **467**(7311): 95–98. doi:10.1038/nature09325.

Hecimovic, S, Wang, J, Dolios, G, Martinez, M, Wang, R, Goate, AM (2004). Mutations in APP have independent effects on Aβ and CTFγ generation. *Neurobiology of Disease*, **17**(2): 205–218. doi:10.1016/j.nbd.2004.04.018.

Henley, DB, May, PC, Dean, RA, Siemers, ER (2009). Development of semagacestat (LY450139), a functional γ-secretase inhibitor, for the treatment of Alzheimer's disease. *Expert Opinion on Pharmacotherapy*, **10**(10): 1657–1664. doi:10.1517/14656560903044982.

Henricson, A, Käll, L, Sonnhammer, ELL (2005). A novel transmembrane topology of presenilin based on reconciling experimental and computational evidence. *FEBS Journal*, **272**(11): 2727–2733. doi:10.1111/j.1742-4658.2005.04691.x.

Henstridge, CM, Hyman, BT, Spires-Jones, TL (2019). Beyond the neuron-cellular interactions early in Alzheimer disease pathogenesis. *Nature Reviews Neuroscience*, **20**(2): 94–108. doi:10.1038/s41583-018-0113-1.

Herreman, A, Van Gassen, G, Bentahir, M, Nyabi, O, Craessaerts, K, Mueller, U, Annaert, W, De Strooper, B (2003). γ-Secretase activity requires the presenilin-dependent trafficking of nicastrin through the Golgi apparatus but not its complex glycosylation. *Journal of Cell Science*, **116**(Pt 6): 1127–1136. doi:10.1242/jcs.00292.

Hitschler, L, Lang, T (2022). The transmembrane domain of the amyloid precursor protein is required for anti-amyloidogenic processing by α-secretase ADAM10. *Journal of Biological Chemistry*, **298**(6): 101911. doi:10.1016/j.jbc.2022.101911.

Hitzenberger, M, Götz, A, Menig, S, Brunschweiger, B, Zacharias, M, Scharnagl, C (2020). The dynamics of γ-secretase and its substrates. *Seminars in Cell and Developmental Biology*, **105**: 86–101. doi:10.1016/j.semcdb.2020.04.008.

Hitzenberger, M, Zacharias, M (2019a). γ-Secretase studied by atomistic molecular dynamics simulations: Global dynamics, enzyme activation, water distribution and lipid binding. *Frontiers in Chemistry*, **6**: 640. doi:10.3389/fchem.2018.00640.

Hitzenberger, M, Zacharias, M (2019b). Structural modeling of γ-secretase Aβn complex formation and substrate processing. *ACS Chemical Neuroscience*, **10**(3): 1826–1840. doi:10.1021/acschemneuro.8b00725.

Hitzenberger, M, Zacharias, M (2019c). Uncovering the binding mode of γ-secretase inhibitors. *ACS Chemical Neuroscience*, **10**(8): 3398–3403. doi:10.1021/acschemneuro.9b00272.

Hoefgen, S, Coburger, I, Roeser, D, Schaub, Y, Dahms, SO, Than, ME (2014). Heparin induced dimerization of APP is primarily mediated by E1 and regulated by its acidic domain. *Journal of Structural Biology*, **187**(1): 30–37. doi:10.1016/j.jsb.2014.05.006.

Holmes, O, Paturi, S, Ye, W, Wolfe, MS, Selkoe, DJ (2012). The effects of membrane lipids on the activity and processivity of purified γ-secretase. *Biochemistry*, **51**(17): 3565. doi:10.1021/bi300303g.

Holtzman, DM, Morris, JC, Goate, AM (2011). Alzheimer's disease: The challenge of the second century. *Science Translational Medicine*, **3**(77): 77sr1. doi:10.1126/scitranslmed.3002369.

Hori, Y, Hashimoto, T, Wakutani, Y, Urakami, K, Nakashima, K, Condron, MM, Tsubuki, S, Saido, TC, Teplow, DB, Iwatsubo, T (2007). The Tottori (D7N) and English (H6R) familial Alzheimer disease mutations accelerate Aβ fibril formation without increasing protofibril formation. *Journal Biological Chemistry*, **282**(7): 4916–4923. doi:10.1074/jbc.M608220200.

Hua, Y, Nair, S (2015). Proteases in cardiometabolic diseases: Pathophysiology, molecular mechanisms and clinical applications. *Biochimica et Biophysica Acta*, **1852**(2): 195–208. doi:10.1016/j.bbadis.2014.04.032.

Hur, JY, Frost, GR, Wu, X, Crump, C, Pan, SJ, Wong, E, Barros, M, Li, T, Nie, P, Zhai, Y, Wang, JC, Tcw, J, Guo, L, McKenzie, A, Ming, C, Zhou, X, Wang, M, Sagi, Y, Renton, AE, Esposito, BT, Kim, Y, Sadleir, KR, Trinh, I, Rissman, RA, Vassar, R, Zhang, B, Johnson, DS, Masliah, E, Greengard, P, Goate, A, Li, YM (2020). The innate immunity protein IFITM3 modulates γ-secretase in Alzheimer's disease. *Nature*, **586**(7831): 735–740. doi:10.1038/s41586-020-2681-2.

Hur, JY, Welander, H, Behbahani, H, Aoki, M, Frånberg, J, Winblad, B, Frykman, S, Tjernberg, LO (2008). Active γ-secretase is localized to detergent-resistant membranes in human brain. *FEBS Journal*, **275**(6): 1174–1187. doi:10.1111/j.1742-4658.2008.06278.x.

Hussain, I, Fabrègue, J, Anderes, L, Ousson, S, Borlat, F, Eligert, V, Berger, S, Dimitrov, M, Alattia, JR, Fraering, PC, Beher, D (2013). The role of γ-secretase activating protein (GSAP) and imatinib in the regulation of γ-secretase activity and amyloid-β generation. *Journal of Biological Chemistry*, **288**(4): 2521–2531. doi:10.1074/jbc.M112.370924.

Hyman, BT, Phelps, CH, Beach, TG, Bigio, EH, Cairns, NJ, Carrillo, MC, Dickson, DW, Duyckaerts, C, Frosch, MP, Masliah, E, Mirra, SS, Nelson, PT, Schneider, JA, Thal, DR, Thies, B, Trojanowski, JQ, Vinters, HV, Montine, TJ (2012). National Institute on Aging–Alzheimer's Association guidelines for the neuropathologic assessment of Alzheimer's disease. *Alzheimer's & Dementia*, **8**(1): 1–13. doi:10.1016/j.jalz.2011.10.007.

Hébert, SS, Serneels, L, Dejaegere, T, Horré, K, Dabrowski, M, Baert, V, Annaert, W, Hartmann, D, De Strooper, B (2004). Coordinated and widespread expression of γ-secretase in vivo: Evidence for size and molecular heterogeneity. *Neurobiology of Disease*, **17**(2): 260–272. doi:10.1016/j.nbd.2004.08.002.

Hébert, SS, Serneels, L, Tolia, A, Craessaerts, K, Derks, C, Filippov, MA, Müller, U, De Strooper, B (2006). Regulated intramembrane proteolysis of amyloid precursor protein and regulation of expression of putative target genes. *EMBO Reports*, **7**(7): 739–745. doi:10.1038/sj.embor.7400704.

Ikeuchi, T, Dolios, G, Kim, SH, Wang, R, Sisodia, SS (2003). Familial Alzheimer disease-linked presenilin 1 variants enhance production of both Aβ 1-40 and Aβ 1-42 peptides that are only partially sensitive to a potent aspartyl protease transition state inhibitor of "γ-secretase". *Journal Biological Chemistry*, **278**(9): 7010–7018. doi:10.1074/jbc.M209252200.

Ikeuchi, T, Kaneko, H, Miyashita, A, Nozaki, H, Kasuga, K, Tsukie, T, Tsuchiya, M, Imamura, T, Ishizu, H, Aoki, K, Ishikawa, A, Onodera, O, Kuwano, R, Nishizawa, M (2008). Mutational analysis in early-onset familial dementia in the Japanese population. The role of PSEN1 and MAPT R406W mutations. *Dementia and Geriatric Cognitive Disorders*, **26**(1): 43–49. doi:10.1159/000141483.

Isoo, N, Sato, C, Miyashita, H, Shinohara, M, Takasugi, N, Morohashi, Y, Tsuji, S, Tomita, T, Iwatsubo, T (2007). Aβ42 overproduction associated with structural changes in the catalytic pore of γ-secretase: Common effects of Pen-2 N-terminal elongation and fenofibrate. *Journal of Biological Chemistry*, **282**(17): 12388–12396. doi:10.1074/jbc.M611549200.

Iwatsubo, T, Odaka, A, Suzuki, N, Mizusawa, H, Nukina, N, Ihara, Y (1994). Visualization of Aβ42(43) and Aβ40 in senile plaques with end-specific Aβ monoclonals: Evidence that an initially deposited species is Aβ42(43). *Neuron*, **13**(1): 45–53. doi:10.1016/0896-6273(94)90458-8.

Jacobsen, H, Reinhardt, D, Brockhaus, M, Bur, D, Kocyba, C, Kurt, H, Grim, MG, Baumeister, R, Loetscher, H (1999). The influence of endoproteolytic processing of familial Alzheimer's disease presenilin 2 on Aβ42 amyloid peptide formation. *Journal of Biological Chemistry*, **274**(49): 35233–35239. doi:10.1074/jbc.274.49.35233.

Jarrett, JT, Berger, EP, Lansbury, PT, Jr. (1993). The carboxy terminus of the β amyloid protein is critical for the seeding of amyloid formation: Implications for the pathogenesis of Alzheimer's disease. *Biochemistry*, **32**(18): 4693–4697. doi:10.1021/bi00069a001.

Jarrett, JT, Lansbury, PT, Jr. (1993). Seeding "one-dimensional crystallization" of amyloid: A pathogenic mechanism in Alzheimer's disease and scrapie? *Cell*, **73**(6): 1055–1058. doi:10.1016/0092-8674(93)90635-4.

Jay, TR, Hirsch, AM, Broihier, ML, Miller, CM, Neilson, LE, Ransohoff, RM, Lamb, BT, Landreth, GE (2017). Disease progression-dependent effects of TREM2 deficiency in a mouse model of Alzheimer's disease. *Journal of Neuroscience*, **37**(3): 637–647. doi:10.1523/jneurosci.2110-16.2016.

Jonsson, T, Atwal, JK, Steinberg, S, Snaedal, J, Jonsson, PV, Bjornsson, S, Stefansson, H, Sulem, P, Gudbjartsson, D, Maloney, J, Hoyte, K, Gustafson, A, Liu, Y, Lu, Y, Bhangale, T, Graham, RR, Huttenlocher, J, Bjornsdottir, G, Andreassen, OA, Jönsson, EG, Palotie, A, Behrens, TW, Magnusson, OT, Kong, A, Thorsteinsdottir, U, Watts, RJ, Stefansson, K (2012). A mutation in APP

protects against Alzheimer's disease and age-related cognitive decline. *Nature*, **488**(7409): 96–99. doi:10.1038/nature11283.

Jumper, J, Evans, R, Pritzel, A, Green, T, Figurnov, M, Ronneberger, O, Tunyasuvunakool, K, Bates, R, Žídek, A, Potapenko, A, Bridgland, A, Meyer, C, Kohl, SAA, Ballard, AJ, Cowie, A, Romera-Paredes, B, Nikolov, S, Jain, R, Adler, J, Back, T, Petersen, S, Reiman, D, Clancy, E, Zielinski, M, Steinegger, M, Pacholska, M, Berghammer, T, Bodenstein, S, Silver, D, Vinyals, O, Senior, AW, Kavukcuoglu, K, Kohli, P, Hassabis, D (2021). Highly accurate protein structure prediction with AlphaFold. *Nature*, **596**(7873): 583–589. doi:10.1038/s41586-021-03819-2.

Jung, JI, Ran, Y, Cruz, PE, Rosario, AM, Ladd, TB, Kukar, TL, Koo, EH, Felsenstein, KM, Golde, TE (2014). Complex relationships between substrate sequence and sensitivity to alterations in γ-secretase processivity induced by γ-secretase modulators. *Biochemistry*, **53**(12): 1947–1957. doi:10.1021/bi401521t.

Jurisch-Yaksi, N, Sannerud, R, Annaert, W (2013). A fast growing spectrum of biological functions of γ-secretase in development and disease. *Biochimica et Biophysica Acta (BBA) - Biomembranes*, **1828**(12): 2815–2827. doi:10.1016/j.bbamem.2013.04.016.

Jäkel, L, Boche, D, Nicoll, JAR, Verbeek, MM (2019). Aβ43 in human Alzheimer's disease: Effects of active Aβ42 immunization. *Acta Neuropathologica Communications*, **7**(1): 141. doi:10.1186/s40478-019-0791-6.

Kaden, D, Munter, LM, Joshi, M, Treiber, C, Weise, C, Bethge, T, Voigt, P, Schaefer, M, Beyermann, M, Reif, B, Multhaup, G (2008). Homophilic interactions of the amyloid precursor protein (APP) ectodomain are regulated by the loop region and affect β-secretase cleavage of APP. *Journal of Biological Chemistry*, **283**(11): 7271–7279. doi:10.1074/jbc.M708046200.

Kaether, C, Capell, A, Edbauer, D, Winkler, E, Novak, B, Steiner, H, Haass, C (2004). The presenilin C-terminus is required for ER-retention, nicastrin-binding and γ-secretase activity. *The EMBO Journal*, **23**(24): 4738–4748. doi:10.1038/sj.emboj.7600478.

Kaether, C, Lammich, S, Edbauer, D, Ertl, M, Rietdorf, J, Capell, A, Steiner, H, Haass, C (2002). Presenilin-1 affects trafficking and processing of βAPP and is targeted in a complex with nicastrin to the plasma membrane. *Journal of Cell Biology*, **158**(3): 551–561. doi:10.1083/jcb.200201123.

Kaether, C, Scheuermann, J, Fassler, M, Zilow, S, Shirotani, K, Valkova, C, Novak, B, Kacmar, S, Steiner, H, Haass, C (2007). Endoplasmic reticulum retention of the γ-secretase complex component Pen2 by Rer1. *EMBO Reports*, **8**(8): 743–748. doi:10.1038/sj.embor.7401027.

Kakuda, N, Takami, M, Okochi, M, Kasuga, K, Ihara, Y, Ikeuchi, T (2021). Switched Aβ43 generation in familial Alzheimer's disease with presenilin 1 mutation. *Translational Psychiatry*, **11**(1): 558. doi:10.1038/s41398-021-01684-1.

Kalvodova, L, Kahya, N, Schwille, P, Ehehalt, R, Verkade, P, Drechsel, D, Simons, K (2005). Lipids as modulators of proteolytic activity of BACE: Involvement of cholesterol, glycosphingolipids, and anionic phospholipids in vitro. *Journal of Biological Chemistry*, **280**(44): 36815–36823. doi:10.1074/jbc.M504484200.

Kamp, F, Winkler, E, Trambauer, J, Ebke, A, Fluhrer, R, Steiner, H (2015). Intramembrane proteolysis of β-amyloid precursor protein by γ-secretase is an unusually slow process. *Biophysical Journal*, **108**(5): 1229–1237. doi:10.1016/j.bpj.2014.12.045.

Kanatsu, K, Morohashi, Y, Suzuki, M, Kuroda, H, Watanabe, T, Tomita, T, Iwatsubo, T (2014). Decreased CALM expression reduces Aβ42 to total Aβ ratio through clathrin-mediated endocytosis of γ-secretase. *Nature Communications*, **5**(3386): 1–12. doi:10.1038/ncomms4386.

Kang, J, Lemaire, HG, Unterbeck, A, Salbaum, JM, Masters, CL, Grzeschik, KH, Multhaup, G, Beyreuther, K, Müller-Hill, B (1987). The precursor of Alzheimer's disease amyloid A4 protein resembles a cell-surface receptor. *Nature*, **325**(6106): 733–736. doi:10.1038/325733a0.

Kao, YC, Ho, PC, Tu, YK, Jou, IM, Tsai, KJ (2020). Lipids and Alzheimer's disease. *International Journal of Molecular Sciences*, **21**(4): 1505. doi:10.3390/ijms21041505.

Kayatekin, C, Amasino, A, Gaglia, G, Flannick, J, Bonner, JM, Fanning, S, Narayan, P, Barrasa, MI, Pincus, D, Landgraf, D, Nelson, J, Hesse, WR, Costanzo, M, Myers, CL, Boone, C, Florez, JC, Lindquist, S (2018). Translocon declogger Ste24 protects against IAPP oligomer-induced proteotoxicity. *Cell*, **173**(1): 62–73.e9. doi:10.1016/j.cell.2018.02.026.

Keren-Shaul, H, Spinrad, A, Weiner, A, Matcovitch-Natan, O, Dvir-Szternfeld, R, Ulland, TK, David, E, Baruch, K, Lara-Astaiso, D, Toth, B, Itzkovitz, S, Colonna,

M, Schwartz, M, Amit, I (2017). A unique microglia type associated with restricting development of Alzheimer's disease. *Cell*, **169**(7): 1276–129017. doi: 10.1016/j.cell.2017.05.018.

Khan, AR, James, MN (1998). Molecular mechanisms for the conversion of zymogens to active proteolytic enzymes. *Protein Science*, **7**(4): 815–836. doi:10.1002/pro.5560070401.

Kim, J, Castellano, JM, Jiang, H, Basak, JM, Parsadanian, M, Pham, V, Mason, SM, Paul, SM, Holtzman, DM (2009). Overexpression of low-density lipoprotein receptor in the brain markedly inhibits amyloid deposition and increases extracellular Aβ clearance. *Neuron*, **64**(5): 632–644. doi:10.1016/j.neuron.2009.11.013.

Kim, J, Onstead, L, Randle, S, Price, R, Smithson, L, Zwizinski, C, Dickson, DW, Golde, T, McGowan, E (2007). Aβ40 inhibits amyloid deposition in vivo. *Journal of Neuroscience*, **27**(3): 627–633. doi:10.1523/jneurosci.4849-06.2007.

Kimberly, WT, LaVoie, MJ, Ostaszewski, BL, Ye, W, Wolfe, MS, Selkoe, DJ (2003). γ-Secretase is a membrane protein complex comprised of presenilin, nicastrin, Aph-1, and Pen-2. *Proceedings of the National Academy of Sciences of the United States of America*, **100**(11): 6382–6387. doi:10.1073/pnas.1037392100.

Kimberly, WT, Xia, W, Rahmati, T, Wolfe, MS, Selkoe, DJ (2000). The transmembrane aspartates in presenilin 1 and 2 are obligatory for γ-secretase activity and amyloid β-protein generation. *Journal of Biological Chemistry*, **275**(5): 3173–3178. doi:10.1074/jbc.275.5.3173.

Kimberly, WT, Zheng, JB, Guénette, SY, Selkoe, DJ (2001). The intracellular domain of the β-amyloid precursor protein is stabilized by Fe65 and translocates to the nucleus in a notch-like manner. *Journal of Biological Chemistry*, **276**(43): 40288–40292. doi:10.1074/jbc.C100447200.

Kimura, A, Hata, S, Suzuki, T (2016). Alternative selection of β-site APP-cleaving enzyme 1 (BACE1) cleavage sites in amyloid β-protein precursor (APP) harboring protective and pathogenic mutations within the Aβ sequence. *Journal Biological Chemistry*, **291**(46): 24041–24053. doi:10.1074/jbc.M116.744722.

Klein, T, Eckhard, U, Dufour, A, Solis, N, Overall, CM (2018). Proteolytic cleavage—mechanisms, function, and "omic" approaches for a near-ubiquitous posttranslational modification. *Chemical Reviews*, **118**(3): 1137–1168. doi: 10.1021/acs.chemrev.7b00120.

Knopman, DS, Jones, DT, Greicius, MD (2021). Failure to demonstrate efficacy of aducanumab: An analysis of the EMERGE and ENGAGE trials as reported by Biogen, December 2019. *Alzheimer's & Dementia*, **17**(4): 696–701. doi:10.1002/alz.12213.

Koffie, RM, Meyer-Luehmann, M, Hashimoto, T, Adams, KW, Mielke, ML, Garcia-Alloza, M, Micheva, KD, Smith, SJ, Kim, ML, Lee, VM, Hyman, BT, Spires-Jones, TL (2009). Oligomeric amyloid β associates with postsynaptic densities and correlates with excitatory synapse loss near senile plaques. *Proceedings of the National Academy of Sciences of the United States of America*, **106**(10): 4012–4017. doi:10.1073/pnas.0811698106.

Koo, EH, Squazzo, SL (1994). Evidence that production and release of amyloid β-protein involves the endocytic pathway. *Journal of Biological Chemistry*, **269**(26): 17386–17389.

Korn, P, Schwieger, C, Gruhle, K, Garamus, VM, Meister, A, Ihling, C, Drescher, S (2022). Azide- and diazirine-modified membrane lipids: Physicochemistry and applicability to study peptide/lipid interactions via cross-linking/mass spectrometry. *Biochimica et Biophysica Acta (BBA) - Biomembranes*, **1864**(10): 184004. doi:10.1016/j.bbamem.2022.184004.

Kornilova, AY, Bihel, F, Das, C, Wolfe, MS (2005). The initial substrate-binding site of γ-secretase is located on presenilin near the active site. *Proceedings of the National Academy of Sciences of the United States of America*, **102**(9): 3230–3235. doi:10.1073/pnas.0407640102.

Kornilova, AY, Das, C, Wolfe, MS (2003). Differential effects of inhibitors on the γ-secretase complex: Mechanistic implications. *Journal of Biological Chemistry*, **278**(19): 16470–16473. doi:10.1074/jbc.C300019200.

Kosik, KS, Joachim, CL, Selkoe, DJ (1986). Microtubule-associated protein tau (τ) is a major antigenic component of paired helical filaments in Alzheimer disease. *Proceedings of the National Academy of Sciences of the United States of America*, **83**(11): 4044–4048. doi:10.1073/pnas.83.11.4044.

Krasemann, S, Madore, C, Cialic, R, Baufeld, C, Calcagno, N, Fatimy, RE, Beckers, L, O'Loughlin, E, Xu, Y, Fanek, Z, Greco, DJ, Smith, ST, Tweet, G, Humulock, Z, Zrzavy, T, Conde-Sanroman, P, Gacias, M, Weng, Z, Chen, H, Tjon, E, Mazaheri, F, Hartmann, K, Madi, A, Ulrich, JD, Glatzel, M, Worthmann, A, Heeren, J, Budnik, B, Lemere, C, Ikezu, T, Heppner, FL, Litvak, V, Holtzman, DM, Lassmann, H, Weiner, HL, Ochando, J, Haass, C, Butovsky, O (2017).

The TREM2-APOE pathway drives the transcriptional phenotype of dysfunctional microglia in neurodegenerative diseases. *Immunity*, **47**(3): 566–5819. doi: 10.1016/j.immuni.2017.08.008.

Kretner, B, Fukumori, A, Kuhn, PH, Pérez-Revuelta, BI, Lichtenthaler, SF, Haass, C, Steiner, H (2013). Important functional role of residue x of the presenilin GxGD protease active site motif for APP substrate cleavage specificity and substrate selectivity of γ-secretase. *Journal of Neurochemistry*, **125**(1): 144–156. doi:10. 1111/jnc.12124.

Kretner, B, Trambauer, J, Fukumori, A, Mielke, J, Kuhn, PH, Kremmer, E, Giese, A, Lichtenthaler, SF, Haass, C, Arzberger, T, Steiner, H (2016). Generation and deposition of Aβ43 by the virtually inactive presenilin-1 L435F mutant contradicts the presenilin loss-of-function hypothesis of Alzheimer's disease. *EMBO Molecular Medicine*, **8**(5): 458–465. doi:10.15252/emmm.201505952.

Kreutzberger, AJB, Ji, M, Aaron, J, Mihaljević, L, Urban, S (2019). Rhomboid distorts lipids to break the viscosity-imposed speed limit of membrane diffusion. *Science*, **363**(6426): eaao0076. doi:10.1126/science.aao0076.

Kuhn, PH, Wang, H, Dislich, B, Colombo, A, Zeitschel, U, Ellwart, JW, Kremmer, E, Rossner, S, Lichtenthaler, SF (2010). ADAM10 is the physiologically relevant, constitutive α-secretase of the amyloid precursor protein in primary neurons. *The EMBO Journal*, **29**(17): 3020–3032. doi:10.1038/emboj.2010.167.

Kukar, T, Murphy, MP, Eriksen, JL, Sagi, SA, Weggen, S, Smith, TE, Ladd, T, Khan, MA, Kache, R, Beard, J, Dodson, M, Merit, S, Ozols, VV, Anastasiadis, PZ, Das, P, Fauq, A, Koo, EH, Golde, TE (2005). Diverse compounds mimic Alzheimer disease-causing mutations by augmenting Aβ42 production. *Nature Medicine*, **11**(5): 545–550. doi:10.1038/nm1235.

Kukar, TL, Ladd, TB, Robertson, P, Pintchovski, SA, Moore, B, Bann, MA, Ren, Z, Jansen-West, K, Malphrus, K, Eggert, S, Maruyama, H, Cottrell, BA, Das, P, Basi, GS, Koo, EH, Golde, TE (2011). Lysine 624 of the amyloid precursor protein (APP) is a critical determinant of amyloid β peptide length: Support for a sequential model of γ-secretase intramembrane proteolysis and regulation by the amyloid β precursor protein (APP) juxtamembrane region. *Journal of Biological Chemistry*, **286**(46): 39804–39812. doi:10.1074/jbc.M111.274696.

Kuo, IY, Hu, J, Ha, Y, Ehrlich, BE (2015). Presenilin-like GxGD membrane proteases have dual roles as proteolytic enzymes and ion channels. *Journal of Biological Chemistry*, **290**(10): 6419–6427. doi:10.1074/jbc.M114.629584.

Kuperstein, I, Broersen, K, Benilova, I, Rozenski, J, Jonckheere, W, Debulpaep, M, Vandersteen, A, Segers-Nolten, I, Van Der Werf, K, Subramaniam, V, Braeken, D, Callewaert, G, Bartic, C, D'Hooge, R, Martins, IC, Rousseau, F, Schymkowitz, J, De Strooper, B (2010). Neurotoxicity of Alzheimer's disease Aβ peptides is induced by small changes in the Aβ42 to Aβ40 ratio. *The EMBO Journal*, **29**(19): 3408–3420. doi:10.1038/emboj.2010.211.

Kwok, JB, Li, QX, Hallupp, M, Whyte, S, Ames, D, Beyreuther, K, Masters, CL, Schofield, PR (2000). Novel Leu723Pro amyloid precursor protein mutation increases amyloid β42(43) peptide levels and induces apoptosis. *Annals of Neurology*, **47**(2): 249–253. doi:10.1002/1531-8249(200002)47:2<249::aid-ana18>3.0.co;2-8.

Köpke, E, Tung, YC, Shaikh, S, Alonso, AC, Iqbal, K, Grundke-Iqbal, I (1993). Microtubule-associated protein tau. Abnormal phosphorylation of a non-paired helical filament pool in Alzheimer disease. *Journal Biological Chemistry*, **268**(32): 24374–24384.

Kühnle, N, Dederer, V, Lemberg, MK (2019). Intramembrane proteolysis at a glance: From signalling to protein degradation. *Journal of Cell Science*, **132**(16): jcs217745. doi:10.1242/jcs.217745.

Lacor, PN, Buniel, MC, Furlow, PW, Clemente, AS, Velasco, PT, Wood, M, Viola, KL, Klein, WL (2007). Aβ oligomer-induced aberrations in synapse composition, shape, and density provide a molecular basis for loss of connectivity in Alzheimer's disease. *Journal of Neuroscience*, **27**(4): 796–807. doi:10.1523/jneurosci.3501-06.2007.

Lai, A, Sisodia, SS, Trowbridge, IS (1995). Characterization of sorting signals in the β-amyloid precursor protein cytoplasmic domain. *Journal of Biological Chemistry*, **270**(8): 3565–3573. doi:10.1074/jbc.270.8.3565.

Lammich, S, Kojro, E, Postina, R, Gilbert, S, Pfeiffer, R, Jasionowski, M, Haass, C, Fahrenholz, F (1999). Constitutive and regulated α-secretase cleavage of Alzheimer's amyloid precursor protein by a disintegrin metalloprotease. *Proceedings of the National Academy of Sciences of the United States of America*, **96**(7): 3922–3927. doi:10.1073/pnas.96.7.3922.

Landman, N, Jeong, SY, Shin, SY, Voronov, SV, Serban, G, Kang, MS, Park, MK, Di Paolo, G, Chung, S, Kim, TW (2006). Presenilin mutations linked to familial Alzheimer's disease cause an imbalance in phosphatidylinositol 4,5-bisphosphate metabolism. *Proceedings of the National Academy of Sciences of the United States of America*, **103**(51): 19524–19529. doi:10.1073/pnas.0604954103.

Langosch, D, Scharnagl, C, Steiner, H, Lemberg, MK (2015). Understanding intramembrane proteolysis: From protein dynamics to reaction kinetics. *Trends in Biochemical Sciences*, **40**(6): 318–327. doi:10.1016/j.tibs.2015.04.001.

Lanz, TA, Hosley, JD, Adams, WJ, Merchant, KM (2004). Studies of Aβ pharmacodynamics in the brain, cerebrospinal fluid, and plasma in young (Plaque-Free) Tg2576 mice using the γ-secretase inhibitor N2-[(2S)-2-(3,5-Difluorophenyl)-2-hydroxyethanoyl]-N1-[(7S)-5-methyl-6-oxo-6,7-dihydro-5H-dibenzo[b,d]azepin-7-yl]-L-alaninamide (LY-411575). *Journal of Pharmacology and Experimental Therapeutics*, **309**(1): 49–55. doi:10.1124/jpet.103.060715.

Lastun, VL, Grieve, AG, Freeman, M (2016). Substrates and physiological functions of secretase rhomboid proteases. *Seminars in Cell and Developmental Biology*, **60**: 10–18. doi:10.1016/j.semcdb.2016.07.033.

Laudon, H, Hansson, EM, Melén, K, Bergman, A, Farmery, MR, Winblad, B, Lendahl, U, von Heijne, G, Näslund, J (2005). A nine-transmembrane domain topology for presenilin 1. *Journal of Biological Chemistry*, **280**(42): 35352–35360. doi:10.1074/jbc.M507217200.

LaVoie, MJ, Fraering, PC, Ostaszewski, BL, Ye, W, Kimberly, WT, Wolfe, MS, Selkoe, DJ (2003). Assembly of the γ-secretase complex involves early formation of an intermediate subcomplex of Aph-1 and nicastrin. *Journal of Biological Chemistry*, **278**(39): 37213–37222. doi:10.1074/jbc.M303941200.

Lazarov, VK, Fraering, PC, Ye, W, Wolfe, MS, Selkoe, DJ, Li, H (2006). Electron microscopic structure of purified, active γ-secretase reveals an aqueous intramembrane chamber and two pores. *Proceedings of the National Academy of Sciences of the United States of America*, **103**(18): 6889–6894. doi:10.1073/pnas.0602321103.

Lee, JY, Feng, Z, Xie, XQ, Bahar, I (2017). Allosteric modulation of intact γ-secretase structural dynamics. *Biophysical Journal*, **113**(12): 2634–2649. doi:10.1016/j.bpj.2017.10.012.

Lee, SF, Shah, S, Li, H, Yu, C, Han, W, Yu, G (2002). Mammalian APH-1 interacts with presenilin and nicastrin and is required for intramembrane proteolysis of amyloid-β precursor protein and Notch. *Journal of Biological Chemistry*, **277**(47): 45013–45019. doi:10.1074/jbc.M208164200.

Leem, JY, Vijayan, S, Han, P, Cai, D, Machura, M, Lopes, KO, Veselits, ML, Xu, H, Thinakaran, G (2002). Presenilin 1 is required for maturation and cell surface accumulation of nicastrin. *Journal of Biological Chemistry*, **277**(21): 19236–19240. doi:10.1074/jbc.C200148200.

Lemberg, MK, Strisovsky, K (2021). Maintenance of organellar protein homeostasis by ER-associated degradation and related mechanisms. *Molecular Cell*, **81**(12): 2507–2519. doi:10.1016/j.molcel.2021.05.004.

Lemieux, MJ, Fischer, SJ, Cherney, MM, Bateman, KS, James, MNG (2007). The crystal structure of the rhomboid peptidase from Haemophilus influenzae provides insight into intramembrane proteolysis. *Proceedings of the National Academy of Sciences of the United States of America*, **104**(3): 750–754. doi:10.1073/pnas.0609981104.

Levy-Lahad, E, Wasco, W, Poorkaj, P, Romano, DM, Oshima, J, Pettingell, WH, Yu, CE, Jondro, PD, Schmidt, SD, K Wang, , et al. (1995). Candidate gene for the chromosome 1 familial Alzheimer's disease locus. *Science*, **269**(5226): 973–977. doi:10.1126/science.7638622.

Li, S, Hong, S, Shepardson, NE, Walsh, DM, Shankar, GM, Selkoe, D (2009). Soluble oligomers of amyloid β protein facilitate hippocampal long-term depression by disrupting neuronal glutamate uptake. *Neuron*, **62**(6): 788–801. doi:10.1016/j.neuron.2009.05.012.

Li, X, Dang, S, Yan, C, Gong, X, Wang, J, Shi, Y (2013). Structure of a presenilin family intramembrane aspartate protease. *Nature*, **493**(7430): 56–61. doi:10.1038/nature11801.

Li, Y, Lu, SHJ, Tsai, CJ, Bohm, C, Qamar, S, Dodd, RB, Meadows, W, Jeon, A, McLeod, A, Chen, F, Arimon, M, Berezovska, O, Hyman, BT, Tomita, T, Iwatsubo, T, Johnson, CM, Farrer, LA, Schmitt-Ulms, G, Fraser, PE, St George-Hyslop, PH (2014). Structural interactions between inhibitor and substrate docking sites give insight into mechanisms of human PS1 complexes. *Structure*, **22**(1): 125–135. doi:10.1016/j.str.2013.09.018.

Li, YM, Xu, M, Lai, MT, Huang, Q, Castro, JL, DiMuzio-Mower, J, Harrison, T, Lellis, C, Nadin, A, Neduvelil, JG, Register, RB, Sardana, MK, Shearman, MS, Smith, AL, Shi, XP, Yin, KC, Shafer, JA, Gardell, SJ (2000). Photoactivated γ-secretase inhibitors directed to the active site covalently label presenilin 1. *Nature*, **405**(6787): 689–694. doi:10.1038/35015085.

Liu, CC, Liu, CC, Kanekiyo, T, Xu, H, Bu, G (2013). Apolipoprotein E and Alzheimer disease: Risk, mechanisms and therapy. *Nature Reviews Neurology*, **9**(2): 106–118. doi:10.1038/nrneurol.2012.263.

Liu, L, Ding, L, Rovere, M, Wolfe, MS, Selkoe, DJ (2019). A cellular complex of BACE1 and γ-secretase sequentially generates Aβ from its full-length precursor. *Journal of Cell Biology*, **218**(2): 644–663. doi:10.1083/jcb.201806205.

Liu, L, Lauro, BM, He, A, Lee, H, Bhattarai, S, Wolfe, MS, Bennett, DA, Karch, CM, Young-Pearse, T, , DIAN, Selkoe, DJ (2022). Identification of the Aβ37/42 peptide ratio in CSF as an improved Aβ biomarker for Alzheimer's disease. *Alzheimer's & Dementia: The Journal of the Alzheimer's Association*, **1-18**. doi: 10.1002/alz.12646.

Loetscher, H, Deuschle, U, Brockhaus, M, Reinhardt, D, Nelboeck, P, Mous, J, Grünberg, J, Haass, C, Jacobsen, H (1997). Presenilins are processed by caspase-type proteases. *Journal of Biological Chemistry*, **272**(33): 20655–20659. doi: 10.1074/jbc.272.33.20655.

Long, JM, Holtzman, DM (2019). Alzheimer disease: An update on pathobiology and treatment strategies. *Cell*, **179**(2): 312–339. doi:10.1016/j.cell.2019.09.001.

Lu, DC, Rabizadeh, S, Chandra, S, Shayya, RF, Ellerby, LM, Ye, X, Salvesen, GS, Koo, EH, Bredesen, DE (2000). A second cytotoxic proteolytic peptide derived from amyloid β-protein precursor. *Nature Medicine*, **6**(4): 397–404. doi:10.1038/74656.

Lu, P, Bai, Xc, Ma, D, Xie, T, Yan, C, Sun, L, Yang, G, Zhao, Y, Zhou, R, Scheres, SHW, Shi, Y (2014). Three-dimensional structure of human γ-secretase. *Nature*, **512**(7513): 166–170. doi:10.1038/nature13567.

Luo, JE, Li, YM (2022). Turning the tide on Alzheimer's disease: Modulation of γ-secretase. *Cell & Bioscience*, **12**(1): 2. doi:10.1186/s13578-021-00738-7.

Luo, Wj, Wang, H, Li, H, Kim, BS, Shah, S, Lee, HJ, Thinakaran, G, Kim, TW, Yu, G, Xu, H (2003). PEN-2 and APH-1 coordinately regulate proteolytic processing of presenilin 1. *Journal of Biological Chemistry*, **278**(10): 7850–7854. doi:10.1074/jbc.C200648200.

López, AR, Dimitrov, M, Gerber, H, Braman, V, Hacker, DL, Wurm, FM, Fraering, PC (2015). Production of active glycosylation-deficient γ-secretase complex for crystallization studies. *Biotechnology and Bioengineering*, **112**(12): 2516–2526. doi:10.1002/bit.25675.

López-Otín, C, Bond, JS (2008). Proteases: Multifunctional enzymes in life and disease. *Journal of Biological Chemistry*, **283**(45): 30433–30437. doi:10.1074/jbc.R800035200.

Manolaridis, I, Kulkarni, K, R. B., D, Ogasawara, S, Zhang, Z, Bineva, G, N. O., R, S. J., H, A. J., T, Cronin, N, Iwata, S, Barford, D (2013). Mechanism of farnesylated CAAX protein processing by the intramembrane protease Rce1. *Nature*, **504**(7479): 301–305. doi:10.1038/nature12754.

Marambaud, P, Shioi, J, Serban, G, Georgakopoulos, A, Sarner, S, Nagy, V, Baki, L, Wen, P, Efthimiopoulos, S, Shao, Z, Wisniewski, T, Robakis, NK (2002). A presenilin-1/γ-secretase cleavage releases the E-cadherin intracellular domain and regulates disassembly of adherens junctions. *The EMBO Journal*, **21**(8): 1948–1956. doi:10.1093/emboj/21.8.1948.

Marambaud, P, Wen, PH, Dutt, A, Shioi, J, Takashima, A, Siman, R, Robakis, NK (2003). A CBP binding transcriptional repressor produced by the PS1/ε-cleavage of N-cadherin is inhibited by PS1 FAD mutations. *Cell*, **114**(5): 635–645. doi:10.1016/j.cell.2003.08.008.

Marquez-Sterling, NR, Lo, AC, Sisodia, SS, Koo, EH (1997). Trafficking of cell-surface β-amyloid precursor protein: Evidence that a sorting intermediate participates in synaptic vesicle recycling. *Journal of Neuroscience*, **17**(1): 140–151. doi:10.1523/jneurosci.17-01-00140.1997.

Martone, RL, Zhou, H, Atchison, K, Comery, T, Xu, JZ, Huang, X, Gong, X, Jin, M, Kreft, A, Harrison, B, Mayer, SC, Aschmies, S, Gonzales, C, Zaleska, MM, Riddell, DR, Wagner, E, Lu, P, Sun, SC, Sonnenberg-Reines, J, Oganesian, A, Adkins, K, Leach, MW, Clarke, DW, Huryn, D, Abou-Gharbia, M, Magolda, R, Bard, J, Frick, G, Raje, S, Forlow, SB, Balliet, C, Burczynski, ME, Reinhart, PH, Wan, HI, Pangalos, MN, Jacobsen, JS (2009). Begacestat (GSI-953): A novel, selective thiophene sulfonamide inhibitor of amyloid precursor protein γ-secretase for the treatment of Alzheimer's disease. *Journal of Pharmacology and Experimental Therapeutics*, **331**(2): 598–608. doi:10.1124/jpet.109.152975.

Masters, CL, Simms, G, Weinman, NA, Multhaup, G, McDonald, BL, Beyreuther, K (1985). Amyloid plaque core protein in Alzheimer disease and Down syndrome. *Proceedings of the National Academy of Sciences of the United States of America*, **82**(12): 4245–4249. doi:10.1073/pnas.82.12.4245.

Matsumura, N, Takami, M, Okochi, M, Wada-Kakuda, S, Fujiwara, H, Tagami, S, Funamoto, S, Ihara, Y, Morishima-Kawashima, M (2014). γ-Secretase associated

with lipid rafts: Multiple interactive pathways in the stepwise processing of β-carboxyl-terminal fragment. *Journal of Biological Chemistry*, **289**(8): 5109–5121. doi:10.1074/jbc.M113.510131.

Mayer, SC, Kreft, AF, Harrison, B, Abou-Gharbia, M, Antane, M, Aschmies, S, Atchison, K, Chlenov, M, Cole, DC, Comery, T, Diamantidis, G, Ellingboe, J, Fan, K, Galante, R, Gonzales, C, Ho, DM, Hoke, ME, Hu, Y, Huryn, D, Jain, U, Jin, M, Kremer, K, Kubrak, D, Lin, M, Lu, P, Magolda, R, Martone, R, Moore, W, Oganesian, A, Pangalos, MN, Porte, A, Reinhart, P, Resnick, L, Riddell, DR, Sonnenberg-Reines, J, Stock, JR, Sun, SC, Wagner, E, Wang, T, Woller, K, Xu, Z, Zaleska, MM, Zeldis, J, Zhang, M, Zhou, H, Jacobsen, JS (2008). Discovery of Begacestat, a Notch-1-sparing γ-secretase inhibitor for the treatment of Alzheimer's disease. *Journal of Medicinal Chemistry*, **51**(23): 7348–7351. doi:10.1021/jm801252w.

Meckler, X, Checler, F (2016). Presenilin 1 and presenilin 2 target γ-secretase complexes to distinct cellular compartments. *Journal of Biological Chemistry*, **291**(24): 12821–12837. doi:10.1074/jbc.M115.708297.

Mekala, S, Nelson, G, Li, YM (2020). Recent developments of small molecule γ-secretase modulators for Alzheimer's disease. *RSC Medicinal Chemistry*, **11**(9): 1003–1022. doi:10.1039/d0md00196a.

Mensch, M, Dunot, J, Yishan, SM, Harris, SS, Blistein, A, Avdiu, A, Pousinha, PA, Giudici, C, Busche, MA, Jedlicka, P, Willem, M, Marie, H (2021). An-α and An-β peptides impair LTP ex vivo within the low nanomolar range and impact neuronal activity in vivo. *Alzheimer's Research & Therapy*, **13**(1): 125. doi:10.1186/s13195-021-00860-1.

Mentrup, T, Cabrera-Cabrera, F, Fluhrer, R, Schröder, B (2020). Physiological functions of SPP/SPPL intramembrane proteases. *Cellular and Molecular Life Sciences*, **77**(15): 2959–2979. doi:10.1007/s00018-020-03470-6.

Moehlmann, T, Winkler, E, Xia, X, Edbauer, D, Murrell, J, Capell, A, Kaether, C, Zheng, H, Ghetti, B, Haass, C, Steiner, H (2002). Presenilin-1 mutations of leucine 166 equally affect the generation of the Notch and APP intracellular domains independent of their effect on Aβ 42 production. *Proceedings of the National Academy of Sciences of the United States of America*, **99**(12): 8025–8030. doi:10.1073/pnas.112686799.

Moin, SM, Urban, S (2012). Membrane immersion allows rhomboid proteases to achieve specificity by reading transmembrane segment dynamics. *eLife*, **1**: e00173. doi:10.7554/eLife.00173.

Moniruzzaman, M, Ishihara, S, Nobuhara, M, Higashide, H, Funamoto, S (2018). Glycosylation status of nicastrin influences catalytic activity and substrate preference of γ-secretase. *Biochemical and Biophysical Research Communications*, **502**(1): 98–103. doi:10.1016/j.bbrc.2018.05.126.

Moore, BD, Martin, J, de Mena, L, Sanchez, J, Cruz, PE, Ceballos-Diaz, C, Ladd, TB, Ran, Y, Levites, Y, Kukar, TL, Kurian, JJ, McKenna, R, Koo, EH, Borchelt, DR, Janus, C, Rincon-Limas, D, Fernandez-Funez, P, Golde, TE (2018). Short Aβ peptides attenuate Aβ42 toxicity in vivo. *Journal of Experimental Medicine*, **215**(1): 283–301. doi:10.1084/jem.20170600.

Morais, VA, Crystal, AS, Pijak, DS, Carlin, D, Costa, J, Lee, VMY, Doms, RW (2003). The transmembrane domain region of nicastrin mediates direct interactions with APH-1 and the γ-secretase complex. *Journal of Biological Chemistry*, **278**(44): 43284–43291. doi:10.1074/jbc.M305685200.

Mucke, L, Masliah, E, Yu, GQ, Mallory, M, Rockenstein, EM, Tatsuno, G, Hu, K, Kholodenko, D, Johnson-Wood, K, McConlogue, L (2000). High-level neuronal expression of Aβ 1-42 in wild-type human amyloid protein precursor transgenic mice: Synaptotoxicity without plaque formation. *Journal of Neuroscience*, **20**(11): 4050–4058. doi:10.1523/jneurosci.20-11-04050.2000.

Mullan, M, Crawford, F, Axelman, K, Houlden, H, Lilius, L, Winblad, B, Lannfelt, L (1992). A pathogenic mutation for probable Alzheimer's disease in the APP gene at the N-terminus of β-amyloid. *Nature Genetics*, **1**(5): 345–347. doi:10.1038/ng0892-345.

Munter, LM, Voigt, P, Harmeier, A, Kaden, D, Gottschalk, KE, Weise, C, Pipkorn, R, Schaefer, M, Langosch, D, Multhaup, G (2007). GxxxG motifs within the amyloid precursor protein transmembrane sequence are critical for the etiology of Aβ42. *The EMBO Journal*, **26**(6): 1702–1712. doi:10.1038/sj.emboj.7601616.

Murray, B, Sorci, M, Rosenthal, J, Lippens, J, Isaacson, D, Das, P, Fabris, D, Li, S, Belfort, G (2016). A2T and A2V Aβ peptides exhibit different aggregation kinetics, primary nucleation, morphology, structure, and LTP inhibition. *Proteins*, **84**(4): 488–500. doi:10.1002/prot.24995.

Murrell, J, Farlow, M, Ghetti, B, Benson, MD (1991). A mutation in the amyloid precursor protein associated with hereditary Alzheimer's disease. *Science*, **254**(5028): 97–99. doi:10.1126/science.1925564.

Müller, UC, Deller, T, Korte, M (2017). Not just amyloid: Physiological functions of the amyloid precursor protein family. *Nature Reviews Neuroscience*, **18**(5): 281–298. doi:10.1038/nrn.2017.29.

Müller, UC, Zheng, H (2012). Physiological functions of APP family proteins. *Cold Spring Harbor Perspectives in Medicine*, **2**(2): a006288. doi:10.1101/cshperspect.a006288.

Naing, SH, Kalyoncu, S, Smalley, DM, Kim, H, Tao, X, George, JB, Jonke, AP, Oliver, RC, Urban, VS, Torres, MP, Lieberman, RL (2018). Both positional and chemical variables control in vitro proteolytic cleavage of a presenilin ortholog. *Journal of Biological Chemistry*, **293**(13): 4653–4663. doi:10.1074/jbc.RA117.001436.

Naing, SH, Vukoti, KM, Drury, JE, Johnson, JL, Kalyoncu, S, Hill, SE, Torres, MP, Lieberman, RL (2015). Catalytic properties of intramembrane aspartyl protease substrate hydrolysis evaluated using a FRET peptide cleavage assay. *ACS Chemical Biology*, **10**(9): 2166–2174. doi:10.1021/acschembio.5b00305.

Nicoll, JAR, Buckland, GR, Harrison, CH, Page, A, Harris, S, Love, S, Neal, JW, Holmes, C, Boche, D (2019). Persistent neuropathological effects 14 years following amyloid-β immunization in Alzheimer's disease. *Brain*, **142**(7): 2113–2126. doi:10.1093/brain/awz142.

Nie, P, Vartak, A, Li, YM (2020). γ-Secretase inhibitors and modulators: Mechanistic insights into the function and regulation of γ-Secretase. *Seminars in Cell and Developmental Biology*, **105**: 43–53. doi:10.1016/j.semcdb.2020.03.002.

Niimura, M, Isoo, N, Takasugi, N, Tsuruoka, M, Ui-Tei, K, Saigo, K, Morohashi, Y, Tomita, T, Iwatsubo, T (2005). Aph-1 contributes to the stabilization and trafficking of the γ-secretase complex through mechanisms involving intermolecular and intramolecular interactions. *Journal of Biological Chemistry*, **280**(13): 12967–12975. doi:10.1074/jbc.M409829200.

Nikolaev, A, McLaughlin, T, O'Leary, DDM, Tessier-Lavigne, M (2009). APP binds DR6 to trigger axon pruning and neuron death via distinct caspases. *Nature*, **457**(7232): 981–989. doi:10.1038/nature07767.

Nilsberth, C, Westlind-Danielsson, A, Eckman, CB, Condron, MM, Axelman, K, Forsell, C, Stenh, C, Luthman, J, Teplow, DB, Younkin, SG, Näslund, J, Lannfelt, L (2001). The 'Arctic' APP mutation (E693G) causes Alzheimer's disease by enhanced Aβ protofibril formation. *Nature Neuroscience*, **4**(9): 887–893. doi: 10.1038/nn0901-887.

Nisticò, R, Borg, JJ (2021). Aducanumab for Alzheimer's disease: A regulatory perspective. *Pharmacological Research*, **171**: 105754. doi:10.1016/j.phrs.2021.105754.

Nordstedt, C, Caporaso, GL, Thyberg, J, Gandy, SE, Greengard, P (1993). Identification of the Alzheimer β/A4 amyloid precursor protein in clathrin-coated vesicles purified from PC12 cells. *Journal of Biological Chemistry*, **268**(1): 608–612.

Oehlrich, D, Berthelot, DJC, Gijsen, HJM (2011). γ-Secretase modulators as potential disease modifying anti-Alzheimer's drugs. *Journal of Medicinal Chemistry*, **54**(3): 669–698. doi:10.1021/jm101168r.

Oh, YS, Turner, RJ (2005a). Evidence that the COOH terminus of human presenilin 1 is located in extracytoplasmic space. *American Journal of Physiology. Cell Physiology*, **289**(3): 576–581. doi:10.1152/ajpcell.00636.2004.

Oh, YS, Turner, RJ (2005b). Topology of the C-terminal fragment of human presenilin 1. *Biochemistry*, **44**(35): 11821–11828. doi:10.1021/bi0509494.

Okochi, M, Fukumori, A, Jiang, J, Itoh, N, Kimura, R, Steiner, H, Haass, C, Tagami, S, Takeda, M (2006). Secretion of the Notch-1 Aβ-like peptide during Notch signaling. *Journal of Biological Chemistry*, **281**(12): 7890–7898. doi:10.1074/jbc.M513250200.

Okochi, M, Tagami, S, Yanagida, K, Takami, M, Kodama, TS, Mori, K, Nakayama, T, Ihara, Y, Takeda, M (2013). γ-secretase modulators and presenilin 1 mutants act differently on presenilin/γ-secretase function to cleave Aβ42 and Aβ43. *Cell Reports*, **3**(1): 42–51. doi:10.1016/j.celrep.2012.11.028.

Olsson, F, Schmidt, S, Althoff, V, Munter, LM, Jin, S, Rosqvist, S, Lendahl, U, Multhaup, G, Lundkvist, J (2014). Characterization of intermediate steps in amyloid β (Aβ) production under near-native conditions. *Journal of Biological Chemistry*, **289**(3): 1540–1550. doi:10.1074/jbc.M113.498246.

Oltersdorf, T, Fritz, LC, Schenk, DB, Lieberburg, I, Johnson-Wood, KL, Beattie, EC, Ward, PJ, Blacher, RW, Dovey, HF, Sinha, S (1989). The secreted form of

the Alzheimer's amyloid precursor protein with the Kunitz domain is protease nexin-II. *Nature*, **341**(6238): 144–147. doi:10.1038/341144a0.

Osawa, S, Funamoto, S, Nobuhara, M, Wada-Kakuda, S, Shimojo, M, Yagishita, S, Ihara, Y (2008). Phosphoinositides suppress γ-secretase in both the detergent-soluble and -insoluble states. *Journal of Biological Chemistry*, **283**(28): 19283–19292. doi:10.1074/jbc.M705954200.

Osenkowski, P, Ye, W, Wang, R, Wolfe, MS, Selkoe, DJ (2008). Direct and potent regulation of γ-secretase by its lipid microenvironment. *Journal of Biological Chemistry*, **283**(33): 22529–22540. doi:10.1074/jbc.M801925200.

Ostrowitzki, S, Lasser, RA, Dorflinger, E, Scheltens, P, Barkhof, F, Nikolcheva, T, Ashford, E, Retout, S, Hofmann, C, Delmar, P, Klein, G, Andjelkovic, M, Dubois, B, Boada, M, Blennow, K, Santarelli, L, Fontoura, P, Investigators, SR (2017). A phase III randomized trial of gantenerumab in prodromal Alzheimer's disease. *Alzheimer's Research & Therapy*, **9**(1): 95. doi:10.1186/s13195-017-0318-y.

Ousson, S, Saric, A, Baguet, A, Losberger, C, Genoud, S, Vilbois, F, Permanne, B, Hussain, I, Beher, D (2013). Substrate determinants in the C99 juxtamembrane domains differentially affect γ-secretase cleavage specificity and modulator pharmacology. *Journal of Neurochemistry*, **125**(4): 610–619. doi:10.1111/jnc.12129.

Page, RM, Baumann, K, Tomioka, M, Pérez-Revuelta, BI, Fukumori, A, Jacobsen, H, Flohr, A, Luebbers, T, Ozmen, L, Steiner, H, Haass, C (2008). Generation of Aβ38 and Aβ42 is independently and differentially affected by familial Alzheimer disease-associated presenilin mutations and γ-secretase modulation. *Journal of Biological Chemistry*, **283**(2): 677–683. doi:10.1074/jbc.M708754200.

Page, RM, Gutsmiedl, A, Fukumori, A, Winkler, E, Haass, C, Steiner, H (2010). β-Amyloid precursor protein mutants respond to γ-secretase modulators. *Journal of Biological Chemistry*, **285**(23): 17798–17810. doi:10.1074/jbc.M110.103283.

Parent, AT, Barnes, NY, Taniguchi, Y, Thinakaran, G, Sisodia, SS (2005). Presenilin attenuates receptor-mediated signaling and synaptic function. *Journal of Neuroscience*, **25**(6): 1540–1549. doi:10.1523/jneurosci.3850-04.2005.

Pawlowski, M, Warnecke, T (2022). Kausale Therapie der Alzheimer-Krankheit: Amyloidantikörper. *Der Internist*, **63**(9): 1–8. doi:10.1007/s00108-022-01291-2.

Peng, T, Yuan, X, Hang, HC (2014). Turning the spotlight on protein–lipid interactions in cells. *Current Opinion in Chemical Biology*, **21**: 144–153. doi:10.1016/j.cbpa.2014.07.015.

Petit, D, Fernández, SG, Zoltowska, KM, Enzlein, T, Ryan, NS, O'Connor, A, Szaruga, M, Hill, E, Vandenberghe, R, Fox, NC, Chávez-Gutiérrez, L (2022). Aβ profiles generated by Alzheimer's disease causing PSEN1 variants determine the pathogenicity of the mutation and predict age at disease onset. *Molecular Psychiatry*, **27**(6): 1–12. doi:10.1038/s41380-022-01518-6.

Petit, D, Hitzenberger, M, Lismont, S, Zoltowska, KM, Ryan, NS, Mercken, M, Bischoff, F, Zacharias, M, Chávez-Gutiérrez, L (2019). Extracellular interface between APP and Nicastrin regulates Aβ length and response to γ-secretase modulators. *The EMBO Journal*, page e101494. doi:10.15252/embj.2019101494.

Pimenova, AA, Raj, T, Goate, AM (2018). Untangling genetic risk for Alzheimer's disease. *Biological Psychiatry*, **83**(4): 300–310. doi:10.1016/j.biopsych.2017.05.014.

Podlisny, MB, Citron, M, Amarante, P, Sherrington, R, Xia, W, Zhang, J, Diehl, T, Levesque, G, Fraser, P, Haass, C, Koo, EHM, Seubert, P, St. George-Hyslop, P, Teplow, DB, Selkoe, DJ (1997). Presenilin proteins undergo heterogeneous endoproteolysis between Thr291and Ala299 and occur as stable N- and C-Terminal fragments in normal and Alzheimer brain tissue. *Neurobiology of Disease*, **3**(4): 325–337. doi:10.1006/nbdi.1997.0129.

Ponting, CP, Hutton, M, Nyborg, A, Baker, M, Jansen, K, Golde, TE (2002). Identification of a novel family of presenilin homologues. *Human Molecular Genetics*, **11**(9): 1037–44. doi:10.1093/hmg/11.9.1037.

Prokop, S, Haass, C, Steiner, H (2005). Length and overall sequence of the PEN-2 C-terminal domain determines its function in the stabilization of presenilin fragments. *Journal of Neurochemistry*, **94**(1): 57–62. doi:10.1111/j.1471-4159.2005.03165.x.

Prokop, S, Shirotani, K, Edbauer, D, Haass, C, Steiner, H (2004). Requirement of PEN-2 for stabilization of the presenilin N-/C-terminal Fragment heterodimer within the γ-secretase complex. *Journal of Biological Chemistry*, **279**(22): 23255–23261. doi:10.1074/jbc.M401789200.

Pryor, EE, Jr., Horanyi, PS, Clark, KM, Fedoriw, N, Connelly, SM, Koszelak-Rosenblum, M, Zhu, G, Malkowski, MG, Wiener, MC, Dumont, ME (2013). Structure of the integral membrane protein CAAX protease Ste24p. *Science*, **339**(6127): 1600–1604. doi:10.1126/science.1232048.

Pérez-Revuelta, BI, Fukumori, A, Lammich, S, Yamasaki, A, Haass, C, Steiner, H (2010). Requirement for small side chain residues within the GxGD-motif of

presenilin for γ-secretase substrate cleavage. *Journal of Neurochemistry*, **112**(4): 940–950. doi:10.1111/j.1471-4159.2009.06510.x.

Qi-Takahara, Y, Morishima-Kawashima, M, Tanimura, Y, Dolios, G, Hirotani, N, Horikoshi, Y, Kametani, F, Maeda, M, Saido, TC, Wang, R, Ihara, Y (2005). Longer forms of amyloid β protein: Implications for the mechanism of intramembrane cleavage by γ-secretase. *Journal of Neuroscience*, **25**(2): 436–445. doi: 10.1523/jneurosci.1575-04.2005.

Quigley, A, Dong, YY, Pike, ACW, Dong, L, Shrestha, L, Berridge, G, Stansfeld, PJ, Sansom, MSP, Edwards, AM, Bountra, C, von Delft, F, Bullock, AN, Burgess-Brown, NA, Carpenter, EP (2013). The structural basis of ZMPSTE24-dependent laminopathies. *Science*, **339**(6127): 1604–1607. doi:10.1126/science.1231513.

Quintero-Monzon, O, Martin, MM, Fernandez, MA, Cappello, CA, Krzysiak, AJ, Osenkowski, P, Wolfe, MS (2011). Dissociation between the processivity and total activity of γ-secretase: Implications for the mechanism of Alzheimer's disease-causing presenilin mutations. *American Chemical Society*. doi:10.1021/bi2007146.

Ramdya, P, Skoch, J, Bacskai, BJ, Hyman, BT, Berezovska, O (2003). Activated Notch1 associates with a presenilin-1/γ-secretase docking site. *Journal of Neurochemistry*, **87**(4): 843–850. doi:10.1046/j.1471-4159.2003.02030.x.

Ran, Y, Hossain, F, Pannuti, A, Lessard, CB, Ladd, GZ, Jung, JI, Minter, LM, Osborne, BA, Miele, L, Golde, TE (2017). γ-Secretase inhibitors in cancer clinical trials are pharmacologically and functionally distinct. *EMBO Molecular Medicine*, **9**(7): 950–966. doi:10.15252/emmm.201607265.

Raut, P, Glass, JB, Lieberman, RL (2021). Archaeal roots of intramembrane aspartyl protease siblings signal peptide peptidase and presenilin. *Proteins: Structure, Function, and Bioinformatics*, **89**(2): 232–241. doi:10.1002/prot.26009.

Rawlings, ND, Barrett, AJ, Thomas, PD, Huang, X, Bateman, A, Finn, RD (2018). The MEROPS database of proteolytic enzymes, their substrates and inhibitors in 2017 and a comparison with peptidases in the PANTHER database. *Nucleic Acids Research*, **46**(D1): D624–D632. doi:10.1093/nar/gkx1134.

Rawson, RB (2013). The site-2 protease. *Biochimica et Biophysica Acta (BBA) - Biomembranes*, **1828**(12): 2801–2807. doi:10.1016/j.bbamem.2013.03.031.

Rawson, RB, Zelenski, NG, Nijhawan, D, Ye, J, Sakai, J, Hasan, MT, Chang, TY, Brown, MS, Goldstein, JL (1997). Complementation cloning of S2P, a gene encoding a putative metalloprotease required for intramembrane cleavage of SREBPs. *Molecular Cell*, **1**(1): 47–57. doi:10.1016/s1097-2765(00)80006-4.

Ren, Z, Schenk, D, Basi, GS, Shapiro, IP (2007). Amyloid β-protein precursor juxtamembrane domain regulates specificity of γ-secretase-dependent cleavages. *Journal of Biological Chemistry*, **282**(48): 35350–35360. doi:10.1074/jbc.M702739200.

Renzi, F, Zhang, X, Rice, WJ, Torres-Arancivia, C, Gomez-Llorente, Y, Diaz, R, Ahn, K, Yu, C, Li, YM, Sisodia, SS, Ubarretxena-Belandia, I (2011). Structure of γ-secretase and its trimeric pre-activation intermediate by single-particle electron microscopy. *Journal of Biological Chemistry*, **286**(24): 21440–21449. doi:10.1074/jbc.M110.193326.

Restrepo, LJ, DePew, AT, Moese, ER, Tymanskyj, SR, Parisi, MJ, Aimino, MA, Duhart, JC, Fei, H, Mosca, TJ (2022). γ-Secretase promotes Drosophila postsynaptic development through the cleavage of a Wnt receptor. *Developmental Cell*, **57**(13): 1643/1660.e7. doi:10.1016/j.devcel.2022.05.006.

Rice, HC, de Malmazet, D, Schreurs, A, Frere, S, Van Molle, I, Volkov, AN, Creemers, E, Vertkin, I, Nys, J, Ranaivoson, FM, Comoletti, D, Savas, JN, Remaut, H, Balschun, D, Wierda, KD, Slutsky, I, Farrow, K, De Strooper, B, de Wit, J (2019). Secreted amyloid-β precursor protein functions as a GABA B R1a ligand to modulate synaptic transmission. *Science*, **363**(6423): eaao4827. doi:10.1126/science.aao4827.

Richter, MC, Ludewig, S, Winschel, A, Abel, T, Bold, C, Salzburger, LR, Klein, S, Han, K, Weyer, SW, Fritz, AK, Laube, B, Wolfer, DP, Buchholz, CJ, Korte, M, Müller, UC (2018). Distinct in vivo roles of secreted APP ectodomain variants APPsα and APPsβ in regulation of spine density, synaptic plasticity, and cognition. *The EMBO Journal*, **37**(11): e98335. doi:10.15252/embj.201798335.

Ring, S, Weyer, SW, Kilian, SB, Waldron, E, Pietrzik, CU, Filippov, MA, Herms, J, Buchholz, C, Eckman, CB, Korte, M, Wolfer, DP, Müller, UC (2007). The secreted β-amyloid precursor protein ectodomain APPsα is sufficient to rescue the anatomical, behavioral, and electrophysiological abnormalities of APP-deficient mice. *Journal of Neuroscience*, **27**(29): 7817–7826. doi:10.1523/jneurosci.1026-07.2007.

Roch, JM, Masliah, E, Roch-Levecq, AC, Sundsmo, MP, Otero, DA, Veinbergs, I, Saitoh, T (1994). Increase of synaptic density and memory retention by a

peptide representing the trophic domain of the amyloid β/A4 protein precursor. *Proceedings of the National Academy of Sciences of the United States of America*, **91**(16): 7450–7454. doi:10.1073/pnas.91.16.7450.

Rogaev, EI, Sherrington, R, Rogaeva, EA, Levesque, G, Ikeda, M, Liang, Y, Chi, H, Lin, C, Holman, K, T Tsuda, , et al. (1995). Familial Alzheimer's disease in kindreds with missense mutations in a gene on chromosome 1 related to the Alzheimer's disease type 3 gene. *Nature*, **376**(6543): 775–778. doi:10.1038/376775a0.

Rogers, MB (2022). Finally: Big win on all outcomes for Lecanemab in phase 3 topline results. *ALZFORUM; accessed 19. Nov. 2022.* https://www.alzforum.org/news/research-news/finally-big-win-all-outcomes-lecanemab-phase-3-topline-results.

Saito, T, Suemoto, T, Brouwers, N, Sleegers, K, Funamoto, S, Mihira, N, Matsuba, Y, Yamada, K, Nilsson, P, Takano, J, Nishimura, M, Iwata, N, Van Broeckhoven, C, Ihara, Y, Saido, TC (2011). Potent amyloidogenicity and pathogenicity of Aβ43. *Nature Neuroscience*, **14**(8): 1023–1032. doi:10.1038/nn.2858.

Sannerud, R, Esselens, C, Ejsmont, P, Mattera, R, Rochin, L, Tharkeshwar, AK, De Baets, G, De Wever, V, Habets, R, Baert, V, Vermeire, W, Michiels, C, Groot, AJ, Wouters, R, Dillen, K, Vints, K, Baatsen, P, Munck, S, Derua, R, Waelkens, E, Basi, GS, Mercken, M, Vooijs, M, Bollen, M, Schymkowitz, J, Rousseau, F, Bonifacino, JS, Van Niel, G, De Strooper, B, Annaert, W (2016). Restricted location of PSEN2/γ-secretase determines substrate specificity and generates an intracellular Aβ pool. *Cell*, **166**(1): 193–208. doi:10.1016/j.cell.2016.05.020.

Sastre, M, Steiner, H, Fuchs, K, Capell, A, Multhaup, G, Condron, MM, Teplow, DB, Haass, C (2001). Presenilin-dependent γ-secretase processing of β-amyloid precursor protein at a site corresponding to the S3 cleavage of Notch. *EMBO Reports*, **2**(9): 835–841. doi:10.1093/embo-reports/kve180.

Sato, C, Takagi, S, Tomita, T, Iwatsubo, T (2008). The C-terminal PAL motif and transmembrane domain 9 of presenilin 1 are involved in the formation of the catalytic pore of the γ-secretase. *Journal of Neuroscience*, **28**(24): 6264–6271. doi:10.1523/jneurosci.1163-08.2008.

Sato, T, Diehl, TS, Narayanan, S, Funamoto, S, Ihara, Y, De Strooper, B, Steiner, H, Haass, C, Wolfe, MS (2007). Active γ-secretase complexes contain only one of each component. *Journal of Biological Chemistry*, **282**(47): 33985–33993. doi:10.1074/jbc.M705248200.

Sawamura, N, Ko, M, Yu, W, Zou, K, Hanada, K, Suzuki, T, Gong, JS, Yanagisawa, K, Michikawa, M (2004). Modulation of amyloid precursor protein cleavage by cellular sphingolipids. *Journal of Biological Chemistry*, **279**(12): 11984–11991. doi:10.1074/jbc.M309832200.

Saxena, MT, Schroeter, EH, Mumm, JS, Kopan, R (2001). Murine notch homologs (N1-4) undergo presenilin-dependent proteolysis. *Journal of Biological Chemistry*, **276**(43): 40268–40273. doi:10.1074/jbc.M107234200.

Schauenburg, L, Liebsch, F, Eravci, M, Mayer, MC, Weise, C, Multhaup, G (2018). APLP1 is endoproteolytically cleaved by γ-secretase without previous ectodomain shedding. *Scientific Reports*, **8**(1916). doi:10.1038/s41598-018-19530-8.

Scheinfeld, MH, Ghersi, E, Laky, K, Fowlkes, BJ, D'Adamio, L (2002). Processing of β-amyloid precursor-like protein-1 and -2 by γ-secretase regulates transcription. *Journal of Biological Chemistry*, **277**(46): 44195–44201. doi:10.1074/jbc.M208110200.

Scheuner, D, Eckman, C, Jensen, M, Song, X, Citron, M, Suzuki, N, Bird, TD, Hardy, J, Hutton, M, Kukull, W, Larson, E, Levy-Lahad, E, Viitanen, M, Peskind, E, Poorkaj, P, Schellenberg, G, Tanzi, R, Wasco, W, Lannfelt, L, Selkoe, D, Younkin, S (1996). Secreted amyloid β-protein similar to that in the senile plaques of Alzheimer's disease is increased in vivo by the presenilin 1 and 2 and APP mutations linked to familial Alzheimer's disease. *Nature Medicine*, **2**(8): 864–870. doi:10.1038/nm0896-864.

Schönherr, C, Bien, J, Isbert, S, Wichert, R, Prox, J, Altmeppen, H, Kumar, S, Walter, J, Lichtenthaler, SF, Weggen, S, Glatzel, M, Becker-Pauly, C, Pietrzik, CU (2016). Generation of aggregation prone N-terminally truncated amyloid β peptides by meprin β depends on the sequence specificity at the cleavage site. *Molecular Neurodegeneration*, **11**(19). doi:10.1186/s13024-016-0084-5.

Seabrook, GR, Smith, DW, Bowery, BJ, Easter, A, Reynolds, T, Fitzjohn, SM, Morton, RA, Zheng, H, Dawson, GR, Sirinathsinghji, DJ, Davies, CH, Collingridge, GL, Hill, RG (1999). Mechanisms contributing to the deficits in hippocampal synaptic plasticity in mice lacking amyloid precursor protein. *Neuropharmacology*, **38**(3): 349–359. doi:10.1016/s0028-3908(98)00204-4.

Selkoe, DJ, Hardy, J (2016). The amyloid hypothesis of Alzheimer's disease at 25 years. *EMBO Molecular Medicine*, **8**(6): 595–608. doi:10.15252/emmm.201606210.

Selkoe, DJ, Podlisny, MB, Joachim, CL, Vickers, EA, Lee, G, Fritz, LC, Oltersdorf, T (1988). β-Amyloid precursor protein of Alzheimer disease occurs as 110- to 135-kilodalton membrane-associated proteins in neural and nonneural tissues. *Proceedings of the National Academy of Sciences of the United States of America*, **85**(19): 7341–7345. doi:10.1073/pnas.85.19.7341.

Sevigny, J, Chiao, P, Bussière, T, Weinreb, PH, Williams, L, Maier, M, Dunstan, R, Salloway, S, Chen, T, Ling, Y, O'Gorman, J, Qian, F, Arastu, M, Li, M, Chollate, S, Brennan, MS, Quintero-Monzon, O, Scannevin, RH, Arnold, HM, Engber, T, Rhodes, K, Ferrero, J, Hang, Y, Mikulskis, A, Grimm, J, Hock, C, Nitsch, RM, Sandrock, A (2016). The antibody aducanumab reduces Aβ plaques in Alzheimer's disease. *Nature*, **537**(7618): 50–56. doi:10.1038/nature19323.

Shah, S, Lee, SF, Tabuchi, K, Hao, YH, Yu, C, LaPlant, Q, Ball, H, Dann, CE, Südhof, T, Yu, G (2005). Nicastrin functions as a γ-secretase-substrate receptor. *Cell*, **122**(3): 435–447. doi:10.1016/j.cell.2005.05.022.

Shankar, GM, Li, S, Mehta, TH, Garcia-Munoz, A, Shepardson, NE, Smith, I, Brett, FM, Farrell, MA, Rowan, MJ, Lemere, CA, Regan, CM, Walsh, DM, Sabatini, BL, Selkoe, DJ (2008). Amyloid-β protein dimers isolated directly from Alzheimer's brains impair synaptic plasticity and memory. *Nature Medicine*, **14**(8): 837–842. doi:10.1038/nm1782.

Sharma, A, Gupta, SP (2017). Fundamentals of viruses and their proteases. *Viral Proteases and Their Inhibitors*, pages 1–24. doi:10.1016/b978-0-12-809712-0.00001-0.

Shearman, MS, Beher, D, Clarke, EE, Lewis, HD, Harrison, T, Hunt, P, Nadin, A, Smith, AL, Stevenson, G, Castro, JL (2000). L-685,458, an aspartyl protease transition state mimic, is a potent inhibitor of amyloid β-protein precursor γ-secretase activity. *Biochemistry*, **39**(30): 8698–8704. doi:10.1021/bi0005456.

Sherrington, R, Rogaev, EI, Liang, Y, Rogaeva, EA, Levesque, G, Ikeda, M, Chi, H, Lin, C, Li, G, Holman, K, Tsuda, T, Mar, L, Foncin, JF, Bruni, AC, Montesi, MP, Sorbi, S, Rainero, I, Pinessi, L, Nee, L, Chumakov, I, Pollen, D, Brookes, A, Sanseau, P, Polinsky, RJ, Wasco, W, Da Silva, HA, Haines, JL, Perkicak-Vance, MA, Tanzi, RE, Roses, AD, Fraser, PE, Rommens, JM, George-Hyslop, PHS (1995). Cloning of a gene bearing missense mutations in early-onset familial Alzheimer's disease. *Nature*, **375**(6534): 754–760. doi:10.1038/375754a0.

Shiraishi, H, Sai, X, Wang, HQ, Maeda, Y, Kurono, Y, Nishimura, M, Yanagisawa, K, Komano, H (2004). PEN-2 enhances γ-cleavage after presenilin

heterodimer formation. *Journal of Neurochemistry*, **90**(6): 1402–1413. doi: 10.1111/j.1471-4159.2004.02597.x.

Shirotani, K, Edbauer, D, Kostka, M, Steiner, H, Haass, C (2004a). Immature nicastrin stabilizes APH-1 independent of PEN-2 and presenilin: Identification of nicastrin mutants that selectively interact with APH-1. *Journal of Neurochemistry*, **89**(6): 1520–1527. doi:10.1111/j.1471-4159.2004.02447.x.

Shirotani, K, Edbauer, D, Prokop, S, Haass, C, Steiner, H (2004b). Identification of distinct γ-secretase complexes with different APH-1 variants. *Journal of Biological Chemistry*, **279**(40): 41340–41345. doi:10.1074/jbc.M405768200.

Shirotani, K, Tomioka, M, Kremmer, E, Haass, C, Steiner, H (2007). Pathological activity of familial Alzheimer's disease-associated mutant presenilin can be executed by six different γ-secretase complexes. *Neurobiology of Disease*, **27**(1): 102–107. doi:10.1016/j.nbd.2007.04.011.

Simons, M, Keller, P, De Strooper, B, Beyreuther, K, Dotti, CG, Simons, K (1998). Cholesterol depletion inhibits the generation of β-amyloid in hippocampal neurons. *Proceedings of the National Academy of Sciences of the United States of America*, **95**(11): 6460–6464. doi:10.1073/pnas.95.11.6460.

Sinha, S, Anderson, JP, Barbour, R, Basi, GS, Caccavello, R, Davis, D, Doan, M, Dovey, HF, Frigon, N, Hong, J, Jacobson-Croak, K, Jewett, N, Keim, P, Knops, J, Lieberburg, I, Power, M, Tan, H, Tatsuno, G, Tung, J, Schenk, D, Seubert, P, Suomensaari, SM, Wang, S, Walker, D, Zhao, J, McConlogue, L, John, V (1999). Purification and cloning of amyloid precursor protein β-secretase from human brain. *Nature*, **402**(6761): 537–540. doi:10.1038/990114.

Sisodia, SS, Koo, EH, Beyreuther, K, Unterbeck, A, Price, DL (1990). Evidence that β-amyloid protein in Alzheimer's disease is not derived by normal processing. *Science*, **248**(4954): 492–495. doi:10.1126/science.1691865.

Song, R, Qiao, W, He, J, Huang, J, Luo, Y, Yang, T (2021). Proteases and their modulators in cancer therapy: Challenges and opportunities. *Journal of Medicinal Chemistry*, **64**(6): 2851–2877. doi:10.1021/acs.jmedchem.0c01640.

Spasic, D, Raemaekers, T, Dillen, K, Declerck, I, Baert, V, Serneels, L, Füllekrug, J, Annaert, W (2007). Rer1p competes with APH-1 for binding to nicastrin and regulates γ-secretase complex assembly in the early secretory pathway. *Journal of Cell Biology*, **176**(5): 629–640. doi:10.1083/jcb.200609180.

Spasic, D, Tolia, A, Dillen, K, Baert, V, De Strooper, B, Vrijens, S, Annaert, W (2006). Presenilin-1 maintains a nine-transmembrane topology throughout the secretory pathway. *Journal of Biological Chemistry*, **281**(36): 26569–26577. doi: 10.1074/jbc.M600592200.

Spitz, C, Schlosser, C, Guschtschin-Schmidt, N, Stelzer, W, Menig, S, Götz, A, Haug-Kröper, M, Scharnagl, C, Langosch, D, Muhle-Goll, C, Fluhrer, R (2020). Non-canonical shedding of TNFα by SPPL2a is determined by the conformational flexibility of its transmembrane helix. *iScience*, **23**(12): 101775. doi:10.1016/j.isci.2020.101775.

Steiner, H, Duff, K, Capell, A, Romig, H, Grim, MG, Lincoln, S, Hardy, J, Yu, X, Picciano, M, Fechteler, K, Citron, M, Kopan, R, Pesold, B, Keck, S, Baader, M, Tomita, T, Iwatsubo, T, Baumeister, R, Haass, C (1999a). A loss of function mutation of presenilin-2 interferes with amyloid β-peptide production and notch signaling. *Journal of Biological Chemistry*, **274**(40): 28669–28673. doi:10.1074/jbc.274.40.28669.

Steiner, H, Kostka, M, Romig, H, Basset, G, Pesold, B, Hardy, J, Capell, A, Meyn, L, Grim, ML, Baumeister, R, Fechteler, K, Haass, C (2000). Glycine 384 is required for presenilin-1 function and is conserved in bacterial polytopic aspartyl proteases. *Nature Cell Biology*, **2**(11): 848–851. doi:10.1038/35041097.

Steiner, H, Romig, H, Pesold, B, Philipp, U, Baader, M, Citron, M, Loetscher, H, Jacobsen, H, Haass, C (1999b). Amyloidogenic function of the Alzheimer's disease-associated presenilin 1 in the absence of endoproteolysis. *Biochemistry*, **38**(44): 14600–14605. doi:10.1021/bi9914210.

Sterchi, EE, Stöcker, W (1999). *Proteolytic enzymes*. Springer, Berlin, Germany. doi:10.1007/978-3-642-59816-6.

Strisovsky, K, Sharpe, HJ, Freeman, M (2009). Sequence-specific intramembrane proteolysis: Identification of a recognition motif in rhomboid substrates. *Molecular Cell*, **36**(6): 1048–1059. doi:10.1016/j.molcel.2009.11.006.

Strittmatter, WJ, Saunders, AM, Schmechel, D, Pericak-Vance, M, Enghild, J, Salvesen, GS, Roses, AD (1993). Apolipoprotein E: High-avidity binding to β-amyloid and increased frequency of type 4 allele in late-onset familial Alzheimer disease. *Proceedings of the National Academy of Sciences of the United States of America*, **90**(5): 1977–1981. doi:10.1073/pnas.90.5.1977.

Struhl, G, Adachi, A (2000). Requirements for presenilin-dependent cleavage of Notch and other transmembrane proteins. *Molecular Cell*, **6**(3): 625–636. doi: 10.1016/s1097-2765(00)00061-7.

Sun, L, Zhou, R, Yang, G, Shi, Y (2017). Analysis of 138 pathogenic mutations in presenilin-1 on the in vitro production of Aβ42 and Aβ40 peptides by γ-secretase. *Proceedings of the National Academy of Sciences of the United States of America*, **114**(4): E476–E485. doi:10.1073/pnas.1618657114.

Sun, X, He, G, Song, W (2006). BACE2, as a novel APP Θ-secretase, is not responsible for the pathogenesis of Alzheimer's disease in Down syndrome. *FASEB Journal*, **20**(9): 1369–1376. doi:10.1096/fj.05-5632com.

Szaruga, M, Munteanu, B, Lismont, S, Veugelen, S, Horré, K, Mercken, M, Saido, TC, Ryan, NS, De Vos, T, Savvides, SN, Gallardo, R, Schymkowitz, J, Rousseau, F, Fox, NC, Hopf, C, De Strooper, B, Chávez-Gutiérrez, L (2017). Alzheimer's-Causing Mutations Shift Aβ Length by Destabilizing γ-Secretase-Aβn Interactions. *Cell*, **170**(3): 443–456.e14. doi:10.1016/j.cell.2017.07.004.

Szaruga, M, Veugelen, S, Benurwar, M, Lismont, S, Sepulveda-Falla, D, Lleo, A, Ryan, NS, Lashley, T, Fox, NC, Murayama, S, Gijsen, H, De Strooper, B, Chávez-Gutiérrez, L (2015). Qualitative changes in human γ-secretase underlie familial Alzheimer's disease. *Journal of Experimental Medicine*, **212**(12): 2003–2013. doi: 10.1084/jem.20150892.

Tagami, S, Yanagida, K, Kodama, TS, Takami, M, Mizuta, N, Oyama, H, Nishitomi, K, Chiu, Yw, Okamoto, T, Ikeuchi, T, Sakaguchi, G, Kudo, T, Matsuura, Y, Fukumori, A, Takeda, M, Ihara, Y, Okochi, M (2017). Semagacestat is a pseudo-inhibitor of γ-secretase. *Cell Reports*, **21**(1): 259–273. doi:10.1016/j.celrep.2017.09.032.

Takami, M, Nagashima, Y, Sano, Y, Ishihara, S, Morishima-Kawashima, M, Funamoto, S, Ihara, Y (2009). γ-Secretase: Successive tripeptide and tetrapeptide release from the transmembrane domain of β-carboxyl terminal fragment. *Journal of Neuroscience*, **29**(41): 13042–13052. doi:10.1523/jneurosci.2362-09.2009.

Takasugi, N, Tomita, T, Hayashi, I, Tsuruoka, M, Niimura, M, Takahashi, Y, Thinakaran, G, Iwatsubo, T (2003). The role of presenilin cofactors in the γ-secretase complex. *Nature*, **422**(6930): 438–441. doi:10.1038/nature01506.

Tamaoka, A, Odaka, A, Ishibashi, Y, Usami, M, Sahara, N, Suzuki, N, Nukina, N, Mizusawa, H, Shoji, S, I Kanazawa, , et al. (1994). APP717 missense mutation affects the ratio of amyloid β protein species (Aβ1-42/43 and Aβ1-40)

in familial Alzheimer's disease brain. *Journal of Biological Chemistry*, **269**(52): 32721–32724.

Thinakaran, G, Borchelt, DR, Lee, MK, Slunt, HH, Spitzer, L, Kim, G, Ratovitsky, T, Davenport, F, Nordstedt, C, Seeger, M, Hardy, J, Levey, AI, Gandy, SE, Jenkins, NA, Copeland, NG, Price, DL, Sisodia, SS (1996). Endoproteolysis of presenilin 1 and accumulation of processed derivatives in vivo. *Neuron*, **17**(1): 181–190. doi:10.1016/s0896-6273(00)80291-3.

Tolia, A, Horré, K, De Strooper, B (2008). Transmembrane domain 9 of presenilin determines the dynamic conformation of the catalytic site of γ-secretase. *Journal of Biological Chemistry*, **283**(28): 19793–19803. doi:10.1074/jbc.M802461200.

Torres-Arancivia, C, Ross, CM, Chavez, J, Assur, Z, Dolios, G, Mancia, F, Ubarretxena-Belandia, I (2010). Identification of an archaeal presenilin-like intramembrane protease. *PLoS One*, **5**(9): e13072. doi:10.1371/journal.pone.0013072.

Trambauer, J, Sarmiento, RMR, Fukumori, A, Feederle, R, Baumann, K, Steiner, H (2020). Aβ43-producing PS1 FAD mutants cause altered substrate interactions and respond to γ-secretase modulation. *EMBO Reports*, **21**(1): e47996. doi:10.15252/embr.201947996.

Tunyasuvunakool, K, Adler, J, Wu, Z, Green, T, Zielinski, M, Žídek, A, Bridgland, A, Cowie, A, Meyer, C, Laydon, A, Velankar, S, Kleywegt, GJ, Bateman, A, Evans, R, Pritzel, A, Figurnov, M, Ronneberger, O, Bates, R, Kohl, SAA, Potapenko, A, Ballard, AJ, Romera-Paredes, B, Nikolov, S, Jain, R, Clancy, E, Reiman, D, Petersen, S, Senior, AW, Kavukcuoglu, K, Birney, E, Kohli, P, Jumper, J, Hassabis, D (2021). Highly accurate protein structure prediction for the human proteome. *Nature*, **596**(7873): 590–596. doi:10.1038/s41586-021-03828-1.

Turk, B (2006). Targeting proteases: Successes, failures and future prospects. *Nature Reviews Drug Discovery*, **5**(9): 785–799. doi:10.1038/nrd2092.

Twining, SS (1994). Regulation of proteolytic activity in tissues. *Critical Reviews in Biochemistry and Molecular Biology*, **29**(5): 315–383. doi:10.3109/10409239409083484.

Urban, S (2010). Taking the plunge: Integrating structural, enzymatic and computational insights into a unified model for membrane-immersed rhomboid proteolysis. *Biochemical Journal*, **425**(3): 501–512. doi:10.1042/bj20090861.

Urban, S, Wolfe, MS (2005). Reconstitution of intramembrane proteolysis in vitro reveals that pure rhomboid is sufficient for catalysis and specificity. *Proceedings of the National Academy of Sciences of the United States of America*, **102**(6): 1883–1888. doi:10.1073/pnas.0408306102.

van Dyck, CH, Swanson, CJ, Aisen, P, Bateman, RJ, Chen, C, Gee, M, Kanekiyo, M, Li, D, Reyderman, L, Cohen, S, Froelich, L, Katayama, S, Sabbagh, M, Vellas, B, Watson, D, Dhadda, S, Irizarry, M, Kramer, LD, Iwatsubo, T (2022). Lecanemab in early Alzheimer's disease. *New England Journal of Medicine*. doi:10.1056/NEJMoa2212948.

van Nostrand, WE, Schmaier, AH, Farrow, JS, Cines, DB, Cunningham, DD (1991). Protease nexin-2/amyloid β-protein precursor in blood is a platelet-specific protein. *Biochemical and Biophysical Research Communications*, **175**(1): 15–21. doi:10.1016/s0006-291x(05)81193-3.

Varadi, M, Anyango, S, Deshpande, M, Nair, S, Natassia, C, Yordanova, G, Yuan, D, Stroe, O, Wood, G, Laydon, A, Žídek, A, Green, T, Tunyasuvunakool, K, Petersen, S, Jumper, J, Clancy, E, Green, R, Vora, A, Lutfi, M, Figurnov, M, Cowie, A, Hobbs, N, Kohli, P, Kleywegt, G, Birney, E, Hassabis, D, Velankar, S (2022). AlphaFold Protein Structure Database: Massively expanding the structural coverage of protein-sequence space with high-accuracy models. *Nucleic Acids Research*, **50**(D1): D439–D444. doi:10.1093/nar/gkab1061.

Vassar, R, Bennett, BD, Babu-Khan, S, Kahn, S, Mendiaz, EA, Denis, P, Teplow, DB, Ross, S, Amarante, P, Loeloff, R, Luo, Y, Fisher, S, Fuller, J, Edenson, S, Lile, J, Jarosinski, MA, Biere, AL, Curran, E, Burgess, T, Louis, JC, Collins, F, Treanor, J, Rogers, G, Citron, M (1999). β-Secretase cleavage of Alzheimer's amyloid precursor protein by the transmembrane aspartic protease BACE. *Science*, **286**(5440): 735–741. doi:10.1126/science.286.5440.735.

Verghese, PB, Castellano, JM, Holtzman, DM (2011). Apolipoprotein E in Alzheimer's disease and other neurological disorders. *Lancet Neurology*, **10**(3): 241–252. doi:10.1016/s1474-4422(10)70325-2.

Vetrivel, KS, Cheng, H, Lin, W, Sakurai, T, Li, T, Nukina, N, Wong, PC, Xu, H, Thinakaran, G (2004). Association of γ-secretase with lipid rafts in post-Golgi and endosome membranes. *Journal of Biological Chemistry*, **279**(43): 44945–44954. doi:10.1074/jbc.M407986200.

Vetrivel, KS, Thinakaran, G (2010). Membrane rafts in Alzheimer's disease β-amyloid production. *Biochimica et Biophysica Acta*, **1801**(8): 860–867. doi: 10.1016/j.bbalip.2010.03.007.

Vetrivel, KS, Zhang, X, Meckler, X, Cheng, H, Lee, S, Gong, P, Lopes, KO, Chen, Y, Iwata, N, Yin, KJ, Lee, JM, Parent, AT, Saido, TC, Li, YM, Sisodia, SS, Thinakaran, G (2008). Evidence that CD147 modulation of β-amyloid (Aβ) levels is mediated by extracellular degradation of secreted Aβ. *Journal of Biological Chemistry*, **283**(28): 19489–19498. doi:10.1074/jbc.M801037200.

Vieira, SI, Rebelo, S, Esselmann, H, Wiltfang, J, Lah, J, Lane, R, Small, SA, Gandy, S, da Cruz e. Silva, EF, da Cruz e. Silva, OAB (2010). Retrieval of the Alzheimer's amyloid precursor protein from the endosome to the TGN is S655 phosphorylation state-dependent and retromer-mediated. *Molecular Neurodegeneration*, **5**(1): 1–21. doi:10.1186/1750-1326-5-40.

Vogrinc, D, Goričar, K, Dolžan, V (2021). Genetic variability in molecular pathways implicated in Alzheimer's disease: A comprehensive review. *Frontiers in Aging Neuroscience*, **13**(646901). doi:10.3389/fnagi.2021.646901.

Wahrle, S, Das, P, Nyborg, AC, McLendon, C, Shoji, M, Kawarabayashi, T, Younkin, LH, Younkin, SG, Golde, TE (2002). Cholesterol-dependent γ-secretase activity in buoyant cholesterol-rich membrane microdomains. *Neurobiology of Disease*, **9**(1): 11–23. doi:10.1006/nbdi.2001.0470.

Wakabayashi, T, Craessaerts, K, Bammens, L, Bentahir, M, Borgions, F, Herdewijn, P, Staes, A, Timmerman, E, Vandekerckhove, J, Rubinstein, E, Boucheix, C, Gevaert, K, De Strooper, B (2009). Analysis of the γ-secretase interactome and validation of its association with tetraspanin-enriched microdomains. *Nature Cell Biology*, **11**(11): 1340–1346. doi:10.1038/ncb1978.

Waldron, E, Isbert, S, Kern, A, Jaeger, S, Martin, AM, Hébert, SS, Behl, C, Weggen, S, De Strooper, B, Pietrzik, CU (2008). Increased AICD generation does not result in increased nuclear translocation or activation of target gene transcription. *Experimental Cell Research*, **314**(13): 2419–2433. doi:10.1016/j.yexcr.2008.05.003.

Wang, J, Beher, D, Nyborg, AC, Shearman, MS, Golde, TE, Goate, A (2006a). C-terminal PAL motif of presenilin and presenilin homologues required for normal active site conformation. *Journal of Neurochemistry*, **96**(1): 218–227. doi:10.1111/j.1471-4159.2005.03548.x.

Wang, J, Brunkan, AL, Hecimovic, S, Walker, E, Goate, A (2004). Conserved "PAL" sequence in presenilins is essential for γ-secretase activity, but not required for formation or stabilization of γ-secretase complexes. *Neurobiology of Disease*, **15**(3): 654–666. doi:10.1016/j.nbd.2003.12.008.

Wang, X, Pei, G (2018). Visualization of Alzheimer's Disease related α-/β-/γ-secretase ternary complex by bimolecular fluorescence complementation based fluorescence resonance energy transfer. *Frontiers in Molecular Neuroscience*, **11**(431). doi:10.3389/fnmol.2018.00431.

Wang, Y, Mandelkow, E (2016). Tau in physiology and pathology. *Nature Reviews Neuroscience*, **17**(1): 5–21. doi:10.1038/nrn.2015.1.

Wang, Y, Zhang, Y, Ha, Y (2006b). Crystal structure of a rhomboid family intramembrane protease. *Nature*, **444**(7116): 179–180. doi:10.1038/nature05255.

Weggen, S, Beher, D (2012). Molecular consequences of amyloid precursor protein and presenilin mutations causing autosomal-dominant Alzheimer's disease. *Alzheimer's Research & Therapy*, **4**(2): 1–14. doi:10.1186/alzrt107.

Weggen, S, Eriksen, JL, Das, P, Sagi, SA, Wang, R, Pietrzik, CU, Findlay, KA, Smith, TE, Murphy, MP, Bulter, T, Kang, DE, Marquez-Sterling, N, Golde, TE, Koo, EH (2001). A subset of NSAIDs lower amyloidogenic Aβ42 independently of cyclooxygenase activity. *Nature*, **414**(6860): 212–216. doi:10.1038/35102591.

Weidemann, A, Eggert, S, Reinhard, FBM, Vogel, M, Paliga, K, Baier, G, Masters, CL, Beyreuther, K, Evin, G (2002). A novel ε-cleavage within the transmembrane domain of the Alzheimer amyloid precursor protein demonstrates homology with Notch processing. *Biochemistry*, **41**(8): 2825–2835. doi:10.1021/bi015794o.

Willem, M, Tahirovic, S, Busche, MA, Ovsepian, SV, Chafai, M, Kootar, S, Hornburg, D, Evans, LDB, Moore, S, Daria, A, Hampel, H, Müller, V, Giudici, C, Nuscher, B, Wenninger-Weinzierl, A, Kremmer, E, Heneka, MT, Thal, DR, Giedraitis, V, Lannfelt, L, Müller, U, Livesey, FJ, Meissner, F, Herms, J, Konnerth, A, Marie, H, Haass, C (2015). η-Secretase processing of APP inhibits neuronal activity in the hippocampus. *Nature*, **526**(7573): 443–447. doi:10.1038/nature14864.

Winblad, B, Amouyel, P, Andrieu, S, Ballard, C, Brayne, C, Brodaty, H, Cedazo-Minguez, A, Dubois, B, Edvardsson, D, Feldman, H, Fratiglioni, L, Frisoni, GB, Gauthier, S, Georges, J, Graff, C, Iqbal, K, Jessen, F, Johansson, G, Jönsson, L, Kivipelto, M, Knapp, M, Mangialasche, F, Melis, R, Nordberg, A, Rikkert, MO, Qiu, C, Sakmar, TP, Scheltens, P, Schneider, LS, Sperling, R, Tjernberg, LO,

Waldemar, G, Wimo, A, Zetterberg, H (2016). Defeating Alzheimer's disease and other dementias: A priority for European science and society. *Lancet Neurology*, **15**(5): 455–532. doi:10.1016/s1474-4422(16)00062-4.

Winkler, E, Hobson, S, Fukumori, A, Dümpelfeld, B, Luebbers, T, Baumann, K, Haass, C, Hopf, C, Steiner, H (2009). Purification, pharmacological modulation, and biochemical characterization of interactors of endogenous human γ-secretase. *Biochemistry*, **48**(6): 1183–1197. doi:10.1021/bi801204g.

Winkler, E, Kamp, F, Scheuring, J, Ebke, A, Fukumori, A, Steiner, H (2012). Generation of Alzheimer disease-associated amyloid β42/43 peptide by γ-secretase can be inhibited directly by modulation of membrane thickness. *Journal of Biological Chemistry*, **287**(25): 21326–21334. doi:10.1074/jbc.M112.356659.

Wischik, CM, Novak, M, Edwards, PC, Klug, A, Tichelaar, W, Crowther, RA (1988a). Structural characterization of the core of the paired helical filament of Alzheimer disease. *Proceedings of the National Academy of Sciences of the United States of America*, **85**(13): 4884–4888. doi:10.1073/pnas.85.13.4884.

Wischik, CM, Novak, M, Thøgersen, HC, Edwards, PC, Runswick, MJ, Jakes, R, Walker, JE, Milstein, C, Roth, M, Klug, A (1988b). Isolation of a fragment of tau derived from the core of the paired helical filament of Alzheimer disease. *Proceedings of the National Academy of Sciences of the United States of America*, **85**(12): 4506–4510. doi:10.1073/pnas.85.12.4506.

Wolfe, MS (2009). Intramembrane proteolysis. *Chemical Reviews*, **109**(4): 1599–1612. doi:10.1021/cr8004197.

Wolfe, MS, Xia, W, Ostaszewski, BL, Diehl, TS, Kimberly, WT, Selkoe, DJ (1999). Two transmembrane aspartates in presenilin-1 required for presenilin endoproteolysis and γ-secretase activity. *Nature*, **398**(6727): 513–517. doi:10.1038/19077.

Wong, GT, Manfra, D, Poulet, FM, Zhang, Q, Josien, H, Bara, T, Engstrom, L, Pinzon-Ortiz, M, Fine, JS, Lee, HJJ, Zhang, L, Higgins, GA, Parker, EM (2004). Chronic treatment with the γ-secretase inhibitor LY-411,575 inhibits β-amyloid peptide production and alters lymphopoiesis and intestinal cell differentiation. *Journal of Biological Chemistry*, **279**(13): 12876–12882. doi:10.1074/jbc.M311652200.

Wouters, R, Michiels, C, Sannerud, R, Kleizen, B, Dillen, K, Vermeire, W, Ayala, AE, Demedts, D, Schekman, R, Annaert, W (2021). Assembly of γ-secretase occurs through stable dimers after exit from the endoplasmic reticulum. *Journal of Cell Biology*, **220**(9): e201911104. doi:10.1083/jcb.201911104.

Wrigley, JDJ, Schurov, I, Nunn, EJ, Martin, ACL, Clarke, EE, Ellis, S, Bonnert, TP, Shearman, MS, Beher, D (2005). Functional overexpression of γ-secretase reveals protease-independent trafficking functions and a critical role of lipids for protease activity. *Journal of Biological Chemistry*, **280**(13): 12523–12535. doi: 10.1074/jbc.M413086200.

Wunderlich, P, Glebov, K, Kemmerling, N, Tien, NT, Neumann, H, Walter, J (2013). Sequential proteolytic processing of the triggering receptor expressed on myeloid cells-2 (TREM2) protein by ectodomain shedding and γ-secretase-dependent intramembranous cleavage. *Journal of Biological Chemistry*, **288**(46): 33027–33036. doi:10.1074/jbc.M113.517540.

Xia, W, Ostaszewski, BL, Kimberly, WT, Rahmati, T, Moore, CL, Wolfe, MS, Selkoe, DJ (2000). FAD mutations in presenilin-1 or amyloid precursor protein decrease the efficacy of a γ-secretase inhibitor: Evidence for direct involvement of PS1 in the γ-secretase cleavage complex. *Neurobiology of Disease*, **7**(6 Pt B): 673–681. doi:10.1006/nbdi.2000.0322.

Yagishita, S, Morishima-Kawashima, M, Tanimura, Y, Ishiura, S, , Ihara, Y (2006). DAPT-induced intracellular accumulations of longer amyloid β-proteins: Further implications for the mechanism of intramembrane cleavage by γ-secretase. *Biochemistry*, **45**(12): 3952–3960. doi:10.1021/bi0521846.

Yamasaki, A, Eimer, S, Okochi, M, Smialowska, A, Kaether, C, Baumeister, R, Haass, C, Steiner, H (2006). The GxGD motif of presenilin contributes to catalytic function and substrate identification of γ-secretase. *Journal of Neuroscience*, **26**(14): 3821–3828. doi:10.1523/jneurosci.5354-05.2006.

Yamazaki, T, Koo, EH, Selkoe, DJ (1996). Trafficking of cell-surface amyloid β-protein precursor. II. Endocytosis, recycling and lysosomal targeting detected by immunolocalization. *Journal of Cell Science*, **109**(Pt 5): 999–1008. doi:10.1242/jcs.109.5.999.

Yan, R, Bienkowski, MJ, Shuck, ME, Miao, H, Tory, MC, Pauley, AM, Brashier, JR, Stratman, NC, Mathews, WR, Buhl, AE, Carter, DB, Tomasselli, AG, Parodi, LA, Heinrikson, RL, Gurney, ME (1999). Membrane-anchored aspartyl protease with Alzheimer's disease β-secretase activity. *Nature*, **402**(6761): 533–537. doi: 10.1038/990107.

Yan, Y, Wang, C (2007). Aβ40 protects non-toxic Aβ42 monomer from aggregation. *Journal of Molecular Biology*, **369**(4): 909–916. doi:10.1016/j.jmb.2007.04.014.

Yang, DS, Tandon, A, Chen, F, Yu, G, Yu, H, Arawaka, S, Hasegawa, H, Duthie, M, Schmidt, SD, Ramabhadran, TV, Nixon, RA, Mathews, PM, Gandy, SE, Mount, HTJ, George-Hyslop, PS, Fraser, PE (2002). Mature glycosylation and trafficking of nicastrin modulate its binding to presenilins. *Journal of Biological Chemistry*, **277**(31): 28135–28142. doi:10.1074/jbc.M110871200.

Yang, G, Zhou, R, Guo, X, Yan, C, Lei, J, Shi, Y (2021). Structural basis of γ-secretase inhibition and modulation by small molecule drugs. *Cell*, **184**(2): 521–53314. doi:10.1016/j.cell.2020.11.049.

Yang, G, Zhou, R, Zhou, Q, Guo, X, Yan, C, Ke, M, Lei, J, Shi, Y (2019). Structural basis of Notch recognition by human γ-secretase. *Nature*, **565**(7738): 192–197. doi:10.1038/s41586-018-0813-8.

Yankner, BA, Duffy, LK, Kirschner, DA (1990). Neurotrophic and neurotoxic effects of amyloid β protein: Reversal by tachykinin neuropeptides. *Science*, **250**(4978): 279–282. doi:10.1126/science.2218531.

Yin, F (2022). Lipid metabolism and Alzheimer's disease: Clinical evidence, mechanistic link and therapeutic promise. *FEBS Journal*. doi:10.1111/febs.16344.

Yu, C, Kim, SH, Ikeuchi, T, Xu, H, Gasparini, L, Wang, R, Sisodia, SS (2001). Characterization of a presenilin-mediated amyloid precursor protein carboxyl-terminal fragment γ. Evidence for distinct mechanisms involved in γ-secretase processing of the APP and Notch1 transmembrane domains. *Journal of Biological Chemistry*, **276**(47): 43756–43760. doi:10.1074/jbc.C100410200.

Yu, G, Nishimura, M, Arawaka, S, Levitan, D, Zhang, L, Tandon, A, Song, YQ, Rogaeva, E, Chen, F, Kawarai, T, Supala, A, Levesque, L, Yu, H, Yang, DS, Holmes, E, Milman, P, Liang, Y, Zhang, DM, Xu, DH, Sato, C, Rogaev, E, Smith, M, Janus, C, Zhang, Y, Aebersold, R, Farrer, LS, Sorbi, S, Bruni, A, Fraser, P, George-Hyslop, PS (2000). Nicastrin modulates presenilin-mediated notch/glp-1 signal transduction and βAPP processing. *Nature*, **407**(6800): 48–54. doi:10.1038/35024009.

Zall, A, Kieser, D, Höttecke, N, Naumann, EC, Thomaszewski, B, Schneider, K, Steinbacher, DT, Schubenel, R, Masur, S, Baumann, K, Schmidt, B (2011). NSAID-derived γ-secretase modulation requires an acidic moiety on the carbazole scaffold. *Bioorganic & Medicinal Chemistry*, **19**(16): 4903–4909. doi:10.1016/j.bmc.2011.06.062.

Zhang, X, Yu, CJ, Sisodia, SS (2015a). The topology of pen-2, a γ-secretase subunit, revisited: Evidence for a reentrant loop and a single pass transmembrane domain. *Molecular Neurodegeneration*, **10**(39). doi:10.1186/s13024-015-0037-4.

Zhang, Z, Song, M, Liu, X, Kang, SS, Duong, DM, Seyfried, NT, Cao, X, Cheng, L, Sun, YE, Yu, SP, Jia, J, Levey, AI, Ye, K (2015b). δ-Secretase cleaves amyloid precursor protein and regulates the pathogenesis in Alzheimer's disease. *Nature Communications*, **6**(8762). doi:10.1038/ncomms9762.

Zhao, G, Cui, MZ, Mao, G, Dong, Y, Tan, J, Sun, L, Xu, X (2005). γ-Cleavage is dependent on ζ-cleavage during the proteolytic processing of amyloid precursor protein within its transmembrane domain. *Journal of Biological Chemistry*, **280**(45): 37689–37697. doi:10.1074/jbc.M507993200.

Zhao, G, Mao, G, Tan, J, Dong, Y, Cui, MZ, Kim, SH, Xu, X (2004). Identification of a new presenilin-dependent ζ-cleavage site within the transmembrane domain of amyloid precursor protein. *Journal of Biological Chemistry*, **279**(49): 50647–50650. doi:10.1074/jbc.C400473200.

Zhou, H, Zhou, S, Walian, PJ, Jap, BK (2010). Dependency of γ-secretase complex activity on the structural integrity of the bilayer. *Biochemical and Biophysical Research Communications*, **402**(2): 291–296. doi:10.1016/j.bbrc.2010.10.017.

Zhou, R, Yang, G, Guo, X, Zhou, Q, Lei, J, Shi, Y (2019). Recognition of the amyloid precursor protein by human γ-secretase. *Science*, **363**(6428): eaaw0930. doi:10.1126/science.aaw0930.

Zhou, S, Zhou, H, Walian, PJ, Jap, BK (2005). CD147 is a regulatory subunit of the γ-secretase complex in Alzheimer's disease amyloid β-peptide production. *Proceedings of the National Academy of Sciences of the United States of America*, **102**(21): 7499–7504. doi:10.1073/pnas.0502768102.

List of Abbreviations

Å	Angstrom
aa	amino acid(s)
AD	Alzheimer's disease
ADAM	a disintegrin and metalloproteinase
AICD	APP intracellular domain
amp	ampicillin
APH-1	anterior pharynx-defective 1
APLP	amyloid precursor-like protein
APP	amyloid precursor protein
ApoE	Apolipoprotein E
BACE	β-site APP cleaving enzyme
BBB	blood-brain barrier
BN-PAGE	blue native polyacrylamide gel electrophoresis
BSA	bovine serum albumin
BV	bead volume(s)
CHAPSO	3-[(3-Cholamidopropyl)dimethyl-ammonio]-1-propanesulfonate
CTF	C-terminal fragment
CuBD	copper binding domain
DCC	deleted in colorectal cancer
DDM	*n*-Dodecyl-β-D-maltopyranoside
DLS	dynamic light scattering
DMSO	dimethyl sulfoxide
DSF	differential scanning fluorimetry
DTT	dithiothreitol
E. coli	*Escherichia coli*
ECL	electrochemiluminescence
ECL-IA	electrochemiluminescence immunoassay
EM	electron microscopy
ER	endoplasmatic reticulum
ERAD	ER associated degradation
E-S	enzyme–substrate complex

FAD	familial AD
FBS	fetal bovine serum
FDA	US Food and Drug Administration
FRET	Förster resonance energy transfer
Fz2	Frizzled2
G	G418, Geniticin
GFLD	growth factor-like domain
GSAP	γ-secretase-activating protein
GSI	γ-secretase inhibitor
GSM	γ-secretase modulator
GWAS	genome-wide association studies
h	hour(s)
IB	immunoblot
ICD	intracellular domain
IFTM3	interferone induced transmembrane protein 3
IMP	intramembrane protease
IP	immunoprecipitation
IPTG	isopropyl β-D-1-thiogalactopyranoside
kB	kilo base pairs
KPI	Kunitz-like protease inhibitor domain
LB medium	lysogeny broth medium
LOAD	late onset AD
LTP	long term potentiation
M. marisnigri	*Methanoculleus marisnigri*
mA	miliampere
MALDI	matrix associated laser distortion
MD	molecular dynamics
min	minute(s)
mm	millimeter
MS	mass spectrometry
NCT	nicastrin
NFT	neurofibrillary tangle
NICD	Notch intracellular domain
NSAID	non-steroidal antiinflammatory agent
NRG1	neuregulin-1 type III
NTF	N-terminal fragment
OD	optical density
PARL	presenilin-associated rhomboid like
PC	proprotein convertase

PCR	poylmerase chain reaction
PEN-2	presenilin enhancer 2
PS	presenilin
PSH	presenilin/SPP homolog
RCE1	Ras-converting enzyme 1
Rer1p	retrieval of ER protein
RHBL	rhomboid-like
rpm	rounds per minute
s	second(s)
S. cerevisiae	*Saccharomyces cerevisiae*
S2P	site-2 protease
sAPP	soluble APP
sAD	sporadic AD
SDS	sodium dodecyl sulfate
SDS-PAGE	SDS polyacrylamide gel electrophoresis
SPP	signal peptide peptidase
SPPL	SPP-like
SREBP	sterol regulatory element binding protein
SUV	small unilamellar vesicles
tet	tetracycline
T_i	inflection temperature
TIMPS	tissue inhibitors of metalloproteases
TM	transmembrane
TMD	transmembrane domain
Trem2	Triggering receptor expressed on myeloid cells-2
TSA	transition state analogue
V	Volt
WT	wild type
Z	Zeocine

Acknowledgements

After this long journey to my doctorate, I would like to thank all the people who have accompanied me during this time and helped me throughout the years to succeed in my projects and in my life.

First of all, I like to thank **Harald Steiner** for giving me the opportunity to work on a bunch of interesting and fascinating projects around intramembrane proteolysis and for his supervision, trust, patience and scientific input throughout the whole time. Furthermore, I like to thank **Christian Haass** for his constant passion in science and for providing a great research environment.

Of course, I need to thank the whole Steiner group for a great time in the lab, for lots of scientific and non-scientific discussions and all your support. **Edith Winkler** and **Gabi Basset** who know all the techniques used since years in the lab and who could tell a lot about the "good old times" and – together with **Claudia Ajram** – for their technical support. **Frits Kamp** and former lab member **Akio Fukumori** for scientific discussions on manuscripts and lab techniques. **Edgar Dawkins**, who created the funniest German expressions ever heard and who was – especially in the last months – a great person to discuss future perspectives. **Alice Sülzen** for help with the antibody generation and the purifications of antibodies. **Johannes Trambauer** who seems to know everything and who always had advices, both asked and unasked. **Nadine Werner**, my seat and lab mate and fellow doctoral researcher in the last 6 years, I think we both managed great to go through our doctorate journey together.

All my projects also involved lots of collaborations and support from other scientists. A special thanks goes to **Shu-Yu Chen** and **Martin Zacharias** for all simulations you performed and all the exciting collaborative projects and discussions that emerged from your simulations. **Regina Feederle** and her team for generating all the antibodies for us which are really crucial for our research. Thanks also to all the people that granted access to machines needed for this study and that gave valuable input: **Axel Imhof**, **Ignasi Forné** and **Shibo Lahiri** from the ZFP for access to the MALDI instruments and **Michela Smolle** for access to the

Nanotemper Tycho. A great thanks goes also to all the collaboration partners of our DFG-funded **"Forschergruppe" FOR2290** for the scientific discussion and all the input throughout the years and for the one or other glass of wine during our regular meetings.

Of course, all my work would have not be possible without a great research environment. Therefore, I would like to thank all the colleagues from the **third floor** that were open for scientific and non-scientific discussions and that gave every now and then valuable input for my projects. Some of you became friends for me and I would like to thank all of you also for a great time in- and outside of the lab. Special thanks goes also to **Sabine Odoy** who put a lot effort to smoothly run the lab and who sometimes made the seemingly impossible possible. A thanks goes also to all the **fellow doctoral researchers** at the DZNE (not only in Munich), for creating a strong doctoral researchers community and for your trust in me to be your elected representative for some time.

There are some people I really have to thank personally since they really supported me a lot also during difficult times. **Georg Werner** who always had an open ear for me, for all our walks, museum visits and dinners, for just being there when I needed someone to talk to. And even though it stressed me also a lot, I was very happy and proud to be your best man. **Franziska Eck** who always had an open kitchen for the one or the other cooking evening and for testing new recipes. **Alexander Siebert** who also was there for me in difficult times and had always an open ears for non-lab and non-scientific related issues. **Karsten Nalbach** for some nice and important personal discussions, for the one or the other wine blissful evening and for some of the best and greatest mountain experiences I had so far. Without you, I would not have reached the one or the other summit. And of course, my long-time friend **Theresa Kordaß**, for all the telephone calls, all the letters and messages, for all the anti-frustration and happiness chocolate, for having each other in hard times, for all the cheering up and also for the scientific discussions. Even though we are separated by several hundred kilometres, I know that there is a person I can truly trust!

Last but not least, I want to thank my whole family and especially my beloved parents who constantly supported me throughout my life so far, who let me go my own way and who trusted me and my decisions even though we faced together some hard times. Before I started my doctorate journey, I promised you to follow my own path no matter what happens. It was not always easy but I tried my best ... and I think I managed quiet well.